



**UNIVERSITÉ PIERRE ET MARIE CURIE
AIRBUS DEFENCE AND SPACE**

Doctoral School **Sciences Mathématiques de Paris Centre**
University Department **Laboratoire Jacques-Louis Lions**

Thesis defended by **Maxime CHUPIN**

Defended on **19th October, 2016**

In order to become Doctor from Université Pierre et Marie Curie

Academic Field **Applied Mathematics**
Speciality **Optimal Control**

Interplanetary transfers with low consumption using the properties of the restricted three body problem

Thesis supervised by Emmanuel TRÉLAT Supervisor
Thomas HABERKORN Co-Supervisor
Max CERF Co-Supervisor

Committee members

<i>Referees</i>	Jean-Baptiste CAILLAU	Professor at Université de Bourgogne Franche-Comté
	Alessandra CELLETTI	Professor at University of Rome Tor Vergata
<i>Examiners</i>	Pascal FREY	Professor at Université Pierre et Marie Curie
	Richard ÉPENROY	Engineer at CNES
<i>Supervisors</i>	Emmanuel TRÉLAT	Professor at Université Pierre et Marie Curie
	Thomas HABERKORN	Lecturer at Université d'Orléans
	Max CERF	Engineer at Airbus DS

UNIVERSITÉ PIERRE ET MARIE CURIE
AIRBUS DEFENCE AND SPACE

École doctorale **Sciences Mathématiques de Paris Centre**
Unité de recherche **Laboratoire Jacques-Louis Lions**

Thèse présentée par **Maxime CHUPIN**

Soutenue le **19 octobre 2016**

En vue de l'obtention du grade de docteur de l'Université Pierre et Marie Curie

Discipline **Mathématiques appliquées**
Spécialité **Contrôle optimal**

Transferts interplanétaires à faible consommation utilisant les propriétés du problème restreint des trois corps

Thèse dirigée par Emmanuel TRÉLAT directeur
Thomas HABERKORN co-directeur
Max CERF co-directeur

Composition du jury

<i>Rapporteurs</i>	Jean-Baptiste CAILLAU Alessandra CELETTI	professeur à l'Université de Bourgogne Franche-Comté professeur à l'University of Rome Tor Vergata
<i>Examineurs</i>	Pascal FREY Richard ÉPENOV	professeur à l'Université Pierre et Marie Curie ingénieur au CNES
<i>Directeurs de thèse</i>	Emmanuel TRÉLAT Thomas HABERKORN Max CERF	professeur à l'Université Pierre et Marie Curie MCF à l'Université d'Orléans ingénieur à l'Airbus DS

Keywords: optimal control, circular restricted three body problem, continuation method, shooting method, indirect methods, spacecraft mission, invariant manifolds

Mots clés : contrôle optimal, problème circulaire restreint des trois corps, méthode de continuation, méthode de tir, mission spatiale, méthodes indirectes, variétés invariantes

This thesis has been prepared at

Laboratoire Jacques-Louis Lions

4 place Jussieu
75005 Paris
France

Web Site <http://ljl1.math.upmc.fr/>



À Nicole, et à ma famille.

*À la mémoire de Philippe Augros, grâce à qui cette thèse a été possible, et qui nous a quittés
bien trop tôt.*

Un monde de mensonges ne peut être détruit
par la vérité, seulement par un monde de
vérité.

Franz Kafka

Freedom is the freedom to say that two plus
two make four. If that is granted, all else
follows.

George Orwell

Les philosophes n'ont fait qu'interpréter le
monde de diverses manières ; ce qui importe,
c'est de le transformer.

Karl Marx

Science is what we understand well enough
to explain to a computer. Art is everything
else we do.

Donald Ervin Knuth

INTERPLANETARY TRANSFERS WITH LOW CONSUMPTION USING THE PROPERTIES OF THE RESTRICTED THREE BODY PROBLEM
Abstract

The first objective of this work is to understand the dynamical properties of the circular restricted three body problem in order to use them to design low consumption missions for spacecrafts with a low thrust engine. A fundamental property is the existence of invariant manifolds associated with periodic orbits around Lagrange points. Following the Interplanetary Transport Network concept, invariant manifolds are very useful to design spacecraft missions because they are gravitational currents. A large part of this work is devoted to designing a numerical method that performs an optimal transfer between invariant manifolds. The cost we want to minimize is the L^1 -norm of the control which is equivalent to minimizing the consumption of the engines. We also consider the L^2 -norm of the control which is easier to minimize numerically. The numerical methods are indirect ones coupled with different continuations on the thrust, on the cost, and on the final state, to provide robustness. These methods are based on the application of the Pontryagin Maximum Principle. The algorithms developed in this work allow for the design of real life missions such as missions between the realms of libration points. The basic idea is to initialize a multiple shooting method with an admissible trajectory that contains controlled parts (local transfers) and uncontrolled parts following the natural dynamics (invariant manifolds). The methods developed here are efficient and fast (less than a few minutes to obtain the whole optimal trajectory). Finally, we develop a hybrid method, with both direct and indirect methods, to adjust the position of the matching points on the invariant manifolds for missions with large energy gaps. The gradient of the value function is given by the values of the costates at the matching points and does not require any additional computation. Hence, the implementation of the gradient descent is easy.

Keywords: optimal control, circular restricted three body problem, continuation method, shooting method, indirect methods, spacecraft mission, invariant manifolds

TRANSFERTS INTERPLANÉTAIRES À FAIBLE CONSOMMATION UTILISANT LES PROPRIÉTÉS DU PROBLÈME RESTREINT DES TROIS CORPS
Résumé

Le premier objectif de cette thèse est de bien comprendre les propriétés de la dynamique du problème circulaire restreint des trois corps et de les utiliser pour calculer des missions pour satellites pourvus de moteurs à faible poussée. Une propriété fondamentale est l'existence de variétés invariantes associées à des orbites périodiques autour des points de LAGRANGE. En suivant l'idée de l'*Interplanetary Transport Network*, la connaissance et le calcul des variétés invariantes, comme courants gravitationnels, sont cruciaux pour le *design* de missions spatiales. Une grande partie de ce travail de thèse est consacrée au développement de méthodes numériques pour calculer le transfert entre variétés invariantes de façon optimale. Le coût que l'on cherche alors à minimiser est la norme L^1 du contrôle car elle est équivalente à minimiser la consommation des moteurs. On considère aussi la norme L^2 du contrôle car elle est, numériquement, plus facile à minimiser. Les méthodes numériques que nous utilisons sont des méthodes indirectes rendues plus robustes par des méthodes de continuation sur le coût, sur la poussée, et sur l'état final. La mise en œuvre de ces méthodes repose sur l'application du Principe du Maximum de Pontryagin. Les algorithmes développés dans ce travail permettent de calculer des missions réelles telles que des missions entre des voisinages des points de LAGRANGE. L'idée principale est d'initialiser un tir multiple avec une trajectoire admissible composée de parties contrôlées (des transferts locaux) et de parties non-contrôlées suivant la dynamique libre (les variétés invariantes). Les méthodes mises au point ici, sont efficaces et rapides puisqu'il suffit de quelques minutes pour obtenir la trajectoire optimale complète. Enfin, on développe une méthode hybride, avec à la fois des méthodes directes et indirectes, qui permettent d'ajuster la positions des points de raccord sur les variétés invariantes pour les missions à grandes variations d'énergie. Le gradient de la fonction valeur est donné par les valeurs des états adjoints aux points de raccord et donc ne nécessite pas de calculs supplémentaire. Ainsi, l'implémentation de l'algorithme du gradient est aisée.

Mots clés : contrôle optimal, problème circulaire restreint des trois corps, méthode de continuation, méthode de tir, mission spatiale, méthodes indirectes, variétés invariantes

Laboratoire Jacques-Louis Lions

4 place Jussieu – 75005 Paris – France

Remerciements

Voilà venu le temps d'écrire mes remerciements venant clôturer ces années de travail sur mon sujet de thèse. C'est donc l'occasion de repenser aux personnes qui ont compté dans cette aventure.

Mes premiers remerciements sont, bien entendu, pour mes directeurs de thèse. J'ai été honoré de rencontrer Philippe AUGROS, ce personnage singulier qui m'a apporté une vision extrêmement profonde du problème alliant une fine compréhension mathématique et une connaissance gigantesque des problématiques d'ingénieries et des enjeux de telles recherches dans le monde de l'industrie. Philippe est malheureusement parti trop tôt, et c'est avec beaucoup d'émotion que je lui dédie une fois de plus ce travail. Je remercie très chaleureusement Max CERF d'avoir accepté de prendre la suite de l'encadrement pour Airbus DS. Ce fut un plaisir de travailler avec toi.

Je tiens à remercier mes directeurs de thèse du monde académique, Emmanuel TRÉLAT et Thomas HABERKORN. Ce duo m'a tant apporté ! Leur temps d'abord, avec une disponibilité sans faille, toujours dans la bonne humeur, toujours encourageants. Ce fut un privilège de travailler avec vous. Chacun avec vos spécificités vous m'avez appris ce qu'était la recherche. J'ai toujours été épaté par votre maîtrise des différents domaines auxquels touche ce travail de thèse. Vous avez été d'excellent conseil, m'aiguillant tout en me laissant toute la liberté que je voulais. Thomas, et nos journées à Orléans, Emmanuel, mon quasi voisin de bureau, merci pour ces années.

Je suis honoré d'avoir eu comme rapporteurs Alessandra CELLETTI et Jean-Baptiste CAILLAU. Si je n'ai jamais eu l'occasion de rencontrer Alessandra CELLETTI, j'ai effleuré quelques uns de ses travaux concernant la stabilité en mécanique spatiale, et je suis impressionné par la complexité du sujet. Je suis heureux d'avoir pu être évalué par cette chercheuse ! Jean-Baptiste, quant à lui, n'est pas seulement un rapporteur de la thèse. Ses travaux sont centraux quand on travaille sur la thématique du contrôle des véhicules spatiaux d'un point de vue mathématique, et tout au long de mon travail, j'ai eu la chance de pouvoir le côtoyer très régulièrement, échanger et apprendre de nos diverses discussions, apportant sa bienveillance et ses conseils. Qu'il ait accepté de rapporter ma thèse me fait très plaisir.

Je tiens aussi à remercier tout particulièrement Richard ÉPENNOY, ingénieur au CNES, avec qui, depuis le début de ma thèse, j'échange régulièrement sur les problématiques qui nous concernent, et duquel, par ses publications et nos discussions, j'ai pu apprendre beaucoup. Je suis très heureux et honoré de pouvoir le compter parmi les membres de mon jury. Enfin, un grand merci au représentant du LJLL de mon jury, Pascal FREY, qui a accepté cette tâche.

Le laboratoire Jacques-Louis Lions a été un endroit très agréable pendant ces années de travail. Il y règne une bonne ambiance, et j'y ai passé du bon temps entre travail et rencontres. J'en profite pour remercier comme il se doit Catherine, Malika et Salima, pour leur travail impressionnant, et pour leur aide inconditionnelle. Je remercie aussi Khashayar, Altaïr, Hugues, et Stéphane, il y a eu un important turnover mais chaque nouvelle recrue a chaque fois été une belle rencontre. J'en profite aussi pour remercier le MAPMO de l'université d'Orléans et en particulier Anne, qui s'est toujours montrée accueillante et tellement efficace. Je remercie aussi le CEREMADE de l'université Paris Dauphine dans lequel je me suis installé depuis le mois d'avril. Là encore, j'ai la chance d'y avoir trouvé une ambiance

chaleureuse et un travail épanouissant.

Je veux aussi remercier mes collègues doctorants du contrôle optimal, Jiamin, Zheng, Mikael, Jérémy et Achile, camarades de conférences à Paris, Toulouse, Linz, Dijon...Ce fut un plaisir de vous connaître, de partager nos recherches et de vous retrouver autour des différents buffets, repas et autres bières.

Je veux aussi rendre hommage à deux personnes qui sont centrales dans ma découverte des mathématiques. En premier lieu, mon prof de maths de PTSI à Poitiers, Jean-Michel SARLAT qui m'a fait découvrir les maths et l'informatique, et me les a fait aimer. Il m'a aussi initié à une de mes passions, à savoir le monde de $\text{T}_\text{E}_\text{X}$. La deuxième personne est Frédéric JEAN, enseignant chercheur à l'ENSTA, qui m'a enseigné le contrôle et la géométrie différentielle, et m'a permis de rencontrer Emmanuel. Il a toujours été de bons conseils et toujours à l'écoute. Merci encore à vous deux !

De l'ENSTA, je garde aussi quelques amis qui comptent toujours : le récemment docteur Gilles, bien évidemment, avec qui on est rarement d'accord, mais avec qui on discute énormément, avec des mots ou des gants sur un ring. Nous avons découvert les mathématiques appliquées ensemble et chacun dans notre voie, le monde de la recherche. Je tiens à saluer notre équipe qui malgré le temps et les disponibilités plus que rares (surtout de ma faute) essaie de garder contact, Antoine, Mathieu, et Maha ! J'en profite pour adresser une pensée à Yassine, ami de prépa, avec qui j'ai fait mes armes mathématiques.

Mes pensées vont aussi à mes collègues et amis du laboratoire. Les vieux d'abord, avec qui j'ai découvert les joies des soirées d'après boulot bien souvent trop arrosées : Pierre LISSY qui connaît si bien ce monde, les histoires, les potins, Charles d'une générosité inégalable, Lise-Marie et son conseil « *tous les jours, faire au moins une chose* », Juliette B. et son indéfectible sourire. S'en suivent mes voisins de bureau. Tout particulièrement, je pense à Pierre JOUNIEAUX, et nos grandes discussions sur tout un tas de sujets (dont la découverte de Picou, merci !). Pierre est fascinant, tout simplement. J'ai eu aussi la chance de partager mon bureau avec Thibault qui a repris le flambeau des soirées d'après boulot, toujours gentil et généreux, et avec Sarah, sa vie débordante, électrique et impulsive. Enfin, plus récemment, j'ai connu les deux nouvelles recrues qui, en seulement quelques mois, me semblent être de très chouettes personnes : bonne continuation Camille et Antoine ! Je remercie également Ludovick, Carlo, Aurora, Mehdi, et Ryadh pour lesquels on pourrait dire beaucoup !

Enfin, il y a mes amis et ma famille, la frontière étant bien floue. Ma Charente natale, avec l'ami Marc pour qui le reste des pages de cette thèse ne suffirait pas à expliquer combien il est important pour moi, JB et notre amitié inébranlable, mes chers Anaïs et Arnau, Pierre mon luthier préféré, Mathilde partie vivre si (trop ?) loin, mon Simon, le plus ancien de tous et qui est si important et enfin le vieil ami Félix ! Je pense aussi à mes amis parisiens, Raphaël, Clara, Miguel, Guillaume, Natalianne, Juliette BOUTIER, Juliette MARIN, Sonia, Clémentine, Aniès, Camille, Antoine, avec qui j'ai la chance de passer mes soirées de jeux, de bières, de whisky, de bouffe, de spectacles, mes randonnées, mes vacances et bien d'autres choses encore. Ce sont toutes des personnes exceptionnelles et chacune mérite bien plus que ces lignes. Je pense aussi à l'ex-londonienne grenobloise Lucie.

Je tiens à remercier tout particulièrement mon frangin, Baptiste, il n'y a pas de mots pour en dire plus. Je remercie aussi Ann et Tony qui m'ont accueilli dans leur famille et qui se sont toujours intéressés à mes recherches. Je pense à mes quatre grands-parents, Annie, Michel, Hélène et Michel, et ma tante, Jacqueline, que j'ai la chance d'avoir, qui m'apprennent toujours autant de choses, à Willy, Virginie, Charlotte, Lisa, Luna, Noé, Lino, Leïla, et Jean-Mi. Et évidemment, je remercie mes parents, Jean-Marc et Josiane, deux personnes simplement extraordinaires, et c'est une fierté d'être leur enfant.

Enfin, je remercie la seule et l'unique, Nicole, qui non seulement a relu toute cette thèse, tentant, avec énormément de patience, d'en améliorer l'anglais et le contenu, mais qui est là toujours pour moi, merci pour tout ! Nicole, cette thèse t'est dédiée.

Contents

Abstract	xiii
Remerciements	xv
Contents	xix
List of Figures	xxiii
Introduction (french version)	1
Introduction	15
1 The Circular Restricted Three-Body Problem (CRTBP)	27
1.1 Equations of Motion	29
1.1.1 Frame transition maps	31
1.2 Libration Points (Lagrange Points)	33
1.2.1 Localization of collinear points	34
1.2.2 Richardson Coordinate System for the CRTBP	35
1.2.3 Stability by Linearization	35
1.3 Jacobi Integral and Hill's Region	37
1.3.1 Jacobi Integral	37
1.3.2 Hill's Region	37
1.4 Periodic Orbits	39
1.4.1 Lyapunov-Poincaré Theorem	40
1.4.2 Numerical Method to Compute Periodic Orbits	42
1.4.3 Analytical Initialization	42
1.4.4 Families of Periodic Orbits	47
1.5 Invariant Manifolds	50
1.5.1 Mathematical Definition	50
1.5.2 Linear Approximation	51
1.5.3 Numerical Computation	53
1.5.4 Stability of Manifolds	55
1.5.5 Theoretical Existence of Invariant Manifolds as Separatrices	56
2 From Impulse Transfer to Low Thrust Transfer between Manifolds	61
2.1 Design of Impulse Transfer Missions using Manifolds	62
2.1.1 Trajectories with Prescribed Itineraries	63
2.1.2 Heteroclinic and Homoclinic Orbits	64
2.2 Model	67
2.2.1 Controlled Dynamics	68

2.2.2	Controllability	69
2.3	Optimal Control Theory in a Nutshell	71
2.3.1	General Framework	71
2.3.2	The Pontryagin Maximum Principle (PMP)	72
2.4	Numerical Methods	73
2.4.1	Direct Methods	74
2.4.2	Indirect Methods	74
2.5	Numerical Continuation Methods	76
2.5.1	Discrete Continuation	77
2.5.2	Piecewise Linear Continuation	78
2.6	Construction of an Optimal Control Problem (OCP)	79
2.6.1	From an Impulse Solution to an Optimal Control Problem	79
2.6.2	Minimization of the L^1 -norm of the Control	83
2.6.3	Minimization of the L^2 -norm of the Control	86
2.7	Numerical Method: From Impulse Transfer to Low Thrust Transfer	88
2.7.1	Final State Continuation	88
2.7.2	Thrust Continuation	89
2.8	Description of the Algorithm	90
2.8.1	Principle	90
2.9	Numerical Results	93
2.9.1	Transfer between Invariant Manifolds: {Earth-Moon} System, Halo Orbits	93
2.9.2	Transfer between Invariant Manifolds: {Sun-Earth} System, Halo Orbits	95
2.9.3	Study of the Transfer Time Parameter	96
3	Low-Thrust Missions between Libration Points with L^2-Minimization	101
3.1	Dynamical Properties to Initialize the Resolution of an OCP	101
3.2	The Lyapunov to Lyapunov Mission as an Optimal Control Problem	102
3.2.1	Optimal Control Problem (OCP)	103
3.2.2	Heteroclinic Orbits	104
3.2.3	From One Orbit to Another	106
3.2.4	Multiple Shooting	110
3.2.5	Thrust Continuation	112
3.2.6	Optimization of the Terminal Points	113
3.2.7	Numerical Results	114
3.3	Variant of the mission	115
3.3.1	With a Heteroclinic Orbit with Two Revolutions	116
3.3.2	Halo to Halo Mission	117
4	Missions Departing from the Geostationary Earth Orbit	125
4.1	Definition of the Mission	126
4.2	An Invariant Manifold as a Gravitational Current	127
4.3	Three-Part Trajectory	129
4.3.1	From GEO to the free trajectory	129
4.3.2	From the free trajectory to the LO	130
4.3.3	The Admissible Trajectory	130
4.4	Hybrid Optimization Method	132
4.4.1	The Algorithm	133
4.4.2	Numerical results	134
4.5	Other Missions	135

4.5.1	GEO to Lyapunov Missions: Two Cases	136
4.5.2	3D case, from the GEO to a Halo orbit	138
4.5.3	About the Maximal Thrust	139
Conclusion		141
A Richardson's Constants		145
B User guide for the Uacamol program – v1.4		147
B.1	Introduction	147
B.2	A Short Review of the Three Body Problem	147
B.2.1	Equations of Motion	148
B.2.2	The Poincaré Cuts	148
B.3	Compile Uacamol	149
B.4	Files to Feed Uacamol	149
B.4.1	Addresses File	149
B.4.2	Parameters Input File	150
B.5	Outputs	153
B.6	Examples of Application	154
B.6.1	Halo Orbit around L_1 – System Earth-Moon	154
B.6.2	Lissajous Orbit around L_2 – System Earth-Moon	155
B.6.3	Eight-shaped Orbit around L_1 – System Earth-Moon	157
B.6.4	Halo Orbit around L_1 – System Sun-Earth	158
C Input File for the Code Performing Transfers between Invariant Manifolds		161
C.1	Principle	161
C.2	Input File	161
Index		165
Bibliography		167

List of Figures

1	Schéma reprenant la carte de métro montrant différentes connexions entre différentes régions du système solaire à faible énergie. <i>Source : NASA, Gary L. Martin, Space Architect.</i>	7
2	Illustration du système {Terre-Lune} : région de Hill, orbites périodiques autour des points de LAGRANGE, et variétés invariantes.	9
3	A metro map showing hubs connected by low energy passageways. <i>Source: NASA, Gary L. Martin, Space Architect.</i>	20
4	Illustration of an {Earth-Moon} system: periodic orbits around Lagrange points, and associated invariant manifolds.	23
1.1	Illustration of the CRTBP, two primaries P_1 and P_2 revolving around their center of mass in circular orbits under their mutual attraction, and the spacecraft P with a negligible mass.	28
1.2	Inertial and rotating frames.	32
1.3	Localization of Lagrange points.	33
1.4	Plot of the potential in the planar case for system {Earth-Moon}. The five equilibrium points $L_i, i \in \llbracket 1, 5 \rrbracket$ are the critical points.	38
1.5	Realms of possible motion (images J.-M. Sarlat).	39
1.6	Halo orbit in the {Sun-Earth} system in Richardson coordinates obtained by a Newton-like method. The fixed excursion is $A_z = 240 \times 10^3$ km.	46
1.7	Eight-shape orbit in the {Earth-Moon} system in Richardson coordinates obtained by a Newton-like method. The fixed excursion is $A_z = 630 \times 10^3$ km.	47
1.8	Lyapunov orbit in the {Earth-Moon} system in Richardson coordinates obtained by a Newton-like method. We are in a planar case.	48
1.9	Family of Halo orbits in the {Sun-Earth} system in Richardson coordinates obtained by a Newton-like method and continuation on the energy. The first fixed excursion is $A_z = 240 \times 10^3$ km and the final energy is -1.50042 in normalized units (corresponding to a quasi-null z -excursion).	50
1.10	Family of eight-shape orbits in the {Earth-Moon} system in Richardson coordinates obtained by a Newton-like method and continuation on the energy. The first fixed excursion is $A_z = 630 \times 10^3$ km and the final energy is -1.59 in normalized units (corresponding to a quasi-null z -excursion).	51
1.11	Family of planar Lyapunov orbits in the {Earth-Moon} system in Richardson coordinates obtained by a Newton-like method and continuation on the energy. The final energy is -1.6001 in normalized units.	52
1.12	Illustration of the method to compute invariant manifolds.	54

1.13	Invariant manifolds of energy $\mathcal{E} = -1.50042$ of the Halo orbit around L_1 in the {Sun-Earth} system. On the left: an unstable manifold near the second primary. On the right: the four manifolds. The propagation time is equal to 5.0 in the normalized system, and the perturbation parameter α is equal to 1×10^{-4}	55
1.14	Invariant manifolds of the eight-shape orbit around L_1 in the {Earth-Moon} system of energy $\mathcal{E} = -1.59$. Top: a 3D view of the manifolds. Left: an unstable manifold near the second primary. Right: The four manifolds. The propagation time is equal to 6.0 in normalized system, and the perturbation parameter α is equal to 1×10^{-4}	56
1.15	Invariant manifolds of the Lyapunov orbit in the {Earth-Moon} system of energy $\mathcal{E} = -1.60$. Left: an unstable manifold near the second primary. Right: The four manifolds. The propagation time is equal to 8.0 in the normalized system, and the perturbation parameter α is equal to 1×10^{-4}	57
1.16	Saddle projection of the flow in the equilibrium region. Only the projection onto the (p_1, q_1) -plane (with axis titled by 45°).	58
2.1	The eight invariant manifolds associated with the Lyapunov orbits of the points L_1 and L_2 in the {Earth-Moon} system, at a specific energy of $\mathcal{E} = -1.59$. The different Poincaré surfaces of section U_i are represented. In such a configuration, one can find a trajectory with a prescribed itinerary visiting the three realms $\mathcal{R}_X, \mathcal{R}_M$ and \mathcal{R}_E	65
2.2	Different Poincaré cuts, U_1 and U_4 , for the {Earth-Moon} system with two Lyapunov orbits around L_1 and L_2 at an energy $\mathcal{E} = -1.56$	66
2.3	Poincaré cut U_2 of invariant manifolds from Lyapunov orbits around L_1 and L_2 . The three intersections correspond to three different heteroclinic orbits connecting the two periodic orbits. We consider the {Earth-Moon} system with two Lyapunov orbits around L_1 and L_2 with an energy of $\mathcal{E} = -1.56$. The U_3 section is similar.	66
2.4	Examples of homoclinic and heteroclinic orbits for the {Earth-Moon} system with two Lyapunov orbits around L_1 and L_2 at energy $\mathcal{E} = -1.56$	67
2.5	Possible continuation zero paths (left) and impossible continuation zero paths (right).	77
2.6	Graphic illustration of the discrete continuation method with constant steps.	79
2.7	Graphic illustration of the Piecewise Linear continuation method with constant steps. Z_c is the prediction constructed with the two previous solutions of intermediary problems.	81
2.8	Drawing of the construction of the end points of the optimal control problem starting with an impulse transfer between invariant manifolds \mathcal{M}_0 and \mathcal{M}_1	81
2.9	Illustration of the continuation on the final state. ξ_1^{nat} is the propagation of the initial point ξ_0^* during the transfer time t_f . Step by step, we reach the final point $\xi_1^\lambda = (1 - \lambda)\xi_1^{\text{nat}} + \lambda\xi_1^*$, with λ going from 0 to 1.	89
2.10	Description of the algorithm to solve the transfer between invariant manifolds with low thrust.	92
2.11	{Earth-Moon} system: Different projections of the intersection with the Poincaré cut U_2 for the invariant manifolds associated with the two Halo orbits around L_1 and L_2 . Note that there is no intersection between the two manifolds, and this is obvious with the (y, \dot{y}) -plane projection.	94
2.12	{Earth-Moon} system: Construction and resolution of the transfer problem between the two invariant manifolds of two Halo orbits around L_1 and L_2	94

2.13	Different continuations during the resolution of the transfer between invariant manifolds in the {Earth-Moon} system.	95
2.14	{Sun-Earth} system: Different projections of the intersection with the Poincaré cut U_2 for the invariant manifolds associated with the two Halo orbits around L_1 and L_2 . Note that there is no intersection between the two manifolds, this is obvious on the (y, \dot{y}) -plane projection.	96
2.15	{Sun-Earth} system: Construction and solution of the transfer problem between the two invariant manifolds of two Halo orbits around L_1 and L_2	97
2.16	Different continuations during the resolution of the transfer between invariant manifolds in the {Sun-Earth} system.	98
2.17	Controls for different transfer times for the transfer between invariant manifolds from Halo orbits in the {Sun-Earth} system. Left: Small times, similar to ΔV . Center: Longer times. Right: After the interval I_{SE} , where the algorithm fails, we get a different structure for the control corresponding to a trajectory with a revolution.	98
2.18	Controls for different transfer time for the transfer between invariant manifolds from Halo orbits in the {Earth-Moon} system. Left: small times, similar to ΔV . Center: Longer times. Right: After the interval I_{SE} , where the algorithm fails, we get a different structure for the control corresponding to a trajectory with a revolution.	99
2.19	Different optimal trajectories for the two considered systems. We observe a bifurcation when the time increases, after respectively I_{SE} and I_{EM} , the trajectories perform a revolution around the second primary.	99
2.20	Evolution of the sequence $(\eta_i)_{i \in I}$. In both cases, we observe that the cost converges to the impulse when the transfer time goes to zero.	100
3.1	Left: Planes U_2 and U_3 in the {Earth-Moon} system. Right: unstable (red) and stable (blue) manifolds respectively from L_1 and L_2 stopping at the plane U_2	104
3.2	Section in the plane U_2 of a unstable manifold from L_1 and a stable manifold from L_2 . The energy is -1.592081 . On the right, a zoom on the interesting area.	105
3.3	Heteroclinic orbit between two Lyapunov orbits in the {Earth-Moon} system. We get a travel time of 8.9613933501964 (normalized time) or 38.974 days.	105
3.4	All relevant points in the construction of the problem.	107
3.5	Command to realize the optimal transfer from the Lyapunov orbit to the heteroclinic orbit. We plot $u(\cdot) \leq 1$ as a function of the normalized time.	108
3.6	Command to realize the optimal transfer from the Lyapunov orbit to the heteroclinic orbit. We plot $u(\cdot) \leq 1$ as a function of the normalized time.	110
3.7	Admissible trajectory in three parts.	111
3.8	Command to realize the optimal transfer from the Lyapunov orbit around L_1 to the Lyapunov orbit around L_2 . We plot $u(\cdot) \leq 1$ before the last optimization step on the first row (we chose two points on L_{y_1} and L_{y_2}) and after the last optimization step consisting in getting the general transversality conditions (second row). We can observe the good turnpike property of the second control.	114
3.9	Optimal trajectory. Left: the optimal trajectory with ξ_0^* and ξ_3^* fixed on L_{y_1} and L_{y_2} . Right: the optimal trajectory with ξ_0^* and ξ_3^* free on L_{y_1} and L_{y_2} . The control is represented by arrows.	115
3.10	Heteroclinic orbit between two Lyapunov orbits in the {Earth-Moon} system. We get a travel time of 11.699681461946 (normalized time) or 50.883 days.	116

3.11	Command to realize the optimal transfer from the Lyapunov orbit to the heteroclinic orbit. We plot $u(\cdot) \leq 1$ before the last optimization step on the first row (we chose two points on L_{y_1} and L_{y_2}) and after the last optimization step consisting in getting the general transversality conditions. We can observe the good turnpike property of the second control.	118
3.12	Optimal trajectory. Left: the optimal trajectory with ξ_0^* and ξ_3^* fixed on L_{y_1} and L_{y_2} . Right: the optimal trajectory with ξ_0^* and ξ_3^* free on L_{y_1} and L_{y_2} . The control is represented by arrows.	119
3.13	Halo orbits around L_1 and L_2 for energies -1.5939 and -1.5805 respectively. This corresponds to a unique excursion of $16\,000$ km.	120
3.14	Left: the propagation of manifolds from Halo around L_1 and Halo around L_2 . Right: the two trajectories of these manifold minimizing the distance on the plane U_2	120
3.15	Norm of the control for the three controlled parts of the admissible trajectory.	122
3.16	Admissible trajectory in five parts. Dashed part are manifold trajectories, <i>i.e.</i> free parts.	122
3.17	Optimal trajectory for the Halo to Halo transfer. Left: a 3 dimensional view. Right: a view in the (x, y) -plane. The control is represented by arrows.	124
3.18	Optimal control for the Halo to Halo Mission $T(\cdot) \in \mathbf{R}^3$ in Newton.	124
4.1	Plot of the propagation in the CRTBP of the initial conditions of the GEO in the 2 body problem. The duration of the propagation is 3.0 and corresponds to nearly 100 revolutions. We see that the embedded trajectory is stable with respect to the perturbation of the Moon.	127
4.2	Plot of the propagation in the CRTBP of an initial condition of a LO in the 2 body problem. The duration of the propagation is 3.0 and corresponds to nearly 10 revolutions. We see that the embedded trajectory is not periodic anymore but stays nearly periodic. The rotation of the Moon is taken into account.	128
4.3	Choice of a condition in the section U_2 , and the trajectory inside the invariant manifolds.	128
4.4	Transfer from a fixed point on the GEO to a fixed point on the free trajectory inside the tube connecting the Earth's realm to the Moon's realm. Left: the trajectory. Right: the norm of the control.	129
4.5	Transfer between a fixed point on the free trajectory to a fixed point on LO. Left: the trajectory. Right: the norm of the control.	130
4.6	Admissible trajectory in three parts from the GEO to the LO.	131
4.7	Evolution of the three-part trajectory during the gradient descent. Note that near the equilibrium point L_1 , the spacecraft makes a detour before coming back to the matching point.	134
4.8	Evolution of the two costs during the optimization. The L^2 -norm of the control decreases as expected, but unfortunately the L^1 -norm of the control increases, so the fuel consumption increases during the optimization.	135
4.9	Two trajectories connecting the GEO to a Lyapunov orbit with different inserting points on the manifold. The energy is $\mathcal{E} = -1.60$	137
4.10	Norm of the control for both trajectories connecting the GEO to the free trajectory of the stable manifold of the Lyapunov orbit. The energy is $\mathcal{E} = -1.60$	137
4.11	Admissible trajectory for the transfer from the GEO to the Halo orbit.	139
4.12	Norm of the control for the two controlled parts of the admissible trajectory connecting the GEO to the Halo orbit. The energy is $\mathcal{E} = -1.59$	139

-
- 4.13 Norm of the control for the two controlled times to reach the invariant manifold trajectory. The energy is $\mathcal{E} = -1.59$ 140
- 4.14 The two admissible trajectories for different times of transfer for the first controlled part of the admissible trajectory. The energy is $\mathcal{E} = -1.59$ 140

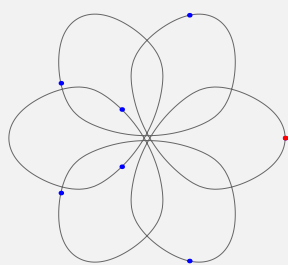
Introduction (french version)

Ce travail de thèse traite du *design* de missions spatiales dans le système solaire, c'est-à-dire, comment trouver, pour un satellite soumis à l'attraction des N corps du système solaire, une trajectoire associée à une commande réalisant le voyage souhaité.

Il est usuel et naturel de considérer que le satellite n'a pas une masse suffisamment importante pour influencer les mouvements des N corps massifs que l'on considère. Ceux-ci se déplacent en suivant des orbites déterminées par leurs influences mutuelles. Le but de *design* de trajectoires est de calculer des transferts pour le satellite le faisant passer d'une orbite de départ à une orbite d'arrivée en contrôlant les moteurs du satellite. De tels transferts peuvent être entre orbites autour de la Terre, par exemple de l'orbite terrestre basse (ou LEO) vers l'orbite géostationnaire (GEO), ou une mission depuis une GEO vers une orbite autour de la lune, autour de Mars, etc. Il y a une multitude de configurations possibles, et c'est un vrai défi scientifique de pouvoir calculer de tels transferts.

Si l'on considère l'influence de N corps sur le satellite, le problème posé en ces termes est bien trop ardu pour être résolu. C'est pourquoi les trajectoires de satellites sont toujours construites par des assemblages d'approximations locales.

Remark 0.1 :



Chorégraphie pour sept corps sur une fleur.

Il existe de très beaux travaux traitant de l'obtention de solutions périodiques dans le problème des N -corps. Montgomery et Chenciner [27] ont déterminé des solutions périodiques pour lesquelles les masses des N corps sont toutes égales et également réparties le long de l'orbite. Ces solutions sont appelées des *chorégraphies* des N corps. Beaucoup d'efforts ont été fournis aussi bien pour prouver l'existence de telles trajectoires que pour les calculer numériquement. Les chorégraphies ont été en particulier découvertes en utilisant des méthodes variationnelles, et plus

récemment des approches topologiques, plus spécifiquement pour établir une classification dans le cas d'orbites planaires.

Les formes produites par de telles solutions ainsi que les animations qui en résultent sont fascinantes, nous renvoyons à [79, 77] pour des tracés et des animations.

Approximation locales par orbites coniques

On considère donc le mouvement d'un satellite dans un champ gravitationnel produit par les N corps. Les lois de la gravité de Newton nous donnent alors

$$\ddot{q}(t) = \sum_{i=1}^N \mu_i \left(\frac{q(t) - q_i(t)}{\|q(t) - q_i(t)\|^3} \right) + \frac{T(t)}{m(t)},$$

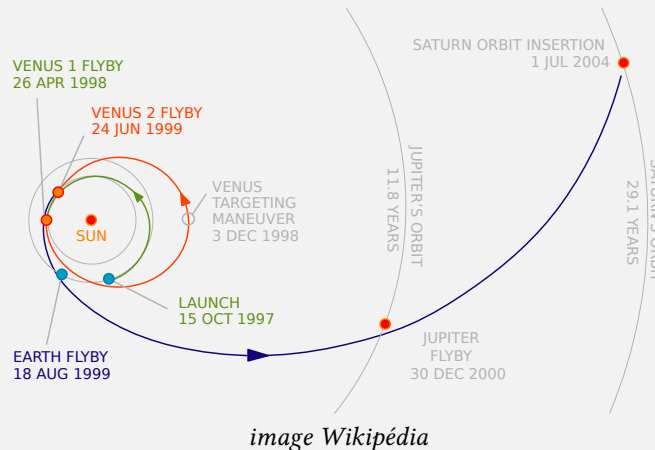
où q est la position du satellite, q_i est la position du i -ème corps, $\mu_i = Gm_i$, G est la constant gravitationnelle, m_i la masse du i -ème corps, T est la poussée du moteur, et m est la masse du satellite.

Comme nous l'avons déjà dit, pour pouvoir espérer résoudre notre problème initial, on cherche à déterminer des approximations locales. Pendant des dizaines d'années les trajectoires étaient décomposées en ne considérant l'attraction que d'un seul astre à la fois. Même pour les trajectoires interplanétaires, et pas uniquement pour des transferts autour d'un unique astre, cette approximation est suffisante pour de nombreux calculs. De spectaculaires missions de la NASA telles que la mission Voyager ou Galileo sont basées sur cette approximation képlérienne, ou approximation locale par orbites coniques. Très récemment, le projet Rosetta conduit par l'ESA a aussi été calculée avec cette méthode pour un trajet de plus de 10 ans ! Pour des références sur le sujet, on peut consulter, par exemple, [8, 9].

Remark 0.2 : Assistance gravitationnelle, Swing-by or Fly-by

L'assistance gravitationnelle ou appui gravitationnel, dans le domaine de la mécanique spatiale, est l'utilisation volontaire de l'attraction d'un corps céleste (planète, Lune) pour modifier en direction et en vitesse la trajectoire d'un engin spatial (sonde spatiale, satellite artificiel...). L'objectif est d'utiliser ce phénomène pour économiser le carburant qui aurait dû être consommé par le moteur-fusée du véhicule pour obtenir le même résultat. (wikipédia)

Ce procédé peut permettre d'augmenter ou de diminuer la vitesse du véhicule ou de changer sa direction. La figure ci-dessous, pour la mission CASSINI-HUYGENS, illustre cette méthode.



Pour choisir à partir de quand nous considérons l'influence d'un corps donné sur le satellite, le concept de *sphère d'influence* a été introduit. Cette sphère consiste en la région entourant un corps céleste et dans laquelle l'influence gravitationnelle est primordiale pour

tout objet en orbite. La méthode consiste à choisir des parties d'orbites hyperboliques héliocentriques de telle façon que le véhicule entre au bon moment dans la sphère d'influence d'un autre astre (disons la terre) de façon à ajuster la vitesse comme on le désire, et ainsi de suite. L'orbite finale, qui est un ensemble d'orbites képlériennes mises bout à bout, peut être alors utilisée pour initialiser une intégration dans le problème complet en considérant les N corps.

Poussée forte ou impulsion

Il existe différentes modélisations pour le contrôle du satellite qui dépend de la technologie utilisée. Pour les impulsions ou poussées fortes, on considère que l'on est capable de changer instantanément la vitesse du véhicule. Les impulsions sont couramment notées ΔV , et appelées Delta-V. Ces impulsions sont produites par des moteurs à réaction et sont proportionnelles à la poussée par unité de masse et au temps de poussée.

Le Delta-V est donné par l'équation de Tsiolkovsky

$$\Delta V = v_e \ln \frac{m_0}{m_f}$$

où

- m_0 est la masse totale de l'astronef au début de la phase propulsée,
- m_f est la masse totale de l'astronef à l'issue de la phase propulsée.
- v_e est la vitesse d'éjection des gaz,
- ΔV est la variation de vitesse entre le début et la fin de la phase propulsée considérée,
- et \ln est la fonction logarithme népérien.

De nombreuses méthodes ont été développées pour optimiser à la fois les impulsions et les fly-bys afin d'établir des missions à faible consommation, les fly-bys étant utilisés pour économiser des impulsions. On peut citer le travail [67] pour une publication récente sur le sujet.

Le véhicule Rosetta, lancé en mars 2004, a subi quatre assistances gravitationnelles permettant ainsi d'atteindre la vitesse et la position de la comète *67P/Churyumov–Gerasimenko* en août 2014. Rosetta a été la première mission de *rendez-vous* avec une comète.

Approximation plus fine

Pour des missions comme Rosetta, Voyager ou Galileo, la vitesse relative du satellite par rapport aux corps considérés est suffisamment élevée pour que l'approximation considérant que les orbites képlériennes ne sont que peu perturbées par les autres corps au sein de la sphère d'influence. Cependant, dès qu'on considère des vitesses faibles, et des poussées faibles, une approximation plus fine est nécessaire.

Le terme de capture balistique (ou phase balistique) est souvent utilisé (*ballistic capture* en anglais).

Definition 1 : *La capture balistique (ou phase balistique) signifie qu'aucun contrôle n'est nécessaire pour réaliser le transfert, ou une partie du transfert, souhaité. En général, les phases balistiques sont temporaires et sont en alternance avec des phases contrôlées. Dans ce travail de thèse, des phases balistiques sont utilisées pour initialiser la résolution d'un problème de contrôle optimal (cf. le chapitre 3).* \diamond

Poussée faible

Comme on l'a déjà mentionné, lors de l'utilisation de moteurs à poussée faible, l'approximation locale par orbites képlériennes n'est plus suffisamment précise. C'est le cas pour ce

travail de thèse où on considère des moteurs ioniques, c'est à dire à propulsion électrique. Pour ces moteurs, la poussée est créée par l'accélération électrique d'ions, ils ont ainsi un rendement plus élevé que les moteurs *chimiques*, et donc permettent d'augmenter soit la charge utile, soit la durée de vie du véhicule.

Ce type de moteur est caractérisé par deux paramètres principaux :

- L'impulsion spécifique (I_{sp}) mesure l'efficacité de moteurs à réaction et des moteurs-fusées et est définie comme l'impulsion totale (ou changement de moment) délivrée par unité de propergol¹ consommé, son unité est alors la seconde.
- Le champ de pesanteur (g_0) est le champ attractif qui s'exerce sur tout corps doté d'une masse au voisinage de la Terre et qui s'exprime en m/s^2 .

Grâce à ces deux paramètres, on définit l'inverse de la vitesse d'éjection de la masse propulsive $\beta = \frac{1}{I_{sp}g_0}$ dont l'unité est s/m. Dans la suite de cette thèse, les valeurs de ces paramètres sont les suivants :

$$I_{sp} = 2000 \text{ s}, \quad \text{and} \quad g_0 = 9.81 \text{ m/s}^2.$$

Le principal inconvénient des moteurs ioniques est la poussée maximale autorisée qui notée T_{max} . En effet, celle-ci est très faible et nous considérons ici qu'elle varie entre 10 et 0.1 Newtons. Pour plus de détails sur les différentes propulsions possibles, nous renvoyons à [82].

L'approximation des trois corps

Lorsque l'on considère un moteur à poussée faible et des trajectoires à faibles énergies, une bien meilleure approximation du problème avec N corps est celle dite des trois corps. En suivant les travaux de Belbruno et Miller [10], on peut imaginer mettre, bout à bout, des solutions locales dans le problème des trois corps reproduisant ainsi ce qui est fait pour les approximations képlériennes. Cette idée est développée en profondeur dans [52]. Par exemple, si on considère un satellite, la lune, la Terre et le soleil, alors localement on va ne prendre en compte que l'influence de la Terre et de la lune (lorsqu'on est proche de ces deux corps), puis ailleurs l'influence du soleil et de la Terre. Cependant pour pouvoir mettre bout à bout les trajectoires issues des approximations des trois corps à la manière des approximations képlériennes, il est nécessaire d'avoir une connaissance précise des trajectoires dans le problème restreint des trois corps.

Dans ce travail de thèse, nous considérons le problème circulaire restreint de trois corps (CRTBP pour l'acronyme anglophone). Cette approximation est discutée en détails dans le chapitre 1. L'étude de ce problème date des travaux de Poincaré [69] à la fin du 19^e siècle dans lesquels il a développé la théorie moderne de l'étude des systèmes dynamiques ainsi que la notion de chaos.

L'approximation CRTBP consiste donc à considérer deux corps massifs appelés *primaires* (par exemple la Terre et la lune), se déplaçant en cercle autour de leur centre de masse, et un troisième corps, le satellite, de masse négligeable se déplaçant dans le champ gravitationnel ainsi créé. On se place alors dans un repère tournant dans lequel les deux primaires sont fixes le long de l'axe x . On donne ici les points clés d'une telle approximation, plus de détails seront donnés dans le chapitre 1. Bien que le mouvement des deux primaires soit planaire, on considère le cas 3D où le mouvement du satellite peut aussi être selon l'axe z .

Avec un peu de mécanique élémentaire, les équations de la dynamique du satellite soumis à ce champs gravitationnel sont facilement obtenues. En normalisant le système par rapport à la distance entre les deux primaires, par rapport au temps de révolution de celle-ci, et par rapport aux masses considérées, le système dynamique s'écrit d'une façon simple

1. Un propergol est un produit de propulsion, constitué d'un mélange de comburant et de combustible, les ergols. La réaction chimique, entre cet oxydant et ce réducteur, fournira l'énergie au moteur-fusée.

et élégante. On introduit ainsi le paramètre de masse

$$\mu = \frac{m_2}{m_1 + m_2},$$

où m_1 et m_2 sont les masses respectives de la plus grande et de la plus petite primaire. Les positions des deux primaires sont alors $(-\mu, 0, 0)$ et $(1-\mu, 0, 0)$, et on note (x, y, z) la position du satellite.

On peut montrer qu'il s'agit d'un système hamiltonien, associé à un lagrangien qui peut s'écrire :

$$\mathcal{L}(x, y, z, \dot{x}, \dot{y}, \dot{z}) = K(x, y, z, \dot{x}, \dot{y}, \dot{z}) - U(x, y, z),$$

où K est l'énergie cinétique

$$K(x, y, z, \dot{x}, \dot{y}, \dot{z}) = \frac{1}{2} [(\dot{x} - \dot{y})^2 + (\dot{y} + \dot{x})^2 + \dot{z}^2],$$

et U est l'énergie potentielle

$$U(x, y, z) = -\frac{1-\mu}{r_1} - \frac{\mu}{r_2},$$

avec r_1 la distance entre le satellite et la première primaire ($r_1 = \sqrt{(x+\mu)^2 + y^2 + z^2}$) et r_2 la distance entre le satellite et la seconde primaire ($r_2 = \sqrt{(x-1+\mu)^2 + y^2 + z^2}$).

On peut alors montrer, en utilisant les outils de l'étude des systèmes dynamiques comme la transformation de LEGENDRE (voir [62, 55]), que l'énergie de notre particule est

$$\mathcal{E} = \frac{1}{2} (\dot{x}^2 + \dot{y}^2 + \dot{z}^2) + \bar{U}(x, y, z),$$

où on a introduit le *potentiel effectif*

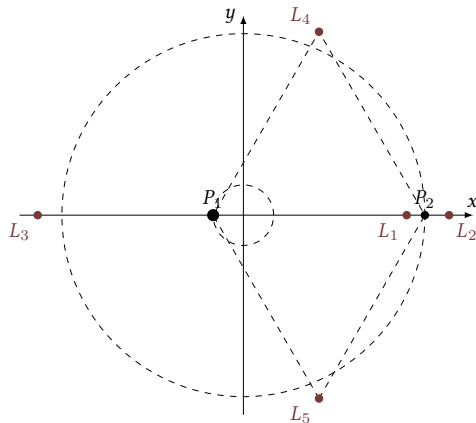
$$\bar{U}(x, y, z) = U(x, y, z) - \frac{x^2 + y^2}{2}.$$

Le système dynamique s'écrit alors

$$\begin{cases} \ddot{x} - 2\dot{y} = \frac{\partial \bar{U}}{\partial x}, \\ \ddot{y} + 2\dot{x} = \frac{\partial \bar{U}}{\partial y}, \\ \ddot{z} = \frac{\partial \bar{U}}{\partial z}. \end{cases}$$

Équilibres

Les équilibres sont des zéros du système dynamique. Ceci est équivalent à trouver des points critiques du potentiel effectif préalablement défini. Nous présentons en détails cette analyse à la section 1.2. Le résultat est qu'il existe cinq points d'équilibre appelés points de LAGRANGE. En effet, les premières études de ces équilibres ont été faites par LAGRANGE suivies par des travaux d'EULER autour de 1750 et 1760. Nous renvoyons à [54] et [34] pour les travaux originaux. Il y a donc trois points *colinéaires* et notés L_1 , L_2 et L_3 , et deux points *équilatéraux* notés L_4 et L_5 . Ces points sont aussi appelés points de *libration*.



Position des points de LAGRANGE.

La connaissance de la stabilité de ces points d'équilibre est crucial pour qui veut construire des missions spatiales. En effet, nous allons voir dans le chapitre suivant que pour certaines configurations du problème restreint des trois corps (par exemple, pour le système {Soleil-Jupiter}), les points équilatéraux sont inutilisables pour la construction de missions car étant stables, un grand nombre de débris se trouve tout autour de ces points et empêche ainsi d'imaginer faire transiter un satellite à cause du trop fort risque de collisions. Les points d'équilibre colinéaires eux sont instables pour tous les systèmes considérés ce qui les rend finalement beaucoup plus intéressants.

Nous allons aussi voir que les points d'équilibre du système restreint des trois corps présentent d'autres propriétés très intéressantes. En effet, l'étude du système linéarisé autour des points L_1 et L_2 montre qu'il s'agit de points d'équilibre de type *center-saddle*. Ainsi, le théorème bien connu de LYAPUNOV-POINCARÉ nous assure l'existence d'une famille d'orbites périodiques autour de ces points d'équilibre. Les orbites périodiques planaires sont alors appelées *orbites de LYAPUNOV* alors que dans le cas 3D, elles sont appelées en fonction de leurs propriétés topologiques, soit *orbites de HALO* soit *orbites de LISSAJOUS*. On peut noter que ce type d'orbites périodiques autour des points de LAGRANGE a déjà été utilisé dans la construction de missions réelles telle que la mission SOHO (voir [75]).

Des courants gravitationnels

Pour notre travail, l'existence de variétés invariantes associées à ces orbites périodiques autour des points de LAGRANGE est une propriété des plus intéressantes dans notre contexte.

Definition 2 (Variétés invariantes) : Une variété invariante stable (resp. instable) d'une orbite périodique est l'ensemble des points de l'espace des phases dont la demi-orbite future (resp. passée) converge vers l'orbite périodique. \diamond

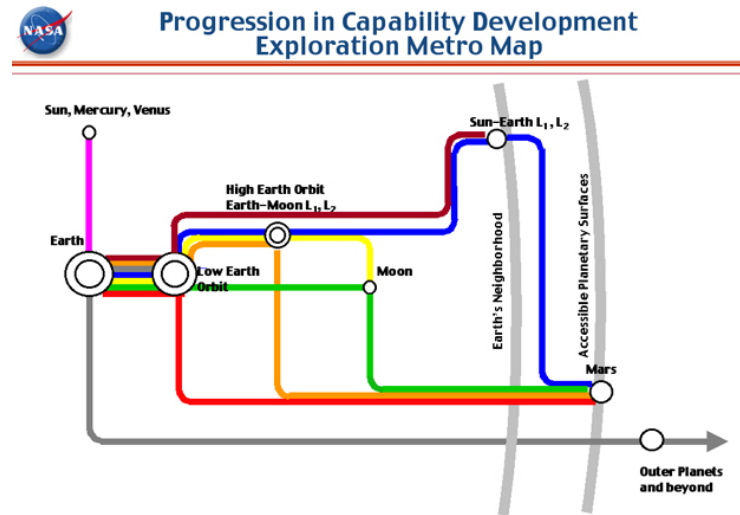
Notons que dans la littérature dédiée, ces variétés invariantes sont appelées *tubes de CONLEY-McGEE*. Nous allons voir que ces variétés invariantes sont des séparatrices de la dynamique, c'est-à-dire qu'elles séparent l'espace des phases, et donc qu'elles peuvent être considérées comme des courants gravitationnels dans le problème restreint des trois corps. Dans les travaux de CONLEY et McGEHEE, et leurs extensions dans [52], le réseau d'orbites homoclines² ou hétéroclines³, obtenues par l'étude des variétés invariantes, reliant les orbites périodiques est étudié précisément.

En s'inspirant des méthodes utilisées pour l'approximation par orbites coniques, on peut connecter des problèmes restreints des trois corps grâce aux variétés invariantes. L'obtention de ces variétés invariantes permet d'établir une carte des connexions entre différentes régions du système solaire par exemple. La connexion entre les variétés invariantes se fait généralement en cherchant une intersection en espace (et non en vitesse), puis en réalisant

2. Une orbite homocline est une trajectoire qui relie un point d'équilibre de type selle, à lui-même, ici une orbite périodique.

3. Une orbite hétérocline est une trajectoire reliant deux différents points d'équilibre, ici des orbites périodiques.

le transfert avec une impulsion ΔV . Ce principe est l'outil principal pour construire le réseau de transport interplanétaire de la NASA (Interplanetary Transport Network (ITN)) qui est une collection d'ensembles de trajectoires naturelles (ou ne nécessitant que peu de contrôle pour être suivies par un satellite) à travers le système solaire (voir la figure 1).



11

FIGURE 1 – Schéma reprenant la carte de métro montrant différentes connexions entre différentes régions du système solaire à faible énergie. *Source : NASA, Gary L. Martin, Space Architect.*

Depuis la fin des années 70, de nombreux travaux ont été consacrés à l'étude des orbites périodiques autour des points de LAGRANGE. En effet, plusieurs missions telles que ISEE-3 (NASA) en 1978, SOHO (ESA-NASA) en 1996, GENESIS (NASA) en 2001, PLANK (ESA) en 2007 etc. ont mis en pratique l'utilisation des propriétés que l'on vient de décrire. De plus, une meilleure compréhension des possibilités de missions interplanétaires a été possible grâce à l'analyse théorique, ainsi que les avancées dans les méthodes numériques pour les divers aspects du *design* de missions autour des points de LAGRANGE.

Il existe un grand nombre de références concernant le problème du calcul de trajectoire à faible coût utilisant les propriétés des points de LAGRANGE. Par exemple, les auteurs des travaux [53, 40, 90] ont développé des méthodes très efficaces pour calculer des trajectoires *gratuites* entre des orbites autour de points de libration. Les méthodes issues de la théorie des systèmes dynamiques y sont utilisées pour construire des orbites hétéroclines ou homoclines à partir de la connaissance des variétés invariantes entre les points de librations. Ceci permet d'obtenir des trajectoires connectant sans contrôle deux orbites périodiques asymptotiquement et donc en temps infini. Ces orbites ont été utilisées pour construire des missions en temps fini en utilisant des impulsions pour joindre l'hétérocline ou en sortir.

Avec les moteurs à poussée faible

Les impulsions nécessaires pour les transferts entre variétés invariantes ou pour atteindre une orbite homocline ou hétérocline ne sont plus possibles lorsque l'on considère des moteurs à poussée faible. Un des problèmes auquel nous nous sommes intéressés est le transfert entre variétés invariantes à poussée faible. C'est un problème à part entière et nous avons développé une méthode numérique s'appuyant sur un transfert impulsif.

pour construire un problème de contrôle optimal. Sa résolution nous permet alors de réaliser le transfert entre variétés invariantes, et ainsi connecter en poussée faible les cartes du type ITN. Ceci est le sujet du chapitre 2.

De plus, les trajectoires naturelles (non contrôlées) appartenant aux variétés invariantes peuvent servir à initialiser la résolution d'un problème de contrôle optimal utilisant ainsi une connaissance *a priori* que la dynamique naturelle nous donne. Il s'agit en fait d'un sujet général, à savoir, comment améliorer la convergence des méthodes indirectes pour les problèmes de contrôle optimal. En effet, les méthodes indirectes telles que les méthodes de tir utilisées grâce au Principe du Maximum de Pontryagin (voir la prochaine section), ont besoin d'une initialisation suffisamment proche de la solution recherchée pour espérer la convergence. Le sujet du chapitre 3 est de construire des missions en utilisant la dynamique naturelle pour initialiser la résolution par méthode indirecte.

Théorie du contrôle optimal

Du fait de la modélisation du moteur et de sa poussée dans notre problème, il est naturel d'utiliser la théorie du contrôle optimal et les méthodes numériques associées et basées sur *le Principe du Maximum de Pontryagin (PMP)*. En effet, d'un point de vue physique, la quantité que l'on souhaite optimiser est la masse du satellite car plus le satellite est lourd, plus il est cher à envoyer. Durant le transfert, l'évolution de la masse est modélisée par

$$\dot{m}(t) = -\beta \|T(t)\| ,$$

où $T(\cdot) \in \mathbf{R}^3$ est le contrôle du satellite qui agit sur l'accélération de celui-ci à travers la dynamique suivante

$$\begin{cases} \ddot{x} - 2\dot{y} = \frac{\partial \bar{U}}{\partial x} + \frac{T_1(t)}{m(t)}, \\ \ddot{y} + 2\dot{x} = \frac{\partial \bar{U}}{\partial y} + \frac{T_2(t)}{m(t)}, \\ \ddot{z} = \frac{\partial \bar{U}}{\partial z} + \frac{T_3(t)}{m(t)}, \\ \dot{m}(t) = -\beta \|T(t)\| . \end{cases}$$

Le coût que l'on cherche alors à minimiser est la norme L^1 du contrôle

$$\int_0^{t_f} \|T\| dt,$$

où t_f est le temps de transfert que l'on considère fixé, la poussée étant bornée par la poussée maximale du moteur notée T_{\max}

$$\forall t, \|T(t)\| \leq T_{\max}.$$

Cette formulation du problème colle parfaitement avec la théorie du contrôle optimal et nous pouvons alors appliquer les résultats connus et les méthodes numériques associées pour le résoudre. Dans ce travail de thèse nous avons développé des algorithmes et des méthodes pour calculer à la fois des transferts optimaux entre variétés invariantes mais aussi pour calculer des missions complètes, le principal avantage de nos méthodes résidant dans la rapidité de résolution.

Rappelons que le PMP nous fournit des conditions nécessaires d'optimalité. Pour cela, un état adjoint est introduit, ainsi qu'un hamiltonien qui nous permet d'établir la dynamique de l'état, de l'état adjoint, et de nous fournir le contrôle optimal comme fonction de l'état

et de l'état adjoint. On peut alors reformuler notre problème comme la recherche d'un zéro d'une certaine fonction dite *fonction de tir*, l'inconnue étant, dans la plupart des cas traités, l'état adjoint initial. Évidemment, la formulation de la fonction de tir dépend du problème considéré, du coût, des conditions terminales. Les principaux avantages des méthodes indirectes sont la rapidité et la précision, cependant elles sont très sensibles à l'initialisation. Pour rendre plus robustes ces méthodes, nous utilisons des méthodes de continuation qui consistent à déformer continûment notre problème initial avec un paramètre réel dans le but d'obtenir un problème plus simple à résoudre. Ensuite, en commençant par résoudre le problème plus simple et en discrétisant par exemple le paramètre réel, de proche en proche, nous nous servons de la solution du problème précédent pour initialiser la résolution du problème suivant. La dernière résolution étant alors le problème objectif initial.

En particulier, dans le contexte de mission de satellite, il est commun d'utiliser la minimisation de la norme L^2 du contrôle comme problème plus simple à résoudre comparé à la minimisation de la norme L^1 . Le coût à minimiser est alors

$$\int_0^{t_f} \|T\|^2 dt.$$

Ce problème est plus simple pour la bonne raison que le contrôle optimal est, dans cas, continu (contrairement à la minimisation L^1), et donc numériquement plus facile à résoudre.

Pour des références sur les techniques que nous utilisons dans cette thèse telles que les continuations, les techniques de régularisation du problème, les techniques et algorithmes d'optimisation, nous renvoyons à [44, 49, 12, 84, 13, 3, 13, 31], bien que la liste soit loin d'être exhaustive. Dans le chapitre 2 nous faisons un bref rappel de la théorie du contrôle optimal ainsi que des méthodes numériques associées.

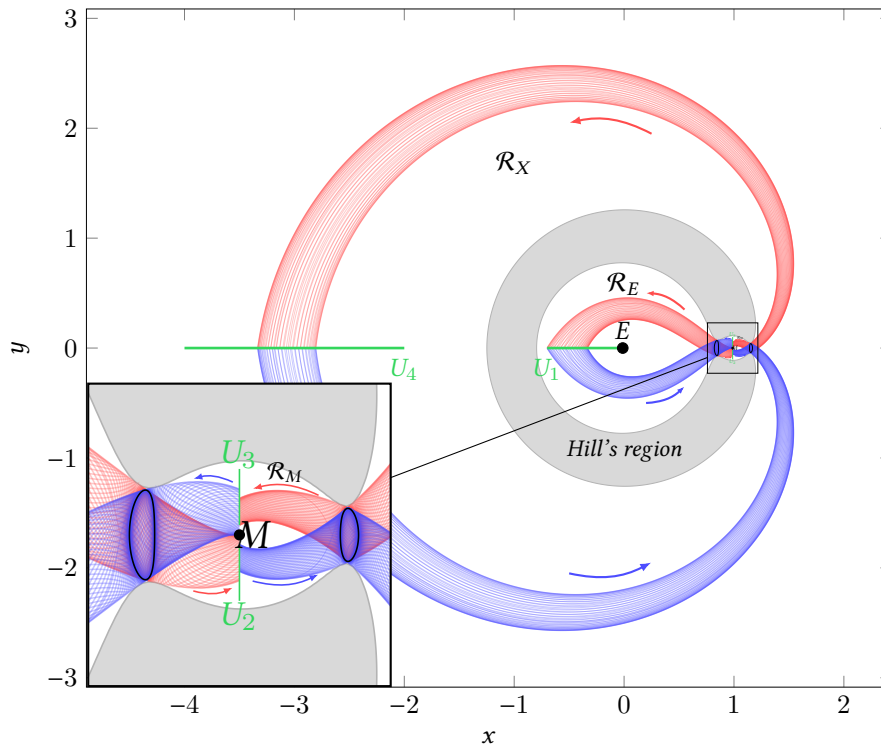


FIGURE 2 – Illustration du système {Terre-Lune} : région de Hill, orbites périodiques autour des points de LAGRANGE, et variétés invariantes.

État de l'art

Tout d'abord, il est à noter que le premier travail combinant l'utilisation de variétés invariantes et de poussée faible est [63].

Les variétés invariantes ont déjà été utilisées dans des travaux tels que [64, 65]. Des ensembles atteignables y sont définis en introduisant la poussée faible (avec un contrôle tangent à la trajectoire), et ces ensembles sont couplés aux variétés invariantes pour définir des solutions admissibles. Ensuite, ces solutions sont optimisées en utilisant un formalisme du contrôle optimal.

Beaucoup d'efforts ont été dédiés à l'élaboration de méthodes efficaces pour atteindre des orbites périodiques autour des points de LAGRANGE (comme des orbites de Halo). Par exemple, dans les travaux [78, 68], les auteurs utilisent des méthodes indirectes et des méthodes directes de tir multiple pour atteindre un point d'insertion sur une variété invariante et ainsi atteindre asymptotiquement l'orbite périodique considérée dans le système {Terre-Lune}. De plus, en utilisant des conditions de transversalité du PMP (voir le chapitre 2), la position du point d'insertion sur la variété invariante est optimisée. Le travail [80] traite aussi du transfert à poussée faible utilisant les variétés invariantes stables vers des orbites de Halo et des méthodes numériques similaires.

Dans des travaux comme [63], des méthodes directes (que nous présentons dans le chapitre 2) sont utilisées pour atteindre une variété invariante stable d'une orbite de Halo à partir d'une orbite GTO. De plus, un transfert d'une orbite de Halo vers une orbite autour de la lune est aussi calculée. Dans ce travail, la norme L^2 du contrôle est minimisée par une discrétisation directe du problème et de la programmation non-linéaire. Dans la continuité de ce travail, dans [61], la position d'insertion sur la variété invariante est optimisée.

Dans les très intéressants travaux [31, 23], des méthodes indirectes couplées avec des méthodes de continuation sont utilisées pour calculer des missions depuis une orbite autour de la Terre (GTO), vers une orbite autour de la lune. Dans un premier temps, le problème de temps minimal est étudié, puis les problèmes de minimisation de la norme L^1 et L^2 du contrôle. Plusieurs continuations sont alors utilisées, une continuation sur la dynamique, introduisant ainsi la perturbation de la lune, une continuation sur la poussée et une continuation sur le coût comme il est usuel de faire. De plus, des résultats de contrôlabilité y sont démontrés.

Les méthodes développées dans [91] consistent aussi à considérer les trois problèmes que sont le temps minimum de transfert, la minimisation de l'énergie (norme L^2) et la minimisation de la consommation (norme L^1). Des continuations sur la poussée, ainsi que des méthodes de Newton et des méthodes indirectes sont aussi utilisées. Notons que dans les deux dernières contributions, la connaissance *a priori* de la dynamique naturelle par les variétés invariantes n'est pas utilisée, cependant, dans notre travail de thèse, ce sont les mêmes techniques numériques qui sont utilisées.

Pour finir, dans l'article [32], l'auteur a développé récemment une méthode très efficace pour calculer un transfert optimal à poussée faible en temps fini entre deux orbites périodiques autour des points L_1 et L_2 . La méthode consiste en trois étapes (que nous ne décrivons pas ici), et utilise des méthodes indirectes ainsi que des continuations en commençant par établir une trajectoire admissible avec une structure imposée au contrôle. Les résultats obtenus sont très bons, et là aussi, les variétés invariantes ne sont pas utilisées.

Comme nous l'avons déjà évoqué, la philosophie des méthodes que nous avons développées dans ce travail de thèse est d'utiliser la connaissance *a priori* de la dynamique avec les variétés invariantes, qui nous fournissent des trajectoires gratuites, pour initialiser la résolution plus « globale ». La contrainte de rester sur les variétés invariantes est alors libérée.

Organisation du manuscrit

Dans le premier chapitre nous établissons le paradigme dynamique dans lequel nous nous plaçons, à savoir, le problème circulaire restreint des trois corps, et nous rappelons les résultats connus. Nous décrivons le calcul des points d'équilibres, dit points de LAGRANGE, en suivant le travail [83]. Nous introduisons ensuite un outil très utile pour l'analyse de missions, à savoir les régions de Hill. Ces régions nous fournissent des informations sur le mouvement possible d'une particule libre dans le CRTBP. Nous présentons aussi les résultats sur les orbites périodiques autour des points de LAGRANGE et les méthodes numériques pour les calculer, méthodes basées sur des méthodes de tir issues des travaux [74, 6, 50]. On rappelle la méthode de LINDSTEDT-POINCARÉ qui permet d'obtenir des approximations analytiques des orbites périodiques qui sont utilisées pour initialiser la méthode de tir afin d'obtenir numériquement les orbites périodiques. Grâce à l'application du théorème de LYAPUNOV-POINCARÉ, nous obtenons l'existence d'une famille d'orbites périodiques autour des points de LAGRANGE que nous calculons grâce à une méthode de continuation. Une des contributions de cette thèse est d'avoir introduit l'énergie comme paramètre de continuation pour obtenir toute la famille. En effet, si on utilise la continuation sur l'excursion comme dans d'autres travaux, on s'aperçoit que la continuation échoue lorsqu'on atteint une excursion trop petite, alors que pour la même énergie, la continuation sur l'énergie fonctionne parfaitement. La dernière section du chapitre 1 traite des variétés invariantes. On y rappelle les résultats théoriques et les études faites sur ces objets et nous introduisons les méthodes numériques utilisées pour les calculer. On conclut le chapitre en rappelant une propriété fondamentale qui permet d'interpréter les variétés invariantes comme des *courants gravitationnels* : les variétés invariantes sont des séparatrices de la dynamique. Il est à noter qu'une partie de cette thèse a été dédiée à développer un code de calcul pour Airbus Defense and Space qui permet de calculer efficacement les variétés invariantes ainsi que plusieurs sections de POINCARÉ (voir l'annexe B).

Dans le chapitre 2, on présente la méthode qu'on a développée pour calculer le transfert optimal entre variétés invariantes. On rappelle dans un premier temps la méthode utilisée pour construire des missions spatiales en utilisant les variétés invariantes et des moteurs à poussée forte et donc en utilisant des impulsions comme décrit dans [52]. Nous présentons ensuite la modélisation de la dynamique contrôlée en poussée faible. Nous donnons des résultats concernant la contrôlabilité du système comme établi dans [31, 23]. Après un rapide rappel de quelques résultats fondamentaux de la théorie du contrôle optimal ainsi que les principales méthodes numériques utilisées dans ce contexte, en particulier les méthodes de continuation (voir, par exemple, [84, 1, 71, 13, 3, 39]), nous présentons l'algorithme que nous avons développé pour résoudre un problème de contrôle optimal réalisant le transfert entre deux variétés invariantes. Pour cela nous utilisons plusieurs continuations, sur l'état final, sur la poussée maximale autorisée, et sur le coût à minimiser nous permettant de rendre la méthode robuste tout en restant très rapide. On construit le problème de contrôle optimal en s'appuyant sur la solution en poussée forte (avec un ΔV), mais la méthode obtenue est plus générale et peut être appliquée à des cas où il n'existe d'intersection ni en position ni en vitesse entre les deux variétés invariantes considérées. Pour illustrer notre méthode, nous donnons quelques résultats numériques pour deux systèmes, le système {Terre-Lune} et le système {Soleil-Terre}. Enfin, nous présentons une courte analyse numérique sur l'impact du paramètre de temps de transfert que nous devons fixer dans notre méthode, et de la convergence vers le transfert impulsif quand ce paramètre tend vers 0.

Dans le chapitre 3, nous appliquons la méthode que nous avons développée couplée à une méthode de tir multiple pour calculer des missions entre orbites périodiques autour des points de LAGRANGE L_1 et L_2 . Dans un premier temps nous introduisons la mission *test* que nous considérons et nous formulons le problème de contrôle optimal correspondant.

On calcule une orbite hétérocline entre les deux orbites de LYAPUNOV de même énergie que l'on considère. Ensuite, en fixant les points de départ et d'arrivée sur les orbites périodiques, et avec une poussée suffisamment grande (60 N), nous réalisons deux transferts *locaux*, du point de l'orbite périodique autour de L_1 vers un point fixe de la trajectoire hétérocline, puis d'un point fixe de la trajectoire hétérocline vers le point choisi sur l'orbite périodique autour de L_2 . Grâce à cela nous obtenons une trajectoire admissible en trois parties dont une est non contrôlée. Ensuite, en utilisant une méthode de tir multiple, on relâche les contraintes de positions sur les points de raccords initialisés sur l'orbite hétérocline (ainsi nous ne forçons plus la trajectoire complète à passer par la trajectoire hétérocline), et nous réalisons la continuation sur la poussée pour atteindre la poussée maximale de 0.3 N. La dernière étape est alors d'optimiser la position (en espace et vitesse) des points terminaux, c'est-à-dire, les points de départ et d'arrivée sur les orbites périodiques pour satisfaire les conditions d'optimalité de transversalité données par le Principe du Maximum de Pontryagin. Nous présentons une autre mission construite avec une orbite hétérocline à deux révolutions autour de la lune. Pour conclure ce chapitre, nous appliquons la méthode à une mission plus générale dans le cas 3D reliant deux orbites de Halo avec des énergies différentes. Dans ce cas, il n'existe pas de trajectoire hétérocline, et donc nous construisons une trajectoire admissible en 5 parties. Deux d'entre elles sont des trajectoires des variétés invariantes instables et stables des deux orbites périodiques, et les trois autres sont des parties contrôlées : 1/ un transfert depuis la première orbite de Halo vers une trajectoire de sa variété invariante instable, 2/ un transfert entre les deux variétés invariantes, et 3/ un transfert entre la trajectoire de la variété invariante stable vers l'orbite de Halo autour de L_2 . Grâce à cette trajectoire admissible en 5 bouts, nous arrivons à initialiser une méthode de tir multiple qui converge vers une trajectoire optimale réalisant le transfert souhaité (et qui n'est pas contrainte à rester sur les variétés invariantes). De plus, comme précédemment, nous optimisons les positions des points de départ et d'arrivée sur les orbites périodiques.

Dans le dernier chapitre de cette thèse, le chapitre 4, nous développons une méthode d'optimisation hybride à deux niveaux utilisant à la fois des méthodes d'optimisation directes et indirectes pour calculer des missions partant de l'orbite géostationnaire (GEO) de faible énergie vers une orbite autour de la lune (LO) ou vers des orbites périodiques autour de L_1 . Encore une fois, nous utilisons les variétés invariantes pour initialiser la méthode en construisant une trajectoire admissible. En effet, on choisit une trajectoire connectant les deux régions de la Terre et de la lune à l'intérieur d'une variété invariante (ou une trajectoire sur une variété invariante stable pour les transferts vers les orbites périodiques autour de L_1). On calcule alors deux transferts *locaux* de l'orbite GEO vers la trajectoire libre de transit, puis de la trajectoire libre vers l'orbite objectif (LO ou une orbite périodique autour de L_1). Cette trajectoire admissible, calculée en seulement quelques minutes, est sous optimale. En effet, aux points de connexion sur la trajectoire libre, l'état adjoint est discontinu car nul sur la partie non contrôlée. La méthode de tir multiple utilisée dans le chapitre 3 échoue en raison des écarts trop importants d'énergie entre les différentes parties et des temps d'intégration trop longs. Pour dépasser cette difficulté, nous optimisons la position (en espace et vitesse) des points de raccords de la trajectoire admissible sans les contraindre à appartenir à la trajectoire non contrôlée. Un résultat bien connu en contrôle optimal est que la sensibilité de la fonction valeur (le coût pour une trajectoire optimale) par rapport aux variations sur l'état initial et final est donnée par les valeurs de l'état adjoint aux temps initial et final. Ainsi, sans aucun calcul supplémentaire, nous avons le gradient par rapport aux variations des points de raccord de la fonction de coût *globale* (comme somme des trois coûts des trois parties de la trajectoire), et donc l'implémentation d'un algorithme du gradient est facile. Remarquons que si on obtient la condition nécessaire d'optimalité pour l'algorithme du gradient, à savoir, le gradient nul, alors, nous obtenons une trajectoire qui satisfait les conditions d'optimalité du PMP pour le transfert total, en particulier la continuité de l'état

adjoint aux points de raccord. Malheureusement, bien que la méthode permette d'améliorer le coût (minimisation L^2), l'algorithme du gradient ne converge pas en temps raisonnable. De plus, lors des itérations, la norme L^1 du contrôle augmente, et comme il s'agit du coût réellement intéressant d'un point de vue industriel, la trajectoire, partiellement optimisée, obtenue n'est pas intéressante physiquement. On finit le chapitre en donnant des trajectoires admissibles à très faible coût (énergétique ou de consommation) pour atteindre l'orbite LO ou des orbites de LYAPUNOV ou de HALO depuis l'orbite GEO. La méthode pour obtenir des trajectoires admissibles à très faible coût se révèle très rapide et efficace, et prend seulement quelques minutes pour tous nos tests numériques.

On finit par conclure et nous donnons quelques perspectives à ce travail de thèse.

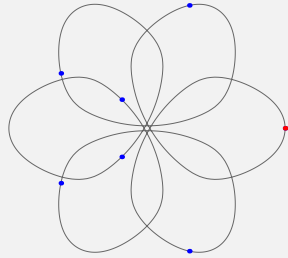
Introduction

This thesis is about the design of trajectories for a spacecraft in the gravitational field of the N bodies of the solar system. With words, we search trajectories and associated controls that perform the wanted travel.

A very standard and obvious assumption is to assume the spacecraft has a small enough mass so that it does not influence the motion of the N massive bodies which move on prescribed orbits under their mutual gravitational attraction. The goal of trajectory design is to find a transfer trajectory which takes the spacecraft from a prescribed initial orbit to a prescribed final orbit using some control applied by the engine. Missions may be between orbits around the Earth: from a Low Earth Orbit (LEO), which is the cheapest orbit to reach from Earth's surface, to a Geostationary Earth Orbit (GEO), or from a GEO to an orbit around the Moon, around Mars, etc. There are many possible configurations, and it is a real challenge to design these trajectories.

Considering the influence of the N bodies on the spacecraft leads to a problem that is far too complex to be treated directly. This is why spacecraft trajectories are always constructed using building blocks which are local approximations.

Remark 0.3:



Choreography seven bodies on a flower.

Note that there exists beautiful work about finding periodic orbits that are solutions of a N -body problem. Montgomery and Chenciner [27] introduced periodic orbits in which all the bodies are equally spread out along a single orbit. They are called N -body choreographies. A lot of effort has been devoted to proving the existence of such periodic orbits and numerically exploring them. Choreographies can be discovered using variational methods, and more recently, topological approaches have been also used to attempt a classification in the planar case.

The shapes and animations of these orbits are fascinating, and we refer to [79, 77] to see plots and animations.

Patched Conic Approximation

We consider the motion of a spacecraft in the gravitational field of N bodies. Newton's law gives us

$$\ddot{q}(t) = \sum_{i=1}^N \mu_i \left(\frac{q(t) - q_i(t)}{\|q(t) - q_i(t)\|^3} \right) + \frac{T(t)}{m(t)},$$

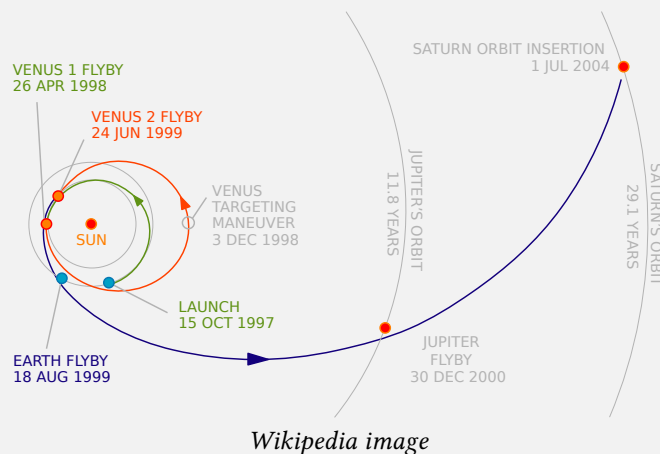
where q is the position of the spacecraft, q_i is the position of the i -th body, $\mu_i = Gm_i$, G is the gravitational constant, m_i is the mass of the i -th body, T is the thrust, and m is the spacecraft mass.

As already stated, we need to use local approximation to build the different parts of the trajectory that we want to design. For decades, people have simplified the general trajectory problem by considering the gravitational force between the spacecraft and only one other body at a time. Even for the case of interplanetary transfer (and not only transfer between orbits around one body), this simplification suffices for many calculations. Note that NASA's spectacular missions such as Voyager and Galileo are based on this Keplerian decomposition of the solar system, known as *the patched conic approximation* (or patched two-body approximation). Very recently, the ESA project Rosetta was built using this simplification for a travel that lasted more than 10 years! For references on the subject, see [8, 9].

Remark 0.4: Gravity Assist Maneuver, Swing-by or Fly-by

In orbital mechanics and aerospace engineering, a gravitational slingshot, gravity assist maneuver, or swing-by is the use of the relative movement (e.g. orbit around the Sun) and gravity of a planet or another astronomical object to alter the path and speed of a spacecraft, typically in order to save propellant, time, and expense. (wikipedia)

This process can increase or decrease the speed of the spacecraft or redirect its path. The figure below, for the Cassini-Huygens mission, illustrates this method.



To choose where to consider the influence of only one body, we need to define its “sphere of influence” which is the radius at which the forces exerted on a particle with negligible mass by the body and the sun are approximately equal. The method consists in choosing the heliocentric hyperbolic trajectory such that the spacecraft enters the sphere of influence at the right moment to increase or decrease the speed, and so on. This patched conic solution could be used as an initial guess for a numerical procedure to integrate a full trajectory in the N -body problem.

High Thrust and Impulse

There are different modelizations of the spacecraft control depending on the technology of the engine. Impulses are instantaneous changes in velocity performed by a high thrust engine. Usually, an impulse is denoted by ΔV , and called Delta-V. Delta-V is produced by reaction engines and it is proportional to the thrust per mass unit and to the burn time.

The Delta-V is given by the Tsiolkovsky rocket equation, or ideal rocket equation

$$\Delta V = v_e \ln \frac{m_0}{m_f}$$

where

- m_0 is the initial total mass of the spacecraft, including propellant.
- m_f is the final total mass without propellant, also known as dry mass.
- v_e is the effective exhaust velocity,
- ΔV is the maximum change of velocity of the vehicle (with no external forces acting),
- and \ln refers to the natural logarithm function.

A lot of effort has been devoted to optimizing the use of both impulses and fly-bys in interplanetary missions. The fly-by is used to save propellant by providing like free impulses (changes of velocity). For instance, a recent publication is [67].

The Rosetta probe, launched in March 2004, used four gravity assist maneuvers to accelerate throughout the inner Solar System - enabling it to match the velocity of the *67P/Churyumov-Gerasimenko* comet at their *rendezvous* point in August 2014. Rosetta is the first spacecraft to match orbit with a comet.

Need for a Better Approximation

For missions like Rosetta, Voyager or Galileo, the speed of the spacecraft relative to the bodies is sufficiently high to allow the assumption of a minor perturbation of the conic solution in the sphere of influence. Unfortunately, when we consider low propulsion, or unpropelled motion where the relative speed is low, a better approximation is necessary.

It is common to use the term ballistic capture.

Definition 3: *Ballistic capture means that no propulsion (or control) is needed to achieve a capture orbit. In general, a ballistic capture is only temporary. In this work, ballistic captures will be used to initialize an optimization problem (see chapter 3).* \diamond

Low Propulsion

The conic approximation is not useful when, instead of impulse control, we use a low thrust engine. We consider here the ion thrusters which are spacecraft engines with electric propulsion. The thrust is created by accelerating ions with electricity. These engines have a better yield than chemical ones, and so, one can extend the payload or the lifetime.

These engines are characterized by two parameters I_{sp} and g_0 . The specific impulse (I_{sp}) is a measure of the efficiency of rockets and jet engines. It is defined by the total impulse (or change of momentum) delivered per unit of propellant⁴ consumed. Its unit is the second. g_0 is the acceleration at the Earth's surface in m/s^2 . The inverse of the average exhaust speed, β , is equal to $\frac{1}{I_{sp}g_0}$. The unit of β is s/m. In this thesis, we use the following values for these parameters

$$I_{sp} = 2000 \text{ s}, \quad \text{and} \quad g_0 = 9.81 \text{ m/s}^2.$$

The main drawback of such engines is that the maximal thrust, denoted by T_{max} , is very low. It could be considered to be between 10 to 0.1 Newtons. For references, see [82].

⁴ A *propellant* or *propellent* is a chemical substance used in the production of energy or pressurized gas that is subsequently used to create movement of a fluid or to generate propulsion of a vehicle, projectile, or other object.

The Three Body Approximation

With low thrust and low energy trajectories, a better local approximation for the N -body problem is the three body model. Indeed, motivated by the work of Belbruno and Miller [10], we can think about patching three body problems to design missions in an N -body problem. This idea is well developed in [52]. For instance, for the Sun, Earth, Moon and spacecraft system, we consider in a certain realm that the principal gravitational attraction is exerted by Earth and the Moon (close to these two bodies) and in a other realm (further away from the Moon orbit), we consider the attraction of the Sun and Earth. To patch three-body solutions as it is done for the conic patching, one needs a very accurate knowledge of the solution in each three-body problem.

In this thesis, we consider the Circular Restricted Three Body Problem (CRTBP) approximation. It is discussed in details in Chapter 1. Note that the study of this problem is by itself an interesting topic. It goes back to the work of Poincaré [69] in the late 1800s. In this context, he developed the modern dynamical systems theory and the notion of chaos.

The CRTBP approximation consists in considering two bodies called *primaries* (e.g., Earth and Moon) moving in circles around their center of mass, and the smaller third body (the spacecraft) moving in the gravitational field of the two others without perturbing it. We place ourselves in a rotating frame so that the two primaries appear to be fixed. We describe in details this problem in Chapter 1, but we give here some notions. Although the motion of the two primaries is planar, we consider the 3D case, where the motion of the spacecraft can be along the z -axis. Note that a better approximation is to consider elliptic trajectories for the two primaries (see [38, 20, 58]).

We consider the system composed by two primaries and a spacecraft. With some elementary mechanics, one can derive the dynamics. The system is written in an elegant way when we normalize it with respect to the distance between the two primaries, their period of revolution, and the masses. We introduce the mass parameter

$$\mu = \frac{m_2}{m_1 + m_2},$$

where m_1 and m_2 are respectively the mass of the bigger and smaller primary. The position of the two primaries are then $(-\mu, 0, 0)$ and $(1 - \mu, 0, 0)$. The position of the third body is denoted by (x, y, z) .

The system is a Hamiltonian system, with an associated Lagrangian that can be written as

$$\mathcal{L}(x, y, z, \dot{x}, \dot{y}, \dot{z}) = K(x, y, z, \dot{x}, \dot{y}, \dot{z}) - U(x, y, z),$$

where K is the kinetic energy

$$K(x, y, z, \dot{x}, \dot{y}, \dot{z}) = \frac{1}{2} [(\dot{x} - \dot{y})^2 + (\dot{y} + \dot{x})^2 + \dot{z}^2],$$

and U is the gravitational potential

$$U(x, y, z) = -\frac{1 - \mu}{r_1} - \frac{\mu}{r_2},$$

with r_1 denoting the distance between the spacecraft and the first body

$$r_1 = \sqrt{(x + \mu)^2 + y^2 + z^2}$$

and r_2 denoting the distance between the second primary to the spacecraft

$$r_2 = \sqrt{(x - 1 + \mu)^2 + y^2 + z^2}.$$

Thanks to that, there exists a conserved energy that can be computed *via* Legendre transformation (see [62, 55])

$$\mathcal{E} = \frac{1}{2} (\dot{x}^2 + \dot{y}^2 + \dot{z}^2) + \bar{U}(x, y, z),$$

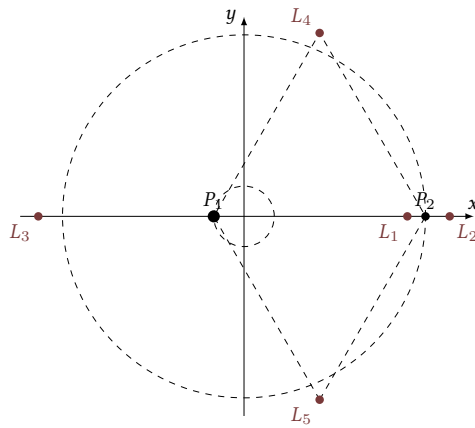
where we have introduced the *effective potential*

$$\bar{U}(x, y, z) = U(x, y, z) - \frac{x^2 + y^2}{2}.$$

The dynamics can then be written as

$$\begin{cases} \ddot{x} - 2\dot{y} = \frac{\partial \bar{U}}{\partial x}, \\ \ddot{y} + 2\dot{x} = \frac{\partial \bar{U}}{\partial y}, \\ \ddot{z} = \frac{\partial \bar{U}}{\partial z}. \end{cases}$$

Equilibria



Localization of Lagrange points.

Equilibria are zeros of the dynamics. This is equivalent to finding the critical points of the effective potential. We discuss this analysis in Section 1.2. The result is that there exist five equilibrium points called Lagrange points. Indeed, one of the first studies of these equilibrium points was done by Lagrange (followed by Euler) around 1750 and 1760, see [54] and [34]. There are three collinear points denoted by L_1 , L_2 and L_3 and two equilibrium equilateral points denoted by L_4 and L_5 . These points are also called *libration points*.

Knowledge of the stability properties of these points is crucial to design spacecraft missions. Indeed, as we will see in the next chapter, one can show that for some three body problems (for instance, the

{Sun-Jupiter} system), the equilateral points are stable. Hence, such points are useless because there is debris all around these points, and a spacecraft, in their vicinity, would be certain to collide with asteroids orbiting around the stable equilibrium points. The other points, the collinear ones, are unstable which is a more interesting property.

The equilibrium points also exhibit other interesting properties. Indeed, a linearized analysis shows the two points L_1 and L_2 closest to the secondary body, are center-saddle points. The well known Lyapunov-Poincaré theorem ensures that there is a family of periodic orbits around these points. These periodic orbits are called *Lyapunov orbits* if they are planar, while their counterparts in 3D are called *Halo* and *Lissajous orbits*. This kind of orbit has already been used to design real life missions such as SOHO (see [75]).

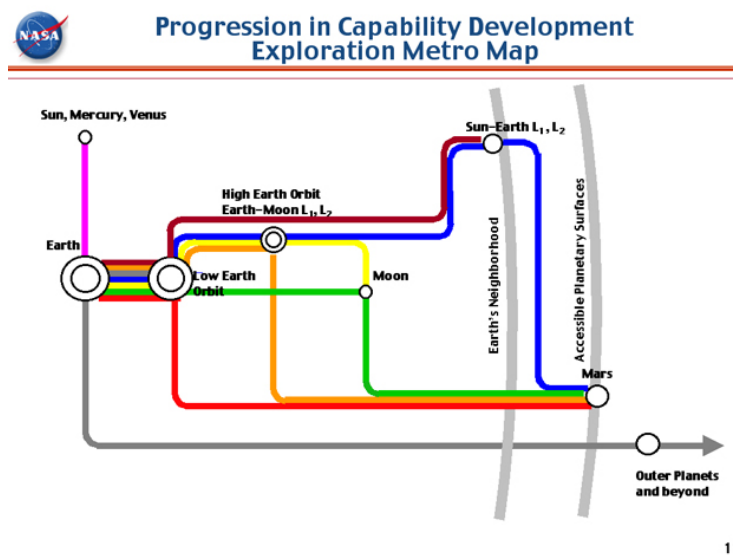
Tubes as Gravitational Currents

The most interesting property for the study performed in this thesis is that there exist invariant manifolds associated with these periodic orbits around Lagrange points.

Definition 4 (Invariant Manifolds): A stable manifold (respectively, unstable) of a periodic orbit is the set of the phase space consisting of all points whose future (respectively, past) semi-orbits converge to it (asymptotic orbits). \diamond

Note that in the dedicated literature, they are called *Conley-McGee tubes*. We will see that these invariant manifolds are separatrices of the dynamics, and so, they can be interpreted as *gravitational currents* in the three body problem. In work by Conley and McGehee, and its extension in [53], the network of homoclinic⁵ and heteroclinic⁶ orbits obtained thanks to the study of the invariant manifolds, connecting these periodic orbits is studied. This gives us very interesting tools to design free trajectories with prescribed itineraries.

Following what was done for the patched conic approximation, we can connect restricted three body problems and, thanks to the invariant manifolds, it is possible to design a map of connections between areas in the solar system. Indeed, intersections in the position variables between invariant manifolds can be computed and with an impulse, ΔV , it is possible to pass from one to another. This principle is the main tool to design the Interplanetary Transport Network (ITN) which is a collection of gravitationally determined pathways through the Solar System that require very little energy for an object to follow.



11

Figure 3 – A metro map showing hubs connected by low energy passageways. *Source: NASA, Gary L. Martin, Space Architect.*

Since the late '70s, the study of Lagrange point orbits has been of great interest. Indeed, several missions such as ISEE-3 (NASA) in 1978, SOHO (ESA-NASA) in 1996, GENESIS (NASA) in 2001, PLANK (ESA) in 2007 etc. have put this knowledge into practice. A more profound understanding of the available mission options has also emerged due to the theoretical, analytical, and numerical advances in many aspects of libration point based mission design.

5. A homoclinic orbit is a flow trajectory of a dynamical system that joins a saddle equilibrium point to itself.

6. A heteroclinic orbit (sometimes called a heteroclinic connection) is a path in the phase space which joins two different equilibrium points.

There exist a huge number of references on the problem of determining low-cost trajectories by using the properties of Lagrange equilibrium points. For instance, the authors in [53, 40, 90] have developed very efficient methods to find “zero cost” trajectories between libration point orbits. Dynamical system methods are used to construct heteroclinic orbits from invariant manifolds between libration point orbits, they allow to obtain infinite time uncontrolled transfers. These orbits have been used with impulse engine spacecrafts to construct finite time transfers.

With Low Thrust

The impulse needed to go from one invariant manifold to another cannot be achieved with a low thrust engine. One of the problems that we have been interested in is how to connect two invariant manifolds from the described map with a low thrust engine. This is a question of its own, and we have developed a generic method to answer. we start with an impulsive transfer to build an optimal control problem that yields a low thrust transfer. This is the subject of chapter 2.

Moreover, the trajectories belonging to the invariant manifolds (or to their inside) can serve as an initialization to solve optimal control problems with the *a priori* knowledge of the dynamics. Note that this is a general research topic: improving the convergence of indirect methods for optimal control problems. Indeed, indirect methods such as shooting methods need an accurate initialization which can be obtained by different means and in particular with the information given by the dynamics. The subject of chapter 3 is precisely to design missions using the natural dynamics as an initialization for an indirect method. These indirect methods can be applied thanks to a formulation of the problem obtained by applying the *Pontryagin Maximum Principle (PMP)* (see below).

Optimal Control Theory

Because of the modelization of the thrust and the problem, in this thesis, we apply the optimal control theory and some associated numerical methods based on the *Pontryagin Maximum Principle (PMP)*. Indeed, physically, the crucial parameter we want to optimize is the mass of the spacecraft because the heavier the satellite, the more expensive the launch. The mass evolution modelization is

$$\dot{m}(t) = -\beta \|T(t)\| ,$$

where $T(\cdot) \in \mathbf{R}^3$ is the control of the spacecraft which modifies the acceleration through the following controlled dynamics

$$\left\{ \begin{array}{l} \ddot{x} - 2\dot{y} = \frac{\partial \bar{U}}{\partial x} + \frac{T_1(t)}{m(t)}, \\ \ddot{y} + 2\dot{x} = \frac{\partial \bar{U}}{\partial y} + \frac{T_2(t)}{m(t)}, \\ \ddot{z} = \frac{\partial \bar{U}}{\partial z} + \frac{T_3(t)}{m(t)}, \\ \dot{m}(t) = -\beta \|T(t)\|. \end{array} \right.$$

The natural cost to minimize is then the L^1 -norm of the control

$$\int_0^{t_f} \|T\| dt,$$

where the time t_f is the fixed transfer time and the thrust is bounded by the maximal thrust T_{\max}

$$\forall t, \|T(t)\| \leq T_{\max}.$$

This formulation of the problem fits the framework of optimal control theory and we can apply available results and numerical techniques to solve our problem. In this thesis, we have developed algorithms and methods to perform transfers between invariant manifolds, and also some complete missions. The main advantage of our techniques is the speed of resolution.

Let us recall that the PMP gives us necessary conditions of optimality. To do that, a costate is introduced, and an associated Hamiltonian that allows to express the state and costate dynamics. Moreover, the optimal control can also be written as a function of the state and the costate. Basically, one can reformulate the problem using a shooting function where, in most cases, the initial costate has to be found to reach the targeted orbit. Note that the formulation of the shooting function depends on the problem, the cost, and the terminal conditions (the set of the initial and final conditions of our problem). Indirect methods are very precise and fast but they are also very sensitive with respect to the initialization. Hence, we use continuation methods which consist in continuously deforming the problem with a real parameter in order to get an easier problem. Then, starting with the resolution of the easiest problem, one can solve the whole family of problems (indexed by a discretization of the parameter) step by step, by using the solution of the previous one to initialize the next one. The final solve is for the difficult targeted problem.

In particular, in the context of spacecraft missions, the minimization of the L^2 -norm of the control is used as an easier problem compared to the L^1 -norm minimization. The cost to minimize is then

$$\int_0^{t_f} \|T\|^2 dt.$$

Indeed, the corresponding optimal control is continuous (this is not the case for the L^1 -minimization), hence, numerically the problem is easier to solve.

For references on techniques used in our work such as continuation on cost, smoothing techniques and, optimization techniques one may read [44, 49, 12, 84, 13, 3, 13, 31] and references therein. In chapter 2, we briefly recall the theory of optimal control and the numerical methods that we use.

State of the Art

First, one can note that [63] is the first work that combines invariant manifolds and low-thrust in the Earth-Moon system.

Invariant manifolds were used in low-thrust missions in [64, 65]. The low-thrust propulsion is introduced by means of special attainable sets that are used in conjunction with invariant manifolds to define a first-guess solution. Then, the solution is optimized using an optimal control formalism.

Much effort has been dedicated to the design of efficient methods to reach periodic orbits around equilibrium points in the three body problem (*e.g.*, Halo orbits). For example, in [78, 68], the authors use indirect methods and direct multiple shooting methods to reach an insertion point on an invariant manifold and then asymptotically reach a Halo orbit in the Earth-Moon system. Moreover, using transversality conditions, the position of the insertion point on the invariant manifold is optimized. Low-thrust stable-manifold transfers to Halo orbits are also shown in [80] using similar numerical methods.

On the same topic, in [63], the authors use direct methods (presented in chapter 2) to reach a point on a stable manifold of a Halo orbit from a GTO orbit. A transfer from the Halo orbit to a Lunar-Orbit is established as well. The L_2 -norm of the control is minimized

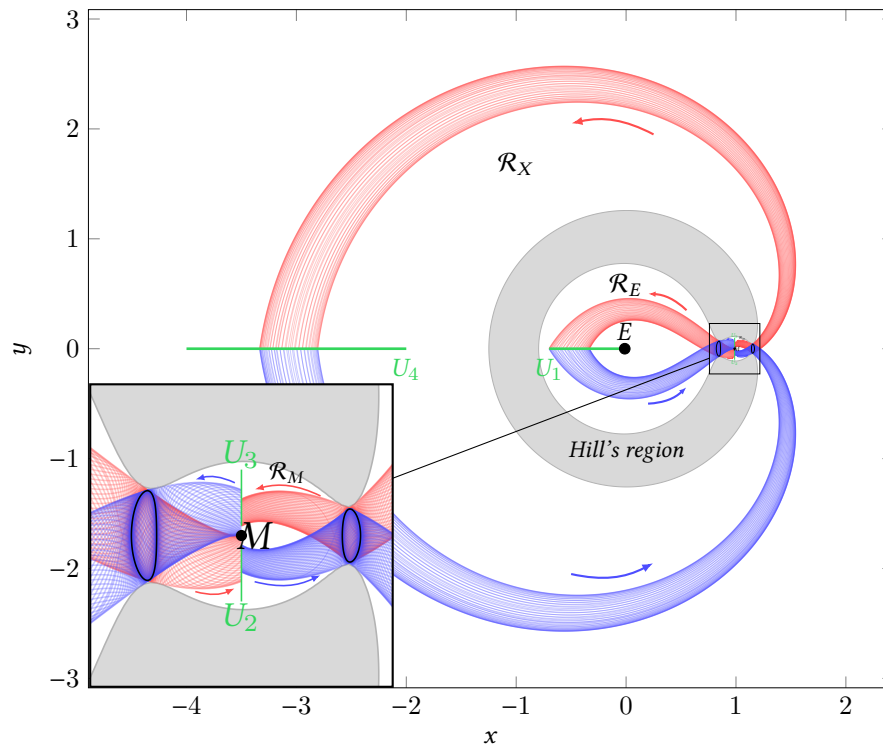


Figure 4 – Illustration of an {Earth-Moon} system: periodic orbits around Lagrange points, and associated invariant manifolds.

by a direct transcription and non linear programming. In [61], the position of the insertion point on the manifold is optimized.

We notice that in the interesting work [31, 23], indirect methods combined with continuation methods were used to design missions from the Earth Geostationary Orbit to a Lunar Orbit. First, the minimum time problem is studied, and then the minimization of the L^1 and L^2 -norms of the control. Continuations are used from the two body problem to the three body problem as well as a continuation on the thrust, and a continuation between energy minimization and fuel consumption minimization. Moreover, the authors prove some controllability results for the CRTBP.

The methods developed in [91] involve the minimum-time problem, the minimum energy problem and the minimum fuel problem to reach a fixed point on a Halo orbit starting from a periodic orbit around Earth. Continuations on the thrust are used, as well as Newton and bisection methods (indirect methods). In these last two contributions, *a priori* information of the natural dynamics with manifolds is not used to help solve the formulated problem. However, in our work, we use similar numerical methods.

In [32], the author recently developed an efficient method to compute an optimal low-thrust transfer trajectory in *finite* time without using invariant manifolds of the three body problem. It is based on a three-step solution method using indirect methods and continuations methods and it gives good results. The first-guess solution is designed by forcing a certain structure for the control.

As already mentioned, the philosophy of the method developed in this work is to use the natural dynamics as invariant manifolds, providing free parts for transfer, and then to initialize a “global” resolution method by freeing the constraints to stay on the manifold.

Organization of the Thesis

The first chapter is devoted to stating the dynamical paradigm and recalling well known results on the circular restricted three body problem. We describe how to compute the equilibrium points following the work in [83]. Then, we introduce a very useful tool to analyze trajectories: the so-called Hill's regions. These regions give us information about the possible motion of a free particle in the CRTBP. We discuss results on periodic orbits and the numerical method to compute them based on shooting method and work in [74, 6, 50]. We recall the Lindstedt-Poincaré method to obtain the analytical approximations of the periodic orbits that are used to initialize the shooting method which computes them. Thanks to the Lyapunov-Poincaré theorem, the existence of a family of periodic orbits is ensured. Therefore, by a continuation method, we are able to compute the whole family of orbits. One of the contributions of this work is to introduce the energy as a continuation parameter to obtain the entire family. Indeed, with the continuation on the excursion parameter used in other work, the continuation fails when the targeted excursion is close to zero whereas, for the same energy, the continuation on energy succeeds. The last section of chapter 1 is about invariant manifolds. We recall theoretical results and the study of these objects and we introduce the numerical methods to compute them. We finish by stating the property that allows to see invariant manifolds as gravitational currents: they are separatrices of the dynamics. Note that as part of this thesis, a code was developed for Airbus Defense and Space that efficiently computes the invariant manifolds and some Poincaré cuts (see appendix B).

In chapter 2, we establish the method to compute an optimal transfer between invariant manifolds. We first recall the method used to design spacecraft missions using invariant manifolds and impulse propulsion as described in [52]. We then introduce precisely the modelization of the controlled dynamics with low thrust. We give some results for the controllability of the system stated in [31, 23]. After a very short introduction of some fundamental results in optimal control theory as well as the associated numerical methods and continuation methods (see, for instance, [84, 1, 71, 13, 3, 39] and references therein), we introduce the algorithm that we have designed to solve an optimal control problem performing the transfer between two invariant manifolds. We use different continuations on the final state, on the thrust and on the cost to improve robustness and to still obtain a solution in a very short computation time. We build an optimal control problem starting with the impulse solution, but our method is more general and can be extended to cases where neither position or velocity intersections exist between the two invariant manifolds considered. To illustrate the method, we give some numerical results for two three body problems: the {Earth-Moon} and {Sun-Earth} system. Finally, we present a short study of the impact of the chosen transfer time and the relation with the impulsive transfer when the transfer time goes to 0.

In chapter 3, we apply the method that we developed and couple it with a multiple shooting method to compute some missions between periodic orbits around Lagrange points L_1 and L_2 . First, we introduce the mission that we consider and state our optimal control problem. We then compute then a heteroclinic orbit between the two Lyapunov periodic orbits sharing a same energy. Then, fixing the departure point near L_1 and the arrival point near L_2 and with a not too small thrust (60 N), we perform two small transfers from the Lyapunov orbit around L_1 to the heteroclinic one, and from the heteroclinic orbit to the Lyapunov orbit around L_2 . This way, we obtain a three-part admissible trajectory with one uncontrolled part. Then, thanks to a multiple shooting method, we release the constraint on the position of the matching points on the heteroclinic orbit and decrease the thrust to the targeted one (0.3 N). The last step is to optimize the departure and arrival points on the periodic orbits to satisfy the necessary transversality conditions given by the Pontryagin

Maximum Principle. Then, we present another mission with a heteroclinic orbit with two revolutions around the Moon. Finally, we apply the method to a more general mission: a Halo to Halo mission for two periodic orbits with different energies. In this case, there is no heteroclinic orbit, so we construct a five-part admissible trajectory. Two of the parts are trajectories on invariant manifolds, and the three others are local transfers: 1/ from one of the Halo orbits to a free trajectory of the unstable manifold, 2/ between both free trajectories and 3/ from the second free trajectory of the stable manifold to the second Halo orbit. Thanks to this five-part admissible trajectory, we are able to initialize a multiple shooting method that computes an optimal trajectory (which is not constrained to reach any invariant manifolds). As previously, we optimize the terminal points on Halo orbits.

In chapter 4, we develop a hybrid bi-level optimization method using both indirect and direct methods to compute a mission from a very low energy geostationary Earth orbit (GEO) to a Lunar Orbit (LO) or to periodic orbits around L_1 . Once again, we use the invariant manifolds to initialize the method building an admissible trajectory. Indeed, we choose a trajectory connecting the realm of the Earth and the realm of the Moon (such a trajectory is inside the stable manifold of the Lyapunov orbit around L_1). We compute two “local” transfers from the GEO to the free trajectory inside the manifold, and one from the free trajectory to the LO. This trajectory, computed in just a few minutes, is a sub-optimal trajectory, or admissible trajectory. Indeed, at the matching points on the free trajectory, the costate vector is discontinuous because it is zero on the uncontrolled part. The multiple shooting method used in Chapter 3 fail in this case because of the long transfer time and the too important energy gap. To overcome this difficulty, we optimize the matching point positions (in space and velocity) without constraining them to belong to a free trajectory. A well known result in optimal control is that the sensitivity of the value function (the cost for an optimal trajectory) with respect to the endpoints is given by the value of the costate at the initial and final times. Hence, without any additional computation, we get the gradient of the “global” cost function (as the sum of the three cost functions on each part) with respect to the variation of the two matching points and so, the implementation of a gradient descent algorithm is easy. We note that if we manage to nullify the gradient of this global cost function, then we obtain the optimal necessary condition given by the PMP for the “global” transfer, in particular, the continuity of the costate at the matching points. Unfortunately, even though this method allows to decrease the cost (L^2 -norm of the control), we do not converge with a gradient descent. Moreover, the L^1 -norm of the control increases (which is the physical cost we want to minimize, the L^2 -norm is just a related cost that is numerically easier to minimize). We finish the chapter with different admissible trajectories to reach the LO orbit, Lyapunov orbit or Halo orbit starting from the GEO orbit. Note that the method to get an admissible trajectory is really fast and only takes a few minutes on all our numerical tests.

We finally conclude and give some perspectives raised by this work.

The Circular Restricted Three-Body Problem (CRTBP)

Contents

1.1	Equations of Motion	29
1.1.1	Frame transition maps	31
1.2	Libration Points (Lagrange Points)	33
1.2.1	Localization of collinear points	34
1.2.2	Richardson Coordinate System for the CRTBP	35
1.2.3	Stability by Linearization	35
1.3	Jacobi Integral and Hill's Region	37
1.3.1	Jacobi Integral	37
1.3.2	Hill's Region	37
1.4	Periodic Orbits	39
1.4.1	Lyapunov-Poincaré Theorem	40
1.4.2	Numerical Method to Compute Periodic Orbits	42
1.4.3	Analytical Initialization	42
1.4.4	Families of Periodic Orbits	47
1.5	Invariant Manifolds	50
1.5.1	Mathematical Definition	50
1.5.2	Linear Approximation	51
1.5.3	Numerical Computation	53
1.5.4	Stability of Manifolds	55
1.5.5	Theoretical Existence of Invariant Manifolds as Separatrices	56

This chapter is inspired by the description in [52]. We consider two bodies revolving around their center of mass on circular orbits under the influence of their mutual gravitational attraction. The purpose is to characterize the motion of a third body with negligible mass, attracted by the two previous bodies without influencing their motions. This is the Circular Restricted Three-Body Problem (CRTBP).

The two massive bodies are called primaries and we denote by M_1 and M_2 their respective masses. Assuming that they may be considered as point masses, we denote by P_1 and P_2

their positions. In some cases, P_1 can be referred to as the primary and P_2 as the secondary. Figure 1.1 illustrates the problem configuration.

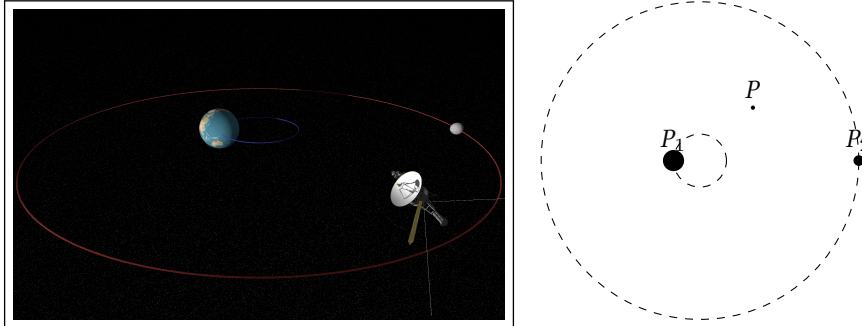


Figure 1.1 – Illustration of the CRTBP, two primaries P_1 and P_2 revolving around their center of mass in circular orbits under their mutual attraction, and the spacecraft P with a negligible mass.

The CRTBP is an approximation of the general three-body problem. In the general problem, each of the three bodies influences the others and there is no assumption on their respective motions. We note that a more realistic approximation is the Elliptic Restricted Three-Body Problem as in [38].

In this thesis, we focus on particular aspects of the three-body problem. We refer to the books by Szebehely [83], Marsden and Ratiu [60], and Meyer, Hall, and Offin [62] for a general introduction and coverage of the literature on the subject.

The reader may think of systems such as {Earth, Moon, spacecraft}, {Sun, Earth, Moon}, {Sun, Jupiter, spacecraft}, etc. Throughout this work, we mostly consider the system {Earth, Moon, spacecraft}. In this chapter, the equations of motion for the CRTBP are introduced in two important coordinate systems: Cross coordinates and Richardson coordinates. The fundamental dynamical properties like *Lagrange points* (equilibrium points of the CRTBP), *Lyapunov orbits* (periodic orbits around Lagrange points), and *invariant manifolds* are introduced, and we use them to construct the mission and to help the resolution of the associated optimal control problem in the next chapters.

Finally, numerical methods to compute periodic orbits around Lagrange points (Lyapunov orbits) and their invariant manifolds are introduced.

Remark 1.1:

All of these properties have been previously used to construct spacecraft missions. For instance, the authors in [53, 40, 90] developed very efficient methods to find “zero cost” trajectories between libration point orbits. They also used dynamical system methods to construct heteroclinic orbits from invariant manifolds between libration point orbits and managed to get infinite time uncontrolled transfers. These orbits, coming from the dynamical study of the CRTBP, have been used with impulse engine spacecrafts to construct finite time transfers.

1.1 Equations of Motion

We consider a spacecraft in the gravitational field of the two primaries. We consider an inertial frame $\mathcal{I} = (\mathbf{E}_x, \mathbf{E}_y, \mathbf{E}_z)$ in which the vector differential equation for the spacecraft motion is written as:

$$m \frac{d^2 \mathbf{R}}{d\tau^2} = -GM_1 m \frac{\mathbf{R}_{13}}{R_{13}^3} - GM_2 m \frac{\mathbf{R}_{23}}{R_{23}^3} \quad (1.1)$$

where M_1 , M_2 and m are the masses respectively of Earth, its moon and the spacecraft, \mathbf{R} is the satellite vector position, \mathbf{R}_{13} is the vector Earth-spacecraft and \mathbf{R}_{23} is the vector Moon-spacecraft, G is the gravitational constant, and τ is the time unit.¹

The system is made adimensional by the following choice of units: the unit of mass is taken to be $M_1 + M_2$; the unit of length is chosen to be the constant distance between P_1 and P_2 ; the unit of time is chosen such that the orbital period of P_1 and P_2 around their center of mass is 2π . The universal constant of gravitation then becomes $G = 1$. Conversion of distances, velocities, and times from the unprimed, normalized unit system to the primed, dimensionalized unit system is

$$\begin{aligned} \text{distance} \quad d' &= l_* d, \\ \text{velocity} \quad s' &= v_* s, \\ \text{time} \quad t' &= \frac{t_*}{2\pi} t, \end{aligned} \quad (1.2)$$

where we denote by l_* the distance between P_1 and P_2 , by v_* the orbital velocity of P_1 and by t_* the orbital period of P_1 and P_2 .

The system then depends on only one parameter, denoted by

$$\mu = \frac{M_2}{M_1 + M_2}, \quad (1.3)$$

and we call it the *mass parameter*, assuming that $M_1 > M_2$.

In table 1.1, we summarize the values of all the constants for some systems.

System	μ	l_*	v_*	t_*
Earth-Moon	1.215×10^{-2}	3.850×10^5 km	1.025 km s ⁻¹	2.361×10^6 s
Sun-Earth	3.036×10^{-6}	1.496×10^8 km	29.784 km s ⁻¹	3.147×10^7 s
Sun-Jupiter	9.537×10^{-4}	7.784×10^8 km	13.102 km s ⁻¹	3.733×10^8 s

Table 1.1 – Table of the parameter values for different Three Body Systems. Sources: see [52]

If we divide equation (1.1) by the spacecraft mass m and use the new unit system, we get:

$$\frac{d^2 \mathbf{r}}{dt^2} = -\frac{(1-\mu)}{r_{13}^3} \mathbf{r}_{13} - GM_2 \frac{\mu}{r_{23}^3} \mathbf{r}_{23}. \quad (1.4)$$

We denote by the non caps \mathbf{r} and \mathbf{r}_{ij} the distances previously introduced in the normalized system.

Now, following [31], we rewrite equation (1.4) in a rotating frame $\mathcal{R} = (\mathbf{e}_x, \mathbf{e}_y, \mathbf{e}_z)$ such that the angular velocity of the frame is the one of the two primaries around their center of

¹ Here, we use τ for the time unit because we will normalize the time, and use the normalized time during the remainder of this manuscript. It will be more natural then to use the usual symbol t .

mass which is also the coordinate origin. In this frame, the two primaries are fixed and the frame is chosen so that they belong to the x -axis. This way, the two coordinates of the two primaries are

$$P_1 = (-\mu, 0, 0) \text{ and } P_2 = (1 - \mu, 0, 0).$$

We denote by $\boldsymbol{\omega} \in \mathbf{R}^3$ the angular velocity of the rotating frame \mathcal{R} with respect to the inertial frame \mathcal{I} , and because the time is normalized by the period of the two primaries, it holds that $\boldsymbol{\omega} = E_z = \mathbf{e}_z$. Hence, it follows that

$$\left(\frac{d^2 \mathbf{r}}{dt^2} \right)_{\mathcal{I}} = \left(\frac{d^2 \mathbf{r}}{dt^2} \right)_{\mathcal{R}} + 2E_z \times \left(\frac{d\mathbf{r}}{dt} \right)_{\mathcal{R}} + E_z \times E_z \times \mathbf{r}. \quad (1.5)$$

Now, let us consider the vector \mathbf{r} and its derivatives expressed in the rotating frame, they can be written as

$$\begin{aligned} \mathbf{r} &= x\mathbf{e}_x + y\mathbf{e}_y + z\mathbf{e}_z, \\ \left(\frac{d\mathbf{r}}{dt} \right)_{\mathcal{R}} &= \dot{x}\mathbf{e}_x + \dot{y}\mathbf{e}_y + \dot{z}\mathbf{e}_z, \\ \left(\frac{d^2\mathbf{r}}{dt^2} \right)_{\mathcal{R}} &= \ddot{x}\mathbf{e}_x + \ddot{y}\mathbf{e}_y + \ddot{z}\mathbf{e}_z. \end{aligned}$$

From (1.5), this leads to

$$\left(\frac{d^2 \mathbf{r}}{dt^2} \right)_{\mathcal{I}} = (\ddot{x} - 2\dot{y} - x)\mathbf{e}_x + (\ddot{y} + 2\dot{x} - y)\mathbf{e}_y + \ddot{z}\mathbf{e}_z.$$

In the rotating frame, because the two primaries are fixed along the x -axis, it holds that

$$\mathbf{r}_{13} = (x + \mu)\mathbf{e}_x + y\mathbf{e}_y + z\mathbf{e}_z,$$

$$\mathbf{r}_{23} = (x - 1 + \mu)\mathbf{e}_x + y\mathbf{e}_y + z\mathbf{e}_z,$$

and injecting all of this into (1.4), we finally obtain the dynamical system expressed in the rotating frame:

$$\begin{cases} \ddot{x} = 2\dot{y} + x - \frac{1-\mu}{r_{13}^3}(x+\mu) - \frac{\mu}{r_{23}^3}(x-1+\mu), \\ \ddot{y} = -2\dot{x} + y - \frac{1-\mu}{r_{13}^3}y - \frac{\mu}{r_{23}^3}y, \\ \ddot{z} = -\frac{1-\mu}{r_{13}^3}z - \frac{\mu}{r_{23}^3}z. \end{cases}$$

As usual we write this system as an ordinary differential equation of order one, we introduce the variables

$$\xi = (x_1, x_2, x_3, x_4, x_5, x_6) = (x, y, z, \dot{x}, \dot{y}, \dot{z}),$$

and we get

$$\begin{cases} \dot{x}_1 = x_4, \\ \dot{x}_2 = x_5, \\ \dot{x}_3 = x_6, \\ \dot{x}_4 = x_1 + 2x_5 - (1 - \mu) \frac{x_1 + \mu}{r_{13}^3} - \mu \frac{x_1 - 1 + \mu}{r_{23}^3}, \\ \dot{x}_5 = x_2 - 2x_4 - (1 - \mu) \frac{x_2}{r_{13}^3} - \mu \frac{x_2}{r_{23}^3}, \\ \dot{x}_6 = -(1 - \mu) \frac{x_3}{r_{13}^3} - \mu \frac{x_3}{r_{23}^3}. \end{cases} \quad (1.6)$$

Remark 1.2:

This coordinate system is called *Cross* coordinates. As we have seen, in such a coordinate system, the two primaries have the following coordinates

- $x_{P_1} = (-\mu, 0, 0, 0, 0, 0)$,
- $x_{P_2} = (1 - \mu, 0, 0, 0, 0, 0)$.

Moreover, their respective masses are

- $\mu_1 = 1 - \mu$,
- $\mu_2 = \mu$.

If we introduce the potential function

$$U_\mu(x_1, x_2, x_3) = -\frac{1}{2}(x_1^2 + x_2^2) - \frac{1 - \mu}{r_{13}} - \frac{\mu}{r_{23}} - \frac{1}{2}\mu(1 - \mu),$$

we can write the system as

$$\begin{cases} \dot{x}_1 = x_4 = f_1(\xi), \\ \dot{x}_2 = x_5 = f_2(\xi), \\ \dot{x}_3 = x_6 = f_3(\xi), \\ \dot{x}_4 = 2x_5 - \frac{\partial U_\mu}{\partial x_1} = f_4(\xi), \\ \dot{x}_5 = -2x_4 - \frac{\partial U_\mu}{\partial x_2} = f_5(\xi), \\ \dot{x}_6 = -\frac{\partial U_\mu}{\partial x_3} = f_6(\xi), \end{cases} \quad (1.7)$$

where we define $F_0 = (f_i)_{1 \leq i \leq 6}$ the vector field of the CRTBP dynamics.

1.1.1 Frame transition maps

In this section, we will write the transition map between the inertial and rotating frames. Let us denote by (X, Y, Z) the coordinates in the inertial frame I :

$$\mathbf{r} = X\mathbf{E}_x + Y\mathbf{E}_y + Z\mathbf{E}_z.$$

According to Figure 1.2, it holds that

$$\begin{pmatrix} X \\ Y \\ Z \end{pmatrix} = A_t \begin{pmatrix} x \\ y \\ z \end{pmatrix},$$

where

$$A_t = \begin{pmatrix} \cos t & \sin t & 0 \\ -\sin t & \cos t & 0 \\ 0 & 0 & 1 \end{pmatrix}.$$

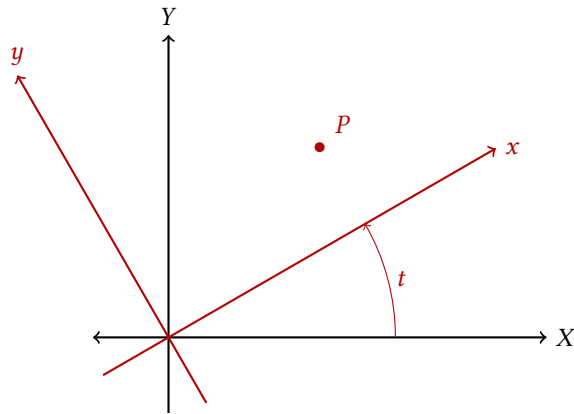


Figure 1.2 – Inertial and rotating frames.

Moreover, a simple computation gives us

$$\begin{aligned} \begin{pmatrix} \dot{X} \\ \dot{Y} \\ \dot{Z} \end{pmatrix} &= \dot{A}_t \begin{pmatrix} x \\ y \\ z \end{pmatrix} + A_t \begin{pmatrix} \dot{x} \\ \dot{y} \\ \dot{z} \end{pmatrix}, \\ &= -A_t J \begin{pmatrix} \dot{x} \\ \dot{y} \\ \dot{z} \end{pmatrix} + A_t \begin{pmatrix} \dot{x} \\ \dot{y} \\ \dot{z} \end{pmatrix}, \\ &= A_t \begin{pmatrix} \dot{x} - y \\ \dot{y} + x \\ \dot{z} \end{pmatrix}. \end{aligned}$$

where

$$J = \begin{pmatrix} 0 & 1 & 0 \\ -1 & 0 & 0 \\ 0 & 0 & 0 \end{pmatrix}.$$

Hence we have

$$\begin{pmatrix} X \\ Y \\ Z \\ \dot{X} \\ \dot{Y} \\ \dot{Z} \end{pmatrix} = \begin{pmatrix} A_t & \mathbf{0}_{3 \times 3} \\ -A_t J & A_t \end{pmatrix} \begin{pmatrix} x \\ y \\ z \\ \dot{x} \\ \dot{y} \\ \dot{z} \end{pmatrix}.$$

1.2 Libration Points (Lagrange Points)

In this section, we investigate the equilibrium points of the CRTBP. They are called Lagrange points or libration points. Euler in [34] and Lagrange in [54] showed that there exist five equilibrium points

- three collinear equilibria on the x -axis, called L_1 , L_2 and L_3 ;
- two equilateral points called L_4 and L_5 (each forms an equilateral triangle with P_1 and P_2).

See Figure 1.3 for an illustration.

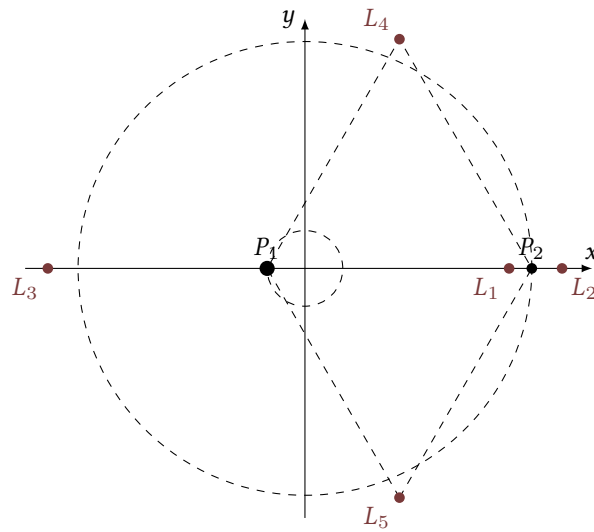


Figure 1.3 – Localization of Lagrange points.

For a complete derivation of the coordinates of the Lagrange points, one may see Szebehely [83] in *Theory of Orbits - The Restricted Problem of Three Bodies*.

Here, we give a sketch of how to compute the coordinates of these points. They correspond to the zeros of $F_0(\cdot)$ defined in (1.7): find $\xi = (x_1, x_2, x_3, x_4, x_5, x_6)$ such that

$$\begin{cases} x_4 = x_5 = x_6 = 0, \\ 2x_5 - \frac{\partial U_\mu}{\partial x_1} = 0, \\ -2x_4 - \frac{\partial U_\mu}{\partial x_2} = 0, \\ -\frac{\partial U_\mu}{\partial x_3} = 0. \end{cases}$$

Immediately, we get

$$x_3 = x_4 = x_5 = x_6 = 0,$$

and we are left to find (x_e, y_e) such that

$$\begin{cases} x_e - (1 - \mu) \frac{x_e + \mu}{r_{13}^3} - \mu \frac{x_e - 1 + \mu}{r_{23}^3} = 0, \\ y_e - (1 - \mu) \frac{y_e}{r_{13}^3} - \mu \frac{y_e}{r_{23}^3} = 0. \end{cases}$$

1.2.1 Localization of collinear points

We consider $y_e = 0$, hence we have to solve the following equation

$$x_e - \frac{1 - \mu}{(x_e + \mu)} - \frac{\mu}{(x_e - 1 + \mu)} = 0. \quad (1.8)$$

Let us focus on the three parts of the x -axis: first, the part between the two primaries, then, the part defined by $x_e > x_{P_2}$, and finally the part defined by $x_e < x_{P_1}$.

Point L_1 . We look for an equilibrium point between the two primaries, and denote it by L_1 . We denote the distance between P_2 and L_1 by γ_1 , so

$$x_{L_1} = x_{P_2} - \gamma_1 = 1 - \mu - \gamma_1.$$

Injecting this into (1.8), one obtains the following equation

$$\gamma_1^5 - (3 - \mu)\gamma_1^4 + (3 - 2\mu)\gamma_1^3 + \mu\gamma_1^2 - 2\mu\gamma_1 + \mu = 0.$$

Point L_2 . We look for an equilibrium point with $x_e > x_{P_2}$, and denote it by L_2 . As before, we denote the distance between P_2 and L_2 by γ_2 , so

$$x_{L_2} = x_{P_2} + \gamma_2 = 1 - \mu + \gamma_2.$$

Injecting this into (1.8), one obtains the equation

$$\gamma_2^5 + (3 - \mu)\gamma_2^4 + (3 - 2\mu)\gamma_2^3 - \mu\gamma_2^2 - 2\mu\gamma_2 - \mu = 0.$$

Point L_3 . We look for an equilibrium point with $x_e < x_{P_1}$, and denote it by L_3 . This time, we denote the distance between P_1 and L_3 by γ_3 , which implies

$$x_{L_3} = x_{P_1} - \gamma_3 = -\mu - \gamma_3.$$

Injecting this into (1.8), one obtains the equation

$$\gamma_3^5 + (2 + \mu)\gamma_3^4 + (1 + 2\mu)\gamma_3^3 - (1 - \mu)\gamma_3^2 - 2(1 - \mu)\gamma_3 - (1 - \mu) = 0.$$

Historically, much effort has been put toward finding the series expansions of such solutions. From Szebehely [83], we get the expression of the two values that we use in this work

$$\begin{aligned} \gamma_1 &= r_h \left(1 - \frac{1}{3}r_h - \frac{1}{9}r_h^{2+\dots} \right), \\ \gamma_2 &= r_h \left(1 + \frac{1}{3}r_h - \frac{1}{9}r_h^{2+\dots} \right), \end{aligned}$$

where $r_h = \left(\frac{\mu}{3}\right)^{1/3}$ is called the *Hill radius*²

2. The corresponding Hill sphere is the 'bubble' in 3D position space surrounding P_2 inside which the satellite with a negligible mass will not be captured by the primary P_1 .

1.2.2 Richardson Coordinate System for the CRTBP

We introduce here a new coordinate system that proves very useful to compute periodic orbits around Lagrange points (see Section 1.4). As for the Cross coordinate system (see remark 1.2), we define the (Ox) -axis as the line defined by the two primary positions P_1 and P_2 , and the (Oy) -axis as the orthogonal. We choose one Lagrange point L_i , $i \in \llbracket 1, 2 \rrbracket$ as the origin, and we normalize the distance by the distance between the Lagrange point and the second primary P_2 (for the Cross system it is the distance between the two primaries).

Change of Coordinates between Cross and Richardson Systems

We consider one of the 2 collinear points L_i of the CRTBP around the second primary P_2 (L_1 or L_2). We denote by d the distance between the two primaries and by d_i the distance between L_i and P_2 . In this section only, we denote respectively by $(x_C, y_C, z_C, \dot{x}_C, \dot{y}_C, \dot{z}_C)$ and $(x_R, y_R, z_R, \dot{x}_R, \dot{y}_R, \dot{z}_R)$ the coordinates in the Cross and Richardson systems.

To convert a set of coordinates from the Cross system to the Richardson system, the following formula holds

$$\begin{aligned} x_R &= \frac{x_C \pm d_i - (1 - \mu)d}{d_i}, & y_R &= \frac{d}{d_i} y_C, & z_R &= \frac{d}{d_i} z_C, \\ \dot{x}_R &= \frac{d}{d_i} \dot{x}_C, & \dot{y}_R &= \frac{d}{d_i} \dot{y}_C, & \dot{z}_R &= \frac{d}{d_i} \dot{z}_C. \end{aligned}$$

The + sign is for L_1 and the – sign for L_2 .

Conversely, it holds that

$$\begin{aligned} x_C &= \frac{d_i x_R \mp d_i + (1 - \mu)d}{d}, & y_C &= \frac{d_i}{d} y_R, & z_C &= \frac{d_i}{d} z_R, \\ \dot{x}_C &= \frac{d_i}{d} \dot{x}_R, & \dot{y}_C &= \frac{d_i}{d} \dot{y}_R, & \dot{z}_C &= \frac{d_i}{d} \dot{z}_R. \end{aligned}$$

Now that we have introduced the dynamics of the CRTBP, we can study some of its dynamical properties.

1.2.3 Stability by Linearization

Stability properties of the Lagrange points have been discussed by Szebehely [83]. This is achieved by studying a linearized system. In this section both the planar and the 2D cases are considered.

Planar case

One can easily write the linearization of the dynamics around a Lagrange point L_i , $i \in \llbracket 1, 5 \rrbracket$. We get

$$\begin{pmatrix} \delta \dot{x} \\ \delta \dot{y} \\ \delta \ddot{x} \\ \delta \ddot{y} \end{pmatrix} = \begin{pmatrix} 0 & 0 & 1 & 0 \\ 0 & 0 & 0 & 1 \\ \frac{\partial U_\mu}{\partial x \partial x}(\xi_i) & \frac{\partial U_\mu}{\partial x \partial y}(\xi_i) & 0 & 2 \\ \frac{\partial U_\mu}{\partial x \partial y}(\xi_i) & \frac{\partial U_\mu}{\partial y \partial y}(\xi_i) & -2 & 0 \end{pmatrix} \begin{pmatrix} \delta x \\ \delta y \\ \delta \dot{x} \\ \delta \dot{y} \end{pmatrix},$$

where ξ_i is the coordinate of L_i . If we evaluate the matrix of the linearized system at the collinear points L_1 , L_2 and L_3 , we obtain that the matrix has four eigenvalues: two real ones including one which is non negative, and two purely imaginary ones that are conjugates. This proves the instability of the collinear points.

If we evaluate the matrix at the equilateral points L_4 and L_5 , we get that if $\mu < \mu_*$ where

$$\mu_* = \frac{1}{2} \left(1 - \frac{\sqrt{69}}{9} \right) = 0.03851, \quad (1.9)$$

then the matrix has purely imaginary eigenvalues.

If $\mu = \mu_*$, the eigenvalues of the matrix of the linearized system are multiples of $\pm i\sqrt{2}/2$ with non trivial Jordan blocks. Finally, for $\mu > \mu_*$, the eigenvalues are λ , $-\lambda$, $\bar{\lambda}$, and $-\bar{\lambda}$ where λ is not purely imaginary.

In this last case, clearly L_4 and L_5 are unstable. Using results on dynamical systems as in Meyer, Hall, and Offin [62], one can show that L_4 and L_5 are stable when $\mu < \mu_*$. In addition to Szebehely [83], the reader may refer to Bonnard, Faubourg, and Trélat [18] for a precise study of the planar case.

Remark 1.3:

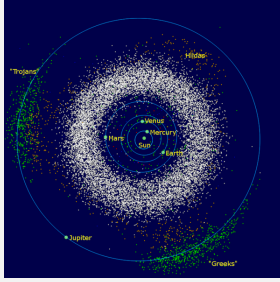


Image Wikipedia.

If we consider the {Sun–Jupiter} system, one can show that the equilateral points are stable and this is coherent with reality.

Indeed, in 1906 a German astronomer Max Wolf discovered the first asteroid captured by the equilibrium region of point L_5 . This kind of asteroid is called a *Trojan asteroid*. In the region of L_4 , it is called *Greek asteroid*. A total of 6,178 Jupiter Trojans had been found in January 2015. The total number of Jupiter Trojans larger than 1 km in diameter is believed to be about 1 million, approximately equal to the number of asteroids larger than 1 km in the asteroid belt.

This illustrates why stable equilibrium points cannot be considered in the design of spacecraft missions because of the collision potential.

3D case

The linearized dynamics around Lagrange points can be written as follows

$$\begin{pmatrix} \delta \dot{x} \\ \delta \dot{y} \\ \delta \dot{z} \\ \delta \ddot{x} \\ \delta \ddot{y} \\ \delta \ddot{z} \end{pmatrix} = \begin{pmatrix} 0 & 0 & 0 & 1 & 0 & 0 \\ 0 & 0 & 0 & 0 & 1 & 0 \\ 0 & 0 & 0 & 0 & 0 & 1 \\ \frac{\partial U_\mu}{\partial x \partial x}(\xi_i) & \frac{\partial U_\mu}{\partial x \partial y}(\xi_i) & \frac{\partial U_\mu}{\partial x \partial z}(\xi_i) & 0 & 2 & 0 \\ \frac{\partial U_\mu}{\partial x \partial y}(\xi_i) & \frac{\partial U_\mu}{\partial y \partial y}(\xi_i) & \frac{\partial U_\mu}{\partial y \partial z}(\xi_i) & -2 & 0 & 0 \\ \frac{\partial U_\mu}{\partial x \partial z}(\xi_i) & \frac{\partial U_\mu}{\partial y \partial z}(\xi_i) & \frac{\partial U_\mu}{\partial z \partial z}(\xi_i) & 0 & 0 & 0 \end{pmatrix} \begin{pmatrix} \delta x \\ \delta y \\ \delta z \\ \delta \dot{x} \\ \delta \dot{y} \\ \delta \dot{z} \end{pmatrix},$$

where ξ_i is the coordinate of L_i .

- At L_1 , L_2 and L_3 , eigenvalues of this matrix are $(\pm\lambda, \pm i\omega_p, \pm i\omega_v)$, where $\lambda > 0$, $\omega_p > 0$, and $\omega_v > 0$. Since one of these values is non negative, collinear points are unstable.
- For L_4 and L_5 , the spectrum is of the form $(\pm i\omega_1, \pm i\omega_2, \pm i\omega_3)$, where $0 < \omega_1 \leq \omega_2 \leq \omega_3$ and the study of stability is harder and depends on the relation between the values ω_i .

1.3 Jacobi Integral and Hill's Region

In this section, to better convey a physical understanding of the phenomena, we denote the state in terms of position and velocity $(x, y, z, \dot{x}, \dot{y}, \dot{z})$.

1.3.1 Jacobi Integral

The CRTBP dynamics are Hamiltonian and autonomous, hence, an energy integral of motion holds

$$\mathcal{E}(\xi) = \frac{1}{2}(\dot{x}^2 + \dot{y}^2 + \dot{z}^2) + U_\mu(x, y, z), \quad (1.10)$$

i.e., $\frac{d\mathcal{E}}{dt} = 0$.

The celestial mechanics and dynamical astronomy communities use $-2\mathcal{E}$ which is called the Jacobi integral and is defined from (1.10) as

$$J(x, y, z, \dot{x}, \dot{y}, \dot{z}) = -2\mathcal{E}(\xi) = -(\dot{x}^2 + \dot{y}^2 + \dot{z}^2) - 2U_\mu(x, y, z).$$

Note that the time-independency of the Jacobi integral can be derived by a straightforward computation of $\frac{dJ}{dt}$.

1.3.2 Hill's Region

Along trajectories of the CRTBP system, the Jacobi integral is constant, hence one can define the energy surface.

Definition 5 (Energy surface): For a given μ and a constant e , we consider the energy surface, or energy manifold $\mathcal{M}(\mu, e)$, as the five-dimensional surface embedded in the six-dimensional phase space defined by

$$\mathcal{M}(\mu, e) = \{(x, y, z, \dot{x}, \dot{y}, \dot{z}); \mathcal{E}(x, y, z, \dot{x}, \dot{y}, \dot{z}) = e\}. \quad \diamond$$

Then, one can define Hill's region from the previous definition.

Definition 6 (Hill's region): The projection of the energy surface onto the position space in the rotating frame is the region of possible motion for a particle of energy e in the CRTBP gravitational field of mass parameter μ . We denote by $M(\mu, e)$ this projection

$$M(\mu, e) = \{(x, y, z); U_\mu(x, y, z) \leq e\}. \quad (1.11)$$

This is historically known as Hill's region. The boundary of $M(\mu, e)$ is known as the zero velocity curve. \diamond

Let us finish by giving one more definition.

Definition 7 (Zero velocity curves): The zero velocity curves (or boundaries of Hill's region) are the locus of the points in the (x, y, z) -space where the kinetic energy vanishes, i.e., for a given energy e and a mass parameter μ

$$\{(x, y, z); e - V_\mu(x, y, z) = 0\},$$

where $V_\mu = \frac{1}{2}(\dot{x}^2 + \dot{y}^2 + \dot{z}^2)$. \diamond

From (1.11), we see that the motion of the spacecraft is possible only on one side of one of these surfaces. Indeed, motion is possible for positive kinetic energy. The other side of the curve is known as the *forbidden realm*.

By multi-variable calculus, one can show that there exist five critical points where the slope of the potential vanishes: three saddle points along the x -axis and two points that are symmetric with respect to the x -axis. Obviously, they correspond to the Lagrange points introduced in Section 1.2.

We denote by \mathcal{E}_i the energy of a particle (a spacecraft) at rest at the libration point L_i ($i \in \llbracket 1, 5 \rrbracket$). It holds that

$$\mathcal{E}_5 = \mathcal{E}_4 > \mathcal{E}_3 > \mathcal{E}_2 > \mathcal{E}_1.$$

Hill's region can be represented as a level section of the graph of the potential U_μ . We plotted the potential for the planar case in Figure 1.4. To have a better understanding of these properties, let us consider the restricted planar case. The extension for the 3D case is easy although we cannot easily represent the different cases.

The intersection of plane $z = e$ with the graph of the effective potential U_μ gives the representation of the different possible zero velocity curves.

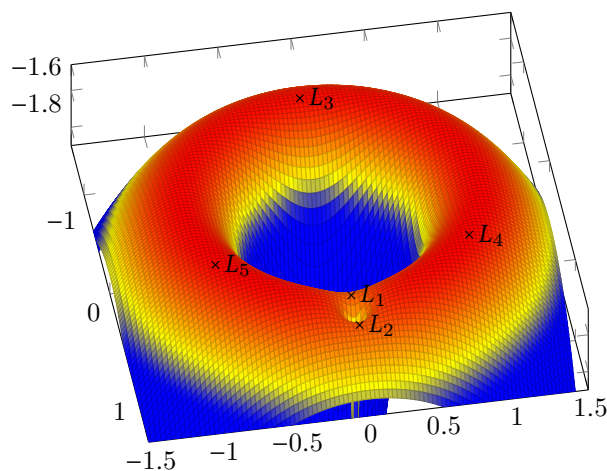


Figure 1.4 – Plot of the potential in the planar case for system {Earth-Moon}. The five equilibrium points L_i , $i \in \llbracket 1, 5 \rrbracket$ are the critical points.

For a given mass parameter μ there are five basic configurations for Hill's region. See Figure 1.5 for a graphical representation.

- Case 1.** $e < \mathcal{E}_1$: If the energy of the spacecraft is lower than \mathcal{E}_1 , the regions around the two primaries are separated and a spacecraft without control cannot move from one to another. See Figure 1.5a.
- Case 2.** $\mathcal{E}_1 < e < \mathcal{E}_2$: In that case, a “neck” between the realms around the two primaries opens up. We can note that the equilibrium point L_1 is in this neck. The spacecraft is still contained in the *interior realm* and cannot go to the *exterior realm*. See Figure 1.5b.
- Case 3.** $\mathcal{E}_2 < e < \mathcal{E}_3$: Here we have a second opening between realm around the point L_2 . This allows to go from the *interior realm* to the *exterior realm*. See Figure 1.5c.
- Case 4.** $\mathcal{E}_3 < e < \mathcal{E}_4 = \mathcal{E}_5$: Here, there are only two separated forbidden realms around the two equilateral points L_4 and L_5 . A third neck appears around point L_3 . See Figure 1.5d.
- Case 5.** $\mathcal{E}_4 = \mathcal{E}_5 < e$: The forbidden realm disappears. The spacecraft is free to move in the entire (x, y) -plane.

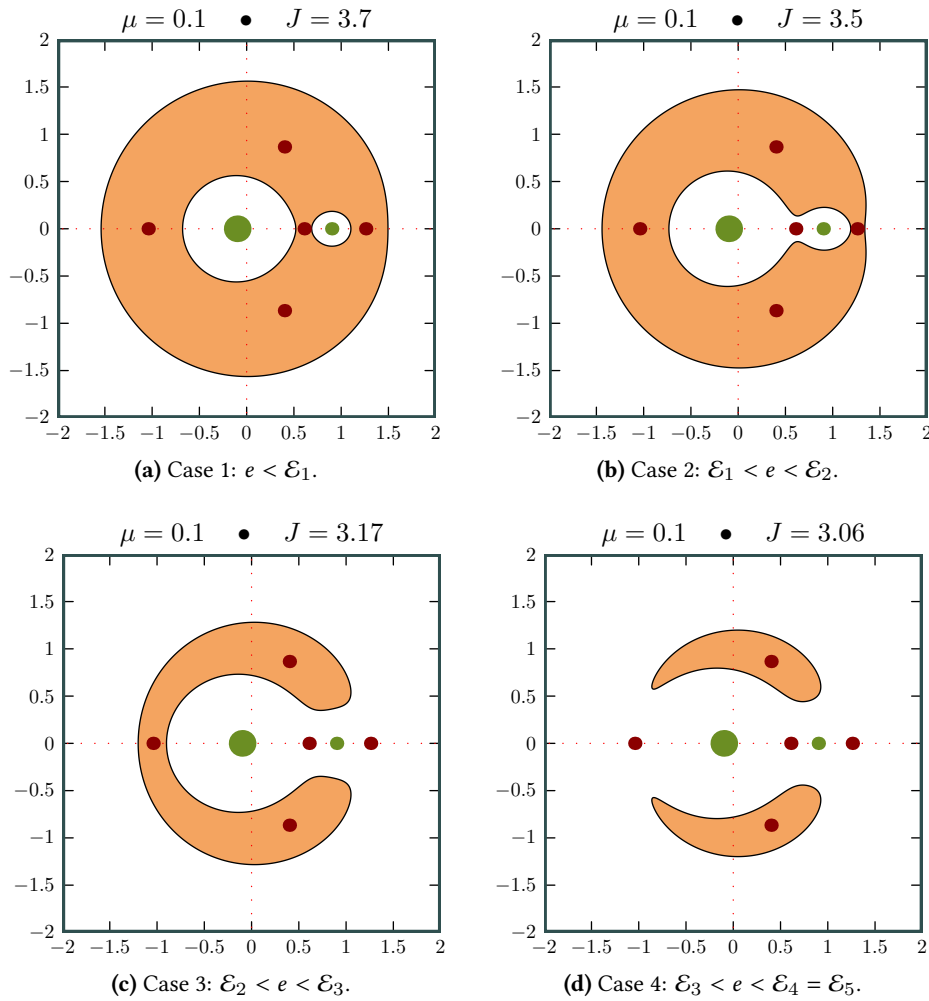


Figure 1.5 – Realms of possible motion (images J.-M. Sarlat).



In this work, we focus on the low thrust transfer in the CRTBP. The study of Hill's regions is crucial because of the good intuition it gives us. Indeed, because we are using low thrust, it will be very interesting to know what regions are accessible without any control. This will become clearer in Section 1.5 about invariant manifolds.

1.4 Periodic Orbits

The equilibrium points in the CRTBP have been known for centuries. As we have seen, Euler in 1767 [34] and Lagrange in 1772 [54] first computed their positions. In 1950, Arthur C. Clarke first suggested that point L_2 could be an ideal place for relaying TV and radio signals.

In 1966, Robert Farquhar discovered trajectories around L_2 on which a communication satellite could be placed to establish a continuous link between Earth and the far side of the Moon. He named such a trajectory a “Halo orbit”. Then NASA became very interested in

the subject and Farquhar published numerous scientific articles covering topics related to Halo orbits (see for instance [35, 36]).

Periodic orbits have been used for real missions such as ISEE-3 (NASA) in 1978, SOHO (ESA-NASA) in 1996, GENESIS (NASA) in 2001, PLANK (ESA) in 2007 etc.

In this section, we will investigate the periodic orbits around the collinear points of the CRTBP. We will introduce the Lyapunov-Poincaré center theorem that ensures that families of periodic orbits exist around the equilibrium points.

1.4.1 Lyapunov-Poincaré Theorem

Let us write the linearized system in the spatial case (the planar case can be easily deduced from it). It is standard to expand the nonlinear terms $\frac{1}{r_1}$ and $\frac{1}{r_2}$ as series in Legendre polynomials, using the formula:

$$\frac{1}{\sqrt{(x-A)^2 + (y-B)^2 + (z-C)^2}} = \frac{1}{D} \sum_{n=0}^{\infty} \left(\frac{\rho}{D}\right)^n P_n\left(\frac{Ax + By + Cz}{D\rho}\right),$$

where $D^2 = A^2 + B^2 + C^2$, $\rho^2 = x^2 + y^2 + z^2$ and P_n is the Legendre polynomial of degree n (see Jorba and Masdemont [50]). Then, using a Richardson coordinate system centered on the equilibrium point L_i introduced in Section 1.2.2, for $i = 1, 2$, the equations of motion (1.6) can be written as

$$\begin{cases} \ddot{x} - 2\dot{y} - (1 + 2c_2)x = \frac{\partial}{\partial x} \sum_{n \geq 3} c_n \rho^n P_n\left(\frac{x}{\rho}\right), \\ \ddot{y} + 2\dot{x} - (c_2 - 1)y = \frac{\partial}{\partial y} \sum_{n \geq 3} c_n \rho^n P_n\left(\frac{x}{\rho}\right), \\ \ddot{z} + c_2 z = \frac{\partial}{\partial z} \sum_{n \geq 3} c_n \rho^n P_n\left(\frac{x}{\rho}\right), \end{cases} \quad (1.12)$$

where

$$c_n = \frac{1}{\gamma_i^{n+1}} \left(\mu + \frac{(1-\mu)\gamma_i^{n+1}}{(1-\gamma_i)^{n+1}} \right).$$

As previously, γ_i denotes the distance between the Lagrange point L_i and the second primary.

Hence, at Lagrange points L_i , $i = 1, 2, 3$, the linearized version of (1.12) is

$$\begin{cases} \ddot{x} - 2\dot{y} - (1 + 2c_2)x = 0, \\ \ddot{y} + 2\dot{x} - (c_2 - 1)y = 0, \\ \ddot{z} + c_2 z = 0. \end{cases} \quad (1.13)$$

This is of the kind saddle×center×center. Indeed, a simple computation leads to the eigenvalues $(\pm\lambda, \pm i\omega_p, \pm i\omega_v)$:

$$\lambda^2 = \frac{c_2 - 2 + \sqrt{9c_2^2 - 8c_2}}{2}, \quad \omega_p^2 = \frac{c_2 - 2 - \sqrt{9c_2^2 - 8c_2}}{2}, \quad \text{and} \quad \omega_v^2 = c_2. \quad (1.14)$$

The following theorem ensures the existence of periodic orbits around equilibrium points (see [62, 18] and references therein).

Theorem 1 (Lyapunov-Poincaré center theorem) Let $\dot{x} = H(x)$ be a hamiltonian system in \mathbb{R}^{2n} , x_0 an equilibrium point identified with 0, and $A = \frac{\partial H}{\partial x}(0)$ the linearized system matrix. Assume that the eigenvalues of A are

$$\sigma(A) = \{\pm i\omega, \lambda_3, \dots, \lambda_{2n}\},$$

where $\omega > 0$. If $\lambda_j/i\omega \notin \mathbb{Z}$ for $j \in \llbracket 3, 2n \rrbracket$, then there exists a one-parameter family of periodic orbits around 0. Moreover, when approaching the equilibrium point along the family, the periods go to $2\pi/\omega$ and the nontrivial multipliers go to $\exp(2\pi\lambda_j/\omega)$, $j \in \llbracket 3, 2n \rrbracket$.

The multipliers are, by definition, the eigenvalues of the monodromy matrix (see Section 1.5.2), and the non-trivial multipliers are the multipliers left after dropping two $+1$ multipliers from the list of eigenvalues (for references, see [62]).

This theorem can be applied to the planar circular restricted three body problem and to the spatial circular restricted three body problem.

Planar case

Let us apply it to the planar case.

- For the collinear points L_1 , L_2 and L_3 , we have seen that the eigenvalues of the linearized system are a pair of real eigenvalues and a pair of pure imaginary eigenvalues (for details, see Meyer, Hall, and Offin [62]). Thus, the Lyapunov-Poincaré theorem implies that there is a one-parameter family of periodic solutions emanating from each of these libration points.
- For the points L_4 and L_5 , for $\mu < \mu_*$ defined in (1.9), we have two pairs of purely imaginary eigenvalues $(\pm i\omega_1, \pm i\omega_2)$ with $0 < \omega_1 < \omega_2$. Applying theorem 1 twice, we obtain the following :
 - since $\omega_2/\omega_1 < 1$: there exists a one-parameter family of periodic orbits emanating from the equilibrium point with a period approaching $2\pi/\omega_1$. This family is called the short period family.
 - If $\omega_2/\omega_1 \notin \mathbb{N}$: there exists a family of periodic orbits emanating from the equilibrium point with period approaching $2\pi/\omega_2$. This family is called the long time period family.

Spatial Case

We have seen that eigenvalues of the spatial circular restricted three body problem are $(\pm\lambda, \pm i\omega_p, \pm i\omega_v)$ with λ , ω_p and ω_v non negative values. Thanks to theorem 1, we obtain the following

- because $\lambda/\omega_v \notin \mathbb{Z}$, there exists a one-parameter family of periodic orbits;
- moreover, if $\omega_p/\omega_v \notin \mathbb{Z}$, we can apply the theorem once again and we obtain another one-parameter family.

When $c_2 > 1$, as for the {Sun-Earth} system, $\omega_p/\omega_v \notin \mathbb{Z}$, and there exists a family of periodic orbits with two parameters around L_1 and L_2 . We will see in the next sections an example of such a periodic orbit: the eight-shape orbit.

Definition 8 (Terminology): *There exists specific terminology for periodic orbits around Lagrange points.*

- In the spatial case, periodic orbits which are homeomorphic to a circle are called Halo orbits, other families of periodic orbits are called Lissajous orbits.
- In the planar case, periodic orbits which are homeomorphic to a circle are called Lyapunov orbits. \diamond

1.4.2 Numerical Method to Compute Periodic Orbits

In Richardson coordinates, the dynamics satisfy a property of symmetry: if $\xi(t)$ is a solution of (1.6), then so is $\xi(-t)$. Hence, if there exists a trajectory on one side of the plane $y = 0$, then its mirror part on the other side propagating backward is also a trajectory.

Consider a trajectory beginning at $t = 0$ in the plane $y = 0$ with an orthogonal velocity vector. If there exists a time t_ξ at which the trajectory crosses the plane $y = 0$ with again an orthogonal velocity, then we get a periodic orbit of period $2t_\xi$.

This can be written in the following way: considering a periodic solution of (1.12)

$$\xi(t) = (x(t), y(t), z(t), \dot{x}(t), \dot{y}(t), \dot{z}(t))$$

of period $2t_\xi$, it holds that

$$\xi(0) = (x_0, 0, z_0, 0, \dot{y}(0), 0) \text{ and } \xi(t_\xi) = (x_1, 0, z_1, 0, \dot{y}_1, 0).$$

Shooting Function

To compute these periodic orbits numerically, we use a Newton-like method. More precisely, the problem can be stated as finding the zero of a shooting function. Indeed, let us denote by ϕ the flow of the dynamical system, we search for the initial values for $\xi(0)$ that yield

$$\begin{pmatrix} y(t_\xi) \\ \dot{x}(t_\xi) \\ \dot{z}(t_\xi) \end{pmatrix} = \begin{pmatrix} \phi_2(t_\xi, \xi(0)) \\ \phi_4(t_\xi, \xi(0)) \\ \phi_6(t_\xi, \xi(0)) \end{pmatrix} = \mathbf{0}.$$

Because we have more degrees of freedom than the dimension of the function that we want to nullify, we fix one parameter, usually, the *excursion* z_0 (see Archambeau, Augros, and Trélat [6]). Having done that, the shooting function for this problem can be defined as

$$\mathcal{S}_{z_0}(t_\xi, x_0, \dot{y}(0)) = \begin{pmatrix} \phi_2(t_\xi, \xi(0)) \\ \phi_4(t_\xi, \xi(0)) \\ \phi_6(t_\xi, \xi(0)) \end{pmatrix}. \quad (1.15)$$

To find the solution of $\mathcal{S}_{z_0}(t_\xi, x_0, \dot{y}(0))$, we use a Newton-like method. Of course, to allow such a method to converge, we have to initialize it with a point in the convergence domain. This is the subject of the next section.

1.4.3 Analytical Initialization

To initialize the Newton-like method for finding the zeros of the shooting function defined in (1.15), we initialize the algorithm with an analytical approximation of the periodic orbits that we want to compute.

Lindstedt-Poincaré Method

The method we follow to compute an analytical approximation is the Lindstedt-Poincaré Method (see Poincaré [70] and Lindstedt [57]).

Let us explain the method on the standard example of the Duffing equation

$$\ddot{q} + q + \epsilon q^3 = 0, \quad (1.16)$$

where $\epsilon \ll 1$. For $\epsilon = 0$, we can easily show that a periodic solution is $q(t) = a \cos(t)$ for initial condition $q(0) = a$ and $\dot{q}(0) = 0$.

For $\epsilon \neq 0$, a very naive approach would be to search for solutions of the form

$$q = \sum_{n=0}^{\infty} \epsilon^n q_n(t),$$

with $q_0(0) = a$, $\dot{q}_0(0) = 0$ and $q_n(0) = 0$, $\dot{q}_n(0) = 0$ for every $n \geq 1$. Then, we could solve, recursively, the equations to the same order of ϵ

$$\begin{aligned} \ddot{q}_0 + q_0 &= 0, \\ \ddot{q}_1 + q_1 &= -q_0^3, \\ \ddot{q}_2 + q_2 &= -2q_0^2 q_1, \\ &\dots \end{aligned}$$

Having performed computations, we get for q_1

$$q_1(t) = -\frac{3}{8}a^3 t \sin(t) + \frac{1}{32}a^3(\cos(3t) - \cos(t)).$$

Because of the so-called *secular term* ($t \sin t$), the first-order approximation grows to infinity in time. Hence, this approach is not valid to compute an approximation of the solution.

The Lindstedt-Poincaré method allows for the creation of an approximation that is accurate at all time. A scaled time is defined

$$\tau = \nu(\epsilon)t,$$

where $\nu = 1 + \epsilon \nu_1 + \epsilon^2 \nu_2 + \dots$. Then, with respect to the scaled time, equation (1.16) becomes

$$q'' + \nu^{-2}(q + \epsilon q^3) = 0,$$

with the same initial conditions. Now, a solution is sought in the form

$$q = \sum_{n=0}^{\infty} \epsilon^n q_n(\tau).$$

The obtained zero-th and first order solution in ϵ are

$$q_0(\tau) = a \cos(\tau) \text{ and } q_1(\tau) = (\nu_1 - \frac{3}{8})a^3 t \sin(t) + \frac{1}{32}a^3(\cos(3t) - \cos(t)).$$

The secular term can be removed by making the choice: $\nu_1 = 3/8$. Higher orders of accuracy can be obtained by propagating this perturbation analysis recursively.

In the end of this very short introduction, this method allows for the removal of the secular terms at any approximation order.

Much effort has been put toward computing analytical approximations of Lissajous orbits around Lagrange points using the Lindstedt-Poincaré method. Let us present the remarkable contributions of Jorba and Masdemont [50], Archaubeau, Augros, and Trélat [6], and Richardson [74].

Halo Orbit Case

In this section, we recall the method that Richardson used in [74] in 1980. He computed analytical approximations for Halo orbits.

Consider the linearized spatial motion equations (1.13)

$$\begin{cases} \ddot{x} - 2\dot{y} - (1 + 2c_2)x = 0, \\ \ddot{y} + 2\dot{x} - (c_2 - 1)y = 0, \\ \ddot{z} + c_2z = 0. \end{cases}$$

A simple computation yields the eigenvalues of this system: $(\pm\lambda, \pm i\omega_p, \pm i\omega_v)$. If initial conditions are restrained to the non-divergent mode, we obtain solutions for the linearized system of the form

$$\begin{cases} x(t) = -A_x \cos(\omega_p t + \phi), \\ y(t) = \kappa A_x \sin(\omega_p t + \phi), \\ z(t) = A_z \cos(\omega_v t + \psi), \end{cases} \quad (1.17)$$

where $\kappa = \frac{\omega_p^2 + 1 + c_2}{2\omega_p} = \frac{2\lambda}{\lambda^2 + 1 - c_2}$ and, A_x and A_z refer to the excursions respectively in x and z .

One can immediately see that if the ratio between ω_p and ω_v is rational, then the bounded solutions of the linearized system are periodic.

Because there are four purely imaginary eigenvalues, classical theorems stating equivalence between the non-linear system and its linearized form do not hold.

However, a generalization of the Lyapunov theorem, established by Moser [66], ensures that for a certain energy greater than the energy of the considered Lagrange point, the behavior of non-linear solutions is qualitatively equivalent to that of the linear solutions. Hence, periodic orbits in the non-linear system are perturbations of the periodic orbits of the linearized system around Lagrange points.

In equation (1.17), values of the frequencies ω_p and ω_v are fixed and “naturally given” by the parameters of the system and the Lagrange point we consider. The non-linearity can induce changes on these two frequencies. Following the work of Richardson and the Lindstedt-Poincaré method we sketch the different steps needed to obtain an approximation of the Halo orbits for which the ratio between the two proper frequencies is equal to one. For other rational ratios, the orbits are referred to as Lissajous orbits.

The first step is to rewrite the system of equations (1.12), enforcing the relation $\omega_p = \omega_v$ for the linearized part

$$\begin{cases} \ddot{x} - 2\dot{y} - (1 + 2c_2)x = \frac{\partial}{\partial x} \sum_{n \geq 3} c_n \rho^n P_n \left(\frac{x}{\rho} \right), \\ \ddot{y} + 2\dot{x} - (c_2 - 1)y = \frac{\partial}{\partial y} \sum_{n \geq 3} c_n \rho^n P_n \left(\frac{x}{\rho} \right), \\ \ddot{z} + \omega_p^2 z = \frac{\partial}{\partial z} \sum_{n \geq 3} c_n \rho^n P_n \left(\frac{x}{\rho} \right) + \Delta z, \end{cases} \quad (1.18)$$

where $\Delta = \omega_p^2 - \omega_v^2$. Equations (1.18) approximated to the fourth order are

$$\begin{cases} \ddot{x} - 2\dot{y} - (1 + 2c_2)x = \frac{3}{2}c_3(2x^2 - y^2 - z^2) + 2c_4x(2x^2 - 3y^2 - 3z^2) + O(\rho^4), \\ \ddot{y} + 2\dot{x} + (c_2 - 1)y = -3c_3xy - \frac{3}{2}c_4y(4x^2 - y^2 - z^2) + O(\rho^4), \\ \ddot{z} + \omega_p^2z = -3c_3xz - \frac{3}{2}c_4z(4x^2 - y^2 - z^2) + \Delta z + O(\rho^4). \end{cases}$$

We look for a periodic solution as a series expansion in the excursions

$$\begin{cases} x = Ax_0(\tau) + A^2x_1(\tau) + A^3x_2(\tau) + \dots \\ y = Ay_0(\tau) + A^2y_1(\tau) + A^3y_2(\tau) + \dots \\ z = Az_0(\tau) + A^2z_1(\tau) + A^3z_2(\tau) + \dots \end{cases} \quad (1.19)$$

where $A^n = \sum_{l,p, l+p=n} \lambda_{l,p} A_x^l A_z^p$, and $\lambda_{i,j}$ are the polynomial coefficients. We then define the scaled time $\tau = vt$ where

$$v = 1 + \sum_{n \geq 1} v_n, \quad v_n < 1.$$

Recursively, we adjust the parameters v_n to cancel secular terms that appear in the expansion of each approximation. Equations (1.19) become

$$\begin{cases} v^2x'' - 2vy' - (1 + 2c_2)x = \frac{3}{2}c_3(2x^2 - y^2 - z^2) + 2c_4x(2x^2 - 3y^2 - 3z^2) + O(\rho^4), \\ v^2y'' + 2vx' + (c_2 - 1)y = -3c_3xy - \frac{3}{2}c_4y(4x^2 - y^2 - z^2) + O(\rho^4), \\ v^2z'' + \omega_p^2z = -3c_3xz - \frac{3}{2}c_4z(4x^2 - y^2 - z^2) + \Delta z + O(\rho^4). \end{cases}$$

Following the Lindstedt-Poincaré method and with quite long calculations, we obtain that $v_1 = 0$ and $v = s_1A_x^2 + s_2A_z^2$ where s_1 and s_2 are defined in appendix A. We also obtain an approximation of the period of the periodic orbit $T = 2\frac{\pi}{\omega_p}v$.

Unfortunately, all secular terms are not canceled, we have to add two more equations

$$\begin{aligned} l_1A_x^2 + l_2A_z^2 + \Delta &= 0 \\ \psi - \phi &= n\pi/2, \quad n \in \{1, 3\} \end{aligned} \quad (1.20)$$

where l_1 and l_2 are also defined in appendix A. For computational details, see [74, 6].

The resulting third order analytical approximation is

$$\begin{cases} x = a_{21}A_x^2 + a_{22}A_z^2 - A_x \cos(\tau_1) + (a_{23}A_x^2 - a_{24}A_z^2) \cos(2\tau_1) + (a_{31}A_x^3 - a_{32}A_xA_z^2) \cos(3\tau_1), \\ y = \kappa A_x \sin(\tau_1) + (b_{21}A_x^2 - b_{22}A_z^2) \sin(2\tau_1) + (b_{31}A_x^3 - b_{32}A_xA_z^2) \sin(3\tau_1), \\ z = \delta_n A_z \cos(\tau_1) + \delta_n d_{21} A_x A_z (\cos(2\tau_1) - 3) + \delta_n (d_{32} A_z A_x^2 - d_{31} A_z^3) \cos(3\tau_1) \end{cases}$$

where $\tau_1 = \omega_p \tau + \phi$, $\delta_n = 2 - n$, n gives the orbit class, which can be interpreted as the direction of rotation. One again, coefficients $a_{i,j}$, $b_{i,j}$ and $d_{i,j}$ are defined in appendix A.

Eight-Shape Periodic Orbit

We will not present the very general method explained in [50, 41] but, an interesting kind of periodic orbit is the ‘‘Eight-Shape’’ periodic orbit. These orbits are nearly vertical and we

will see that their invariant manifolds are very stable compared to the Halo manifolds. This is proved thanks to the study of the local Lyapunov exponents (see Archambeau, Augros, and Trélat [6]).

Despite a mistake in the work in [6]³, the author, following the ideas of Richardson's study, gives an analytical approximation for eight-shape periodic orbits that is accurate enough to initialize a Newton-like method and achieve convergence. The author derives the following expression of the approximation

$$\begin{cases} x = a_{21}A_x^2 + a_{22}A_z^2 - A_x \cos(\tau_1) + (a_{23}A_x^2 - a_{24}A_z^2) \cos(2\tau_1) + (a_{31}A_x^3 - a_{32}A_xA_z^2) \cos(3\tau_1), \\ y = \kappa A_x \sin(\tau_1) + (b_{21}A_x^2 - b_{22}A_z^2) \sin(2\tau_1) + (b_{31}A_x^3 - b_{32}A_xA_z^2) \sin(3\tau_1), \\ z = \delta_r A_z \cos(\tau_2) + \delta_n d_{21} A_x A_z (\cos(2\tau_2) - 3) + \delta_n (d_{32} A_z A_x^2 - d_{31} A_z^3) \cos(3\tau_2), \end{cases}$$

where $\tau_1 = \omega_p \tau + \phi$ and $\tau_2 = \frac{\omega_p}{2} \tau + \psi$. Relations between excursion and phase are the ones introduced in (1.20).

Numerical results

In figures 1.6 and 1.7, we see different periodic orbits for different CRTBPs: the Halo orbit in the {Sun-Earth} system, and an eight-shape orbit in the {Earth-Moon} system. In Figure 1.8, we plot a planar Lyapunov orbit in the {Earth-Moon} system. All examples are computed around L_1 but it could easily be done for L_2 . Thanks to the two analytical approximation for periodic orbits, the Newton-like method converges easily.

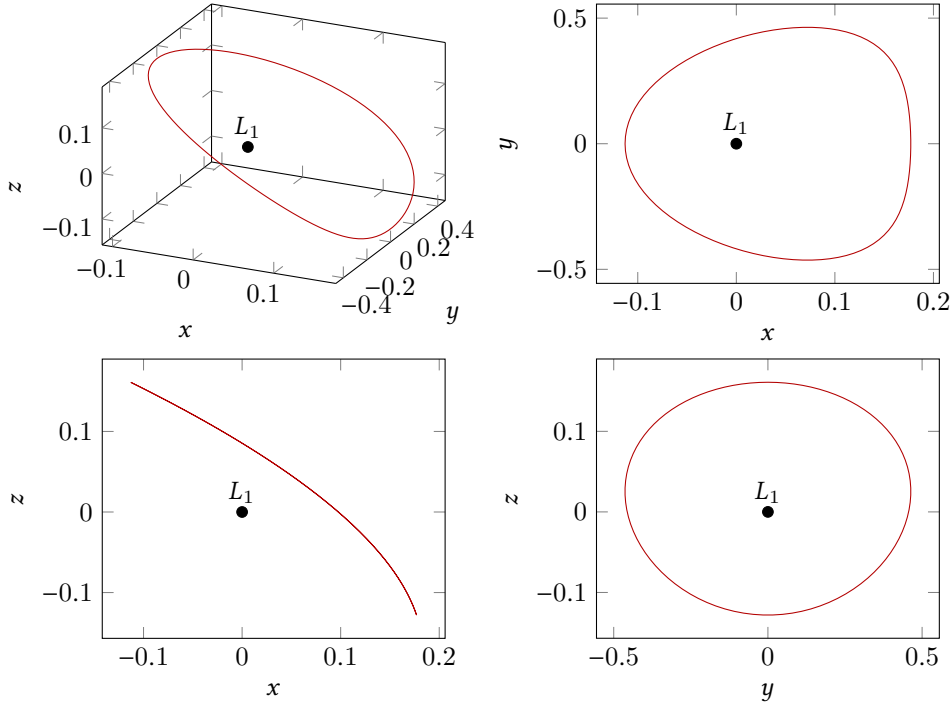


Figure 1.6 – Halo orbit in the {Sun-Earth} system in Richardson coordinates obtained by a Newton-like method. The fixed excursion is $A_z = 240 \times 10^3$ km.

³. Indeed, the argument to cancel the secular term for z_0^2 does not hold for the eight-shape periodic orbit.

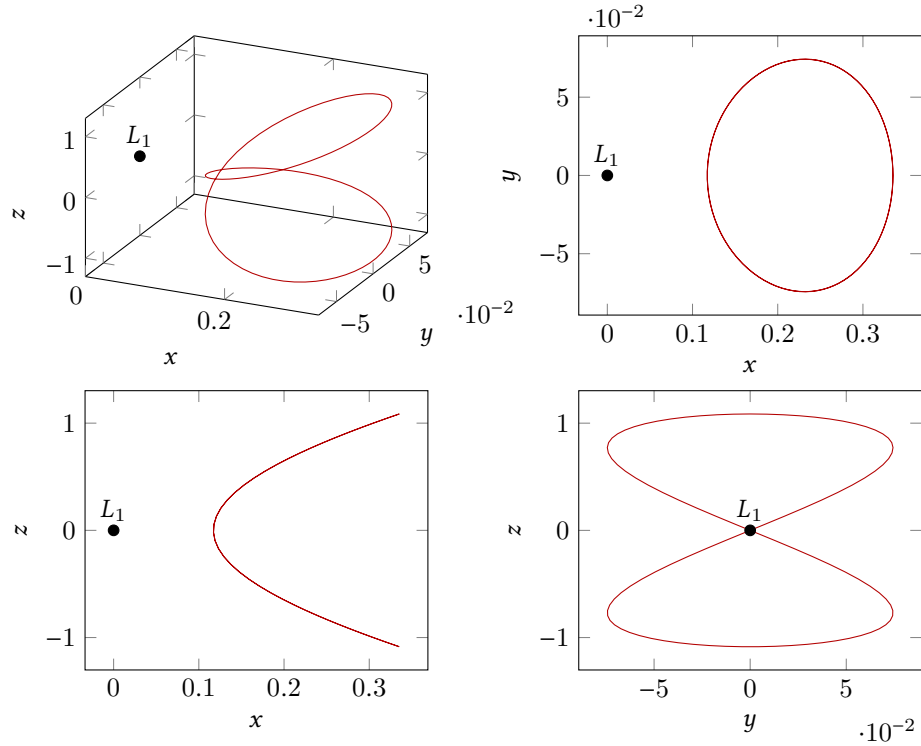


Figure 1.7 – Eight-shape orbit in the {Earth-Moon} system in Richardson coordinates obtained by a Newton-like method. The fixed excursion is $A_z = 630 \times 10^3$ km.

1.4.4 Families of Periodic Orbits

To design spacecraft missions, it is very useful to be able to compute the family of all periodic orbits, providing a variety of orbits that have different energies. In order to achieve this, we first introduce the continuation methods. These methods will be used throughout this thesis, here we introduce the basic concept.

Continuation Method

To compute the family of periodic orbits, we introduce continuation methods also known as homotopy methods. We consider a problem \mathcal{P}_1 that we want to solve. The principle is to *embed* this problem into a family of problems depending on a parameter $\lambda \in [0, 1]$: $(\mathcal{P}_\lambda)_{\lambda \in [0, 1]}$. The initial problem \mathcal{P}_0 is assumed to be easy to solve, while the final problem \mathcal{P}_1 is the one we actually want to solve (and too hard to solve directly).

The continuation method is to follow the zeros of the problems $(\mathcal{P}_\lambda)_{\lambda \in [0, 1]}$ using shooting functions from $\lambda = 0$ to $\lambda = 1$ to finally obtain a solution for \mathcal{P}_1 . There are many types of continuation methods, for a complete presentation, see Allgower and Georg [3]. First, we consider discrete continuation.

Let us assume that we have solved \mathcal{P}_0 numerically, and consider a subdivision $0 = \lambda_0 < \lambda_1 < \dots < \lambda_p = 1$ of the interval $[0, 1]$. The solution of \mathcal{P}_0 is used to initialize the Newton-like method applied to \mathcal{P}_{λ_1} . And so on: solution of $\mathcal{P}_{\lambda_{i-1}}$ is used to initialize \mathcal{P}_{λ_i} . Of course, the sequence (λ_i) has to be well chosen, and should be refined if necessary. See Section 2.5 for general explanations on discrete continuation methods.

Theoretically, for this method to converge, we need the family of problems to depend

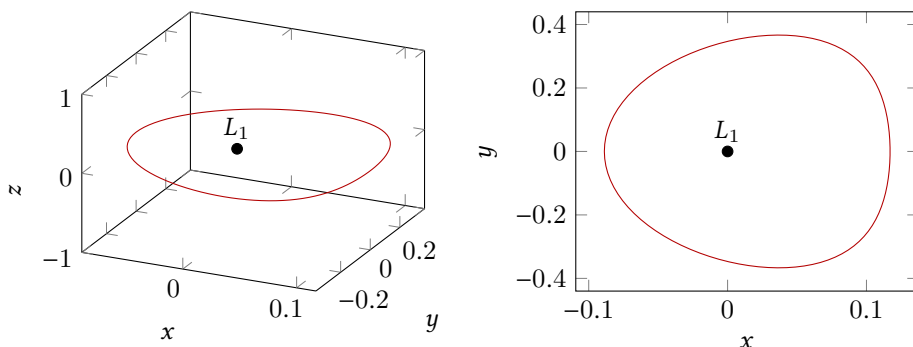


Figure 1.8 – Lyapunov orbit in the {Earth-Moon} system in Richardson coordinates obtained by a Newton-like method. We are in a planar case.

continuously on the parameter λ . See [18, chap. 9] for some justification of the method.

We note that there exist many continuation codes available on the web, such as the well-known Hompack90 [89] or Hampath [30]. For a survey of different results, challenges and issues on continuation methods, see [85].

Application to the family of orbits

Since we had to choose a parameter the excursion z_0 to write the zero function \mathcal{S}_{z_0} in (1.15), it seems natural to use this parameter to perform the continuation that computes the family of orbits. We choose to reach a certain z_0^{obj} (respectively x_0^{obj} in the planar case). So we define our continuation as

$$\mathcal{P}_\lambda : \begin{cases} z_0^\lambda = (1 - \lambda)z_0 + \lambda z_0^{\text{obj}} \\ \mathcal{S}_{z_0}^\lambda(t_\xi, x_0, \dot{y}_0) = \begin{pmatrix} \phi_2(t_\xi, \xi_0^\lambda) \\ \phi_4(t_\xi, \xi_0^\lambda) \\ \phi_6(t_\xi, \xi_0^\lambda) \end{pmatrix} = \begin{pmatrix} 0 \\ 0 \\ 0 \end{pmatrix} \end{cases}$$

where $\xi_0^\lambda = (x_0, 0, z_0^\lambda, 0, \dot{y}_0, 0)$. Thanks to the analytical approximation provided by [74] or [50], we can solve the initial problem \mathcal{P}_0 as described in the previous section. Note that such an analytical approximation does not work for every z_0 , in particular for small ones. Using the continuation method described previously, we derive a family of periodic orbit.



Unfortunately, for some periodic orbits (Halo family), we observe that the continuation fails when we converge to the equilibrium point ($z_0^{\text{obj}} \rightarrow 0$). A much better continuation parameter is *energy*. It releases the constraint on the parameter z_0 , and allows us to reach any periodic orbit. In particular the algorithm converges to the energy of L_i , $i \in \{1, \dots, 3\}$.

We can explain the failure of the continuation on the z -excursion by the fact that for, energy value close to the one of the libration point, the z -excursion is too small. Moreover, the energy parameter provides monotony to the path of zeros.

Moreover, it is a significantly more natural parameter, keeping in mind the fact that we will construct a controlled transfer method. To the author's knowledge, this is the first time that this continuation is performed with the energy as the continuation parameter. This avoids numerical problems when reaching energies close to L_i .

Thanks to the analytical approximation, we get a first periodic orbit with energy \mathcal{E}_0 , and

we want to reach a prescribed energy \mathcal{E}_1 so we define the following family of problems:

$$\mathcal{P}_\lambda^\mathcal{E} : \mathcal{S}_\mathcal{E}^\lambda(t_\chi, x_0, z_0, \dot{y}_0) = \begin{pmatrix} \phi_2(t_\xi, \xi_0) \\ \phi_4(t_\xi, \xi_0) \\ \phi_6(t_\xi, \xi_0) \\ \mathcal{E}(\xi_0) = \mathcal{E}_\lambda \end{pmatrix} = \begin{pmatrix} 0 \\ 0 \\ 0 \\ 0 \end{pmatrix}$$

where $\mathcal{E}(\xi_0)$ is the energy of the trajectory starting at ξ_0 and

$$\mathcal{E}_\lambda = (1 - \lambda)\mathcal{E}_0 + \lambda\mathcal{E}_1.$$

See Algorithm 1.1 for a precise description of the method.

Algorithm 1.1: Orbit Continuation Algorithm

Require: the objective energy \mathcal{E}_1 , $\epsilon > 0$, ϵ_{\min} and ϵ_{\max} .
Require: $\xi_0 = (x_0, 0, z_0, 0, \dot{y}_0, 0)$ and t_ξ provided by the first shoot (with the analytical approximation initialization).
1: $\mathcal{E}_0 = \mathcal{E}(\xi_0)$, $\lambda = 0$.
2: $x_s = x_0$, $z_s = z_0$, $\dot{y}_s = \dot{y}_0$ and $t_s = t_\xi$.
3: $i = 0$.
4: **while** $\lambda < 1$ and $\epsilon > \epsilon_{\min}$ **do**
5: $\epsilon = \min(\epsilon, 1 - \lambda)$
6: we increase : $\lambda \leftarrow \lambda + \epsilon$.
7: we initialize : $(t_c, x_c, z_c, \dot{y}_c) \leftarrow (t_s, x_s, z_s, \dot{y}_s)$
8: $\mathcal{E}_\lambda \leftarrow (1 - \lambda)\mathcal{E}_0 + \lambda\mathcal{E}_1$
9: Newton-like Method to solve $\mathcal{S}_\mathcal{E}^\lambda(t_c, x_c, z_c, \dot{y}_c) = \mathbf{0}$.
10: **if** success **then**
11: we keep the solution : $(t_s, x_s, \dot{y}_s) \leftarrow (t_c, x_c, \dot{y}_c)$
12: we increase : $\epsilon = \min(\alpha\epsilon, \epsilon_{\max})$, $\alpha > 1$.
13: **else**
14: we restore : $\lambda \leftarrow \lambda - \epsilon$.
15: we decrease : $\epsilon = \beta\epsilon$, $\beta < 1$.
16: **end if**
17: **end while**

Numerical Results

In Figures 1.9 and 1.10, we plotted, respectively, the family of Halo orbits for decreasing energies in the {Sun-Earth} system, and the family of eight-shape orbits for decreasing energies in the {Earth-Moon} system. In Figure 1.11, we see the family of planar Lyapunov orbits in the {Earth-Moon} system. All examples are computed around L_1 but the same could easily be done for L_2 . One may note that this continuation is a discrete one with no linear prediction. We can obviously improve this continuation but because the computation time is very small (around 0.01 s including the printing of each orbit during the continuation), we did not add this feature.

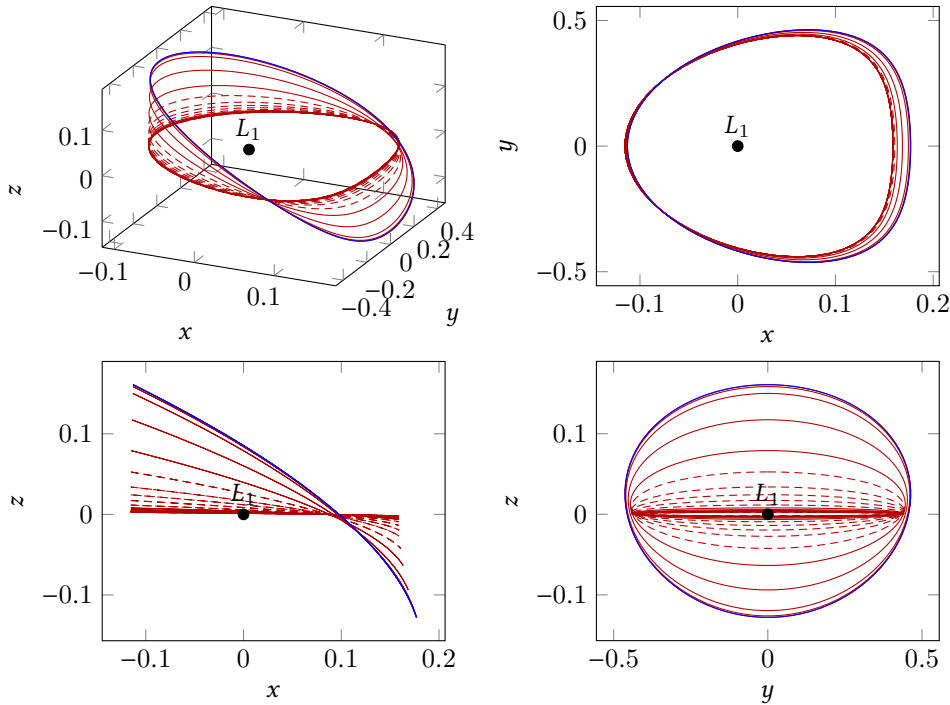


Figure 1.9 – Family of Halo orbits in the {Sun-Earth} system in Richardson coordinates obtained by a Newton-like method and continuation on the energy. The first fixed excursion is $A_z = 240 \times 10^3$ km and the final energy is -1.50042 in normalized units (corresponding to a quasi-null z -excursion).

1.5 Invariant Manifolds

In this section, we introduce the concept of *invariant manifold* of a periodic orbit. In the next chapters, it will become apparent that the existence of such mathematical object is of a great interest. Indeed, the invariant manifolds can be considered as *gravitational currents*, and so, they can be used in interplanetary missions.

1.5.1 Mathematical Definition

We consider a periodic orbit around a libration point L_i , $i \in \llbracket 1, 3 \rrbracket$. Let us begin with the mathematical definition of these objects.

Definition 9 (Invariant Manifolds): A *stable manifold* (resp., *unstable*) of a periodic orbit is the set of the phase space consisting of all points whose *future* (resp., *past*) semi-orbits converge to it (asymptotic orbits). \diamond

Because there is no analytical expression for the periodic orbits around libration points, there is no analytical way of computing the associated invariant manifolds. However, the computation of the stable and unstable invariant manifolds can be accomplished numerically. The procedure is based on the monodromy matrix discussed next.

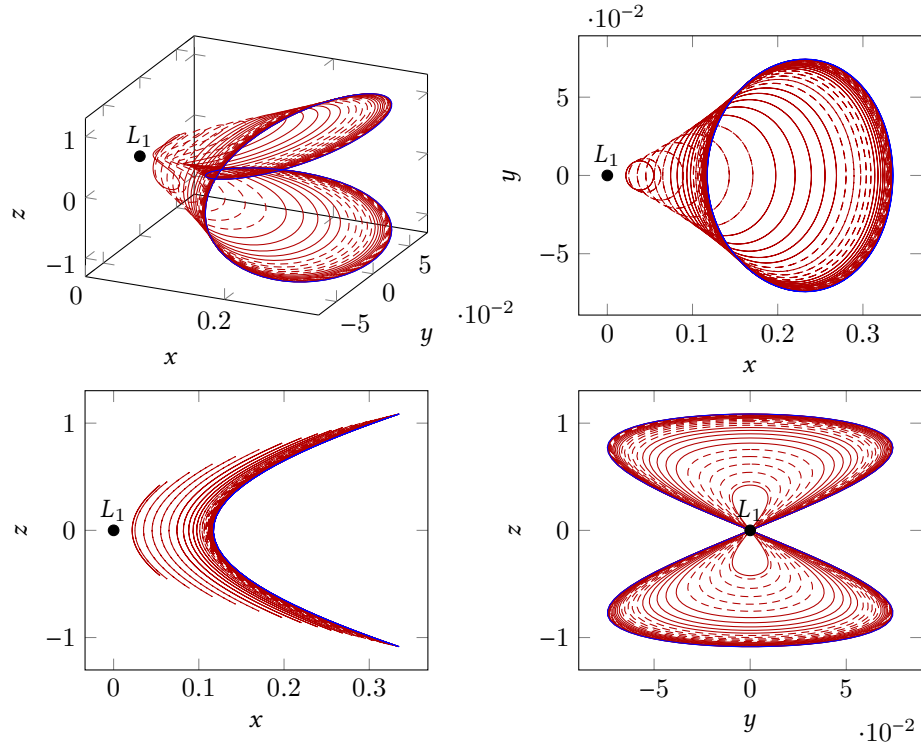


Figure 1.10 – Family of eight-shape orbits in the {Earth-Moon} system in Richardson coordinates obtained by a Newton-like method and continuation on the energy. The first fixed excursion is $A_z = 630 \times 10^3$ km and the final energy is -1.59 in normalized units (corresponding to a quasi-null z -excursion).

1.5.2 Linear Approximation

Let us introduce some basic dynamical tools.

Monodromy Matrix

The monodromy matrix gives us information about the influence of perturbations around the periodic orbit. Let us consider a periodic solution $x^*(\cdot)$ of period T , the flow from the initial point $x_0^* = x^*(0)$ is denoted by $\phi(t, x_0^*)$.

We consider a small perturbation δx_0^* , and we defined the evolution of the perturbation for $t \geq 0$

$$\delta x(t) = \phi(t, x_0^* + \delta x_0^*) - \phi(t, x_0^*).$$

At time T , it holds that

$$\delta x(T) = \phi(T, x_0^* + \delta x_0^*) - \phi(T, x_0^*),$$

which first-order approximation is

$$\delta x(T) = \frac{\partial \phi(T, x_0^*)}{\partial x_0} \delta x_0^*.$$

This leads to the definition of the monodromy matrix.

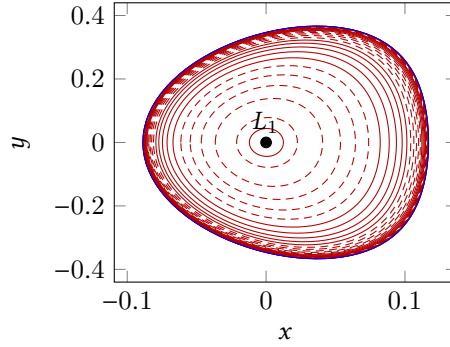


Figure 1.11 – Family of planar Lyapunov orbits in the {Earth-Moon} system in Richardson coordinates obtained by a Newton-like method and continuation on the energy. The final energy is -1.6001 in normalized units.

Definition 10 (Monodromy matrix): *The matrix*

$$M = \frac{\partial \phi(T, x_0^*)}{\partial x_0}$$

determines whether initial perturbations x_0^ from the periodic orbit $x^*(\cdot)$ decay or grow. This matrix is called the monodromy matrix.* \diamond

For a complete presentation, see [46].

Next, a well known property of the monodromy matrix is introduced.

Proposition 1: *Let us consider the dynamical system $\dot{x} = f(x)$ and a periodic solution x^* . The monodromy matrix M is the matrix $\Phi(T)$ where Φ is a solution of the linearized system*

$$\begin{cases} \frac{\partial \Phi}{\partial t} = \frac{\partial f(x^*)}{\partial x} \Phi, \\ \Phi(0) = \text{Id}. \end{cases}$$

Proof: The flow satisfies the following equation

$$\frac{\partial \phi}{\partial t}(t, x_0) = f(\phi(t, x_0))$$

with the initial condition $\phi(0, x_0) = x_0$. We differentiate this equation with respect to the initial condition and obtain

$$\frac{\partial}{\partial t} \frac{\partial \phi(t, x_0)}{\partial x_0} = \frac{\partial f(\phi)}{\partial \phi} \frac{\partial \phi(t, x_0)}{\partial x_0}. \quad \blacksquare$$

Eigenvalues of Monodromy Matrix

Definition 11 (Floquet multipliers): *The eigenvalues of the monodromy matrix are called the Floquet multipliers (or characteristic multipliers).* \diamond

Using the Floquet theorem (see [46]), it can be proved that the monodromy matrix has $+1$ as an eigenvalue with a corresponding eigenvector $f(x_0^*)$ which is tangent to the periodic orbit at x_0^* (see [52, p. 101]).

Drawing a connection between the monodromy matrix and the Poincaré map, one can show that $+1$ is an eigenvalue of the matrix. Moreover, because the CRTBP is a Hamiltonian system (see Meyer, Hall, and Offin [62] and Vogtmann, Weinstein, and Arnold [87]), this

eigenvalue has algebraic multiplicity of at least 2. Because the monodromy matrix of an autonomous Hamiltonian system is symplectic, it holds that, if λ is an eigenvalue, then so are λ^{-1} , $\bar{\lambda}$ and $\bar{\lambda}^{-1}$ with the same multiplicity. For details about all these properties, refer to [52, section 4.3].

This leads to the following property for the CRTBP system.

Proposition 2 : *For the CRTBP, eigenvalues of the monodromy matrix satisfy*

$$\lambda_1 > 1, \quad \lambda_2 < 1, \quad \lambda_3 = \lambda_4 = 1, \quad \lambda_5 = \bar{\lambda}_6, \quad |\lambda_5| = 1,$$

where λ_1 and λ_2 are reals.

Note that this is true for the restricted planar system without the complex eigenvalues λ_5 and λ_6 .

Stability of Periodic Orbits

Let us introduce another dynamical tool: the Poincaré map.

Definition 12: *Let Σ be a section surface of co-dimension 1 chosen in such a way that all trajectories that cross Σ in a neighborhood of $q \in \Sigma$ meet two requirements*

- *the trajectories intersect Σ transversely,*
- *they cross Σ in the same direction.*

Let $t_\Sigma(q)$ be the time taken for a trajectory $\phi(t, q)$ to first return to Σ . The Poincaré map is defined by

$$P(q) = \phi(t_\Sigma(q), q). \quad \diamond$$

We remark that a periodic orbit is a fixed point of $P(\cdot)$.

Note that the monodromy matrix has 1 as an eigenvalue with corresponding eigenvectors tangent to the transversal periodic orbit. Since this eigenvector is not in Σ , one can choose an appropriate basis such that the remaining $(n - 1)$ eigenvalues of M are those of $\frac{\partial P(q^*)}{\partial q}$. These eigenvalues are independent of the choice of Σ . As a result of this independence, the periodic orbit is stable if the remaining $(n - 1)$ eigenvalues of M are smaller than 1 in modulus. The orbit $x^*(\cdot)$ is unstable if there exists one eigenvalue λ with $|\lambda| > 1$. The eigenvalues of the Poincaré map determine what happens to small perturbations around q^* within Σ .

1.5.3 Numerical Computation

Local Approximation

Using the Poincaré map it can be shown that the eigenvectors corresponding to eigenvalues other than 1 of the monodromy matrix are linear approximations of the invariant manifolds of the periodic orbit. The eigenvector associated with eigenvalue λ_1 is in the unstable direction and the eigenvector associated with eigenvalue λ_2 is in the stable direction.

Algorithm

Based on that, the method to compute invariant manifolds is the following:

1. First, for ξ_0 a point of the periodic orbit, we compute the monodromy matrix and its eigenvectors. Let's denote by $Y^s(\xi_0)$ the normalized stable eigenvector and by $Y^u(\xi_0)$ the normalized unstable eigenvector.

2. Then, let

$$\begin{aligned}\xi^{s\pm}(\xi_0) &= \xi_0 \pm \alpha Y^s(\xi_0), \\ \xi^{u\pm}(\xi_0) &= \xi_0 \pm \alpha Y^u(\xi_0),\end{aligned}\tag{1.21}$$

be the initial guesses for (respectively) the stable and unstable manifolds. The magnitude of α should be small enough to be within the validity of the linear estimate but not too small to keep a reasonable time of escape or convergence (for instance, see [42] for a discussion on the value of α).

3. Finally, we integrate numerically the unstable vector forward in time, using both α and $-\alpha$ to generate the two branches of the unstable manifold denoted by $W^{u\pm}(\xi_0)$. We do the same for the stable vector only backward in time, and we obtain the two branches of the stable manifold $W^{s\pm}(\xi_0)$ (see Figure 1.12).

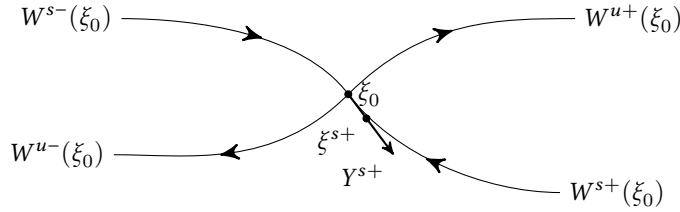


Figure 1.12 – Illustration of the method to compute invariant manifolds.

With this procedure, we are able to compute the invariant manifolds of any Lissajous, Halo, or Lyapunov orbit for any energy greater than the energy of L_i . The complete algorithm is described in Algorithm 1.2. We present an algorithm to propagate the invariant manifolds during a given time parameter. We can easily adjust this algorithm to propagate until a certain plane, for instance the set defined by $x = 1 - \mu$, etc. (see Chapter 2).

Algorithm 1.2: Numerical Computation of Invariant Manifolds

Require: α : parameter defined in (1.21) (depends on the CRTBP)

Require: $(\xi_i)_{i \in I}$: set of points of the considered periodic orbit

Require: T : time of propagation

- 1: **for all** $i \in I$ **do**
- 2: Compute the monodromy matrix by finite differences
- 3: Compute the normalized stable eigenvector $Y^s(\xi_i)$ and the normalized unstable eigenvector $Y^u(\xi_i)$
- 4: Perturb in the four directions to get four branches

$$\begin{aligned}\xi_i^{s\pm} &\leftarrow \xi_i \pm \alpha Y^s(\xi_i), \\ \xi_i^{u\pm} &\leftarrow \xi_i \pm \alpha Y^u(\xi_i)\end{aligned}$$

- 5: Propagate the trajectories with the initial conditions $\xi_i^{s\pm}$ and $\xi_i^{u\pm}$

$$\phi(T, \xi_i^{s-}), \quad \phi(T, \xi_i^{s+}), \quad \phi(T, \xi_i^{u-}), \quad \phi(T, \xi_i^{u+}).$$

- 6: **end for**

Some examples

In appendix B, we present a software developed in FORTRAN90 for Airbus Defence and Space. This software computes periodic orbits with prescribed energy, and its associated invariant manifolds.

Invariant manifolds can be seen as *tubes*, especially in the spatial case. Here we plot some manifolds coming from the periodic orbits that we presented in the previous sections. In Figure 1.13, we plotted the manifolds for the previous Halo orbit with an energy of -1.50042 . We propagate the manifolds during a time equal to 5.0 in the normalized system. The perturbation parameter introduced in (1.21) is $\alpha = 1 \times 10^{-4}$.

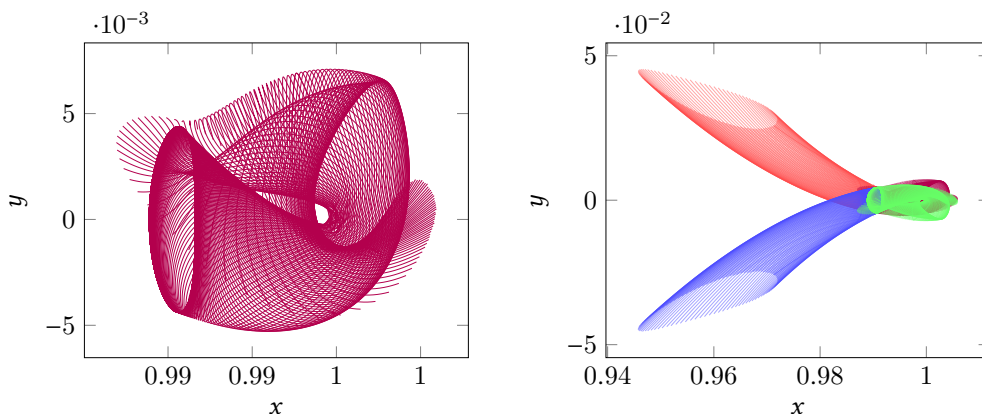


Figure 1.13 – Invariant manifolds of energy $\mathcal{E} = -1.50042$ of the Halo orbit around L_1 in the {Sun-Earth} system. On the left: an unstable manifold near the second primary. On the right: the four manifolds. The propagation time is equal to 5.0 in the normalized system, and the perturbation parameter α is equal to 1×10^{-4} .

In Figure 1.14, we plot the manifolds for an “eight-shape” periodic orbit around L_1 in the {Earth-Moon} system. We propagate the manifolds during a time of 6.0 in the normalized units. We used the same perturbation parameter as for the Halo manifolds.

To finish, we plot in Figure 1.15 the invariant manifolds of a Lyapunov orbit (in planar case) in the {Earth-Moon} system. We have chosen an energy of -1.60 . We propagate the invariant manifolds during a time equal to 8.0. Once again, we used the same perturbation parameter α .

1.5.4 Stability of Manifolds

The study of the stability of invariant manifolds is of great interest. Indeed, in order to design spacecraft missions using invariant manifolds, the general rule is: the more stable the manifolds, the better they can be followed. There are two kinds of stability. The first one is shape conserving stability. We observe in with Figures 1.13, 1.14 and 1.15 that this stability depends on the system considered and the periodic orbit type. We see that manifolds of Halo orbits are not very stable and cannot be used for long time propagation whereas the invariant manifolds of eight-shape orbits are very stable but with low amplitude. Finally, the invariant manifolds of Lyapunov orbits are stable but for very low energy.

Another stability concept is measured by Lyapunov exponents. The concept of Lyapunov exponents (also known as characteristic exponents) was introduced in [59] to investigate the stability properties of solutions of differential equations, and has been used extensively and studied in the literature. Lyapunov exponents measure the exponential

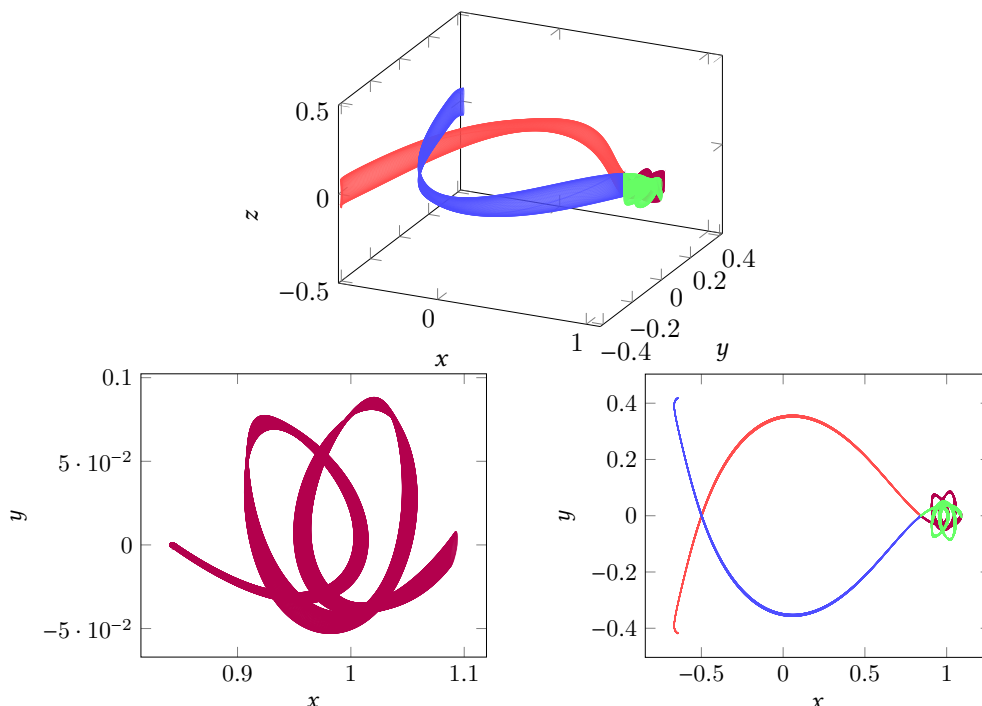


Figure 1.14 – Invariant manifolds of the eight-shape orbit around L_1 in the {Earth-Moon} system of energy $\mathcal{E} = -1.59$. Top: a 3D view of the manifolds. Left: an unstable manifold near the second primary. Right: The four manifolds. The propagation time is equal to 6.0 in normalized system, and the perturbation parameter α is equal to 1×10^{-4} .

convergence or divergence of nearby trajectories in a dynamical system, and provide indications on the behavior in large time of solutions under infinitesimal perturbations. We refer to Archambeau, Augros, and Trélat [6] for a study in the case of the eight-shape orbits.

1.5.5 Theoretical Existence of Invariant Manifolds as Separatrices

To finish this chapter, we sketch the study of the linear flow around equilibrium points. Indeed, this study gives us crucial information for designing spacecraft missions. Studying the linearization of the dynamics near the equilibria is an essential ingredient for understanding the more complete nonlinear dynamics. It can be shown that for a value of energy just above that of L_i (where L_i is the equilibrium point we are considering), the nonlinear dynamics in the equilibrium region is qualitatively the same as the linearized one, we will briefly describe this in the remainder of this section. See [29, 46, 50] and [52, chap. 9].

Canonical Transformation

By a canonical (symplectic) transformation, the linearized Hamiltonian can be written. It is the second-order part of the general Hamiltonian

$$H_2 = \lambda q_1 p_1 + \frac{\omega_p}{2} (q_2^2 + p_2^2) + \frac{\omega_v}{2} (q_3^2 + p_3^2), \quad (1.22)$$

where λ , ω_v and ω_p are the ones defined in (1.14). Variables q_i and p_i are the canonical variables, see Jorba and Masdemont [50] for the details of the canonical transformation.

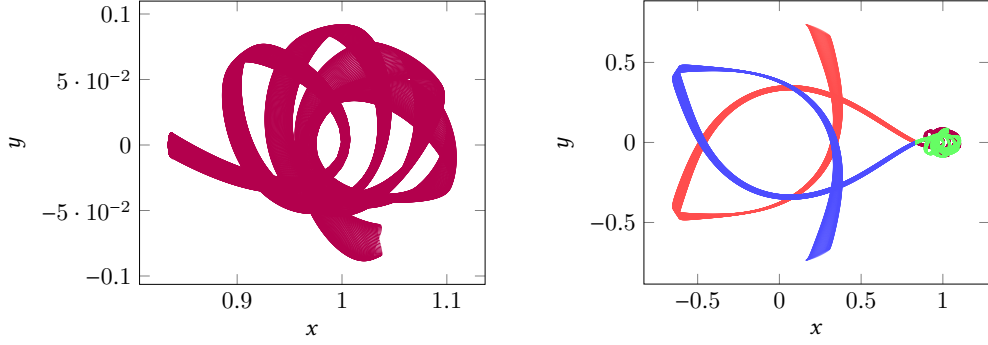


Figure 1.15 – Invariant manifolds of the Lyapunov orbit in the {Earth-Moon} system of energy $\mathcal{E} = -1.60$. Left: an unstable manifold near the second primary. Right: The four manifolds. The propagation time is equal to 8.0 in the normalized system, and the perturbation parameter α is equal to 1×10^{-4} .

A short computation gives the linearized equations in the form

$$\begin{aligned} \dot{q}_1 &= \lambda q_1, & \dot{p}_1 &= -\lambda p_1, \\ \dot{q}_2 &= \omega_p p_2, & \dot{p}_2 &= -\omega_p q_2, \\ \dot{q}_3 &= \omega_v p_3, & \dot{p}_3 &= -\omega_v q_3. \end{aligned}$$

Then solutions can easily be written as

$$\begin{aligned} q_1(t) &= q_1^0 e^{\lambda t}, & p_1(t) &= p_1^0 e^{-\lambda t}, \\ q_2(t) + ip_2(t) &= (q_2^0 + ip_2^0) e^{-i\omega_p t}, \\ q_3(t) + ip_3(t) &= (q_3^0 + ip_3^0) e^{-i\omega_v t}. \end{aligned}$$

Invariant Manifolds as Separatrices

For positive h and c , we defined the region denoted by \mathcal{R} as

$$H_2 = h, \quad |p_1 - q_1| \leq c.$$

This region is homeomorphic to the product of a 4-sphere by an interval I : $\mathbf{S} \times I$. Indeed, for each value of $(p_1 - q_1)$ in $[-c, c]$, the equation (1.22) can be written as

$$\frac{\lambda}{4}(q_1 + p_1)^2 + \frac{\omega_p}{2}(q_2^2 + p_2^2) + \frac{\omega_v}{2}(q_3^2 + p_3^2) = h + \frac{\lambda}{4}(q_1 - p_1)^2.$$

The bounding 4-sphere of \mathcal{R} for $p_1 - q_1 = -c$ is denoted by n_1 and the one for $p_1 - q_1 = c$ by n_2 .

Following the nomenclature of [52], we call the set of points where $q_1 + p_1 = 0$ the *equator* and the sets where $q_1 + p_1 > 0$ and $q_1 + p_1 < 0$, the *northern* and the *southern hemispheres*, respectively.

Classification of orbits for the linear flow. To analyze the flow in \mathcal{R} , we consider the different projections onto the (q_1, p_1) -plane, the (q_2, p_2) -plane, and the (q_3, p_3) -plane. In Figure 1.16, we only plot the representation of the *saddle* projection onto the (q_1, p_1) -plane, the two other projections are only circles.

Note that each point in the projection (q_1, p_1) -plane corresponds to a 3-sphere \mathbf{S}^3 in \mathcal{R}

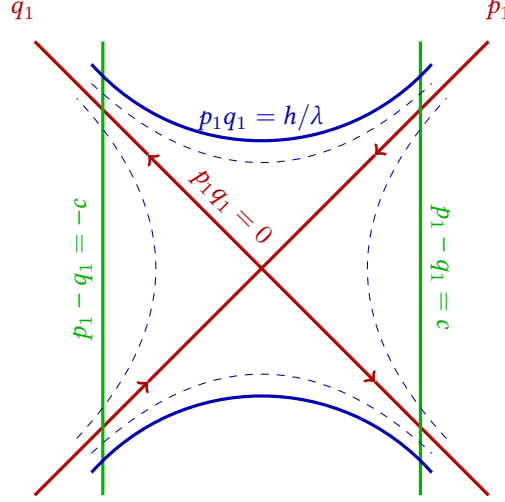


Figure 1.16 – Saddle projection of the flow in the equilibrium region. Only the projection onto the (p_1, q_1) -plane (with axis titled by 45°).

given by

$$\frac{\omega_p}{2}(q_2^2 + p_2^2) + \frac{\omega_v}{2}(q_3^2 + p_3^2) = h - \lambda q_1 p_1.$$

We distinguish 4 categories of orbits:

1. The points $q_1 = p_1 = 0$ correspond to an invariant 3-sphere \mathbf{S}_h^3 of *bounded orbits* (periodic and quasi-periodic) in \mathcal{R} .
2. The four half open segments on the axes, $q_1 p_1 = 0$, correspond to four cylinders of orbits asymptotic to the previous invariant 3-sphere ($q_1 = p_1 = 0$). They are called *asymptotic orbits* and form the stable (for $p_1 = 0$ and increasing time) and the unstable (for $q_1 = 0$ and decreasing time) manifolds presented in definition 9. The stable manifolds are given by

$$\frac{\omega_p}{2}(q_2^2 + p_2^2) + \frac{\omega_v}{2}(q_3^2 + p_3^2) = h, \quad q_1 = 0.$$

We denote by $W_+^s(\mathbf{S}_h^3)$ the branch going from right to left ($p_1 > 0$) and by $W_-^s(\mathbf{S}_h^3)$ the branch going from left to right ($p_1 < 0$).

The unstable manifolds are given by

$$\frac{\omega_p}{2}(q_2^2 + p_2^2) + \frac{\omega_v}{2}(q_3^2 + p_3^2) = h, \quad p_1 = 0.$$

We denote by $W_+^u(\mathbf{S}_h^3)$ the branch going from right to left ($q_1 > 0$) and by $W_-^u(\mathbf{S}_h^3)$ the branch going from left to right ($q_1 < 0$).

3. The hyperbolic segments defined by $q_1 p_1$ equal to a positive constant corresponds to orbits which cross the region \mathcal{R} from one bounding 4-sphere to the other: $p_1 - q_1 = -c$ to $p_1 - q_1 = +c$ in the southern hemisphere and $p_1 - q_1 = +c$ to $p_1 - q_1 = -c$ in the northern hemisphere. Because these orbits transit from one realm to another, we call them *transit orbits*.

4. Finally, the hyperbolic segments defined by $q_1 p_1$ equal to a negative constant corresponds to orbits connecting the two hemispheres on the same bounding-sphere n_1 or n_2 . Since these orbits return to the same realm, we call them *non-transit orbits*.

Using the *reduction to the center manifold*, one can show that these results can be extended for the nonlinear dynamics. For details, see [52, sec. 9.8].

Remark 1.4: Invariant Manifolds as Separatrices

The main purpose of this section is that, together, the asymptotic orbits form 4-dimensional stable and unstable manifolds, that can be seen as “tubes” $\mathbf{S}^3 \times \mathbf{R}$ to the invariant 3-sphere \mathbf{S}_h^3 in a 5-dimensional energy surface. Moreover, as we have seen, these manifolds separate two distinct types of orbits: transit and non-transit orbits. The transit orbits are those *inside* the 4-dimensional manifold tube. The non-transit orbits are those outside the tube.

Let us remark that this is coherent with the plot of the Hill region (see Section 1.5). The forbidden realm can be seen as barrier for non-transit orbits.

This is a very useful property to construct spacecraft missions. Indeed, by computing the manifolds and interpreting them as *gravitational currents*, one can easily find which trajectories realize a transit path or not. This will be the focus of the next chapter.

From Impulsive Transfer to Low Thrust Transfer between Manifolds

Contents

2.1	Design of Impulse Transfer Missions using Manifolds	62
2.1.1	Trajectories with Prescribed Itineraries	63
2.1.2	Heteroclinic and Homoclinic Orbits	64
2.2	Model	67
2.2.1	Controlled Dynamics	68
2.2.2	Controllability	69
2.3	Optimal Control Theory in a Nutshell	71
2.3.1	General Framework	71
2.3.2	The Pontryagin Maximum Principle (PMP)	72
2.4	Numerical Methods	73
2.4.1	Direct Methods	74
2.4.2	Indirect Methods	74
2.5	Numerical Continuation Methods	76
2.5.1	Discrete Continuation	77
2.5.2	Piecewise Linear Continuation	78
2.6	Construction of an Optimal Control Problem (OCP)	79
2.6.1	From an Impulse Solution to an Optimal Control Problem	79
2.6.2	Minimization of the L^1 -norm of the Control	83
2.6.3	Minimization of the L^2 -norm of the Control	86
2.7	Numerical Method: From Impulse Transfer to Low Thrust Transfer	88
2.7.1	Final State Continuation	88
2.7.2	Thrust Continuation	89
2.8	Description of the Algorithm	90
2.8.1	Principle	90
2.9	Numerical Results	93

2.9.1	Transfer between Invariant Manifolds: {Earth-Moon} System, Halo Orbits	93
2.9.2	Transfer between Invariant Manifolds: {Sun-Earth} System, Halo Orbits	95
2.9.3	Study of the Transfer Time Parameter	96

In chapter 1, the dynamical paradigm used in this thesis was introduced. We noted that there exist periodic orbits around equilibrium points of the dynamical system and that in turn there exist invariant manifolds associated with these periodic orbits.

In the first section of this chapter, we briefly recall how these manifolds can be used to design spacecraft missions with high thrust (or impulse). The principle is to use the invariant manifolds as a map of *gravitational currents* and to realize transfers from one current to another using impulses, *i.e.*, instantaneous changes of velocity usually denoted by ΔV . This section also contains some results on the state of the art, namely on the homoclinic and heteroclinic orbits.

In this thesis we consider a low thrust engine, hence, such methods fail. Indeed, as we will see in Section 2.2, the low thrust model does not allow for instantaneous changes in velocity. We then introduce tools from optimal control theory (Section 2.3) and associated numerical methods (Section 2.4). We recall the principle of continuation methods and we develop the corresponding algorithms (Section 2.5) because we use them extensively in the method that we developed. After that, we explain how we can use an impulsive transfer to build an optimal control problem (Section 2.6). To do that we define both cost functions considered in this thesis (that we want to minimize): the L^1 -norm of the control, which corresponds to the physical mass that we want to maximize but which is numerically difficult to optimize, and the L^2 -norm of the control, which corresponds to the physical energy and is smoother. We introduce the continuation performed between these two related problems.

The last sections are about the numerical resolution of the previously formulated problems and the general method we developed. We use indirect methods based on the application of the Pontryagin Maximum Principle (PMP), and because the main difficulty of these methods is to initialize them, we introduce other continuations for the final state and the thrust to improve robustness (Section 2.7). The general algorithm is summarized and some numerical results are presented in sections 2.8 and 2.9.

What we do in this thesis is to use the dynamical information of the invariant manifolds as *gravitational current* to initialize the resolution of an optimal control problem of orbital transfer in the CRTBP. The purpose of this chapter is to introduce the tools that will contribute to our method for interplanetary mission design. One particularly important issue is how to connect two invariant manifolds with low thrust control.

2.1 Design of Impulsive Transfer Missions using Manifolds

The study of invariant manifolds has been of great interest for half a century. The reason is that invariant manifolds provide a geometric understanding of the dynamics in the CRTBP which is a local approximation of the N -body problem. Thanks to the computation of invariant manifolds (or tubes), we are able to understand, at a given energy, a part of the capture region of the moon (with the stable manifolds of the L_1 and L_2 Halo orbits). Of course, the Moon is just an example, and this process can be applied to other primaries.

Invariant manifolds also provide a set of natural trajectories connecting regions of the three body problem. This is because they are separatrices of the dynamics as explained in

Section 1.5.5. In order to find trajectories that minimize the fuel consumption, the use of these orbits is crucial. The basic idea is to patch CRTBPs, as is done for two-body problems, so the knowledge of different invariant manifolds for the different CRTBPs provides a *map of gravitational currents*. Using this map, one can then design a mission by minimizing the sum of the different impulses ΔV_i that allow to go from one manifold to another (or to enter the interior of the cylinders of asymptotic orbits).

Remark 2.1: Interplanetary Transport Network (Wikipedia)

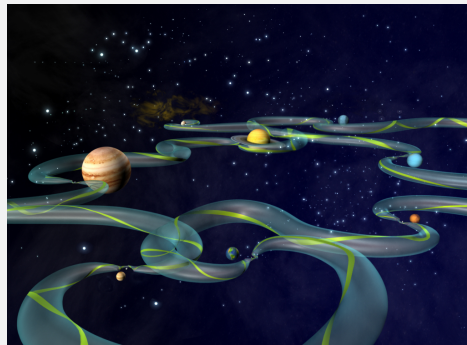


Image Wikipedia.

The Interplanetary Transport Network (ITN) [76] is a collection of gravitationally determined pathways through the Solar System that require very little energy for an object to follow.

The ITN makes particular use of Lagrange points as locations where trajectories through space are redirected using little or no energy.

These points have the peculiar property of allowing objects to orbit around them, despite lacking an object to orbit. While they use little energy, the transport can take a very long time.

We see in Remark 2.1 that much effort has been devoted to computing a network of these manifolds. The artistic illustration gives us a good intuition on how this network can be used. For a precise description of this, one can see [52] and more specifically the article by Ross [76] in the American Scientist Magazine. Let us note that we can draw a connection to the *gravitational assist* used for patching orbits of the 2-body problem.

In this thesis, the instantaneous transfer from one tube to another is not possible. Indeed, because we want to design spacecraft mission with low thrust, we cannot approximate the control as an instantaneous change of velocity (ΔV). Hence, we establish a method to go from one invariant manifold to another (or inside manifolds) using low thrust.

2.1.1 Trajectories with Prescribed Itineraries

Invariant manifolds can be used to find trajectories with prescribed itineraries. To illustrate the method, we consider the planar motion of a spacecraft in the {Earth-Moon} system. This is called the *planar circular restricted three body problem* (PCRTBP). We label the realm around Earth with \mathcal{R}_E , the realm around the Moon with \mathcal{R}_M and the exterior realm with \mathcal{R}_X (see Figure 2.1). Let us describe a method to find a trajectory with a prescribed itinerary.

Step 1. First, we choose an appropriate energy that allows for motion in the area that we want to reach. Assume that we want the particle to go between all three realms \mathcal{R}_X , \mathcal{R}_M and \mathcal{R}_E , then we need to choose an energy greater than the one of the point L_2 (see Section 1.3): for instance, $\mathcal{E} = -1.59$.

Step 2. We compute the L_1 and L_2 periodic orbits around the two equilibrium points using the numerical method described in Section 1.4. In Figure 2.1, we have computed two Lyapunov orbits.

Step 3. We define the four Poincaré surfaces of section U_i , $i \in \llbracket 1, 4 \rrbracket$ in the general 3D case but this can easily be restricted to the planar case to obtain the examples shown in Figure 2.1. The definitions of these surfaces are

$$\begin{aligned} U_1 &= \{(x, y, z); x < 0, y = 0\}, \\ U_2 &= \{(x, y, z); x = 1 - \mu, y < 0\}, \\ U_3 &= \{(x, y, z); x = 1 - \mu, y > 0\}, \\ U_4 &= \{(x, y, z); x < -1, y = 0\}. \end{aligned}$$

This way, the U_i are strategically placed (see [52]): if each U_i contains the (non empty) intersection between two of the invariant manifolds, then by computing it, we find a trajectory which connects different realms. This result is based on the fact that invariant manifolds are separatrices of the dynamics as stated in Remark 1.4.

Step 4. We compute the invariant manifolds associated with the two periodic orbits as explained in Section 1.5. We propagate them to the different Poincaré surfaces of section U_i , $i \in \llbracket 1, 4 \rrbracket$ to obtain the intersection of each manifolds with the Poincaré cuts. Figure 2.1 presents the example of the {Earth-Moon} system. There are eight invariant manifolds, four for each of the two periodic orbits. Thanks to this method we are able, either to find a trajectory without any impulse respecting the prescribed itinerary, or, one with a finite number of impulses (for instance, when we can find an intersection in the positions of two invariant manifolds but with a velocity gap).

This method can be extended for patched CRTBP. For instance, we may consider in a close realm of the Earth, the {Earth-Moon} system, then the {Sun-Earth} system and so on.

This method cannot be used with a low thrust engine. Indeed, an instantaneous velocity change cannot be performed. In this chapter, we develop a methodology to go from one invariant manifold to another with low thrust.

2.1.2 Heteroclinic and Homoclinic Orbits

Heteroclinic and homoclinic orbits are classical concepts of the dynamical system theory.

Definition 13: *In the phase portrait of a dynamical system, a heteroclinic orbit (sometimes called a heteroclinic connection) is a path in the phase space which joins two different equilibrium points. If the equilibrium points at the start and end of the orbit are the same, then the orbit is called a homoclinic orbit.*

This definition is extended to the case where the equilibria are periodic orbits, hence, in our context, we talk about heteroclinic and homoclinic orbits between periodic orbits around Lagrange points. Note that such periodic orbits must have the same energy.

Following [52], the method to find heteroclinic or homoclinic orbit in the CRTBP is to find intersections between invariant manifolds in both position and velocity. Indeed, if there exists an intersection between the stable and unstable invariant manifolds of the same periodic orbit around one libration point, then there exists a homoclinic orbit asymptotically starting and going to the considered periodic orbit. Hence, the trajectory belongs both to the stable and the unstable invariant manifolds.

If there exists an intersection between stable and unstable manifolds of two different periodic orbits of the same CRTBP system (*i.e.*, around two different Lagrange points),

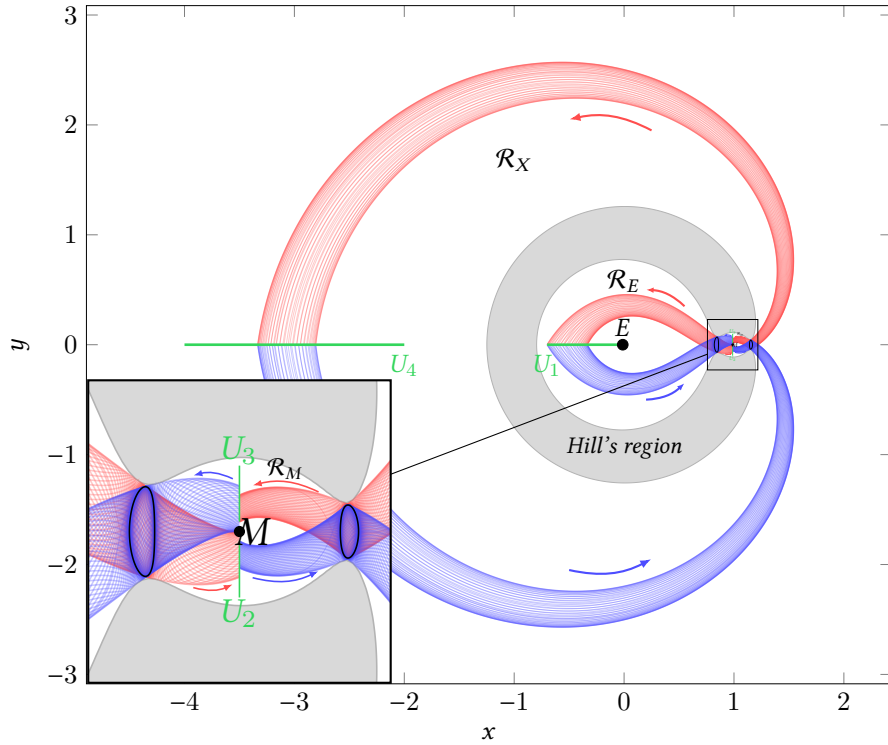


Figure 2.1 – The eight invariant manifolds associated with the Lyapunov orbits of the points L_1 and L_2 in the {Earth-Moon} system, at a specific energy of $\mathcal{E} = -1.59$. The different Poincaré surfaces of section U_i are represented. In such a configuration, one can find a trajectory with a prescribed itinerary visiting the three realms \mathcal{R}_X , \mathcal{R}_M and \mathcal{R}_E .

then there exists a heteroclinic orbit asymptotically connecting two different periodic orbits around two different libration points.

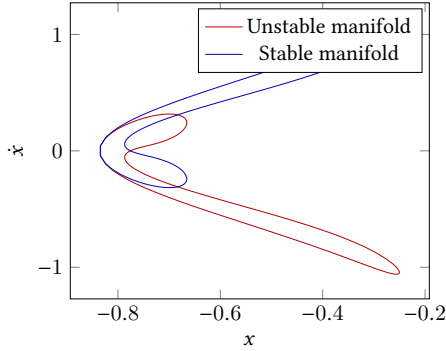
To compute these possible intersections, we use the Poincaré surface of section defined above in Section 2.1.1 step 3, and plotted in Figure 2.1.

There is no general method to find these intersections for the circular restricted three body problem because of the dimension of the manifolds. Indeed, the spacecraft is embedded in \mathbf{R}^6 . We saw in Section 1.5.5 that the tubes are topologically $\mathbf{S}^3 \times \mathbf{R}$, so the Poincaré cut (e.g., U_i) is a topological 3-sphere \mathbf{S}^3 (in \mathbf{R}^4). It is not obvious how to find the intersection region inside the Poincaré cuts since its projection onto the (y, \dot{y}) -plane (for U_2 or U_3) or the (x, \dot{x}) -plane (for U_1 or U_4) and the (z, \dot{z}) -plane are 2-dimensional disks. To overcome this difficulty, one can fix for example $z = c$ and impose that $\dot{z} = 0$. For details about this problem, see [52, chap. 9].

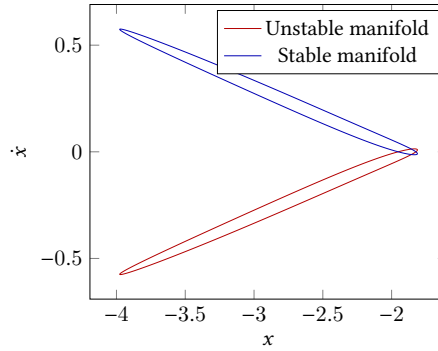
To illustrate the method, we consider here the simpler *planar circular restricted three body problem* (PCRTBP). Indeed, in that case, $z = 0$ and $\dot{z} = 0$, and the intersection has to be searched for only in the (y, \dot{y}) -plane for the $U_{2,3}$ Poincaré cuts (and in the (x, \dot{x}) -plane for the $U_{1,4}$ Poincaré cuts).

Let's apply the method to find these connecting orbits in the system illustrated in Figure 2.1. We consider the {Earth-Moon} system and Lyapunov periodic orbits around L_1 and L_2 with an energy $\mathcal{E} = -1.56$. We have changed the energy to allow for the existence of intersections in each Poincaré cut.

For each Poincaré cut, we have fixed one variable x or y , hence we look for an intersection in \mathbf{R}^3 . We are considering invariant manifolds of the same energy, so this reduces



(a) Poincaré cut U_1 of invariant manifolds from a Lyapunov orbit around L_1 . The three intersections correspond to three different homoclinic orbits to the periodic orbit.



(b) Poincaré cut U_4 of invariant manifolds from a Lyapunov orbit around L_2 . The three intersections correspond to three different homoclinic orbits to the periodic orbit.

Figure 2.2 – Different Poincaré cuts, U_1 and U_4 , for the {Earth-Moon} system with two Lyapunov orbits around L_1 and L_2 at an energy $\mathcal{E} = -1.56$.

the search space further to \mathbf{R}^2 . Once both variables, (x, \dot{x}) or (y, \dot{y}) , have been found in the Poincaré cut, the last one, \dot{y} or \dot{x} , is deduced by the energy relation (see equation (1.10))

$$\mathcal{E} = \frac{1}{2}(\dot{x}^2 + \dot{y}^2) + U_\mu(x, y).$$

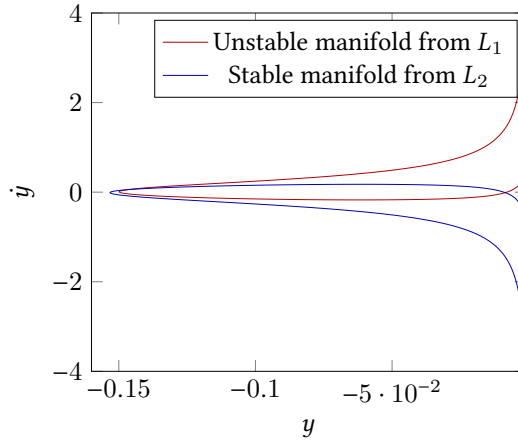
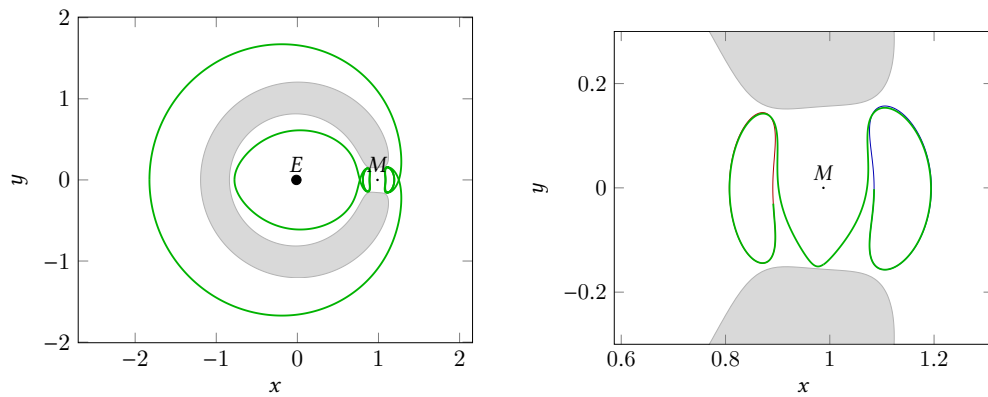


Figure 2.3 – Poincaré cut U_2 of invariant manifolds from Lyapunov orbits around L_1 and L_2 . The three intersections correspond to three different heteroclinic orbits connecting the two periodic orbits. We consider the {Earth-Moon} system with two Lyapunov orbits around L_1 and L_2 with an energy of $\mathcal{E} = -1.56$. The U_3 section is similar.

In figures 2.2 and 2.3, we plot the different Poincaré cuts for the system. Sub-figures 2.2a and 2.2b illustrate the intersections used to compute homoclinic orbits and Figure 2.3 is for the computation of heteroclinic orbits between the two Lyapunov orbits around Lagrange points L_1 and L_2 . Finally, see Figure 2.4 for two examples of the obtained orbits. The two homoclinic orbits to the Lyapunov orbits around L_1 and L_2 , respectively in the *interior* and *exterior* realms, are plotted in Figure 2.4a. The heteroclinic orbit between the two Lyapunov

orbits computed with the intersection on the U_2 -plane is plotted in Figure 2.4b



(a) Two homoclinic orbits for the two Lyapunov orbits around L_1 and L_2 . They have been computed using intersections with the Poincaré cuts U_1 and U_4 .

(b) One heteroclinic orbit connecting the two Lyapunov orbits around L_1 and L_2 . It has been computed using an intersection with the U_2 Poincaré cut. A similar symmetric trajectory can be computed using the Poincaré cut U_3 .

Figure 2.4 – Examples of homoclinic and heteroclinic orbits for the {Earth-Moon} system with two Lyapunov orbits around L_1 and L_2 at energy $\mathcal{E} = -1.56$.

2.2 Model

Let us first introduce the model for the controlled spacecraft and some results on the controllability of the system. Recall that in chapter 1, we introduced the dynamics of the circular restricted three-body problem (CRTBP)

$$\begin{cases} \dot{x}_1 = x_4, \\ \dot{x}_2 = x_5, \\ \dot{x}_3 = x_6, \\ \dot{x}_4 = x_1 + 2x_5 - (1-\mu)\frac{x_1+\mu}{r_{13}^3} - \mu\frac{x_1-1+\mu}{r_{23}^3}, \\ \dot{x}_5 = x_2 - 2x_4 - (1-\mu)\frac{x_2}{r_{13}^3} - \mu\frac{x_2}{r_{23}^3}, \\ \dot{x}_6 = -(1-\mu)\frac{x_3}{r_{13}^3} - \mu\frac{x_3}{r_{23}^3}. \end{cases}$$

Denoting by $F_0(\cdot)$ the associated vector field, in condensed form, we write the system as

$$\dot{\xi}(t) = F_0(\xi),$$

where $\xi = (x_1, x_2, x_3, x_4, x_5, x_6)$.

Note that, depending on the context, we use the notation $\xi = (x, y, z, \dot{x}, \dot{y}, \dot{z})$ or $x = (x_1, x_2, x_3, x_4, x_5, x_6)$, because it is more standard in the field of optimal control theory to use the second.

2.2.1 Controlled Dynamics

We first describe the model for the evolution of our spacecraft in the CRTBP. In non normalized coordinates (see (1.6)), the controlled dynamical system is as follow

$$m(t)\frac{d\mathbf{R}(t)}{dt} = -GM_1m(t)\frac{\mathbf{R}_{13}(t)}{R_{13}^3(t)} - GM_2m(t)\frac{\mathbf{R}_{23}(t)}{R_{23}^3(t)} + T(t),$$

where T is the spacecraft driving force, and m is the time dependent mass of the spacecraft. The equation for the evolution of the mass is

$$\dot{m}(t) = -\beta \|T(t)\|,$$

where β is computed from two parameters I_{sp} and g_0 . The specific impulse parameter (I_{sp}) is a measure of the efficiency of rockets and jet engines. It is defined by the total impulse (or change of momentum) delivered per unit of propellant consumed. Its time unit is the second. g_0 is the acceleration at the Earth's surface in m/s^2 . The inverse of the average exhaust speed, β , is equal to $\frac{1}{I_{sp}g_0}$. The units of β is second per meter. Throughout this manuscript we use the following values for these parameters

$$I_{sp} = 2000 \text{ s}, \quad \text{and} \quad g_0 = 9.81 \text{ m/s}^2.$$

Moreover, the thrust is constrained as follows

$$\forall t, \|T(t)\| \leq T_{\max}, \quad T_{\max} \in \mathbf{R}_+^*.$$

T_{\max} is the maximal thrust that the engine can generate.

Using the normalization parameters (1.2), and denoting by β_* the normalized counterpart of β , we obtain the normalized controlled dynamics:

$$\left\{ \begin{array}{l} \dot{x}_1 = x_4, \\ \dot{x}_2 = x_5, \\ \dot{x}_3 = x_6, \\ \dot{x}_4 = x_1 + 2x_5 - (1 - \mu) \frac{x_1 - x_1^0}{r_1^3} - \mu \frac{x_1 - x_2^0}{r_2^3} + \frac{t_*^2}{4\pi^2 l_*} T_{\max} \frac{u_1(t)}{m(t)}, \\ \dot{x}_5 = x_2 - 2x_4 - (1 - \mu) \frac{x_2}{r_1^3} - \mu \frac{x_2}{r_2^3} + \frac{t_*^2}{4\pi^2 l_*} T_{\max} \frac{u_2(t)}{m(t)}, \\ \dot{x}_6 = -(1 - \mu) \frac{x_3}{r_1^3} - \mu \frac{x_3}{r_2^3} + \frac{t_*^2}{4\pi^2 l_*} T_{\max} \frac{u_3(t)}{m(t)}, \\ \dot{m}(t) = -\beta_* \frac{t_*^2}{4\pi^2 l_*} T_{\max} \|u(t)\|, \end{array} \right.$$

where for all t , $\|u(t)\| \leq 1$. In the remainder of this thesis, we will denote the coefficient $\frac{t_*^2}{4\pi^2 l_*} T_{\max}$ by ϵ . Hence, we get :

$$\left\{ \begin{array}{l} \dot{x}_1 = x_4 \\ \dot{x}_2 = x_5 \\ \dot{x}_3 = x_6 \\ \dot{x}_4 = x_1 + 2x_5 - (1 - \mu) \frac{x_1 - x_1^0}{r_1^3} - \mu \frac{x_1 - x_2^0}{r_2^3} + \epsilon \frac{u_1(t)}{m(t)} \\ \dot{x}_5 = x_2 - 2x_4 - (1 - \mu) \frac{x_2}{r_1^3} - \mu \frac{x_2}{r_2^3} + \epsilon \frac{u_2(t)}{m(t)} \\ \dot{x}_6 = -(1 - \mu) \frac{x_3}{r_1^3} - \mu \frac{x_3}{r_2^3} + \epsilon \frac{u_3(t)}{m(t)} \\ \dot{m}(t) = -\beta_* \epsilon \|u(t)\| \end{array} \right.$$

In condensed form, we write the system as :

$$\left\{ \begin{array}{l} \dot{x} = F_0(x) + \frac{\epsilon}{m} \sum_{i=1}^3 u_i F_i(x), \\ \dot{m} = -\beta_* \epsilon \|u\|, \end{array} \right.$$

where F_0 is defined in (1.7) and

$$F_1(x) = \begin{pmatrix} 0 \\ 0 \\ 0 \\ 1 \\ 0 \\ 0 \\ 0 \end{pmatrix}, \quad F_2(x) = \begin{pmatrix} 0 \\ 0 \\ 0 \\ 0 \\ 1 \\ 0 \\ 0 \end{pmatrix}, \quad F_3(x) = \begin{pmatrix} 0 \\ 0 \\ 0 \\ 0 \\ 0 \\ 0 \\ 1 \end{pmatrix}.$$

Remark 2.2:

This system belongs to a well known class of controlled systems: the affine control systems. F_0 is called a *drift vector field* while the F_i are called *control vector fields*. Let us note that for these systems, the geometric control theory is very efficient (see [51, 48]).

2.2.2 Controllability

Controllability of the system is a natural and primordial question before beginning any transfer design. At present time, there is no general proof of controllability for the CRTBP. Next, we present some existing partial results.

In [23], it is proved that the CRTBP is controllable for a suitable sub-region of the phase-space, denoted by X_μ^1 , where the energy is greater than the energy of L_1 . The authors use geometric control techniques.

Theorem 2 For any $\mu \in (0, 1)$, and any positive ϵ , the circular restricted three-body problem is controllable on X_μ^1 .

The proof is based on the Poincaré recurrence theorem. In the next definition, we introduce the notion of recurrence.

Definition 14: A vector field F is said to be recurrent on a set X if, for each open set of X , there exist orbits that intersect the set infinitely many times

$$\forall x \in X, \forall V \in \mathcal{V}(x), \forall T \geq 0, \exists t > T, \exp(tF(x)) \in V. \quad \diamond$$

We sketch the proof of theorem 2 followed by the authors (see [31] or [23]).

Proof: The authors first defined the subset of the subspace

$$Q_\mu = \{x_{1,2,3} \in \mathbf{R}^3; x_{1,2,3} \neq (-\mu, 0, 0), x_{1,2,3} \neq (1 - \mu, 0, 0)\}$$

and $X_\mu = TQ_\mu \simeq Q_\mu \times \mathbf{R}^3$. Then, X_μ^1 is defined as the subset $X_\mu^1 = \{x \in X_\mu; \mathcal{E}(x) < \mathcal{E}(L_2)\}$. Based on that, the authors apply the control theorem of recurrent systems from [51] to obtain the following.

- X_μ^1 is a connected set.
- The control set defined by $\|u\| \leq 1$ is a neighborhood of the origin.
- For all $x \in X_\mu$, the set

$$\text{Span}_x \{F_1, F_2, F_3, [F_0, F_1], [F_0, F_2], [F_0, F_3]\}$$

is of rank 6. The $[\cdot, \cdot]$ operator is the Lie bracket, and it holds, for $i \in \{1, 2, 3\}$

$$[F_0, F_i](x) = F'_i(x)F_0(x) - F'_0(x)F_i(x) = -F'_0(x)F_i(x) = \frac{\partial F_0}{\partial x_{i+3}}.$$

This leads to

$$[F_0, F_1](x) = -\begin{pmatrix} 1 \\ 0 \\ 0 \\ 0 \\ -2 \\ 0 \end{pmatrix}, [F_0, F_2](x) = -\begin{pmatrix} 0 \\ 1 \\ 0 \\ 2 \\ 0 \\ 0 \end{pmatrix}, [F_0, F_3](x) = -\begin{pmatrix} 0 \\ 0 \\ 1 \\ 0 \\ 0 \\ 0 \end{pmatrix}.$$

Then, it holds that $\text{Span}_x \{F_1, F_2, F_3, [F_0, F_1], [F_0, F_2], [F_0, F_3]\} = \mathbf{R}^6$.

- The crucial point is to show that the vector field F_0 (the drift) is recurrent on X_μ^1 . Indeed, the uncontrolled CRTBP is a Hamiltonian system, and the system orbits are bounded on X_μ^1 . To show the last point, the projection of X_μ^1 onto the (x_1, x_2, x_3) -space has to be bounded. ■

The last step of the proof is the key point that cannot be extended to other subsets of the CRTBP. See [31, 23] for details.

The previous theorem is stated for a system with a non-varying mass. Using [24, prop. 2.2], one can extend it to the system with an evolving mass.

Theorem 3 For any $\mu \in (0, 1)$ and $\epsilon > 0$, there is a proper mass $\chi_0 > 0$ of the spacecraft (mass without fuel) that makes the system controllable on X_μ^1 .

Let us sketch the proof of [24, prop. 2.2].

Proof: Considering the initial mass m_0 , once the controllability is stated for a certain maximal thrust ϵ/m_0 , and denoting the control for the non-evolving system by γ , we set

$$m = m_0 \exp\left(-\beta_* \epsilon \int_0^t \|\gamma\| ds\right) > 0,$$

$$u = m\gamma.$$

That way, $\dot{m} = -\beta_* \epsilon \|u\|$ and $\|u\| < \epsilon$. If T is the resulting transfer time, the proper mass $\chi_0 = m_0 \exp(-\beta_* \epsilon T/m_0) > 0$ is such that $m \geq \chi_0$ on $[0, T]$. ■

Remark 2.3:

The controllability of the complete CRTBP has not yet been proved. Although for the different missions considered in this thesis, we do not satisfy the condition of staying on X_μ^1 , these results give an indication that we can indeed control our spacecraft.

2.3 Optimal Control Theory in a Nutshell

Let us first begin by stating the main theorem of optimal control theory. For references on Optimal Control Theory, see [84, 1, 16, 11, 56, 19, 71].

2.3.1 General Framework

We introduce a general framework which contains the problems that we consider.

Let n and m be two positive integers and consider a control system in \mathbf{R}^n

$$\dot{x}(t) = f(t, x(t), u(t)), \quad (2.1)$$

where $f : \mathbf{R} \times \mathbf{R}^n \times \mathbf{R}^m \rightarrow \mathbf{R}^n$ is of class C^1 , and the controls are measurable essentially bounded functions of time taking their values in some measurable subset Ω of \mathbf{R}^m (the set of control constraints).

Let $f^0 : \mathbf{R} \times \mathbf{R}^n \times \mathbf{R}^m \rightarrow \mathbf{R}$ and $g : \mathbf{R} \times \mathbf{R}^n \rightarrow \mathbf{R}$ be functions of class C^1 . For every $x_0 \in \mathbf{R}^n$, every $t_f \geq 0$, and every admissible control $u \in \mathcal{U}_{x_0, t_f, \Omega}$, the *cost* of the trajectory $x(\cdot)$, solution of (2.1), corresponding to the control u , and such that $x(0) = x_0$, is defined by

$$C_{x_0, t_f}(u) = \int_0^{t_f} f^0(t, x(t), u(t)) dt + g(t_f, x(t_f)). \quad (2.2)$$

Many variants of the cost can be chosen, the one above is already quite general and covers a very large class of problems. If needed, one could easily add some term penalizing the initial point. Note also that the term $g(t_f, x(t_f))$ could alternately be written in integral form and included in the definition of the function f^0 .

Let us now define the optimal control problem that we consider. Let M_0 and M_1 be two measurable subsets of \mathbf{R}^n . We consider the optimal control problem (denoted in short (OCP) in what follows) of determining a trajectory $x(\cdot)$, defined on $[0, t_f]$ (where the final time t_f can be fixed or not in (OCP)), corresponding to an admissible control $u \in \mathcal{U}_{x(0), t_f, \Omega}$, solution of (2.1), such that

$$x(0) \in M_0, \quad x(t_f) \in M_1,$$

and minimizing the cost (2.2) over all possible trajectories steering as well the control system from M_0 to M_1 .

Formulation of The Generic Problem

We write the problem as follows

$$\mathcal{P}_{(OCP)} \begin{cases} \min C_{x_0, t_f}(u) = \int_0^{t_f} f^0(t, x(t), u(t)) dt + g(t_f, x(t_f)), \\ \dot{x}(t) = f(t, x(t), u(t)), \\ u \in \mathcal{U}_{x_0, t_f, \Omega} \\ x(0) \in M_0, \quad x(t_f) \in M_1. \end{cases} \quad (2.3)$$

2.3.2 The Pontryagin Maximum Principle (PMP)

Next we formulate the strong version of the PMP.

The historical proof can be found in [71]. As in [1, 16], it is based on the use of needle-like variations combined with a Brouwer fixed point argument. A concise sketch of the proof, also based on an implicit function argument as in the proof of the weak PMP (and using needle-like variations) can be found in [43].

General statement

Theorem 4 Let $x(\cdot)$ be a solution of (OCP), corresponding to a control u on $[0, t_f]$. Then there exists an absolutely continuous vector-valued function $p(\cdot) : [0, t_f] \rightarrow \mathbf{R}^n$ called the adjoint vector or costate and a real number $p^0 \leq 0$, with $(p(\cdot), p^0) \neq (0, 0)$, such that

$$\dot{x}(t) = \frac{\partial H}{\partial p}(t, x(t), p(t), p^0, u(t)), \quad \dot{p}(t) = -\frac{\partial H}{\partial x}(t, x(t), p(t), p^0, u(t)), \quad (2.4)$$

for almost every $t \in [0, t_f]$, where the function $H : \mathbf{R} \times \mathbf{R}^n \times \mathbf{R}^n \times \mathbf{R} \times \mathbf{R}^m \rightarrow \mathbf{R}$, called Hamiltonian of (OCP), is defined by

$$H(t, x, p, p^0, u) = \langle p, f(t, x, u) \rangle + p^0 f^0(t, x, u).$$

Moreover, the following maximization condition holds

$$H(t, x(t), p(t), p^0, u(t)) = \max_{v \in \Omega} H(t, x(t), p(t), p^0, v), \quad (2.5)$$

for almost every $t \in [0, t_f]$.

If the final time t_f is not fixed in (OCP), then it also holds that

$$\max_{v \in \Omega} H(t_f, x(t_f), p(t_f), p^0, v) = -p^0 \frac{\partial g}{\partial t}(t_f, x(t_f)). \quad (2.6)$$

Moreover, the adjoint vector can be chosen such that the so-called transversality conditions hold (if they make sense)

$$p(0) \perp T_{x(0)}M_0, \quad (2.7)$$

$$p(t_f) - p^0 \frac{\partial g}{\partial x}(t_f, x(t_f)) \perp T_{x(t_f)}M_1, \quad (2.8)$$

where the notation $T_x M$ stands for the usual tangent space to M at point x (these conditions can be written as soon as the tangent space is well defined).

Let us introduce some vocabulary.

Definition 15: A quadruple $(x(\cdot), p(\cdot), p^0, u(\cdot))$ solution of (2.4) and (2.5) is called an extremal.

- If $p^0 < 0$, then the extremal is said to be normal. In that case, it is usual (but not mandatory) to normalize the adjoint vector so that $p^0 = -1$.
- If $p^0 = 0$, then the extremal is said to be abnormal. ◇

Remark 2.4:

Let us insist on the fact that the PMP is nothing but a first-order necessary condition for optimality.^a As already stressed, the PMP states that every optimal trajectory $x(\cdot)$, associated with a control $u(\cdot)$, is the projection onto \mathbf{R}^n of an extremal $(x(\cdot), p(\cdot), p^0, u(\cdot))$. However, conversely, an extremal (i.e., a solution of the equations in the PMP) is not necessarily optimal. The study of the optimality status of extremals can be conducted with the theory of conjugate points. More precisely, as in classical optimization where extremal points are characterized by a first-order necessary condition (the vanishing of some appropriate derivative), there exists in optimal control a theory of second-order conditions for optimality. It consists in investigating a quadratic form that is the intrinsic second-order derivative of the end-point mapping: if this quadratic form is positive definite then this means that the extremal under consideration is locally optimal (for some appropriate topology), and if it is indefinite then the extremal is not optimal; conversely if the extremal is optimal then this quadratic form is non-negative. Times at which the index of this quadratic form changes are called conjugate times. The optimality status of an extremal is then characterized by its first conjugate time. We refer to [17] (and references therein) for a survey on that theory and on algorithms that compute conjugate times.

^a This is an elaborate version of the first-order necessary condition $\nabla f(x) = 0$ when minimizing a C^1 function over \mathbf{R}^n !

Thanks to the PMP, we have a necessary condition to get optimal trajectory. Let us now see how we can numerically apply this principle.

2.4 Numerical Methods

In optimal control, there exist two kinds of numerical method: direct and indirect methods. Direct methods consist in discretizing the state and the control, and hence, consist in solving a nonlinear optimization problem (nonlinear programming). Indirect methods consist in solving a boundary value problem that results from the PMP by applying the so-called *shooting method*.

In this work, we quasi-exclusively use indirect methods, but for the sake of completeness, and because direct methods can be used to initialize indirect methods, we recall the principle of direct methods.

For a complete survey on numerical methods (both direct and indirect) see the article by Trélat [85].

2.4.1 Direct Methods

There exist many different direct methods. By discretizing both the state and the control, the problem reduces to a nonlinear programming problem in finite dimension. For references on direct methods, see [13, 15], and for a general introduction to numerical analysis, see [81].

A very common choice of discretization for optimal control problem is to discretize time. Consider a subdivision of the time interval $[0, t_f]$ during which the transfer occurs into $0 = t_1 < t_2 < \dots < t_N = t_f$. Then, let us consider the control as piecewise constant, *i.e.*, as a sequence $(u_i)_{i \in \llbracket 1, N \rrbracket}$. Meanwhile, the differential dynamics are discretized using, for instance, an explicit (or implicit) Euler method, midpoint method, Runge-Kutta, etc. We set $h_i = t_{i+1} - t_i$ and we define a *discretized cost* by an interpolation procedure. This allows to reduce an optimal control problem to a nonlinear programming problem (NLP) of the form

$$\begin{cases} \min C(x_1, \dots, x_N, u_1, \dots, u_{N-1}), \\ x_{i+1} = x_i + h_i f(t_i, x_i, u_i), \forall i \in \llbracket 2, N-1 \rrbracket, \\ u_i \in \Omega, \forall i \in \llbracket 1, N-1 \rrbracket, \\ x_1 \in M_1, \text{ and } x_N \in M_2. \end{cases}$$

The numerical resolution of such a problem is standard. There exist plenty of methods: gradient methods, quasi-Newton methods, dual methods, etc. See the book by Bonnans, Gilbert, Lemaréchal, and Sagastizábal [15] and [13].

Note that there exists some very useful software to solve optimization problems. One can use the modeling language AMPL [37] coupled with IpOpt [88] for the interior-point filter line search algorithm. This is a very user-friendly and powerful association, although a direct use of IpOpt, for instance with C++, allows for finer tuning. Another very easy to use and powerful tool is the Bocop software. This tool is well designed to solve optimal control problem. The original Bocop package implements a local optimization method. The NLP problem is solved by the well known software IpOpt, using sparse exact derivatives computed by Adol-C. Note that Bocop allows to choose the ordinary differential equation (ODE) approximation such as Euler (implicit or explicit), midpoint, Gauß, etc. See [14].

Remark 2.5:

Although there exist a variety of software options, direct methods are also quite easy to implement from scratch. Moreover, the constraints on state and control are not an issue for such methods.

2.4.2 Indirect Methods

Single Shooting Method

Let us consider the problem $\mathcal{P}_{(OCP)}$ defined in (2.3). According to the PMP (Theorem 4), and the maximization condition (2.5), we are able to express the control as a function of the state and the costate: $(x(\cdot), p(\cdot))$. Hence, the extremal system can be written as

$$\dot{z}(t) = F(t, z(t)),$$

where $z(\cdot) = (x(\cdot), p(\cdot))$. The initial and final conditions and the transversality conditions (2.7) and (2.8) can be written as

$$R(z(0), z(t_f), t_f) = 0.$$

Therefore, we have to solve a *boundary value problem*

$$\begin{cases} \dot{z}(t) = F(z(t)), \\ R(z(0), z(t_f), t_f) = 0. \end{cases} \quad (2.9)$$

Denote by $z(t, z_0)$ the solution of the Cauchy problem

$$\dot{z}(t) = F(t, z(t)), \quad z(0) = z_0,$$

and let us define $\mathcal{S}(z_0) = R(z_0, z(t_f, z_0), t_f)$. Then, the problem (2.9) is equivalent to finding z_0 such that

$$\mathcal{S}(z_0) = 0.$$

This can be done by using a Newton-like method. Note that we have written the principle for a general case, but it is the application of the PMP which determines the function R and its variables (fixed final time, M_1 and M_2 reduced to one point, etc.).

Multiple Shooting Method

Compared to the single shooting method, the multiple shooting method has a better numerical stability. It consists in dividing the interval $[0, t_f]$ into $N - 1$ intervals $[t_i, t_{i+1}]$ (with $t_1 = 0$ and $t_N = t_f$). Then, the values of $z_i = z(t_i) = (x(t_i), p(t_i))$ are introduced as unknowns. A standard reference on multiple shooting methods is [81].

The result is a multi-point boundary value problem. Indeed, we add the matching conditions

$$z_{i+1} = \phi_{\text{ext}}(h_i, z_i),$$

where we denote by ϕ_{ext} the flow of the extremal system and set $h_i = t_{i+1} - t_i$. We denote this condition by $r_i(z_{i+1}, z_i, h_i) = 0$. Let $Z = \{z_1, z_2, \dots, z_N\}$ such that we can finally define the *multiple shooting function*

$$\mathcal{S}_{\text{multi}}(Z) = \begin{pmatrix} R(z_1, z(t_N, z_0), t_N) \\ r_1(z_2, z_1, h_1) \\ \dots \\ r_{N-2}(z_{N-1}, z_{N-2}, h_{N-2}) \end{pmatrix},$$

and the problem (2.9) is equivalent to finding Z such that

$$\mathcal{S}_{\text{multi}}(Z) = 0.$$

This problem can also be solved by iterative Newton-like methods.

For problems which involve discontinuous controls (e.g., L^1 -minimization), the nodes of the multiple shooting method may involve switching times, and junction times (entry, contact, or exit times) with boundary arcs. In this case, an *a priori* knowledge of the structure of the optimal solution is required and this in turn requires an *a priori* knowledge of the switching times. This can be obtained through geometric analysis of the problem.

For a more precise introduction to multiple shooting method, see [81] as well as [84] for applications to optimal control.

Remark 2.6: Initialization

In general, the family of Newton-like methods (descent direction method, quasi-Newton, etc.) allows to achieve a very precise resolution. The accuracy comes from the integration of the BVP. Unfortunately, to ensure that the method will converge, the initial guess must be chosen sufficiently close to the researched solution. From the point of view of optimal control, we need to have some *a priori* intuition about the trajectory we are looking for.

For the mission construction, there are different ways to get this intuition.

- One can use a coarse approximation obtained by a direct resolution.
- One can use geometric insight (by applying geometric optimal control tools).
- One can use the properties of the dynamical system as *a priori* information. For the problem under consideration, we discussed this idea in chapter 1.
- One can use continuation methods to robustify the shooting method. This will be introduced in the next section.

For a very good survey on some results and challenges on optimal control and applications to aerospace, see the article by Trélat [85].

2.5 Numerical Continuation Methods

The principle of continuation methods is to solve a difficult problem using the solution of a similar, but easier, problem by parameter deformation. The theory of the continuation method is well known (see, e.g., [5, 3, 2, 4, 22, 73] and a survey in [85]). One can find many continuation algorithms. For a specific application to controlled systems and spacecraft missions, we refer to [44]. Here, we introduce briefly two continuation algorithms. The first one, the discrete continuation, has already been explained in Section 1.4.4. The second one is a Predictor-Corrector continuation (PC continuation) and more precisely the Piecewise Linear Method (PL continuation). In the remainder of this thesis, we only use this type of continuation.

Let us define continuation in the context of indirect methods applied to the optimal control problem.

Definition 16 (Homotopy/Continuation): *Let us consider two smooth maps \mathcal{S}_0 and \mathcal{S}_1 from \mathbf{R}^n to \mathbf{R}^n , where n is the dimension of the unknown zero of the shooting function (single or multiple shooting) denoted by Z . We define a homotopy or continuation as the following smooth map*

$$G : \mathbf{R}^n \times [0, 1] \rightarrow \mathbf{R}^n,$$

such that $\mathcal{S}(\cdot, 0) = \mathcal{S}_0(\cdot)$ and $\mathcal{S}(\cdot, 1) = \mathcal{S}_1(\cdot)$. ◇

Existence result. We next state the result for the existence of the zero paths. Local existence of *zero paths* is ensured by the implicit function theorem. To guarantee the global existence of zero paths, we need some regularity assumptions. Let us state the theorem presented in [21] and [44].

Theorem 5 (Existence of the zero paths) Let Ω be an open bounded subset of \mathbb{R}^n . Let $S : \Omega \times [0, 1] \rightarrow \mathbb{R}^n$ be continuously differentiable and such that:

- $\forall (Z, \lambda) \in \{(Z, \lambda) \in \Omega \times [0, 1]; S(Z, \lambda) = 0\}$, the Jacobian matrix

$$\begin{bmatrix} \frac{\partial S}{\partial Z_1} & \frac{\partial S}{\partial Z_2} & \cdots & \frac{\partial S}{\partial Z_n} & \frac{\partial S}{\partial \lambda} \end{bmatrix}$$

is of maximum rank n .

- $\forall Z \in \{Z \in \Omega; S(Z, 0) = 0\} \cup \{Z \in \Omega; S(Z, 1) = 0\}$, the matrix

$$\begin{bmatrix} \frac{\partial S}{\partial Z_1} & \frac{\partial S}{\partial Z_2} & \cdots & \frac{\partial S}{\partial Z_n} \end{bmatrix}$$

is of maximum rank n .

Then, the set $\{(Z, \lambda) \in \Omega \times [0, 1]; S(Z, \lambda) = 0\}$ consists of paths that are

1. a finite number of loops in $\Omega \times [0, 1]$;
2. a finite number of paths with end points in the set $\partial\Omega \times [0, 1]$.

These curves type (1 and 2) are continuously differentiable and disjoint.

In Figure 2.5, an illustration in one dimension of possible and impossible paths is presented. The proof is in [21, Theo. 2.1].

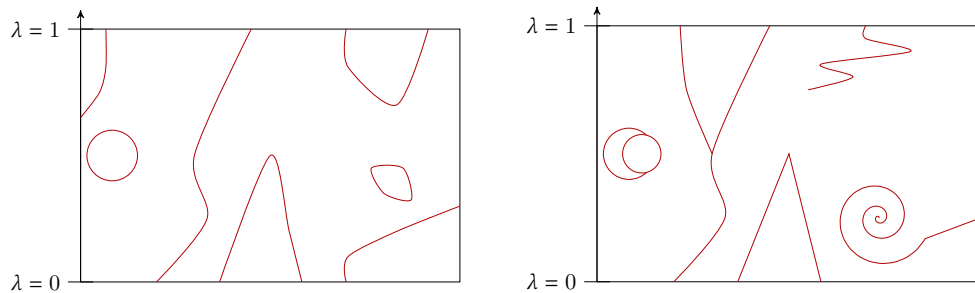


Figure 2.5 – Possible continuation zero paths (left) and impossible continuation zero paths (right).

Remark 2.7:

In [85, sec. 4.1.], it is shown that, as long as no minimizing singular control nor conjugate point along the continuation procedure is encountered, the continuation method works locally and the extremal solution is of class C^1 with respect to the parameter λ . These two assumptions ensure the existence of a local solution in the continuation procedure. In other words, under these two sufficient conditions, the continuation method is locally feasible.

2.5.1 Discrete Continuation

Let $\mathcal{S} : \mathbf{R}^n \times [0, 1] \rightarrow \mathbf{R}^n$ be a continuation. We denote by \bar{Z}_λ the solution of $\mathcal{S}(Z, \lambda) = 0$ where λ is fixed. We assume that there is an algorithm available to find the root of a function called the “search algorithm” (e.g., a Newton-like method). In other words, we assume that the solution \bar{Z}_0 of $\mathcal{S}(Z, 0) = 0$ is known. The discrete homotopy consists in constructing an increasing sequence $(\lambda_k)_{k \in \llbracket 0, N \rrbracket}$ with $\lambda_0 = 0$ and $\lambda_N = 1$. Then, step by step, we look for a zero \bar{Z}_{λ_k} of $\mathcal{S}(Z, \lambda_k)$ with the search algorithm initialized by $\bar{Z}_{\lambda_{k-1}}$. The drawback of this method is that we assume that $\bar{Z}_{\lambda_{k-1}}$ is in the convergence radius of the search algorithm. This problem can generally be overcome by refining the step between λ_{k-1} and λ_k . The sequence $(\lambda_k)_{k \in \mathbb{N}}$ depends on the different successful or failed iterations of the discrete continuation algorithm. See Algorithm 2.1 for a precise description as well as Figure 2.6 with an illustration for a one dimensional zero path.

Algorithm 2.1: Discrete continuation algorithm

```

Require:  $\bar{Z}_0$  solution of  $\mathcal{S}(Z, 0) = 0$ 
1: Initialization:  $\bar{\lambda} = 0$ 
2:  $\bar{Z} = \bar{Z}_0$ 
3:  $\Delta\lambda \in ]0, 1]$  (e.g.  $1 \times 10^{-1}$ )
4:  $\Delta\lambda_{\min} \in ]0, \Delta\lambda]$  (e.g.  $1 \times 10^{-9}$ )
5: while  $\bar{\lambda} < 1$  and  $\Delta\lambda > \Delta\lambda_{\min}$  do
6:    $\Delta\lambda = \min(\Delta\lambda, 1 - \bar{\lambda})$ 
7:    $\tilde{\lambda} \leftarrow \bar{\lambda} + \Delta\lambda$ 
8:    $\tilde{Z} \leftarrow \text{Solve}(\mathcal{S}(\tilde{Z}, \tilde{\lambda}))$  with the initialization  $\bar{Z}$ 
9:   if Success of Solve then
10:     $\bar{Z} = \tilde{Z}$ 
11:     $\bar{\lambda} = \tilde{\lambda}$ 
12:   else
13:     $\Delta\lambda = \epsilon\Delta\lambda$  (e.g.  $\epsilon = \frac{1}{2}$ )
14:   end if
15: end while
16: if  $\bar{\lambda} = 1$  then
17:   The discrete continuation is successful.
18:   return  $\bar{Z}$ 
19: else
20:   The discrete continuation has failed.
21: end if

```

Of course, one can increase the step $\Delta\lambda$ when the search algorithm succeeds. We applied this continuation technique to the computation of the family of periodic orbits around Lagrange points (see Section 1.4.4, algorithm 1.1).

A noticeable drawback of such a method is the detection of the failure to converge of the search algorithm. Indeed, a Newton-like method is very fast to converge if it is well initialized but can run for a long time before failing.

2.5.2 Piecewise Linear Continuation

This method is based on a piecewise linear approximation of the zero paths. We refer to [4] for a precise and complete description. The advantage of this method is that it only requires the continuity of the zero path. Indeed, more sophisticated methods such as differentiable

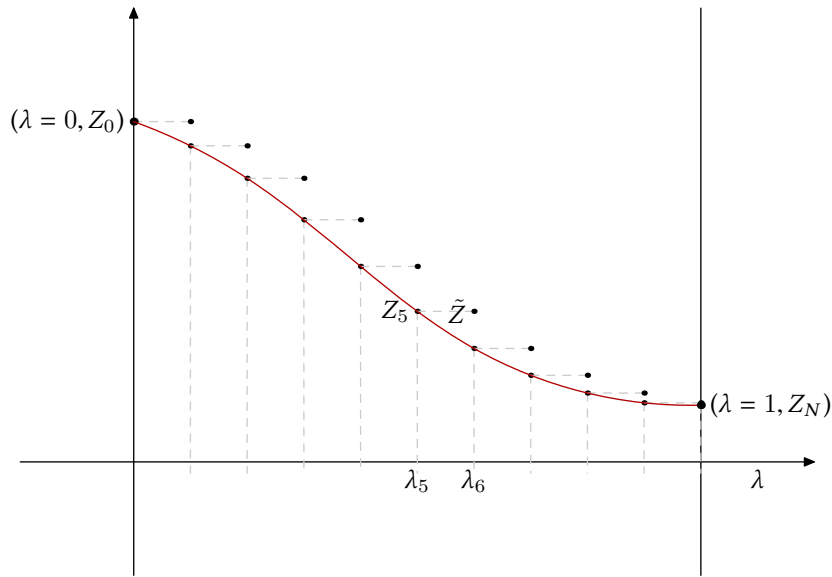


Figure 2.6 – Graphic illustration of the discrete continuation method with constant steps.

continuation require the path to be C^1 . We do not use these methods and we refer to [44] for an introduction in the context of optimal control.

After the first step of the PL method (which is a discrete step continuation), we predict the initial guess for the search algorithm with the relation

$$\tilde{Z}_c \leftarrow \bar{Z}_i + \Delta\lambda(\bar{Z}_i - \bar{Z}_{i-1}),$$

as it is written in the line numbered 8 in Algorithm 2.2. In Figure 2.7, we illustrate this linear prediction for a simple one dimensional zero path. For a complete description of this algorithm, see algorithm 2.2.

Once again, the step $\Delta\lambda$ can be increased when the search algorithm succeeds.

2.6 Construction of an Optimal Control Problem (OCP)

In the previous sections, we have explained how a mission can be designed using *impulse* and *invariant manifolds* to save a lot of propellant. The fact that invariant manifolds are separatrices of the dynamics makes them *gravitational currents*.

Then we introduced the model for the low thrust engine spacecraft. Because of the low thrust engine, the method for mission design introduced in Section 2.1 cannot be applied. Indeed, to go from one invariant manifold to another, an instantaneous change of velocity is not possible anymore.

For this reason, we develop a method to connect two invariant manifolds using low thrust. With this model, the natural context is the optimal control theory. Indeed, because the control is permanent during the transfer time, one can write the minimization of the mass consumption in terms of an integral of the control norm. We will discuss that in the next sections.

First, let us explain the method we developed to write an optimal control problem to perform the transfer between two invariant manifolds.

Algorithm 2.2: Piecewise Linear Continuation algorithm

Require: \bar{Z}_0 solution of $S(Z, 0) = 0$

- 1: Initialization: $\bar{\lambda} = 0$
- 2: $\bar{Z}_1 = \bar{Z}_0, i = 1$
- 3: $\Delta\lambda \in]0, 1]$ (e.g. 1×10^{-1})
- 4: $\Delta\lambda_{\min} \in]0, \Delta\lambda]$ (e.g. 1×10^{-9})
- 5: **while** $\bar{\lambda} < 1$ **and** $\Delta\lambda > \Delta\lambda_{\min}$ **do**
- 6: $\Delta\lambda = \min(\Delta\lambda, 1 - \bar{\lambda})$
- 7: $\tilde{\lambda} \leftarrow \bar{\lambda} + \Delta\lambda$
- 8: $\tilde{Z}_c \leftarrow \bar{Z}_i + \Delta\lambda(\bar{Z}_i - \bar{Z}_{i-1})$
- 9: $\tilde{Z} \leftarrow \text{Solve}(S(\tilde{Z}, \tilde{\lambda}))$ with the initialization \bar{Z}_c
- 10: **if** Success of Solve **then**
- 11: $\bar{Z}_{i+1} = \tilde{Z}$
- 12: $\bar{\lambda} = \tilde{\lambda}$
- 13: $i \leftarrow i + 1$
- 14: **else**
- 15: $\Delta\lambda = \epsilon\Delta\lambda$ (e.g. $\epsilon = \frac{1}{2}$)
- 16: **end if**
- 17: **end while**
- 18: **if** $\bar{\lambda} = 1$ **then**
- 19: The PL continuation is successful.
- 20: **return** \bar{Z}
- 21: **else**
- 22: The PL continuation has failed.
- 23: **end if**

2.6.1 From an Impulse Solution to an Optimal Control Problem

We start with an impulsive transfer between two manifolds. We denote respectively by \mathcal{M}_0 and \mathcal{M}_1 the two invariant manifolds that we consider. The goal of this section is to find a trajectory performing the transfer between these two invariant manifolds.



The choice of the two invariant manifolds \mathcal{M}_0 and \mathcal{M}_1 depends on the complete mission that we want to design. In chapter 3, we apply the tools developed in this chapter for real missions.

Of course, the two invariant manifolds should be chosen such that the transfer from one to another is useful. For example, they must be “directed” in the same direction. Moreover, the two chosen invariant manifolds must be such that there exists a section where the distance in position and velocity is not too big.

These notions are not mathematically well defined here, but the key is the knowledge of the map of invariant manifolds as explained in Section 2.1.

The Impulsive Transfer

We start with an impulsive transfer between \mathcal{M}_0 and \mathcal{M}_1 . We define a Poincaré surface of section denoted by U (see, e.g., Section 2.1.1) where there exists an intersection in position of the two invariant manifolds. Denote by $\xi_0^U = (\mathbf{x}_0^U, \mathbf{v}_0^U)$ and $\xi_1^U = (\mathbf{x}_1^U, \mathbf{v}_1^U)$ the two points

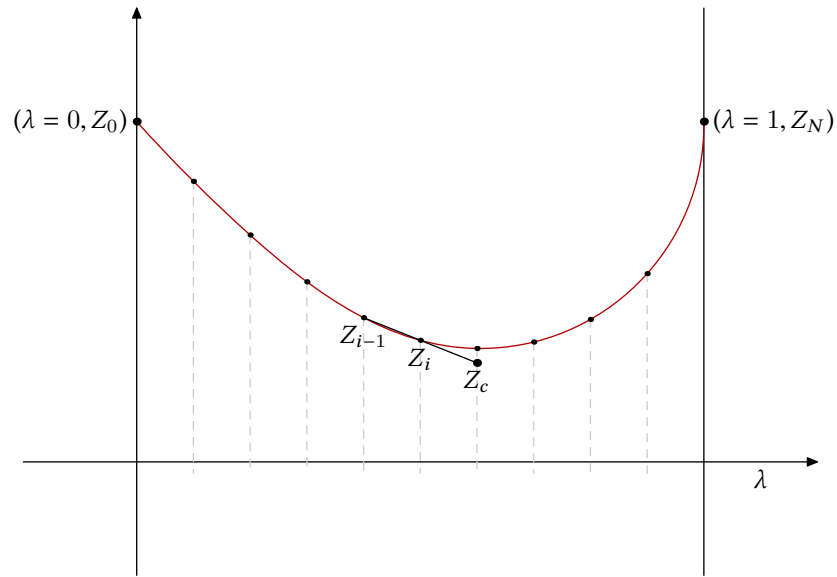


Figure 2.7 – Graphic illustration of the Piecewise Linear continuation method with constant steps. Z_c is the prediction constructed with the two previous solutions of intermediary problems.

in this surface of section where

$$\begin{aligned} \mathbf{x}_i^U &= (x_1^i, x_2^i, x_3^i) = (x_i, y_i, z_i), i \in \{0, 1\}, \\ \mathbf{v}_i^U &= (x_4^i, x_5^i, x_6^i) = (\dot{x}_i, \dot{y}_i, \dot{z}_i), i \in \{0, 1\}, \end{aligned}$$

and such that

$$\mathbf{x}_0^U = \mathbf{x}_1^U.$$

Denote by \mathcal{A}_0 (resp. \mathcal{A}_1) the orbit to which ξ_0^U (resp. ξ_1^U) belongs. Hence, to go from \mathcal{A}_0 belonging to \mathcal{M}_0 to \mathcal{A}_1 belonging to \mathcal{M}_1 , we just have to perform the impulse

$$\Delta V = \mathbf{v}_1^U - \mathbf{v}_0^U.$$

Thanks to that, we are able to go from one orbit belonging to the first manifold to another belonging to the second manifold. See Figure 2.8 for a drawing of this, and Section 2.9 for real applications.

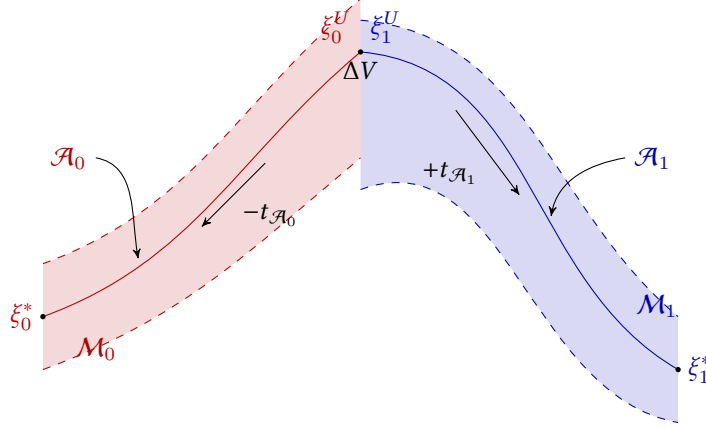


Figure 2.8 – Drawing of the construction of the end points of the optimal control problem starting with an impulsive transfer between invariant manifolds \mathcal{M}_0 and \mathcal{M}_1 .

Intersection Problem. Let us enumerate the different cases.

1. If we consider *the planar case*, then there are four state variables ($\xi \in \mathbf{R}^4$) on the surface of section U , we look for an intersection in \mathbf{R}^3 . Moreover, if both manifolds share the same energy, then a complete intersection in position and velocity is possible (not guaranteed). In that case, we do not need any control to perform the transfer. See the section on heteroclinic and homoclinic orbits (Section 2.1.2).
2. If we consider *the planar case* but without the same energy, then it is possible to find a position intersection, but with a gap in velocity. Once again, the existence is only empirical.
3. If we consider *the spatial case*, then the state $\xi \in \mathbf{R}^6$ so on the surface of section U , we look for an intersection in \mathbf{R}^5 . In that case, an intersection is difficult to find and, we actually give up searching for such a point. Instead, we restrict ourselves to finding an intersection in the position space. Note that the method we describe can be applied when there is no intersection (nor in position nor in velocity), but with a small

$$\Delta\xi = (\Delta\mathbf{x}, \Delta V) = (\mathbf{x}_1^U - \mathbf{x}_0^U, \mathbf{v}_1^U - \mathbf{v}_0^U),$$

where $\mathbf{x} = (x_1, x_2, x_3) = (x, y, z)$ and $\mathbf{v} = (x_4, x_5, x_6) = (\dot{x}, \dot{y}, \dot{z})$ depending of the notation. Keeping that in mind, for pedagogical reason, we consider the case when we only have a ΔV .

Optimal Control Problem

Thanks to the impulsive transfer between the two invariant manifolds, we have two trajectories $\mathcal{A}_0 \in \mathcal{M}_0$ and $\mathcal{A}_1 \in \mathcal{M}_1$ and two points $\xi_0^U \in \mathcal{A}_0$ and $\xi_1^U \in \mathcal{A}_1$ such that

$$\xi_1^U - \xi_0^U = (0, \Delta V).$$

Perturbation Time. Starting with these two points $\xi_0^U \in \mathbf{R}^6$ and $\xi_1^U \in \mathbf{R}^6$, we choose two times $t_{\mathcal{A}_0}$ and $t_{\mathcal{A}_1}$ to respectively propagate backward the point ξ_0^U and forward the ξ_1^U . Mathematically, denoting by ϕ^{nat} the flow of the (uncontrolled) natural dynamics, we

define two points in \mathbf{R}^6 by

$$\xi_0^* = \phi^{\text{nat}}(-t_{\mathcal{A}_0}, \xi_0^U), \quad \text{and} \quad \xi_1^* = \phi^{\text{nat}}(t_{\mathcal{A}_1}, \xi_1^U).$$

See Figure 2.8 for an illustration of this construction.

The Optimal Control Problem. Let us define a new transfer time t_f such that

$$t_f = t_{\mathcal{A}_0} + t_{\mathcal{A}_1}.$$

At this point, the optimal control problem is ready to be constructed. We want to maximize the final mass (this in turn minimizes the weight of propellant burnt during the mission). Indeed, because the real cost for the launch of the spacecraft is to send it “away from Earth”, *i.e.*, to send it to a first *parking orbit* around Earth (for example a *low Earth orbit* is the simplest and cheapest for satellite positioning), the lighter the spacecraft, the cheaper the launch.

Therefore, the problem we formulate is the following

$$\mathcal{P}_{m_f} \begin{cases} C_{m_f}(u) = m(t_f) \rightarrow \max, \\ \dot{x} = F_0(x) + \frac{\epsilon}{m} \sum_{i=1}^3 u_i F_i(x), \\ \dot{m} = -\beta_* \epsilon \|u\|, \\ \|u\| \leq 1, \\ x(0) = \xi_0^*, m(0) = m_0^*, \text{ and } x(t_f) = \xi_1^*. \end{cases} \quad (2.10)$$

Application of the PMP. It is obvious that the maximization of the final mass is equivalent to the minimization of the L^1 -norm of the control u . So problem (2.10) is equivalent to the following one

$$\mathcal{P}_{L^1} \begin{cases} C_{L^1}(u) = \int_0^{t_f} \|u\| dt \rightarrow \min, \\ \dot{x} = F_0(x) + \frac{\epsilon}{m} \sum_{i=1}^3 u_i F_i(x), \\ \dot{m} = -\beta_* \epsilon \|u\|, \\ \|u\| \leq 1, \\ x(0) = \xi_0^*, m(0) = m_0^*, \text{ and } x(t_f) = \xi_1^*. \end{cases} \quad (2.11)$$

2.6.2 Minimization of the L^1 -norm of the Control

In this section, we apply the Pontryagin Maximum Principle to the problem (2.11) to get the structure of the control. We introduce the costate denoted by $(p^0, p, p_m) = (p^0, p_x, p_v, p_m)$ associated with the state denoted by $(\xi, m) = (x, v, m)$. The Hamiltonian of the system defined in theorem 4 is

$$\mathcal{H}(x, m, u, p^0, p, p_m) = (p^0 - \beta_* \epsilon p_m) \|u\| + H_0 + u_1 \frac{\epsilon}{m} H_1 + u_2 \frac{\epsilon}{m} H_2 + u_3 \frac{\epsilon}{m} H_3,$$

where $H_i = \langle p, F_i \rangle$ for $i \in \llbracket 0, 3 \rrbracket$. The application of the maximum principle yields

$$\begin{aligned}\dot{x} &= \frac{\partial \mathcal{H}}{\partial p}(x, u, p), \\ \dot{p} &= -\frac{\partial \mathcal{H}}{\partial x}(x, u, p), \\ u(t) &= \arg \max_{\|v\| \leq 1} \mathcal{H}(x, m, v, p^0, p, p_m).\end{aligned}$$

The costate dynamics system are too long to write here. They can easily be computed by a *computer algebra system*, but using the notation $p = (p_x, p_v) = (p_1, p_2, p_3, p_4, p_5, p_6)$, and the notation $F_0 = (f_i)_{i \in \llbracket 1, 6 \rrbracket}$ introduced in Section 1.1, it is easy to see that

$$\begin{cases} \dot{p}_1 = \sum_{i=1}^3 p_{i+3} \frac{\partial f_{i+3}(x)}{\partial x_1}, \\ \dot{p}_2 = \sum_{i=1}^3 p_{i+3} \frac{\partial f_{i+3}(x)}{\partial x_2}, \\ \dot{p}_3 = \sum_{i=1}^3 p_{i+3} \frac{\partial f_{i+3}(x)}{\partial x_3}, \\ \dot{p}_4 = -p_1 - 2p_4, \\ \dot{p}_5 = -p_2 + 2p_5, \\ \dot{p}_6 = -p_3, \\ \dot{p}_m = \frac{\epsilon}{m^2} \langle u, p_v \rangle. \end{cases}$$

In order to obtain the structure of the optimal control, we recall results and proofs from the contributions in [44, 39, 25, 31].

Proposition 3 : *If ξ_0^* and ξ_1^* do not belong to the same natural trajectory, then $\|p_v\|$ has a finite number of zeros.*

Proof : Let us assume that there are an infinite number of zeros, and consequently an infinite sequence $(t_k)_{k \in \mathbb{N}}$ where $t_k \in [0, t_f]$ such that $\|p_v(t_k)\| = 0$, for all $k \in \mathbb{N}$. Then there exists a convergent subsequence $(t_{\phi(k)})_{k \in \mathbb{N}}$ of limit \bar{t} . By the continuity of p_v , we have $p_v(\bar{t}) = 0$.

The costate dynamics imply that p_v is continuously differentiable, therefore

$$\frac{p_v(t_{\phi(i)}) - p_v(\bar{t})}{t_{\phi(i)} - \bar{t}} = 0 \xrightarrow{i \rightarrow +\infty} \dot{p}_v(\bar{t}) = -p_x(\bar{t}) + \begin{pmatrix} 2p_4(\bar{t}) \\ -2p_3(\bar{t}) \\ 0 \end{pmatrix},$$

where we have used the notation $p = (p_1, p_2, p_3, p_4, p_5, p_6)$. Then, $p_v(\bar{t}) = 0$ implies that $p_x(\bar{t}) = 0$ which implies that, for all $t \in [0, t_f]$, $p_x(t) = p_v(t) = 0$ and $\dot{p}_m(t) = 0$. Thanks to the transversality condition (free final mass), $p_m(t_f) = 0$, and for all $t \in [0, t_f]$, $p_m(t) = 0$. Because of the non-triviality of (p^0, p, p_m) , this implies that $p^0 \neq 0$, and the maximization of the Hamiltonian gives us $u(\cdot) = 0$ almost everywhere. This contradicts the hypothesis on the two points ξ_1^* and ξ_2^* . ■

Let us define $\varphi(p) = (H_1, H_2, H_3) = p_v = (p_4, p_5, p_6)$.

Proposition 4 : *If t_f is greater than the minimum transfer time¹ t_f^{\min} and if ξ_0^* and ξ_1^* do not belong to the same natural trajectory, then $p^0 \neq 0$.*

1. The minimum transfer time is the solution time of the minimum time problem when the cost to minimize is t_f .

Proof: Assume that $p^0 = 0$, then by the Cauchy-Schwarz inequality, it holds that

$$\mathcal{H}(x, m, u, p, p_m) \leq H_0 + \left(\frac{\epsilon}{m} \|\varphi(p)\| + \beta_* \epsilon p_m \right) \|u\|. \quad (2.12)$$

Property 3 implies that $\|\varphi(p)\| \neq 0$ a.e., and the maximization condition yields $u(t) = a(\zeta(t)) \frac{\varphi(p)}{\|\varphi(p)\|}$ where

$$\zeta(t) = (x(t), m(t), p(t), p_m(t)), \quad \text{and } a(\zeta(t)) \in [0, 1].$$

Then, $\dot{p}_m = a(\zeta(t)) \frac{\epsilon}{m^2(t)} \|\varphi(p)\| \geq 0$, hence, because $p_m(t_f) = 0$, for all $t \in [0, t_f]$, $p_m(t) \leq 0$. Therefore, equality in the inequality labeled (2.12) holds if $\|u\| = 1$ almost everywhere and

$$C_{L^1} = \int_0^{t_f} \|u\| dt = \int_0^{t_f} dt,$$

with $t_f > t_f^{\min}$ by assumption. But the trajectory corresponding to the minimum time problem is admissible for problem (2.11), and is better since $t_f^{\min} < t_f$, absurd. ■

Thanks to Property 4, we are considering the normal case (see [16]), that is to say that $p^0 \neq 0$, so the costate (p^0, p) can be normalized with $p^0 = -1$

Denoting by $\zeta = (x, m, p, p_m)$, let us introduce the *switching function*:

$$\psi(\zeta) = 1 - \beta_* \epsilon p_m - \frac{\epsilon}{m} \|\varphi(p)\|.$$

Then, the control is:

- if $\|\varphi(p)\| \neq 0$, then

$$\begin{cases} u(\zeta) = 0 & \text{if } \psi(\zeta) < 0, \\ u(\zeta) = \alpha \frac{\varphi(p)}{\|\varphi(p)\|}, \alpha \in [0, 1] & \text{if } \psi(\zeta) = 0, \\ u(\zeta) = \frac{\varphi(p)}{\|\varphi(p)\|} & \text{otherwise,} \end{cases}$$

- if $\|\varphi(p)\| = 0$, then

$$\begin{cases} u(\zeta) = 0 & \text{if } \psi(\zeta) < 0, \\ u(\zeta) \in \mathbf{B}(0, 1) & \text{if } \psi(\zeta) = 0, \\ u(\zeta) \in \mathbf{S}(0, 1) & \text{otherwise,} \end{cases}$$

where $\mathbf{S}(a, b)$ is the \mathbf{R}^2 -sphere centered in a with radius b , and $\mathbf{B}(a, b)$ is the \mathbf{R}^2 ball.

Remark 2.8: Singular Arcs

Note that the case $\|\varphi(p)\| = 0$ can be a problem. However, Proposition 3 and the assumption that it remains true on a neighborhood of the solution guarantee that the numerical evaluation of the control is not problematic as long as there are no singular arcs. Hence, we assume that ψ has a finite number of zeros.

This assumption can be checked *a posteriori*, once the numerical computation has been performed.

Shooting Function

We have established the structure of the control using the maximization condition of the PMP. Then, as explained in Section 2.4.2, the resolution of the problem is equivalent to finding the root of a shooting function.

First, the free final mass transversality conditions gives us $p_m(t_f) = 0$. Because we consider isolated end points (M_0 and M_1 in Theorem 4 are reduced to two points ξ_0^* and ξ_1^*), transversality conditions for the costate p associated to the state x do not give any information. The boundary value problem defined by the application of the PMP is reduced to find initial costate values $(p(0), p_m(0))$ such that the extremal solution $\zeta(\cdot) = (x(\cdot), m(\cdot), p(\cdot), p_m(\cdot))$ is well defined and reach the final state $x(t_f) = \xi_1^*$ starting at $(x(0), m(0)) = (\xi_0^*, m_0^*)$. Finally, the shooting function can be written as

$$\mathcal{S}_{L_1}(p(0), p_m(0)) = \begin{pmatrix} \phi_{1, \dots, 6}^{\text{ext}}(\xi_0^*, m_0^*, p(0), p_m(0)) - \xi_1^* \\ \phi_{14}^{\text{ext}}(\lambda_0^*, m_0^*, p(0), p_m(0)) \end{pmatrix} = \begin{pmatrix} \mathbf{0} \\ 0 \end{pmatrix}.$$

To solve such a problem, we use a Newton-like method. For that kind of method, we need the shooting function to be differentiable. It can be shown (see [44, 39]) that the regularity of the shooting function can only be guaranteed around the optimal control structure. This reduces the convergence domain of the Newton-like method applied to the problem.



With the assumption on singular arcs, the minimization of the L^1 -norm of the control leads to a control called *bang-bang*, indeed $\|u\|$ alternates between $\|u\| = 0$ and $\|u\| = 1$.

Numerically, this problem is difficult to solve. Hence, one has to know, *a priori*, the structure of the controlled solution, and the search for the zero of the shooting function is very hard to initialize.

To overcome this difficulty, we use continuation from a simpler problem: the L^2 -norm of the control minimization.

2.6.3 Minimization of the L^2 -norm of the Control

We consider the following problem

$$\mathcal{P}_{L^2} \begin{cases} C_{L^2}(u) = \int_0^{t_f} \|u\|^2 dt \rightarrow \min, \\ \dot{x} = F_0(x) + \frac{\epsilon}{m} \sum_{i=1}^3 u_i F_i(x), \\ \dot{m} = -\beta_* \epsilon \|u\|, \\ \|u\| \leq 1, \\ x(0) = \xi_0^*, m(0) = m_0^*, \text{ and } x(t_f) = \xi_1^*. \end{cases} \quad (2.13)$$

The problem is simpler because the optimal control is not *bang-bang* anymore (that will be clearer with the analysis of the structure of the optimal control) and we use it as the initial problem for a continuation to solve problem (2.11). Problem (2.13) has a cost defined by the L^2 -norm of the control. This cost corresponds to the minimization of the energy which is not too far from the minimization of the consumption.

For the sake of conciseness, we directly introduce the family of problems indexed by

$\lambda \in [0, 1]$

$$\mathcal{P}_{C_\lambda} \begin{cases} C_\lambda(u) = \int_0^{t_f} \left((1-\lambda) \|u\|^2 + \lambda \|u\| \right) dt \rightarrow \min, \\ \dot{x} = F_0(x) + \frac{\epsilon}{m} \sum_{i=1}^3 u_i F_i(x), \\ \dot{m} = -\beta_* \epsilon \|u\|, \\ \|u\| \leq 1, \\ x(0) = \xi_0^*, m(0) = m_0^*, \text{ and } x(t_f) = \xi_1^*. \end{cases} \quad (2.14)$$

Indeed, the analysis of the control structure is the same for problems (2.13) and (2.14) for $\lambda \in [0, 1]$. The Hamiltonians of these problems are

$$\mathcal{H}_\lambda(x, m, u, p^0, p, p_m) = (-\lambda - \beta_* \epsilon p_m) \|u\| - (1-\lambda) \|u\|^2 + H_0 + u_1 \frac{\epsilon}{m} H_1 + u_2 \frac{\epsilon}{m} H_2 + u_3 \frac{\epsilon}{m} H_3. \quad (2.15)$$

Let us note that we can extend the previous properties to problem \mathcal{P}_{C_λ} .

Proposition 5: *Under the same assumptions as for the property 3, $\|p_\lambda^\lambda\|$ has a finite number of zeros. Moreover, $p_\lambda^0 = 0$. The superscript and subscript λ are for the costate of for problems (2.14).*

Note that for $\lambda \in [0, 1[$, the Hamiltonian is strictly concave with respect to u , so the control is a *continuous function* of (x, m, p, p_m) . To get the structure of the control, we follow the presentation in [31]. This key point makes the numerical computation easier. By Cauchy-Schwarz, it holds that

$$\mathcal{H}_\lambda(x, m, u, p, p_m) \leq H_0 + \underbrace{\left(\frac{\epsilon}{m} \|\varphi(p)\| + \beta_* \epsilon p_m - \lambda \right) \|u\| - (1-\lambda) \|u\|^2}_{g_\lambda(\|u\|)}.$$

The maximization condition implies that, for all $\lambda \in [0, 1[$

$$\begin{aligned} g'_\lambda(\|u\|) &= 0 \\ \iff 2(1-\lambda) \|u\| &= \left(\frac{\epsilon}{m} \|\varphi(p)\| + \beta_* \epsilon p_m - \lambda \right) \\ \iff \|u\| = \psi_\lambda(\zeta) &= \frac{\frac{\epsilon}{m} \|\varphi(p)\| + \beta_* \epsilon p_m - \lambda}{2(1-\lambda)} \end{aligned}$$

We get the structure of the control

- if $\|\varphi(p)\| \neq 0$, then

$$\begin{cases} u(\zeta) = 0 & \text{if } \psi_\lambda(\zeta) \leq 0, \\ u(\zeta) = \psi_\lambda(\zeta) \frac{\varphi(p)}{\|\varphi(p)\|} & \text{if } \psi_\lambda(\zeta) \in [0, 1], \\ u(\zeta) = \frac{\varphi(p)}{\|\varphi(p)\|} & \text{otherwise,} \end{cases} \quad (2.16)$$

- if $\|\varphi(p)\| = 0$, then

$$\begin{cases} u(\zeta) = 0 & \text{if } \psi_\lambda(\zeta) \leq 0, \\ u(\zeta) \in \mathbf{S}(0, \psi(\zeta)) & \text{if } \psi_\lambda(\zeta) \in [0, 1], \\ u(\zeta) \in \mathbf{S}(0, 1) & \text{otherwise,} \end{cases}$$

where $S(a, b)$ is the \mathbf{R}^2 -sphere centered in a with radius b .

The shooting function is exactly the same as before but the control is different, and so are the extremal dynamics. The result on the regularity of the shooting function still holds, because the shooting function for $\lambda < 1$ is more regular than the one for $\lambda = 1$ (the control is now continuous).

Let us enunciate a classical but remarkable result on costs for the different problems in the family (see [39]).

Proposition 6 : *Let $(x_\lambda, m_\lambda, u_\lambda)$ be a solution of problem \mathcal{P}_{C_λ} , then for $0 \leq \lambda \leq \lambda' \leq 1$, we have*

1. $C_\lambda(u_\lambda) \leq C_{\lambda'}(u_\lambda) \leq C_{L^1}(u_1) \leq C_{L^1}(u_\lambda)$
2. $|C_{L^1}(u_\lambda) - C_\lambda(u_\lambda)| \xrightarrow{\lambda \rightarrow 1} 0$
3. $C_\lambda(u_\lambda) \xrightarrow{\lambda \rightarrow 1} C_{L^1}(u_1)$ and $C_{L^1}(u_\lambda) \xrightarrow{\lambda \rightarrow 1} C_{L^1}(u_1)$

2.7 Numerical Method: From Impulsive Transfer to Low Thrust Transfer

We have now established the main results for the two problems that we want to solve: the L^1 -norm minimization of the problem (\mathcal{P}_{L^1}), the L^2 -norm minimization of the problem (\mathcal{P}_{L^2}) as well as all continuations between the two problems with the family of problems (\mathcal{P}_{C_λ}).

However, the transfer is still too difficult to initialize. Indeed, we still do not know how to initialize the simpler problem \mathcal{P}_{L^2} . To manage to achieve this, we have designed a general method using several continuations.

2.7.1 Final State Continuation

Let us start with the first continuation in our multistep method. We consider the problem described in Section 2.6.1, that is to say, with the L^2 -norm of the control as the cost function

$$\mathcal{P}_{L^2} \begin{cases} C_{L^2}(u) = \int_0^{t_f} \|u\|^2 dt \rightarrow \min, \\ \dot{x} = F_0(x) + \frac{\epsilon}{m} \sum_{i=1}^3 u_i F_i(x), \\ \dot{m} = -\beta_* \epsilon \|u\|, \\ \|u\| \leq 1, \\ x(0) = \xi_0^*, m(0) = m_0^*, \text{ and } x(t_f) = \xi_1^*. \end{cases}$$

Instead of the final state ξ_1^* , we consider the point ξ_1^{nat} defined by

$$\xi_1^{\text{nat}} = \phi^{\text{nat}}(t_f, \xi_0^*).$$

To say it with words, we have just propagated the initial point by following the natural dynamics during the transfer time. See Figure 2.9 for an illustration. It is obvious then that

we know how to solve the following optimal control problem

$$\mathcal{P}_{L^2} \begin{cases} C_{L^2}(u) = \int_0^{t_f} \|u\|^2 dt \rightarrow \min, \\ \dot{x} = F_0(x) + \frac{\epsilon}{m} \sum_{i=1}^3 u_i F_i(x), \\ \dot{m} = -\beta_* \epsilon \|u\|, \\ \|u\| \leq 1, \\ x(0) = \xi_0^*, m(0) = m_0^*, \text{ and } x(t_f) = \xi_1^{\text{nat}}. \end{cases}$$

Indeed, a *constant null control*, with a null costate, constitutes the optimal extremal solution which follows the natural dynamics.

We can then construct a continuation of problems to manage to solve \mathcal{P}_{L^2} . We define the following family of problems depending continuously on the parameter $\lambda \in [0, 1]$ (see Figure 2.9 for an illustration)

$$\mathcal{P}_{\text{FS}}^\lambda \begin{cases} C_{L^2}(u) = \int_0^{t_f} \|u\|^2 dt \rightarrow \min, \\ \dot{x} = F_0(x) + \frac{\epsilon}{m} \sum_{i=1}^3 u_i F_i(x), \\ \dot{m} = -\beta_* \epsilon \|u\|, \\ \|u\| \leq 1, \\ x(0) = \xi_0^*, m(0) = m_0^*, \text{ and } x(t_f) = (1 - \lambda)\xi_1^{\text{nat}} + \lambda\xi_1^*. \end{cases}$$

This problem is associated to the corresponding shooting function

$$\mathcal{S}_{\text{FS}}^\lambda(p(0), p_m(0)) = \begin{pmatrix} \phi_{1, \dots, 6}^{\text{ext}}(\xi_0^*, m_0^*, p(0), p_m(0)) - \xi_1^\lambda \\ \phi_{14}^{\text{ext}}(\lambda_0^*, m_0^*, p(0), p_m(0)) \end{pmatrix} = \begin{pmatrix} 0 \\ 0 \end{pmatrix},$$

where

$$\xi_1^\lambda = (1 - \lambda)\xi_1^{\text{nat}} + \lambda\xi_1^*.$$

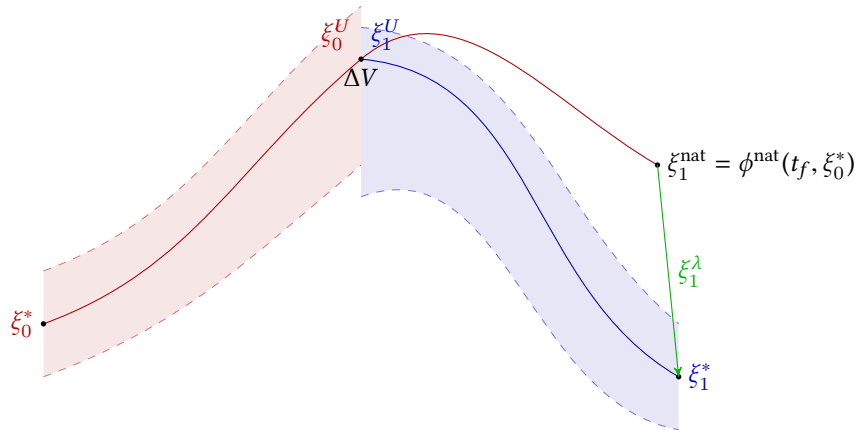


Figure 2.9 – Illustration of the continuation on the final state. ξ_1^{nat} is the propagation of the initial point ξ_0^* during the transfer time t_f . Step by step, we reach the final point $\xi_1^\lambda = (1 - \lambda)\xi_1^{\text{nat}} + \lambda\xi_1^*$, with λ going from 0 to 1.

2.7.2 Thrust Continuation

The maximal thrust can also be an issue. Indeed, the lower the magnitude of the maximal thrust, the smaller the attainable set, and so the more difficult the problem is to initialize. To overcome this difficulty, we use another continuation, but this time, on the maximal thrust.

Let ϵ_{obj} be the maximal thrust corresponding to the real engine that we want to use for the transfer. We also consider a greater thrust ϵ_{init} . For instance, consider the example of $\epsilon_{\text{obj}} = 0.3 \text{ N}$ and $\epsilon_{\text{init}} = 60 \text{ N}$. We denote by

$$\epsilon_\lambda = (1 - \lambda)\epsilon_{\text{init}} + \lambda\epsilon_{\text{obj}},$$

the intermediary thrust that allows us to define the following family of problems for all $\lambda \in [0, 1]$.

$$\mathcal{P}_{\text{thrust}}^\lambda \begin{cases} C_{L^2}(u) = \int_0^{t_f} \|u\|^2 dt \rightarrow \min, \\ \dot{x} = F_0(x) + \frac{\epsilon_\lambda}{m} \sum_{i=1}^3 u_i F_i(x), \\ \dot{m} = -\beta_* \epsilon_\lambda \|u\|, \\ \|u\| \leq 1, \\ x(0) = \xi_0^*, m(0) = m_0^*, \text{ and } x(t_f) = \xi_1^*. \end{cases}$$

2.8 Description of the Algorithm

We designed an algorithm (and implemented it in C++) to solve the problem of performing the transfer between two *natural* trajectories of two invariant manifolds (but not only). The description of the interface is given in appendix C. In this section, we briefly describe the algorithm.

2.8.1 Principle

The main idea is described by the following items and summarized in Figure 2.10.

- We start with the two points denoted by ξ_0^U and ξ_1^U in Section 2.6.1 and Figure 2.8. These points are chosen in such a way that they minimize the distance between the two intersections between invariant manifolds and the Poincaré cut we chose.
- We give two times of propagation $t_{\mathcal{A}_0}$ and $t_{\mathcal{A}_1}$ to build the end-points of the transfer and an additional parameter $\alpha_T \in]0, 1]$. This parameter allows to start the resolution with two points denoted by $\xi_0^{\alpha_T}$ and $\xi_1^{\alpha_T}$ and defined as

$$\xi_0^{\alpha_T} = \phi(-\alpha_T t_{\mathcal{A}_0}, \xi_0^U), \quad \text{and} \quad \xi_1^{\alpha_T} = \phi(\alpha_T t_{\mathcal{A}_1}, \xi_1^U).$$

These two points are closer than the two end-points defined as

$$\xi_0^* = \phi(-t_{\mathcal{A}_0}, \xi_0^U), \quad \text{and} \quad \xi_1^* = \phi(t_{\mathcal{A}_1}, \xi_1^U)$$

We then reach the two objective states ξ_0^* and ξ_1^* by continuation on the initial and final state as described in Section 2.7.1.²

- A (boolean) parameter is given to activate the continuation between the minimization of the L^2 -norm of the control and the minimization of the L^1 -norm. If it is active, then,

2. The continuation on the initial state can easily be derived from the explanation of the final state continuation.

to overcome some numerical difficulties, we add another parameter, to indicate the position of this continuation in the algorithm (see Figure 2.10).

- If we give two different maximal thrusts, the algorithm performs a continuation on the thrust as explained in Section 2.7.2.
- Checking the L^i -norm of the control ($i \in \{1, 2\}$) during the thrust continuation, we can verify if the border of the accessible set is reached (or at least get an indication of whether this is the case). If so, then we allow for an increase in the transfer time by another continuation on this parameter.

Of course, we allow for the initialization of a non zero costate to help convergence of the first step of the algorithm.

Coding Perspective

Although there exists excellent software to perform continuations for optimal control problem such as the well-known Hompack90 [89] or Hampath [30], because of the structure of the algorithm we developed, we chose to write our own code.

We implemented our code in C++, with interfaces to some very efficient FORTRAN codes. We used:

- the DOP853 explicit Runge-Kutta method developed by Hairer, Nørsett, and Wanner [45]. To verify our implementation of the method we developed, we added another integrator, `ode.f`, by Shampine and Gordon, which can be found on the website <http://www.netlib.org/ode/ode.f>.
- For the Newton-like method, we used the well known FORTRAN90 code: `hbrd.f90`, by A. Miller. In this file, there is an implementation of Powell's Hybrid algorithm used to solve sets of non-linear equations. This file can be found on the website <http://jblevins.org/mirror/amiller/#f>.

Note that we have not used automatic differentiation for the computation of the costate dynamics. We could have used, for instance, the very efficient software TAPENADE [47].

Our code is not ready to be published on the web, but we plan to clean it up and distribute it in a near future.

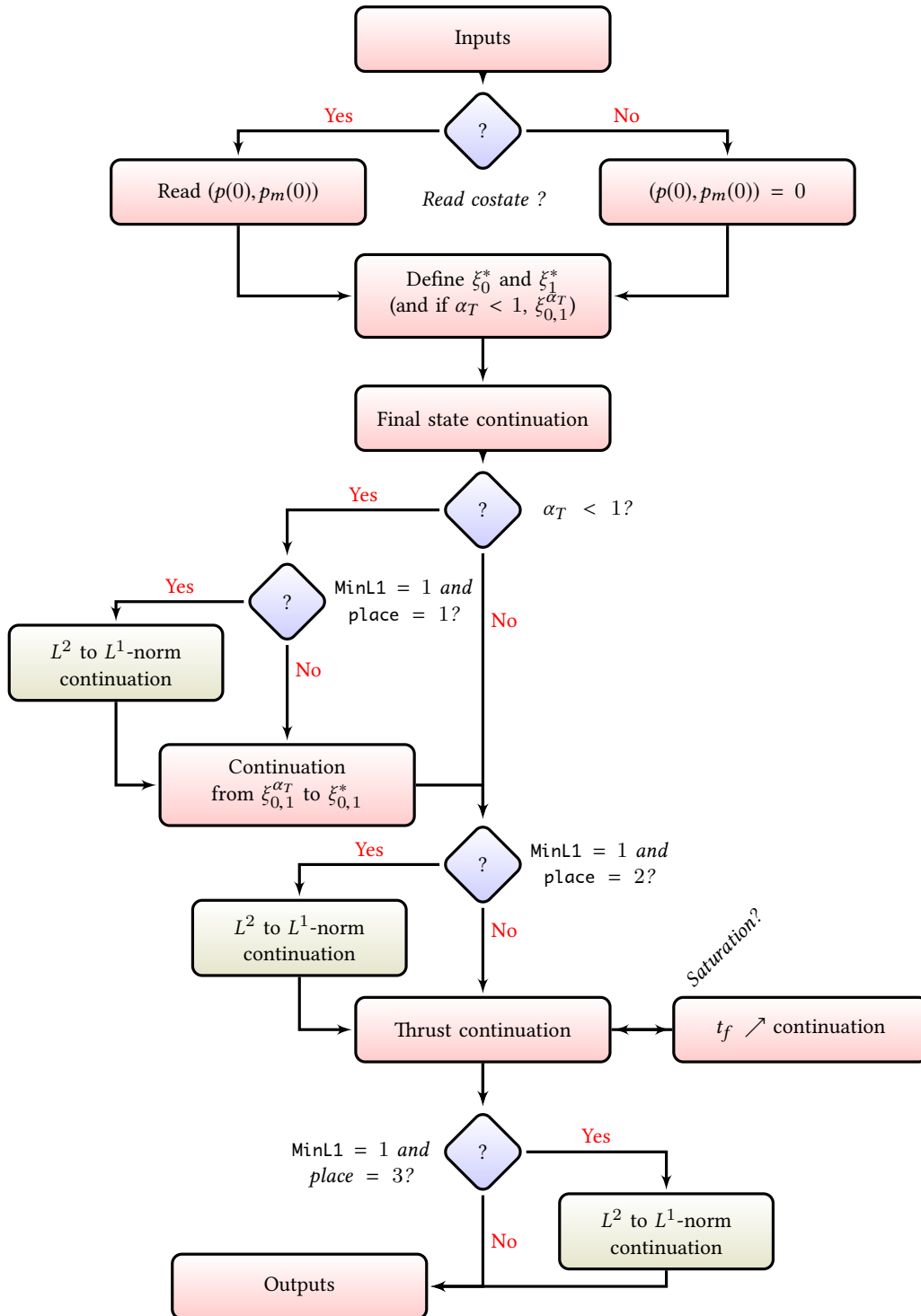


Figure 2.10 – Description of the algorithm to solve the transfer between invariant manifolds with low thrust.

2.9 Numerical Results

In this section, we apply the method that we developed to real transfers between invariant manifolds.

2.9.1 Transfer between Invariant Manifolds: {Earth-Moon} System, Halo Orbits

Let us consider once again the {Earth-Moon} system, and two Halo orbits around L_1 and L_2 with different energies. In table 2.1, we give the initial conditions and the periods for the two considered Halo orbits. These two Halo orbits have been computed with the same z -excursion of 16×10^3 km. Let us recall that the parameters for this CRTBP system can be found in table 1.1.

	x	y	z	
Halo L_1	8.23362033247E-01	0.0E+00	4.16230924917E-05	
Halo L_2	1.12040065667E+00	0.0E+00	4.16230924917E-05	
	\dot{x}	\dot{y}	\dot{z}	Period
Halo L_1	0.0E+00	1.26343508887E-01	0.0E+00	2.74294400617E+00
Halo L_2	0.0E+00	1.76071039637E-01	0.0E+00	3.41558381117E+00

Table 2.1 – Initial conditions and periods for the two Halo orbits around L_1 and L_2 used to perform the transfer between their invariant manifolds. Values are expressed in the normalized system of units of the {Earth-Moon} system.

We follow the method that was previously described:

1. We compute the manifolds from the two periodic orbits around L_1 and L_2 . Here, we consider Halo orbits (which are diffeomorphic to a circle). See Figure 1.9, page 50, for a plot of such an orbit.
2. We compute the intersections with the Poincaré cut U_2 . See Figure 2.11. We plot the different projections onto the (y, z) -plane (recall that x is set to $1 - \mu$ on U_2), the (y, \dot{y}) -plane and the (z, \dot{z}) -plane.
3. We find the two points ξ_0^U and ξ_1^U that minimize $\Delta\xi = \|\xi_0^U - \xi_1^U\|$. Note that we obtain not only a $\Delta V = \Delta\boldsymbol{v}$ but also a $\Delta\boldsymbol{x}$. Indeed, we observe in Figure 2.11 that there is no intersection in the projections onto the (y, \dot{y}) -plane.
4. We choose two times, previously denoted by $t_{\mathcal{A}_0}$ and $t_{\mathcal{A}_1}$. Here, we choose 0.5 for both times, expressed in the normalized system of units. This corresponds to a travel time of 4.34 days. Thanks to this choice, the two end-points can be built. We denote them by ξ_0^* and ξ_1^* . The two natural trajectories are plotted in Figure 2.12.

The final state continuation is straightforward as long as the maximal thrust is large enough. In Figure 2.13a, we plot the norm of the control during each step of the final state continuation, and we remark that even though the final control is smaller than 0.55 N, it reaches nearly 3 N during the continuation.

We compute the transfer starting with a maximal thrust of 60 N to reach 0.45 N by continuation. See Figure 2.13b for the plot of the evolution of the control norm with respect to time during the continuation. We observe that the control is saturated only for the last step of the continuation. Indeed, for a maximal thrust greater than 0.55 N, the control is not saturated, and so, the continuation on the maximal thrust does not change the optimal

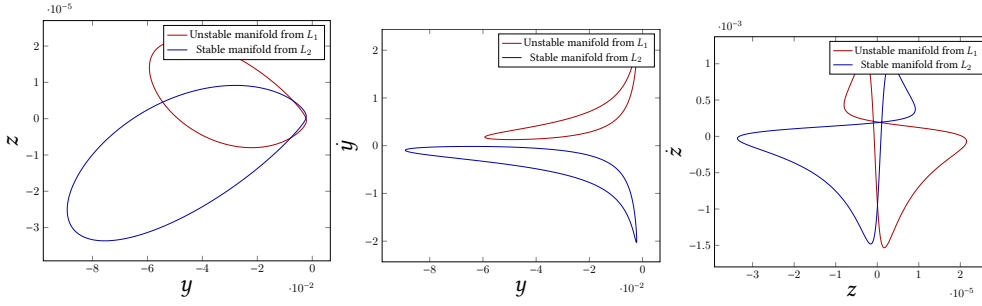
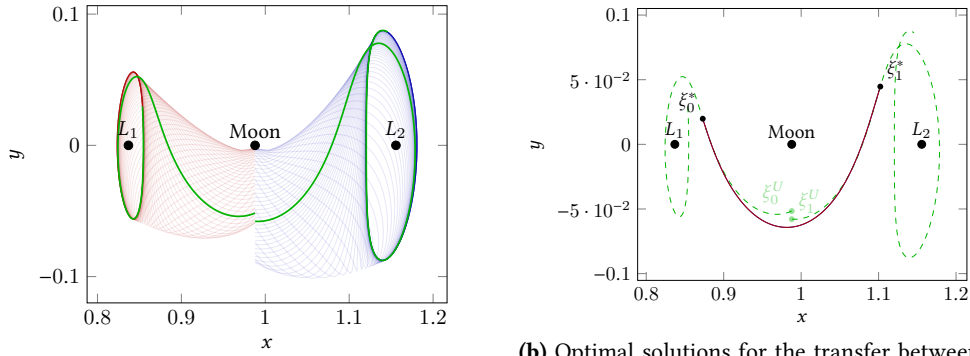


Figure 2.11 – {Earth-Moon} system: Different projections of the intersection with the Poincaré cut U_2 for the invariant manifolds associated with the two Halo orbits around L_1 and L_2 . Note that there is no intersection between the two manifolds, and this is obvious with the (y, \dot{y}) -plane projection.



(a) Intersection of the two invariant manifolds, and the two trajectories that correspond to ξ_0^U and ξ_1^U that minimize the distance between the two sections.

(b) Optimal solutions for the transfer between the two invariant manifolds. The solutions for the minimization of the L^2 -norm of the control and the solution for the L^1 -norm overlap because of the tiny difference between them.

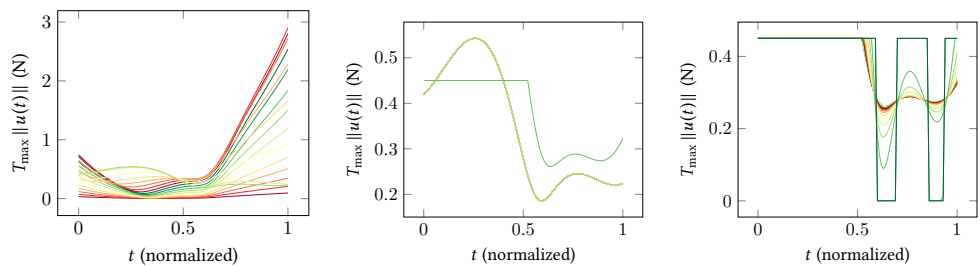
Figure 2.12 – {Earth-Moon} system: Construction and resolution of the transfer problem between the two invariant manifolds of two Halo orbits around L_1 and L_2 .

control, until reaching the critical value. One can think that it is useless to start this continuation with the value of 60 N, but, for instance, if we start with a value of 1 N, the final state continuation fails. Even though the control is not saturated, a large starting value provides us with a suitable attainable set, and allows the final step continuation to converge. This way the continuation on the thrust is very fast, and smooth.

The continuation on the cost between the L^2 -norm and the L^1 -norm is then performed and succeeds easily. The different steps in the continuation for the norm of the control are plotted in Figure 2.13c.

The final trajectories are plotted in Figure 2.12. The trajectories for both the L^1 -minimization and the L^2 -minimization are very close to each other and differences cannot be seen on the plot. Obviously, the more times we have to perform the transfer (that is to say the choice of $t_{\mathcal{A}_0}$ and $t_{\mathcal{A}_1}$), the smaller both the L^1 -cost and L^2 -cost are.

Because we are using exclusively indirect methods, the computation of the transfer, including all steps and continuations, only takes 13.18 s on a standard desktop computer. Each of the three continuations is very efficient, and they converge in, respectively, 19, 20 and 22 iterations. We used an initial mass of 1500 kg for the spacecraft, and the final mass



(a) Norm of the control in Newton during the final state continuation. (19 iterations)

(b) Norm of the control in Newton during the thrust continuation. Before reaching a maximal thrust below 0.55 N nothing changes. The last step of the continuation saturates the control. (20 iterations)

(c) Norm of the control in Newton during the continuation from the L^1 -norm of the control to the L^2 -norm. We finally get a bang-bang control. (22 iterations)

Figure 2.13 – Different continuations during the resolution of the transfer between invariant manifolds in the {Earth-Moon} system.

is 1492.885 68 kg for the minimization of the L^1 -norm of the control.

Remark 2.9:

We will see in the next chapter that this transfer method can be used in to design a complete mission initialized with several controlled and uncontrolled parts, the uncontrolled ones being trajectories belonging to invariant manifolds.

This is the idea of this work: we want to use, as explained in Section 2.1, the invariant manifolds in the Interplanetary Transport Network, connected by small optimal transfer between invariant manifolds, to initialize the complete mission. The final mission will consist of several uncontrolled parts (following the invariant manifolds) and controlled parts (the connection between manifolds computed with our algorithm).

2.9.2 Transfer between Invariant Manifolds: {Sun-Earth} System, Halo Orbits

This time we consider the {Sun-Earth} system, and two Halo orbits around L_1 and L_2 with different energies, respectively $\mathcal{E}_{L_1} = -1.500444$ and $\mathcal{E}_{L_2} = -1.500443$. In table 2.2, we give the initial conditions and the periods for the two considered Halo orbits. Once again, let us recall that the parameters for this CRTBP system can be found in table 1.1.

Once again, we follow exactly the same method, and perform the computation as easily as in the previous case. We plot the different projections of the intersection with the Poincaré cut U_2 in Figure 2.14.

As previously, we compute the two end-points ξ_0^U and ξ_1^U that minimize the distance between the two invariant manifolds and we choose the normalized time of propagation (backward and forward) to build the end-points of the transfer ξ_0^* and ξ_1^* . See Figure 2.15 for the plot of the manifolds and the two *natural* trajectories. Here, we have chosen $t_{\mathcal{A}_0} = t_{\mathcal{A}_1} = 0.5$. This corresponds to approximately 58 days. We choose a starting thrust of 60 N to reach a targeted thrust of 0.3 N.

The final state continuation is smooth and fast thanks to the rather large initial maximal thrust (see Figure 2.16a). Then, the thrust continuation is easier than for the {Earth-Moon}

	x	y	z	
Halo L_1	9.88877586385E-01	0.0E+00	4.01075229212E-06	
Halo L_2	1.00838140029E+00	0.0E+00	1.61657961732E-05	
	\dot{x}	\dot{y}	\dot{z}	Period
Halo L_1	0.0E+00	8.79724315850E-03	0.0E+00	3.06024482087E+00
Halo L_2	0.0E+00	9.75059689672E-03	0.0E+00	3.10252118223039E+00

Table 2.2 – Initial conditions and periods for the two Halo orbits around L_1 and L_2 used to perform the transfer between their manifolds. Values are expressed in the normalized system of unit of the {Sun-Earth} system.

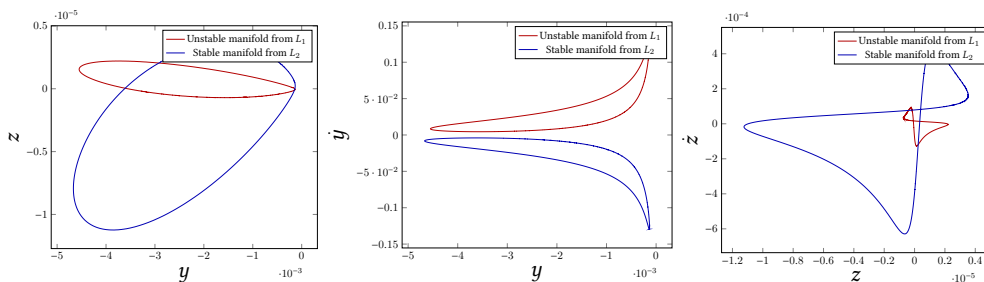


Figure 2.14 – {Sun-Earth} system: Different projections of the intersection with the Poincaré cut U_2 for the invariant manifolds associated with the two Halo orbits around L_1 and L_2 . Note that there is no intersection between the two manifolds, this is obvious on the (y, \dot{y}) -plane projection.

system, indeed, here we never reach the maximal thrust, and so, this continuation does not change the control at all (see Figure 2.16b).

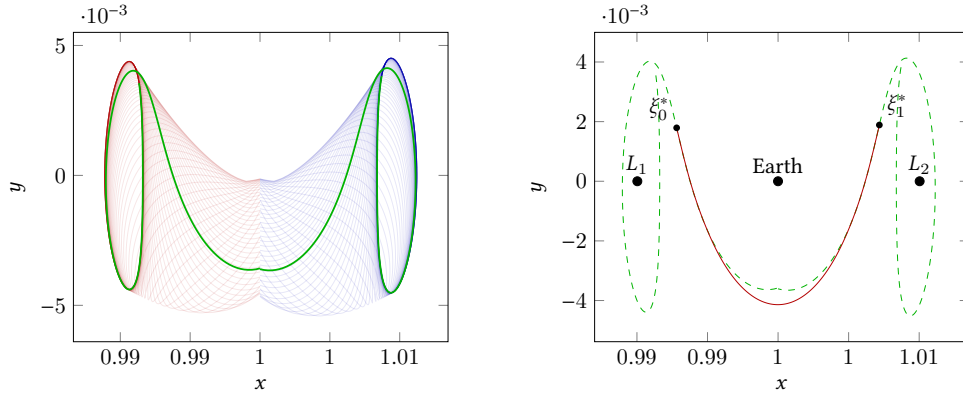
The continuation between the L^2 -minimization and the L^1 -minimization is straightforward. Note that we obtain a different structure for the bang-bang control, and here, we do not start this continuation with a saturated control.

Finally, we obtain an optimal trajectory. As before, the initial mass is of 1500 kg, and the final mass is 1490.1144 kg. The computational time on a simple desktop computer is 21.86 s for the entire computation of the transfer (from initial states computation to the last continuation on the cost). The final optimal trajectory is plotted in Figure 2.15 and the different controls for the different continuations are plotted in Figure 2.16.

2.9.3 Study of the Transfer Time Parameter

We have seen that one of the parameters that we fix is the transfer time. Of course, the larger the transfer time, the lower the cost (L^1 -norm or L^2 -norm). Moreover, it seems intuitive that the larger the time, the lower the maximum of the control norm during the transfer. We perform a numerical study of the influence of this parameter for the two transfers previously introduced: the transfer between invariant manifolds from Halo orbits in the {Sun-Earth} and {Earth-Moon} systems.

We vary the time parameter to test in different cases the efficiency of our algorithm. We consider the states ξ_0^U and ξ_1^U defined for the two transfer problems as the two states minimizing the distance in position and velocity (see Section 2.6.1). We then choose a sequence $(t_f^i)_{i \in \llbracket 1, N \rrbracket}$ discretizing interval $[0.001, 2.914]$ and we execute the algorithm for each t_f^i . The method is efficient and succeeds for almost every t_f^i . We plot in Figure 2.17 three sets



(a) Intersection of the two invariant manifolds, and the two trajectories that correspond to the two computed points ξ_0^U and ξ_1^U that minimize the distance between the two sections.

(b) Optimal solutions for the transfer between the two invariant manifolds. The solutions for the minimization of the L^2 -norm of the control and the solution for the L^1 -norm overlap because of the tiny difference between them.

Figure 2.15 – {Sun-Earth} system: Construction and solution of the transfer problem between the two invariant manifolds of two Halo orbits around L_1 and L_2 .

of tests for the {Sun-Earth} system and in Figure 2.18 for the {Earth-Moon} system. First, we plot the control for small times, when the norm of the control is high and looks like an impulse ΔV . The second set is a control for longer times (similar to the control obtained in the previous section). We observe that when we increase the transfer time, the method fails for a certain time interval. For the {Earth-Moon} system, the interval is

$$I_{EM} = [1.724, 2.224]$$

and for the {Sun-Earth} system the interval is

$$I_{SE} = [2.126, 2.526].$$

Note that these two intervals are discrete approximations. If we pass this interval, then the method succeeds again but it gives a different structure of the control and we observe that the optimal trajectories obtained have one revolution around the second primary (respectively Earth and Moon). There is a bifurcation in the structure of the optimal trajectory with respect to the time parameter. We plot the different trajectories for the two systems in 2.19a and 2.19b.



The time parameter is crucial. We have to pick it very carefully to obtain the desired result. Note that, whereas there is an interval in which our method fails, it succeeds for a very large range and so, it is not difficult to pick a suitable time.

Finally, because one can expect that when the transfer time goes to zero ($t_f \rightarrow 0$), we converge to the equivalent ΔV corresponding to an impulsive transfer, in Figure 2.20, we plotted the sequence η_i defined by

$$\eta_i = \left\| \int_0^{t_f^i} \epsilon_* \frac{\|u(t)\|}{m(t)} dt - \Delta V \right\|,$$

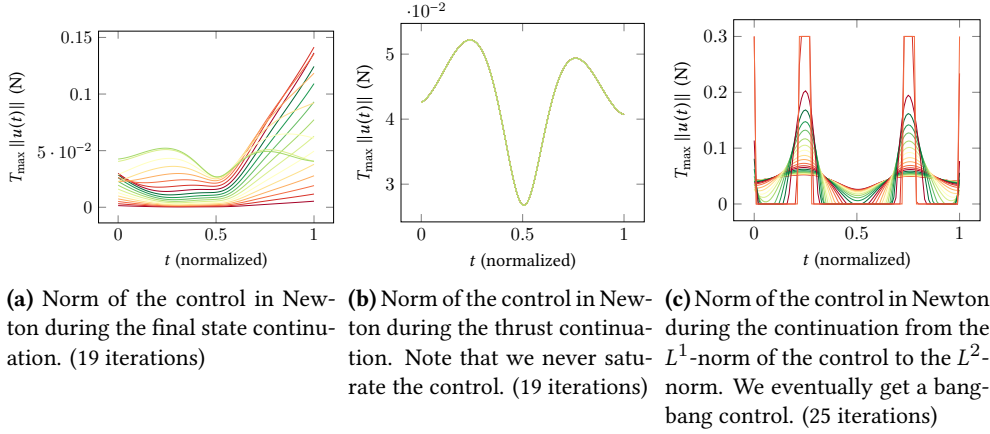


Figure 2.16 – Different continuations during the resolution of the transfer between invariant manifolds in the {Sun-Earth} system.

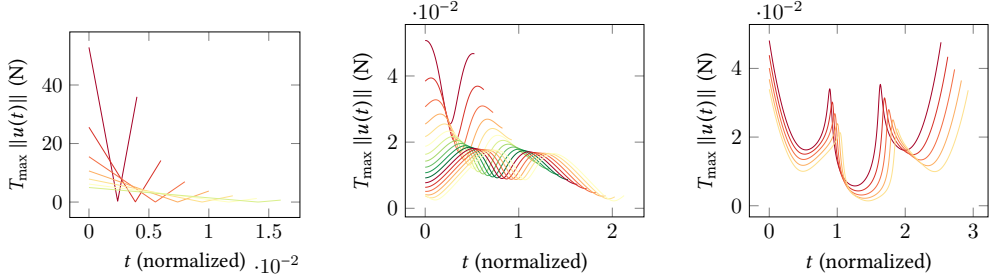


Figure 2.17 – Controls for different transfer times for the transfer between invariant manifolds from Halo orbits in the {Sun-Earth} system. Left: Small times, similar to ΔV . Center: Longer times. Right: After the interval I_{SE} , where the algorithm fails, we get a different structure for the control corresponding to a trajectory with a revolution.

where ΔV is defined by

$$\Delta V = \|\mathbf{v}_0^U - \mathbf{v}_1^U\|,$$

with $\xi_0^U = (\mathbf{x}_0^U, \mathbf{v}_0^U)$ and $\xi_1^U = (\mathbf{x}_1^U, \mathbf{v}_1^U)$

We observe that in both considered examples, we converge to the ΔV when the transfer time decrease. Note that, because there is also a $\Delta \mathbf{x}$ for the {Earth-Moon} example, we can expect that the convergence may not be to ΔV exactly. However, the main gap concerns the velocity, hence, in both case the Figure 2.20 shows that when t_f goes to 0, then $\eta_i \rightarrow 0$. This is coherent with the construction of the problem recalling that we have designed an optimal control problem starting with an impulsive transfer between the two invariant manifolds.

Conclusion

To conclude, we have designed a general algorithm (associated with software written in C++) that performs the transfer between two invariant manifolds. This relies on a few parameters that we have to choose. Of course, because we minimize the norm of the control (L^2 or L^1), we have to fix the transfer time. This is a crucial parameter. The study of the influence of this parameter should be done more precisely. Indeed, we know that the longer

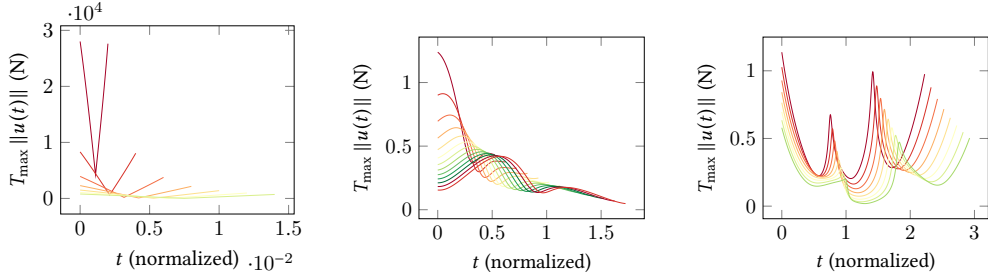
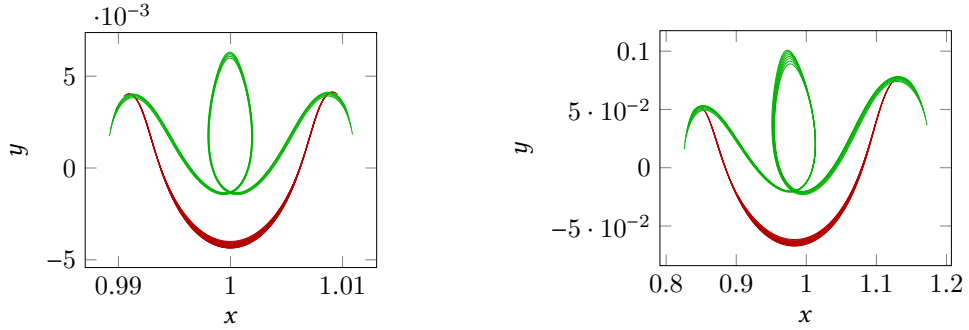


Figure 2.18 – Controls for different transfer time for the transfer between invariant manifolds from Halo orbits in the {Earth-Moon} system. Left: small times, similar to ΔV . Center: Longer times. Right: After the interval I_{SE} , where the algorithm fails, we get a different structure for the control corresponding to a trajectory with a revolution.



(a) For the {Sun-Earth} system.

(b) For the {Earth-Moon} system.

Figure 2.19 – Different optimal trajectories for the two considered systems. We observe a bifurcation when the time increases, after respectively I_{SE} and I_{EM} , the trajectories perform a revolution around the second primary.

the transfer time is, the smaller the cost is, but the drawback is that when we choose too long a transfer time, the first final state continuation can fail. We have seen that there exist some values of time for which our method fails but these times are sort of transition times between two structures of the trajectory with and without a revolution around the second primary. Before these times interval, the method is robust and succeeds for a large range of transfer times. Moreover, we observe that when the transfer time goes to 0, it seems that the control converges to the impulse control as expected. Finally, on our two experiments, we observe that the behavior with respect to the time parameter is independent of the CRTBP we consider.

We think that this algorithm and this method constitute a brick for designing interplanetary missions using invariant manifolds, and more precisely the Interplanetary Transport Network. We use it in such a way in the next chapter where a complete mission is designed, but we also think that it could be a good first step to initialize missions patching three body problems with some uncontrolled parts (trajectories in invariant manifolds) and some controlled parts computed by this method to connect the invariant manifolds.

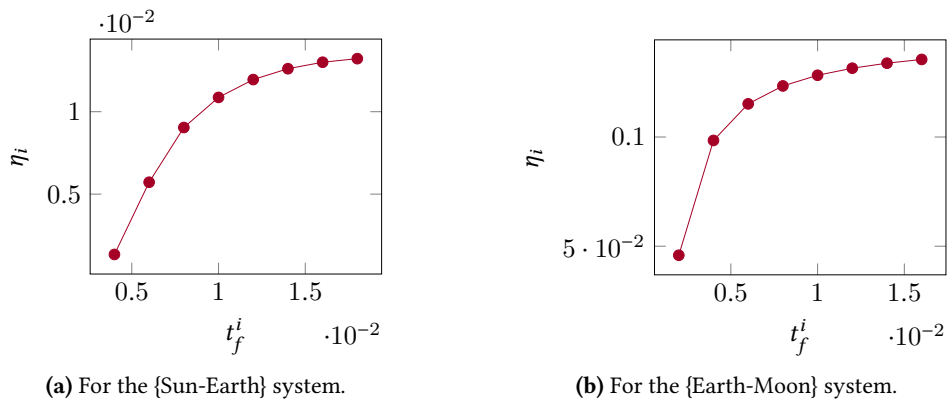


Figure 2.20 – Evolution of the sequence $(\eta_i)_{i \in I}$. In both cases, we observe that the cost converges to the impulse when the transfer time goes to zero.

Low-Thrust Missions between Libration Points with L^2 -Minimization

Contents

3.1	Dynamical Properties to Initialize the Resolution of an OCP . . .	101
3.2	The Lyapunov to Lyapunov Mission as an Optimal Control Problem	102
3.2.1	Optimal Control Problem (OCP)	103
3.2.2	Heteroclinic Orbits	104
3.2.3	From One Orbit to Another	106
3.2.4	Multiple Shooting	110
3.2.5	Thrust Continuation	112
3.2.6	Optimization of the Terminal Points	113
3.2.7	Numerical Results	114
3.3	Variants of the mission	115
3.3.1	With a Heteroclinic Orbit with Two Revolutions	116
3.3.2	Halo to Halo Mission	117

The content of this chapter is presented in the article [28] in collaboration with Emmanuel Trélat and Thomas Haberkorn (accepted for publication online and printed versions in ESAIM: Mathematical Modelling and Numerical Analysis).

3.1 Dynamical Properties to Initialize the Resolution of an OCP

In this chapter, we design missions using invariant manifolds. We consider missions between periodic orbits around the libration points L_1 and L_2 of the {Earth-Moon} system.

We develop here a method using invariant manifolds to initialize the resolution of an optimal control problem. Of course, this is built on the algorithm that was introduced in the

previous chapter. Indeed, it has been established how to perform transfers between invariant manifolds, and the same techniques can be applied between every natural trajectories of the CRTBP dynamical system, and in particular to periodic orbits.

We initialize an L^2 -minimization optimal control problem with an admissible trajectory in several parts: controlled ones to perform the transfer between natural trajectories which are the uncontrolled parts. An admissible trajectory is a sub-optimal trajectory performing the mission (it does not satisfy the necessary conditions of optimality). The controlled parts, between natural trajectories (belonging or not to invariant manifolds) are computed following the algorithm that we developed. We then use a multiple shooting method initialized with these different parts. Finally, thanks to the general transversality conditions given by the PMP, we optimize the start and end-points of the mission on the periodic orbits.

We first design a Lyapunov to Lyapunov mission using an heteroclinic orbit *asymptotically* connecting the two periodic orbits. This is a simple example of a planar mission between libration points. We consider this case to show that when a heteroclinic orbit exists, we observe the *turnpike structure* for the optimal solution (see [86]). Moreover, our method can be compared to the one in [33]. The author recently developed an efficient method to compute an optimal low-thrust transfer trajectory in *finite* time without using invariant manifolds of the three body problem. It is based on a three-step solution method using indirect methods and continuations methods and it gives good results.

In Section 3.3, we design two other missions. The first one is also a Lyapunov to Lyapunov mission, but with a different energy which allows for the existence of a heteroclinic orbit with two revolutions around the moon. The duration of this heteroclinic orbit is longer than the duration of the single revolution heteroclinic orbit, hence, we expect a smaller cost for the optimal solution.

Finally, in Section 3.3.2, we design a more useful mission between two 3D Halo orbits. We consider a very general case with two different energies for the two periodic orbits. Since we have chosen 3D periodic orbits and with different energies, there is no heteroclinic orbit. Hence, we initialize the resolution with three controlled parts, one to go from the first Halo orbit to the first invariant manifold, one to perform the connection between the two invariant manifolds, and one to go from the second invariant manifold to the second Halo orbit. One can note that we do not observe the turnpike property here because there is no “steady-state” trajectory connecting the two periodic orbits.

3.2 The Lyapunov to Lyapunov Mission as an Optimal Control Problem

We want to design a mission going from a periodic Lyapunov orbit around L_1 to a periodic Lyapunov orbit around L_2 using a low-thrust engine in the {Earth-Moon} system (see Figure 3.1). A full description of these periodic orbits is given in Section 1.4. Let us recall that these orbits are planar orbits diffeomorphic to a circle. In order to perform such a mission, we will use the properties introduced in Section 1.5: the existence of invariant manifolds. Indeed, if we are able to find an intersection between an “ L_1 unstable manifold” and an “ L_2 stable manifold”, we obtain an asymptotic trajectory that performs the mission with a zero thrust, called a heteroclinic orbit (see Section 2.1.2).

In the classical literature, such a mission is usually designed by using an impulse to reach the heteroclinic orbit from the Lyapunov orbit around L_1 and then another impulse to reach the Lyapunov orbit from the heteroclinic one. Since we design a low-thrust transfer, following this method is not allowed. In [32], the author developed a three-step method to perform a low-thrust, low-energy trajectory between Lyapunov orbits of the same energy without using invariant manifolds. At his first step, he uses a feasible quadratic-zero-quadratic con-

trol structure to initialize his method. In this work we will use the knowledge of a zero cost trajectory, the heteroclinic orbit, to initialize an indirect shooting method (Newton-like method for optimal control problem) set up by applying the Pontryagin Maximum Principle.

3.2.1 Optimal Control Problem (OCP)

Our main goal in this work is to solve an optimal control problem. We want to go from the Lyapunov orbit around L_1 to the Lyapunov orbit around L_2 with minimal energy. We respectively denote by Lya_1 and by Lya_2 the Lyapunov orbit around L_1 and L_2 . Mathematically we write this problem as follows

$$\mathcal{P}_g \begin{cases} C_g = \min \int_0^{t_f} \|u\|^2 dt, \\ \dot{x} = F_0(x) + \frac{\epsilon}{m} \sum_{i=1}^2 u_i F_i(x), \\ \dot{m} = -\beta_* \epsilon \|u\|, \\ \|u\| \leq 1, \\ x(0) \in \text{Lya}_1, \text{ and } x(t_f) \in \text{Lya}_2. \end{cases} \quad (3.1)$$

Let us summarize the steps in the method we developed to solve this problem :

1. First, we find a heteroclinic orbit from the Lyapunov orbit around L_1 to the Lyapunov orbit around L_2 . We denote by *Het* this orbit.
2. Then, we realize a short transfer from a *fixed point* on the Lyapunov orbit around L_1 to the heteroclinic orbit.
3. Similarly, we realize a transfer from the heteroclinic orbit to a *fixed point* on the Lyapunov orbit around L_2 .
4. Then we release the constraint on the position of the matching connections on the heteroclinic orbit by using a multiple shooting method and we decrease the maximal thrust.
5. Finally, we optimize the position of the two fixed points on Lya_1 and Lya_2 to satisfy the transversality condition for problem (3.1).

We note that in steps 2 to 4 (in which we solve optimal control problems), we have fixed the departure and arrival points to simplify the problem. The last step consists in releasing these constraints.

Remark 3.1:

The *real* problem that we want to solve is the minimization of the fuel consumption (the maximization of the final mass). This is done by considering the minimization of the L_1 -norm of u

$$C_g^{L_1} = \min \int_0^{t_f} \|u\| dt.$$

Unfortunately, this implies numerical difficulties and for simplicity, we only consider here the L_2 -minimization problem. One of the perspectives of this work is to use, for example, another continuation on the cost.

This is due to the very low optimal control that we get after the L^2 -minimization. Indeed, the continuation between the L^2 -minimization and the L^1 -minimization fails be-

cause the engine thrust specification of 0.3 N we have picked is far too big to allow for convergence to a bang-bang control.

3.2.2 Heteroclinic Orbits

Let us first find the heteroclinic orbit between a Lyapunov orbit around L_1 and a Lyapunov orbit around L_2 . One condition to be able to find such an orbit is to compute an intersection between two manifolds. Hence, these two manifolds should have the same energy. Since the manifold and the Lyapunov orbit have the same energy, we must compute two Lyapunov orbits around L_1 and L_2 at a given, shared, energy.

The study of the well known Hill regions (see [52] and references therein), *i.e.* the projection of the energy surface of the uncontrolled dynamics onto the position space gives us an indication of the interval of energy we can use. Indeed, we have to compute an orbit with an energy greater than the energy of L_2 . Because we want to realize a low-thrust transfer, we choose to keep a low energy. Moreover, we have a smaller region of possible motion, and so, a possibly shorter transfer.

Using the method described in 1.4.4, we choose to get two orbits with an energy of -1.592081 in the normalized system.

Finding the intersection. To find an intersection, we introduce two 2D sections $U_2 = \{(x, y) \in \mathbb{R}^2, x = 1 - \mu, y < 0\}$, and $U_3 = \{(x, y) \in \mathbb{R}^2, x = 1 - \mu, y > 0\}$. We represent them in Figure 3.1.

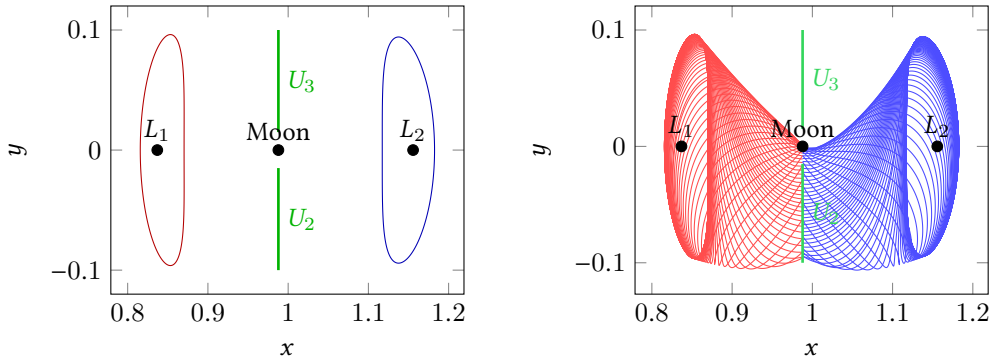


Figure 3.1 – Left: Planes U_2 and U_3 in the {Earth-Moon} system. Right: unstable (red) and stable (blue) manifolds respectively from L_1 and L_2 stopping at the plane U_2

Then, we compute the intersection of the unstable manifold from L_1 and the stable manifold from L_2 with the plane U_2 (of course, we can do the symmetric counterpart: stable manifold from L_1 and unstable manifold from L_2 with the plane U_3). Since the x -coordinate is fixed by U_2 and because the energies of the two manifolds are equal, we just have to compute the intersection in the (y, \dot{y}) -plan (values of \dot{x} are deduced from the energy equation (1.10)).

We show in Figure 3.2 the U_2 -section and the existence of intersections for our particular energy. To find precisely one intersection point, we have used once more a Newton-like method. We can parametrize the section of one manifold with U_2 with only one parameter, the parameter of the Lyapunov orbit. We denote by $\phi_{x=1-\mu}^+$, the flow propagating forward a state point from L_{y_1} onto the plane U_2 , and by $\phi_{x=1-\mu}^-$ the flow propagating backward

a state point from Lya_2 onto the plane U_2 . Time of propagation is fixed by the condition $x = 1 - \mu$.

We want to find two points $\xi_{L_1} \in \text{Lya}_1$ and $\xi_{L_2} \in \text{Lya}_2$ such that

$$\phi_{x=1-\mu}^+(\xi^{u+}(\xi_{L_1})) - \phi_{x=1-\mu}^-(\xi^{s-}(\xi_{L_2})) = 0,$$

where ξ^{u+} and ξ^{s-} are defined in (1.21). This is an equality in \mathbf{R}^2 , and because each of the Lyapunov orbits is parametrized with a one dimensional parameter (the time), our problem is well posed.

To initialize the method we use a discretisation (100 points in this particular example) of the Lyapunov orbits and we take the two points minimizing the Euclidean norm in the U_2 section.

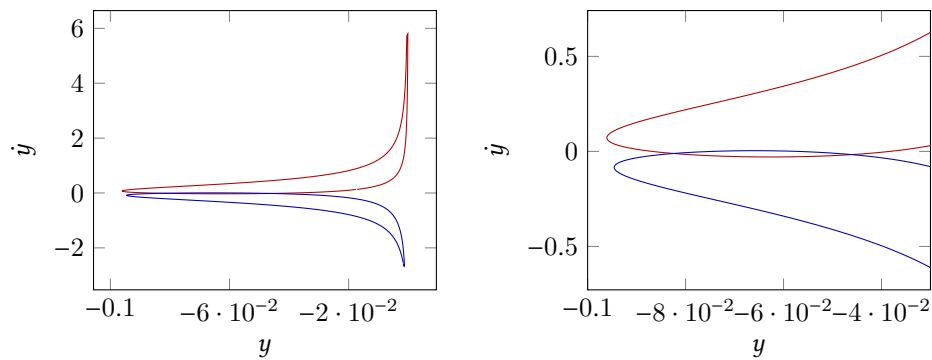


Figure 3.2 – Section in the plane U_2 of a unstable manifold from L_1 and a stable manifold from L_2 . The energy is -1.592081 . On the right, a zoom on the interesting area.

In our case, with a value of energy equal to -1.592081 and $\alpha = \frac{1}{384402}$ from (1.21), we obtain the heteroclinic trajectory represented in Figure 3.3. From now on, we will denote this heteroclinic orbit by Het. Note that this computation only takes a few seconds on a standard desktop computer.

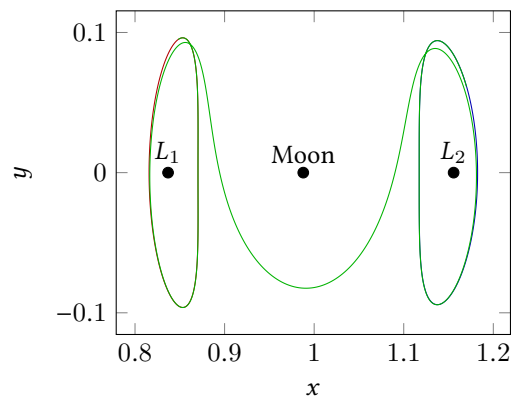


Figure 3.3 – Heteroclinic orbit between two Lyapunov orbits in the {Earth-Moon} system. We get a travel time of 8.9613933501964 (normalized time) or 38.974 days.

3.2.3 From One Orbit to Another

Here, we construct two rather simple problems: first we compute an optimal control using the Pontryagin Maximum Principle reaching the heteroclinic orbit from the Lyapunov orbit around L_1 , then we compute an optimal control to reach the Lyapunov orbit around L_2 from the heteroclinic orbit. This way, we get an admissible control that follows the null control heteroclinic orbit during a certain time.

Around L_1

Problem Statement. Consider two points $\xi_0^* \in \text{Lya}_1$ and $\xi_1^* \in \text{Het}$, a time t_0 and an initial mass $m_0^* = 1500$ kg. We apply the Pontryagin Maximum Principle to the following problem:

$$\mathcal{P}_{L_1} \begin{cases} \min \int_0^{t_0} \|u\|^2 dt, \\ \dot{x} = F_0(x) + \frac{\epsilon}{m} \sum_{i=1}^2 u_i F_i(x), \\ \dot{m} = -\beta_* \epsilon \|u\|, \\ \|u\| \leq 1, \\ x(0) = \xi_0^*, m(0) = m_0^* \text{ and } x(t_0) = \xi_1^*. \end{cases} \quad (3.2)$$

Here, we have fixed the two points ξ_0^* and ξ_1^* on the Lyapunov orbit and the heteroclinic orbit. We will see how we choose these points later. We will release the constraint on the position of these two points by an optimization and satisfy the transversality conditions for problem 3.1 in the last steps of our method.

If t_0 is greater than the *minimum time*, we can show that we are in the *normal* case for the Pontryagin Maximum Principle, that is to say p^0 can be normalized to -1 (see proposition 4 page 84). Although we have not proved that this assumption holds, we will see that it is a reasonable one because of the construction of our two points. Moreover, because normality of the trajectories relies on the invariance of the target with respect to the zero control (see [39] and [26]), the normality property holds for the *targeted problem* (3.1).

We have established the structure of the control given by the maximization condition of the PMP for this cost on page 87. Hence, we can write this problem as a shooting function. We denote by ϕ^{ext} the extremal flow of the extremal system. Hence, we define the shooting function:

$$\mathcal{S}_{L_1}(p(0), p_m(0)) = \begin{pmatrix} \phi_{1,\dots,4}^{\text{ext}}(\xi_0^*, m_0^*, p(0), p_m(0)) - \xi_1 \\ \phi_{10}^{\text{ext}}(\xi_0^*, m_0^*, p(0), p_m(0)) \end{pmatrix} = \begin{pmatrix} \mathbf{0} \\ 0 \end{pmatrix}. \quad (3.3)$$

We compute the solution, that is to say $p(0)$ and $p_m(0)$ using a shooting method (Newton-like method applied to (3.3)). As we have seen in the previous chapter, the main difficulty is to *initialize* the Newton-like algorithm. To do that, we apply the same algorithm that we developed for the transfer between invariant manifolds.

Construction of ξ_0^* and ξ_1^* . We want to realize the transfer from Lya_1 to Het and we have already computed the heteroclinic orbit. The method is the following:

1. If we denote by $\xi_{\text{Het}}^{L_1}$ the first point of the “numerical” heteroclinic orbit near the Lyapunov orbit, we find $\xi_{\text{Lya}_1} \in \text{Lya}_1$ by minimizing the euclidean norm :

$$\xi_{\text{Lya}_1} = \arg \min_{\xi \in \text{Lya}_1} \left\| \xi_{\text{Het}}^{L_1} - \xi \right\|.$$

2. Then, we propagate backward in time ξ_{Lya_1} following the uncontrolled dynamics during a time t_{Lya_1} (smaller than the period of the Lyapunov orbit) to get ξ_0^*
3. We propagate forward in time $\xi_{\text{Het}}^{L_1}$ during a reasonable time $t_{\text{Het}}^{L_1}$ to get ξ_1^* (small compared to the travel time to reach the other extremity of Het).

We define the transfer time t_0 in (3.2) as

$$t_0 = t_{\text{Lya}_1} + t_{\text{Het}}^{L_1}.$$

Although it seems to be more simple a problem than problem (3.1), the main difficulty is still to initialize the shooting method. We use a continuation method on the final state, as introduced in Section 2.7.1, page 88.

Final State Continuation. As explained in Section 2.7.1, we construct a family of problems $\mathcal{P}_{L_1}^\lambda$ depending continuously on one parameter λ such that $\mathcal{P}_{L_1}^0$ is easy to solve and $\mathcal{P}_{L_1}^\lambda$ corresponds to the targeted problem, that is to say (3.2).

First, let us define $\xi_{\text{Lya}_1}^{\text{nat}}$ as the forward propagation of ξ_{Lya_1} following the uncontrolled dynamics during time t_0 . Then we define the family of problems:

$$\mathcal{P}_{L_1}^\lambda \begin{cases} \min \int_0^{t_0} \|u\|^2 dt, \\ \dot{x} = F_0(x) + \frac{\epsilon}{m} \sum_{i=1}^2 u_i F_i(x), \\ \dot{m} = -\beta_* \epsilon \|u\|, \\ \|u\| \leq 1, \\ x(0) = \xi_0^*, \quad m(0) = m_0^*, \\ x(t_0) = (1 - \lambda)\xi_{\text{Lya}_1}^{\text{nat}} + \lambda\xi_1^*. \end{cases}$$

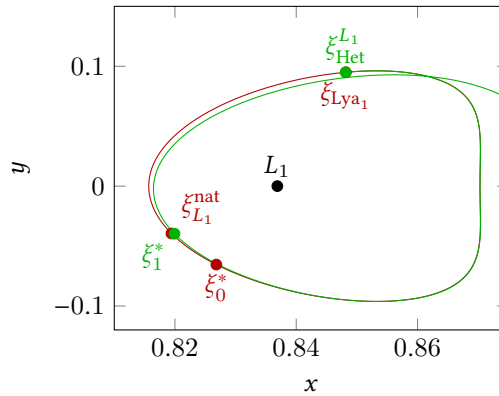


Figure 3.4 – All relevant points in the construction of the problem.

Since $\xi_{\text{Lya}_1}^{\text{nat}}$ corresponds to the uncontrolled dynamics, the corresponding initial costate $(p(0), p_m(0))$ is zero. Then, step by step, we initialize the shooting method of $\mathcal{P}_{L_1}^{\lambda_i}$ using the solution of $\mathcal{P}_{L_1}^{\lambda_{i-1}}$ to reach problem (3.2). This is done by a PL continuation (see Section 2.5.2 page 78), *i.e.*, the solution of the two previous iterations of the continuation are used to initialize the resolution of the next step by a linear prediction.

Figure 3.4 shows the different points defined for some parameters described below.

Numerical Results. We show here the numerical results for this transfer. We choose a maximal thrust equal to 60 N. We postpone to Section 3.2.4 the problem of the maximum thrust which should be very small. In fact, a high thrust implies that the magnitude of the costate stays very low, and it will be necessary for the multiple shooting to converge. Indeed, for a non-saturating control, the higher the maximal magnitude of the thrust, the lower the control u between $[0, 1]$, and so the lower the magnitude of $\psi(\zeta)$ and in turn of the costate. Recall that ψ is the switching function defined in (2.16) and ζ is the extremal state. Moreover, we choose the two times of propagation in the normalized system as

$$t_{\text{Lya}_1} = 1.0, \text{ and } t_{\text{Het}}^{L_1} = 2.0.$$

We obtain the optimal trajectory plotted in Figure 3.4. The optimal command is shown in Figure 3.5. One can see that we are far from the saturation of the command, indeed, the maximum value is approximately 6×10^{-6} , whereas we are constrained by one. We postpone the discussion on the real value in Newton to the final trajectory.

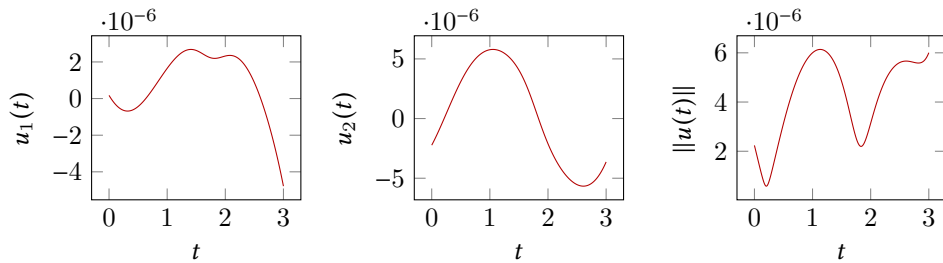


Figure 3.5 – Command to realize the optimal transfer from the Lyapunov orbit to the heteroclinic orbit. We plot $u(\cdot) \leq 1$ as a function of the normalized time.

This continuation gives us an initial adjoint vector (costate) that we will denote by p_0^* and p_m^{0*} in the remainder of this section.

Around L_2

We design a very similar problem around L_2 .

Problem Statement. Consider two points $\xi_2^* \in \text{Het}$ and $\xi_3^* \in \text{Lya}_2$, a time t_2 and an initial mass m_2^* .¹ The mass m_2^* is the final mass obtained after solving for the transfer around L_1 (between the two problems we follow a heteroclinic orbit without any fuel consumption). We apply the Pontryagin Maximum Principle to the following problem:

$$\mathcal{P}_{L_2} \begin{cases} \min \int_0^{t_2} \|u\|^2 dt, \\ \dot{x} = F_0(x) + \frac{\epsilon}{m} \sum_{i=1}^2 u_i F_i(x), \\ \dot{m} = -\beta_* \epsilon \|u\|, \\ \|u\| \leq 1, \\ x(0) = \xi_2^*, m(0) = m_2^* \text{ and } x(t_2) = \xi_3^*. \end{cases} \quad (3.4)$$

As before, we have fixed ξ_2^* and ξ_3^* on the heteroclinic and Lyapunov orbits. The final steps will allow us to release these constraints.

1. We will see later on why we use 2 as subscript.

Note that the problem is very similar to the problem around L_1 hence, we get the following shooting function

$$\mathcal{S}_{L_2}(p(0), p_m(0)) = \begin{pmatrix} \phi_{1, \dots, 4}^{\text{ext}}(\xi_2^*, m_2^*, p(0), p_m(0)) - \xi_3^* \\ \phi_{10}^{\text{ext}}(\xi_2^*, m_2^*, p(0), p_m(0)) \end{pmatrix} = \begin{pmatrix} \mathbf{0} \\ 0 \end{pmatrix}.$$

Construction of ξ_2^* and ξ_3^* . We construct the two points following the same method as for the problem around L_1 .

1. If we denote by $\xi_{\text{Het}}^{L_2}$ the last point of the heteroclinic orbit near the Lyapunov orbit, we find $\xi_{\text{Lya}_2} \in \text{Lya}_2$ minimizing the euclidean norm :

$$\xi_{\text{Lya}_2} = \arg \min_{\xi \in \text{Lya}_2} \left\| \xi_{\text{Het}}^{L_2} - \xi \right\|$$

2. Then, we propagate forward ξ_{Lya_2} following the uncontrolled dynamics during a time t_{Lya_2} (smaller than the period of the Lyapunov orbit) to get ξ_3^* .
3. We propagate backward $\xi_{\text{Het}}^{L_2}$ during a reasonable time $t_{\text{Het}}^{L_2}$ (small compared to the traveling time to reach the other extremity) to get ξ_2^* .

We define the transfer time t_2 in (3.4) as

$$t_2 = t_{\text{Lya}_2} + t_{\text{Het}}^{L_2}.$$

Final State Continuation. As before, we construct a family of problems $\mathcal{P}_{L_2}^\lambda$ depending continuously on a parameter λ such that $\mathcal{P}_{L_2}^0$ is easy to solve and $\mathcal{P}_{L_2}^1$ corresponds to the targeted problem, that is to say (3.2).

First, let us define $\xi_{\text{Het}}^{\text{nat}}$ as the forward propagation of ξ_{Het} following the uncontrolled dynamics during the time t_2 . Then we define the family of problems

$$\mathcal{P}_{L_2}^\lambda \begin{cases} \min \int_0^{t_2} \|u\|^2 dt, \\ \dot{x} = F_0(x) + \frac{\epsilon}{m} \sum_{i=1}^2 u_i F_i(x), \\ \dot{m} = -\beta_* \epsilon \|u\|, \\ \|u\| \leq 1, \\ x(0) = \xi_2^*, \quad m(0) = m_2^*, \\ x(t_2) = (1 - \lambda)\xi_{\text{Het}}^{\text{nat}} + \lambda\xi_3^*. \end{cases}$$

Numerical Results. As before, we set $T_{\text{max}} = 60$ N, and we compute the continuation for the two times chosen as

$$t_{\text{Het}}^{L_2} = 2.0, \text{ and } t_{\text{Lya}_2} = 1.0.$$

Figure 3.6 shows the optimal control to realize the final transfer from the heteroclinic orbit to the Lyapunov one around L_2 . We see that, once again, we are far from the saturation of u .

This continuation gives us an initial costate that we will denote by p_2^* and p_m^{2*} in the remainder of this section.

Table 3.1 summarizes all the parameters for the continuation computation. We observe that, because we are using indirect shooting methods, the computation is very fast even

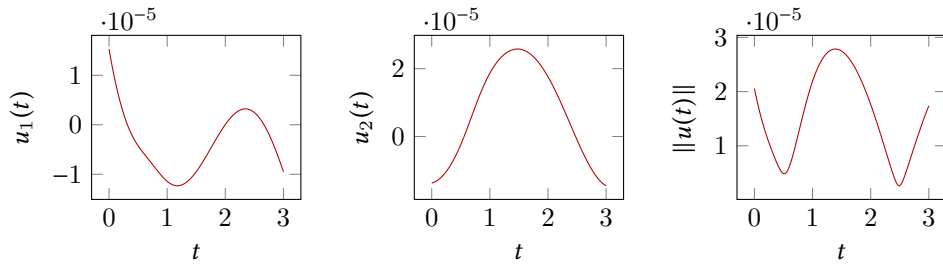


Figure 3.6 – Command to realize the optimal transfer from the Lyapunov orbit to the heteroclinic orbit. We plot $u(\cdot) \leq 1$ as a function of the normalized time.

though it is performed on a simple desktop computer or on a single-board computer (the Raspberry Pi).

I_{sp}	g_0	Earth Mass	Moon Mass	Distance	Period
2000 s	$9.8 \text{ m}^3 \text{ kg}^{-1} \text{ s}^{-2}$	$5.972 \times 10^{24} \text{ kg}$	$7.349 \times 10^{22} \text{ kg}$	$384\,402 \times 10^3 \text{ m}$	$2.361 \times 10^6 \text{ s}$

Transfer	Iterations	Cost	T_{\max}
L_1	21	$6.309\,67 \times 10^{-11}$	60 N
L_2	19	$9.061\,24 \times 10^{-10}$	60 N

System	Transfer	Execution time
Core i7	L_1	98% cpu 2,821s total
	L_2	96% cpu 1,439s total
Raspberry Pi A	L_1	38% cpu 8,009s total
	L_2	22% cpu 7,879s total

Table 3.1 – Numerical results for the two transfers around L_1 and L_2 . Computations are performed on a simple laptop Core i7, and on a Raspberry Pi A, a credit card-sized single-board computer.

Remark 3.2:

The computational time with the Raspberry Pi A shows that this kind of methods are very fast and do not require big units of computation. Hence, we can imagine to embed this software on a spacecraft to compute optimal trajectories on the fly.

3.2.4 Multiple Shooting

Thanks to the results from previous sections, we have designed an admissible control to perform the transfer from a Lyapunov orbit around L_1 to a Lyapunov orbit around L_2 . We first reach a point on a heteroclinic orbit, then we follow the natural dynamics (null control), and finally reach a point on the final Lyapunov orbit from a certain point on the heteroclinic orbit. This admissible trajectory is however not energy optimal, since the stay on the heteroclinic orbit is forced.

The two points on the heteroclinic orbit were arbitrarily chosen. There is no guarantee that they provide a good choice in terms of optimality. Hence, we want to release the constraints on the position of these two points. We use a multiple shooting method on top of the first two local transfers to get a better optimum.



This is a key point of our method. In different contributions such as [31, 23, 91], the authors use the resolution of a time minimum problem to initialize the L^2 -minimization (and then a L^1 -minimization). Here, we use the dynamical information given *a priori* to initialize the L^2 -minimization.

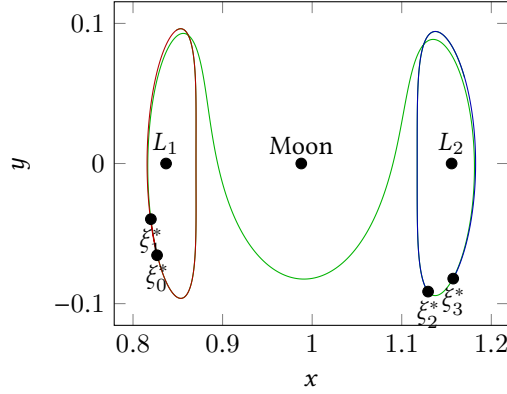


Figure 3.7 – Admissible trajectory in three parts.

Let us describe how we state the multiple shooting problem. As we can see in Figure 3.7, there are two points ξ_1^* and ξ_2^* belonging to the heteroclinic orbit that we want to free. Moreover, we consider three times:

- t_0 which is the time defined for the transfer around L_1 ;
- t_2 which is the time defined for the transfer around L_2 ;
- t_1 which is the total time of the computed heteroclinic orbit minus the two times $t_{\text{Het}}^{L_1}$ and $t_{\text{Het}}^{L_2}$ used in the two previous transfers.

We define $t_{\text{tot}} = t_0 + t_1 + t_2$ and we write a new optimal control problem with the same structure as the previous one around L_1 and L_2 .

$$\mathcal{P}_{\text{tot}} \begin{cases} C_{\text{tot}} = \min \int_0^{t_{\text{tot}}} \|u\|^2 dt, \\ \dot{x} = F_0(x) + \frac{\epsilon}{m} \sum_{i=1}^2 u_i F_i(x), \\ \dot{m} = -\beta_* \epsilon \|u\|, \\ \|u\| \leq 1, \\ x(0) = \xi_0^* \in \text{Lya}_1, \quad m(0) = m_0^*, \\ x(t_{\text{tot}}) = \xi_3^* \in \text{Lya}_2. \end{cases} \quad (3.5)$$

As before, we apply the Pontryagin Maximum Principle to get a necessary condition for the optimal control. We are able to write the control u with respect to the state (x, m) and the costate (p, p_m) , we can write a shooting function, with the same results as the ones obtained in Section 3.2.3.

Thanks to the following method, we get an admissible trajectory in three parts, and it is quite natural to use it to construct a multiple shooting function. This is where we use the dynamical information. We define

$$Z = \underbrace{(p_0, p_m^0)}_{P_0}, \underbrace{\xi_1, m_1, p_1, p_m^1}_{X_1}, \underbrace{\xi_2, m_2, p_2, p_m^2}_{X_2} \in \mathbf{R}^{25},$$

then we write the multiple shooting function with two matching conditions on the state and the costate, the final state condition, and the free final mass:

$$\mathcal{S}_{\text{multi}}(Z) = \begin{pmatrix} \phi_{1,\dots,5}^{\text{ext}}(\xi_0^*, m_0^*, P_0) - X_1 \\ \phi_{6,\dots,10}^{\text{ext}}(\xi_0^*, m_0^*, P_0) - P_1 \\ \phi_{1,\dots,5}^{\text{ext}}(X_1, P_1) - X_2 \\ \phi_{6,\dots,10}^{\text{ext}}(X_1, P_1) - P_2 \\ \phi_{1,\dots,4}^{\text{ext}}(X_2, P_2) - \xi_3^* \\ \phi_{10}^{\text{ext}}(X_2, P_2) \end{pmatrix}. \quad (3.6)$$

We want to find the vector Z such that $\mathcal{S}_{\text{multi}}(Z) = 0$ and, as in previous sections, we use a Newton-like algorithm. The main difficulty is as usual to initialize the algorithm. This time, it is done by the previous *local* transfers, since we choose²

$$\begin{cases} p_0 = p_0^*, & \xi_1 = \xi_1^*, & p_1 = \mathbf{0}, & \xi_2 = \xi_2^*, & p_2 = p_2^*, \\ p_m^0 = p_m^{0*}, & m_1 = m_2^*, & p_m^1 = 0, & m_2 = m_2^*, & p_m^2 = p_m^{2*}. \end{cases}$$

The choices $m_1 = m_2^*$, $p_1 = \mathbf{0}$ and $p_m^1 = 0$ are made because we initialize the trajectory with the heteroclinic part that we have computed, that is to say with a null control and without consumption of mass.

The Newton-like algorithm gives us a complete trajectory which is not constrained to follow the heteroclinic orbit. In Figure 3.9 and Figure 3.8, we can see the trajectory and the associated control.

We keep the maximum thrust equal to 60 N to allow the Newton-like algorithm to converge. But, we want to be able to give the right specification for the engine of the spacecraft. Let us see how we make this possible.

3.2.5 Thrust Continuation

Using, the continuation method that we introduced in Section 2.7.2, we want to constrain the thrust to a real value for a low-thrust engine, let us say 0.3 N. To do that, we construct a family of problems as before. Let us denote by ϵ_0 the initial maximal thrust in normalized units corresponding to $T_{\text{max}} = 60$ N. Similarly, let us denote by ϵ_1 the maximal thrust that we want to get corresponding to $T_{\text{max}} = 0.3$ N. Finally, we define the maximal continuation thrust:

$$\epsilon_\lambda = (1 - \lambda)\epsilon_0 + \lambda\epsilon_1.$$

2. Note that the notation p_1 and p_2 is not for the first and second components of the costate but for two different costate belonging to \mathbf{R}^4 .

We can now define the family of problems:

$$\mathcal{P}_{\text{thrust}}^\lambda \begin{cases} \min \int_0^{t_{\text{tot}}} \|u\|^2 dt, \\ \dot{x} = F_0(x) + \frac{\epsilon_\lambda}{m} \sum_{i=1}^2 u_i F_i(x), \\ \dot{m} = -\beta_* \epsilon_\lambda \|u\|, \\ \|u\| \leq 1, \\ x(0) = \xi_0^* \in \text{Lya}_1, \quad m(0) = m_0^*, \\ x(t_{\text{tot}}) = \xi_3^* \in \text{Lya}_2. \end{cases} \quad (3.7)$$

We solve each step of the continuation with the previously defined multiple shooting method (3.6). Indeed, the multiple shooting method is totally compatible with the continuation method. This way, we manage to constrain the thrust to the given engine value. Since the control is smaller than 0.3 N, this continuation is easy, and the command does not change during it. In Section 3.2.7 we summarize the numerical results. Let us remark that in our numerical experiment, the continuation takes 22 iterations.

3.2.6 Optimization of the Terminal Points

The last remaining step is to free the initial and final points on the two Lyapunov orbits. The only constraints are that $x(0)$ has to belong to Lya_1 and $x(t_{\text{tot}})$ to Lya_2 . To simplify the problem, we have fixed by construction two points ξ_0^* on Lya_1 and ξ_3^* on Lya_2 . Now we want to find the optimal points where to start and end the mission on these two periodic orbits. So we want to solve the more general problem (3.1). The Pontryagin Maximum Principle gives us two transversality conditions that we have to satisfy:

$$p_{1,\dots,4}(0) \perp T_{x(0)}\text{Lya}_1 \quad \text{and} \quad p_{1,\dots,4}(t_{\text{tot}}) \perp T_{x(t_{\text{tot}})}\text{Lya}_2, \quad (3.8)$$

where the notation $T_x M$ stands for the usual tangent space to M at point x (these conditions can be written as soon as the tangent space is well defined).

To perform this optimization we consider the two previously chosen points $\xi_0^* \in \text{Lya}_1$ and $\xi_3^* \in \text{Lya}_2$. First we perturb the point around Lya_2 following the decrease of the transversality condition until it changes sign so as to find a good zero for the transversality condition. Since we checked that the evolution of this transversality condition along the periodic orbit is not monotone, we are just able to reach a local minimum. By doing this we manage to reach a transversality condition at t_{tot} around 1×10^{-8} . Secondly, we realize the same perturbation along Lya_1 and we manage to reach a value around 1×10^{-8} . We have checked that the inverse process beginning with the point on Lya_1 gives the same result.

Although this seems to cause very little change on the transfer (see numerical results in the next section), the structure of the control is completely changed. We will describe this result in depth in the next section.

Remark 3.3:

To perform this optimization, we could use a gradient method on the one-dimensional periodic orbits initializing it with the solution of problem (3.7). Although, because the method we used is sufficiently efficient, this does not seem to be necessary.

3.2.7 Numerical Results

Recall that we use the CRTBP parameters given in table 1.1.



We observe in Figure 3.8 that the last optimization step changes the shape of the control. Indeed, by construction, we make the spacecraft go onto the heteroclinic orbit before we free that constraint. Hence, it can be expected that the mission has *turnpike properties* (see [86]). That is to say that the optimal solution settled in large time consists approximately of three pieces, the first and the last of which are transient short-time arcs, and the middle piece is a long-time arc staying exponentially close to the optimal steady-state solution.

In Figure 3.8, we see that before the transversality conditions are satisfied following the last optimization step, the command structure does not have the shape of a turnpike command: the control is spread along the trajectory. After the last optimization step, the control is clearly a turnpike control and the trajectory consists approximately in three pieces as expected.

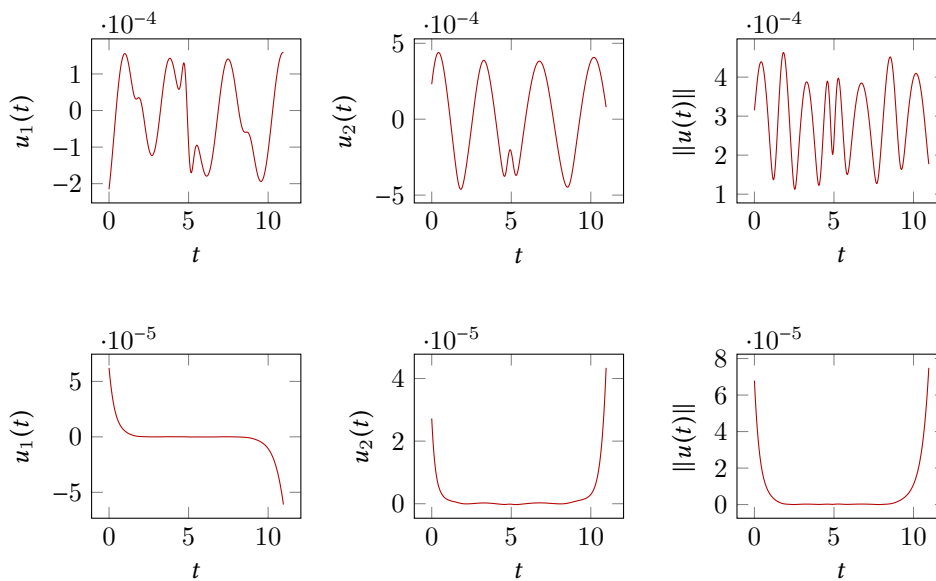


Figure 3.8 – Command to realize the optimal transfer from the Lyapunov orbit around L_1 to the Lyapunov orbit around L_2 . We plot $u(\cdot) \leq 1$ before the last optimization step on the first row (we chose two points on L_{y_1} and L_{y_2}) and after the last optimization step consisting in getting the general transversality conditions (second row). We can observe the good turnpike property of the second control.

We show in Figure 3.9 the two corresponding trajectories. We observe that, to satisfy to transversality conditions corresponding to $x(0) \in L_{y_1}$ and $x(t_{\text{tot}}) \in L_{y_2}$, the two fixed points were not moved very much.

Cost. In this problem we are minimizing the cost $\int_0^{t_{\text{tot}}} \|u\|^2 dt$. We consider a mass evolving dynamical system, and a maximum thrust so to try to compare fairly the cost with other

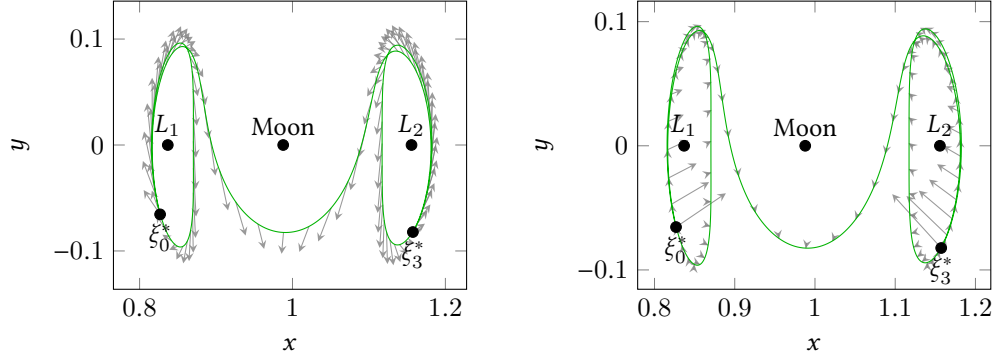


Figure 3.9 – Optimal trajectory. Left: the optimal trajectory with ξ_0^* and ξ_3^* fixed on Lya_1 and Lya_2 . Right: the optimal trajectory with ξ_0^* and ξ_3^* free on Lya_1 and Lya_2 . The control is represented by arrows.

results, we define three different costs:

$$C_{\text{tot}}^1 = \int_0^{t_{\text{tot}}} \|u(t)\|^2 dt, \quad C_{\text{tot}}^2 = \int_0^{t_{\text{tot}}} \frac{\epsilon^2}{m^2(t)} \|u(t)\|^2 dt, \quad \text{and} \quad C_{\text{tot}}^3 = \int_0^{t_{\text{tot}}} \frac{T_{\text{max}}^2}{m^2(t)} \|u(t)\|^2 dt. \quad (3.9)$$

Results are summarized in table 3.2. We observe that, although the two points ξ_0^* and ξ_3^* are not perturbed very much to satisfy the general transversality conditions, for the costs and the mass consumption, it causes real improvement.

Initial Mass	Transfer time	T_{max}
1500 kg	10.961 39 or 47.67 days	0.3 N

	C_{tot}^1	C_{tot}^2	C_{tot}^3	Mass of fuel
Problem (3.7)	$1.065\,018 \times 10^{-6}$	$5.747\,987 \times 10^{-9}$	$1.852\,784 \times 10^{-13}$	0.018 687 kg
Problem (3.1)	$2.230\,596 \times 10^{-9}$	$1.203\,855 \times 10^{-11}$	$3.880\,463 \times 10^{-16}$	$3.670\,958 \times 10^{-4}$ kg

	System	Execution time
Problem (3.7)	Core i7	99% cpu 26,912s total
Problem (3.1)	Core i7	99% cpu 1min18,64s total
Problem (3.7)	Raspberry Pi A	20% cpu 15min3,545s total
Problem (3.1)	Raspberry Pi A	23% cpu 56min45,921s total

Table 3.2 – Numerical results for the final trajectory of the first mission obtained after the multiple shooting with fixed departure and final points (problem (3.7)) and for the optimized departure and final points on Lya_1 and Lya_2 (problem (3.1)).

3.3 Variant of the mission

In this section, we show two other applications of our method to design two different missions. The first one is the Lyapunov to Lyapunov mission but with an energy $\mathcal{E} = -1.5890$ that allows for the existence of a heteroclinic orbit with two revolutions around the moon.

The second mission is a Halo to Halo mission with two different energies and with no heteroclinic orbit. In this case, we use two trajectories belonging to two invariant manifolds.

3.3.1 With a Heteroclinic Orbit with Two Revolutions

In this section we present another mission going from a Lyapunov orbit around L_1 to a Lyapunov orbit around L_2 . We follow exactly the same method than the one we presented except that we compute the second crossing of both invariant manifolds through the Poincaré cut U_2 . Our final trajectory will perform two revolutions around the Moon. Because the Ly_2 target is invariant with respect to the zero control, the larger the duration of the heteroclinic orbit, the smaller (and better) the fuel consumption. Having considered that, we expect a better cost for the transfer. Indeed, the heteroclinic orbit is longer (in time and distance) than the previous one.

Because we follow exactly the same steps as for the mission with only one revolution around the Moon, we do not explain in details each of the steps.

The Heteroclinic orbit

To compute the heteroclinic orbit with two revolutions around the Moon, we have to choose a certain energy allowing for the second intersection to exist. We have chosen the energy (we follow a mission in [32, 33] to motivate this choice) $\mathcal{E}_{Ly_{1,2}} = -1.5890$, and computed the heteroclinic orbit plotted in Figure 3.10. There are indeed two revolutions around the Moon.

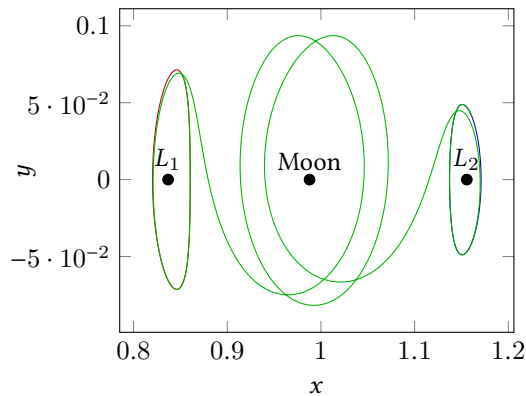


Figure 3.10 – Heteroclinic orbit between two Lyapunov orbits in the {Earth-Moon} system. We get a travel time of 11.699681461946 (normalized time) or 50.883 days.

Once we have computed this trajectory, we have the *a priori* information of the natural dynamics, and so, we can use it to initialize the resolution of the complete mission.

Two Local Transfers

As before, we compute two local transfers: one from the periodic orbit around L_1 to the heteroclinic orbit, and another from the end of the heteroclinic orbit to the periodic orbit around L_2 . We choose the maximal thrust equal to 60 N as before to help the success of the shooting. We do not report the partial results here as they are comparable to the ones of the previous mission. Thanks to this step, we obtain an admissible trajectory in three parts. The first one is controlled to reach the heteroclinic orbit (the *turnpike*), the second part is the

uncontrolled heteroclinic orbit, and the last part is a controlled one from the heteroclinic to the Lyapunov orbit around L_2 .

Multiple Shooting Method

As before, to free the two matching connections on the heteroclinic orbit and to decrease the maximum thrust we use a multiple shooting method associated with a continuation method. Since the transfer time is larger than for the previous mission, we have to add some grid points along the heteroclinic orbit (which are initialized with a zero adjoint vector). This is due to the very unstable nature of the Hamiltonian system. Here we chose 5 grid points. Thanks to the multiple shooting method and a thrust continuation, we manage to reach the required maximal thrust: $T_{\max} = 0.3 \text{ N}$ and we get an admissible trajectory with two fixed points on Lya_1 and Lya_2 . The last step consists in finding the optimal departure and arrival points on the two periodic orbits.

Remark 3.4:

Note that the addition of grid nodes along the “invariant manifold part” is due to the sensibility of these invariant tubes (and of the Hamiltonian system). And for that very reason, other invariant manifolds could be a better choice. For example, the ones with an “eight-shape” studied in [6] are more stable and so, less sensitive. Because we want to compare our method with some academic ones, we consider here the invariant manifolds from Lyapunov orbits.

Optimization of the Terminal Points

Once again, because we have simplified the problem by fixing the departure and arrival points on Lya_1 and Lya_2 , we want to free these points on the periodic orbits to satisfy the general transversality conditions (3.8). As before, we perturb first $\xi_3^* \in \text{Lya}_2$ following the decrease of the transversality condition and we do the same with ξ_0^* . We manage to satisfy the transversality conditions up to 1×10^{-9} .

Results

We plot in Figure 3.11 the command before and after the last optimization step. We observe the same phenomenon as for the previous mission. Indeed, before we satisfy the transversality conditions, the command does not have the *turnpike structure*, that is to say, the three parts, first a short thrust to reach the *highway* (or turnpike), then a null controlled part, and finally a controlled part to reach the periodic orbit.

Whereas the perturbations of the two points ξ_0^* and ξ_3^* to satisfy the transversality conditions are very small (see Figure 3.12), the structure of the control is very different and the costs are much smaller after getting the transversality conditions. We summarize the numerical results in Table 3.3.

3.3.2 Halo to Halo Mission

In this section, we will adapt the previous method to another mission: a Halo to Halo mission. Recall that Halo orbits are periodic orbits around equilibrium points like Lyapunov orbits but in the 3D dynamics.

For the Halo to Halo mission, because we are in the 3D case, for the energies of the periodic orbits that we have chosen, the intersection between unstable and stable manifolds does not exist. However, our method is still valid and can be applied.

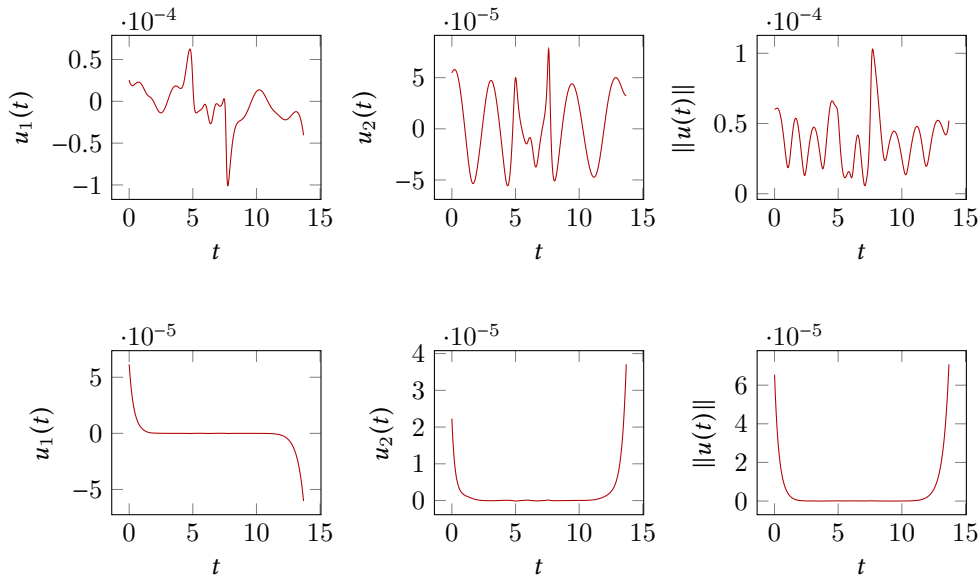


Figure 3.11 – Command to realize the optimal transfer from the Lyapunov orbit to the heteroclinic orbit. We plot $u(\cdot) \leq 1$ before the last optimization step on the first row (we chose two points on L_{y_1} and L_{y_2}) and after the last optimization step consisting in getting the general transversality conditions. We can observe the good turnpike property of the second control.



Whereas previously we used a natural trajectory that *asymptotically* perform the mission (in infinite time), here, the natural dynamics is not as helpful as an heteroclinic orbit.

However, the general approach is clearer in this example. Indeed, we do not require the intersection between manifolds to exist, and we only use part of them to help to initialize the resolution of the complete mission. This is a first step toward the general approach with ITN (see Remark 2.1 page 63) and patching together several invariant manifolds parts.

We will first design an admissible trajectory with 5 parts:

1. first, we propagate the unstable and stable manifolds from L_1 and L_2 as described in Section 3.2.2. We compute, in the plane U_2 , the two points (one on each manifolds) that minimize the distance in position and velocity. This gives us two trajectories.
2. Then, we compute the optimal transfer from a fixed point on the Halo orbit around L_1 to a fixed point on the trajectory on the associated unstable manifold.
3. We compute a transfer from a fixed point on the trajectory of the unstable manifold from the Halo orbit around L_1 to a fixed point on the trajectory on the stable manifold of the Halo orbit around L_2 .
4. We then compute the optimal control to reach a fixed point on the Halo orbit around L_2 from a fixed point on the trajectory of the associated stable manifold.

With this admissible trajectory in 5 parts (with two uncontrolled parts in each of the two invariant manifolds), we initialize a multiple shooting method to get an optimal trajectory

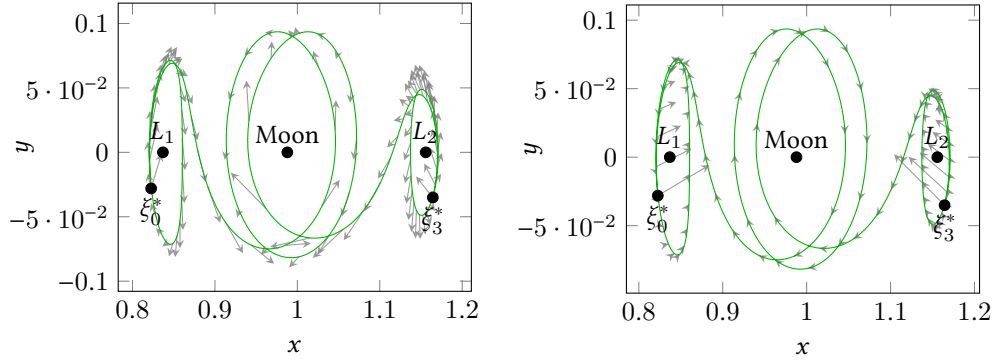


Figure 3.12 – Optimal trajectory. Left: the optimal trajectory with ξ_0^* and ξ_3^* fixed on L_{y_1} and L_{y_2} . Right: the optimal trajectory with ξ_0^* and ξ_3^* free on L_{y_1} and L_{y_2} . The control is represented by arrows.

Initial Mass	Transfer time	T_{\max}
1500 kg	13.699 681 461 or 59.582 days	0.3 N

	C_{tot}^1	C_{tot}^2	C_{tot}^3	Mass of fuel
Problem (3.7)	$2.463\,890 \times 10^{-8}$	$1.329\,766 \times 10^{-10}$	$4.286\,320 \times 10^{-15}$	0.003 013 kg
Problem (3.1)	$1.969\,593 \times 10^{-9}$	$1.062\,991 \times 10^{-11}$	$3.426\,407 \times 10^{-16}$	$3.359\,975 \times 10^{-4}$ kg

	System	Execution time
Problem (3.7)	Core i7	99% cpu 44,949s total
Problem (3.1)	Core i7	99% cpu 2min54,79s total
Problem (3.7)	Raspberry Pi A	33% cpu 22min52,8s total
Problem (3.1)	Raspberry Pi A	29% cpu 1h32min46s total

Table 3.3 – Numerical results for the final trajectory of the second mission obtained after the multiple shooting with fixed departure and final points (problem (3.7)) and for the optimized departure and final points on L_{y_1} and L_{y_2} (problem (3.1)).

reaching a fixed point on the Halo orbit around L_2 from a fixed point on the Halo orbit around L_1 . Finally, following the method described for the Lyapunov to Lyapunov mission, we optimize the position of the end points.

Free Parts on Manifolds

As described in the introduction, we compute two trajectories on unstable and stable manifolds respectively from the Halo orbit around L_1 and from the Halo orbit around L_2 .

Halo Orbits

For the sake of generality, we compute two Halo orbits with different energies. For the Halo orbit around L_1 denoted by Halo_1 , we have chosen $\mathcal{E}(\text{Halo}_1) = -1.5939$. For the Halo orbit around L_2 denoted by Halo_2 , we have chosen $\mathcal{E}(\text{Halo}_2) = -1.5805$. These two energy values correspond to a unique z -excursion of 16 000 km. The numerical computation of such orbits

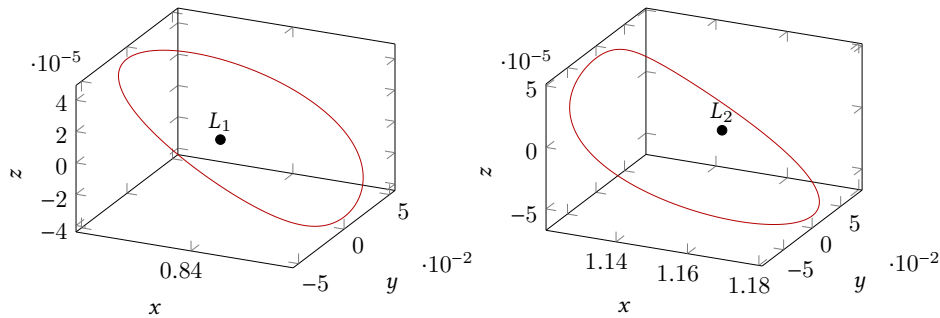


Figure 3.13 – Halo orbits around L_1 and L_2 for energies -1.5939 and -1.5805 respectively. This corresponds to a unique excursion of 16 000 km.

is done using the method described in Section 1.4.3 page 1.4.3. See Figure 3.13 for a plot of these two periodic orbits.

Propagation of Manifolds and Choice of Trajectories

Using the same parameter α as defined in (1.21) for the Lyapunov to Lyapunov mission, *i.e.* $\frac{1}{384402}$, we compute the intersection with the plane U_2 (see sec 3.2.2). One can see the result in Figure 3.14. We denote by \mathcal{M}_1 and \mathcal{M}_2 these two manifolds.

We compute the intersection of each manifold with U_2 and find the closest pair of points (one from the manifold of Halo₁ and one from the manifold of Halo₂). This is done with a fine discretization of 1000 points per Halo orbits. That way, we get two points for $x = 1 - \mu$, denoted respectively by $\xi_{\mathcal{M}_1}^{U_2}$ and $\xi_{\mathcal{M}_2}^{U_2}$. The distance in \mathbf{R}^6 is

$$\left\| \xi_{\mathcal{M}_1}^{U_2} - \xi_{\mathcal{M}_2}^{U_2} \right\|^2 = 0.098\ 644\ 604\ 436.$$

The two corresponding trajectories are plotted in Figure 3.14. Let $t_{\mathcal{M}_1}$ and $t_{\mathcal{M}_2}$ denote the two times of propagation for the two free trajectories, themselves denoted by \mathcal{A}_1 and \mathcal{A}_2 (see Figure 3.14).

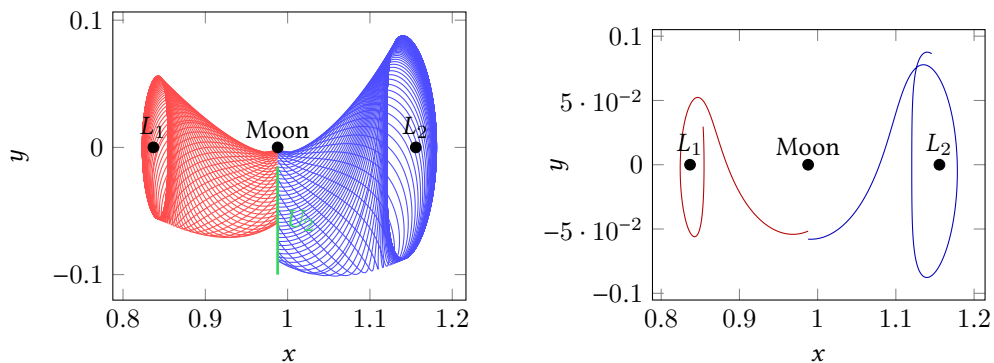


Figure 3.14 – Left: the propagation of manifolds from Halo around L_1 and Halo around L_2 . Right: the two trajectories of these manifold minimizing the distance on the plane U_2 .

Three Short Transfers

Following our method, we compute three short transfers in order to initialize a multiple indirect shooting method and get the optimal trajectory.

From Halo₁ to \mathcal{A}_1 . Once again, we follow the method described in Section 3.2.3, we construct two fixed points, one on Halo₁, the other on \mathcal{A}_1 . To do that, we consider the two closest points on Halo₁ and \mathcal{A}_1 . We choose two time parameters: t_{Halo_1} to propagate backward the point on Halo₁ and $t_{\mathcal{A}_1}^{L_1}$ to propagate forward on \mathcal{A}_1 . Here, we pick:

$$t_{\text{Halo}_1} = t_{\mathcal{A}_1}^{L_1} = 1.0.$$

We are now ready to build the first optimal control problem as defined in (3.2). Using continuation on the final state solves this problem in an easy and fast (4.1 s) manner. The norm of the control is plotted in Figure 3.15. Let us denote by

$$t_0 = t_{\text{Halo}_1} + t_{\mathcal{A}_1}^{L_1},$$

the transfer time and by $X_0^* = (\xi_0^*, m_0^*)$ and $X_1 = (\xi_1, m_1)$ the terminal points of this transfer. The resulting final mass is $m_1 = 1499.996\,743\,927\,8$ kg.

From \mathcal{A}_1 to \mathcal{A}_2 . In this part, we apply our method to compute the transfer from trajectory \mathcal{A}_1 to trajectory \mathcal{A}_2 . There is a rather large gap to resorb. We already have the two points that we will perturb backward and forward: $\xi_{\mathcal{M}_1}^{U_2}$ and $\xi_{\mathcal{M}_2}^{U_2}$. We choose the two corresponding times

$$t_{\mathcal{A}_1}^{U_2} = t_{\mathcal{A}_2}^{U_2} = 0.5,$$

and define the transfer time as³

$$t_2 = t_{\mathcal{A}_1}^{U_2} + t_{\mathcal{A}_2}^{U_2}.$$

After the first transfer from Halo₁ to \mathcal{A}_1 , we follow a free trajectory on the manifold, so we choose the initial mass of the transfer from \mathcal{A}_1 to \mathcal{A}_2 as the final mass of the previous part, that is to say $m_2 = m_1 = 1499.996\,743\,927\,8$ kg.

Once again, the continuation on the final state allows for a fast convergence to obtain the solution of this problem. Indeed we obtained the solution in 4.4 s. In this problem, we denote by $X_2 = (\xi_2, m_2)$ the initial point on \mathcal{A}_1 and by $X_3 = (\xi_3, m_3)$ the final point on \mathcal{A}_2 . The final mass we get is $m_3 = 1493.318\,462\,201\,5$ kg and the norm of the control is plotted in Figure 3.15.

From \mathcal{A}_2 to Halo₂. We consider here the last short transfer from \mathcal{A}_2 to Halo₂. As for the transfer from Halo₁ to \mathcal{A}_1 , we pick the two closest points on \mathcal{A}_2 and Halo₂ and we perturb them with two time parameters denoted by $t_{\mathcal{A}_2}^{L_2}$ and t_{Halo_2} . We then

define the transfer⁴ time

$$t_4 = t_{\mathcal{A}_2}^{L_2} + t_{\text{Halo}_2} = (1.0 + 1.0)$$

to go from $X_4 = (\xi_4, m_4)$ to the final points ξ_5^* . As before, $m_4 = m_3 = 1493.318\,462\,201\,5$ kg because after the transfer around U_2 , we follow a free trajectory on the stable manifold.

3. We keep the index 1 for the remaining time on the free part, *i.e.*, the remaining part of the unstable manifold trajectory.

4. Once again we keep the index 3 for the free part between transfer between manifolds and transfer to Halo₂.

Once again, the resolution is easy and fast (4.14 s) thanks to the continuation method. The final mass we obtain is $m_5 = 1493.315\ 673\ 696\ 6$ kg. The norm of the control is plotted in Figure 3.15.

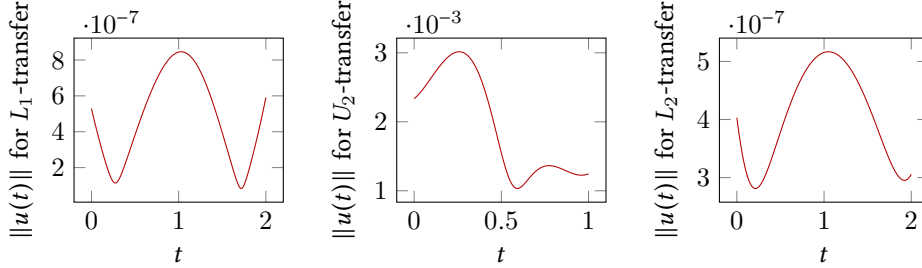


Figure 3.15 – Norm of the control for the three controlled parts of the admissible trajectory.

Admissible Trajectory in Five Parts. To summarize, we have constructed an admissible trajectory going from Halo_1 to Halo_2 with three controlled parts and two free parts. This trajectory is plotted in the Figure 3.16 and the control for the three controlled parts is in Figure 3.15. The local transfers are computed with a maximal thrust equal to 180 N, indeed this helps the convergence of local transfers (but we do not reach the targeted maximal thrust of 0.3 N), and the multiple shooting for the reason described in Section 3.2.3.

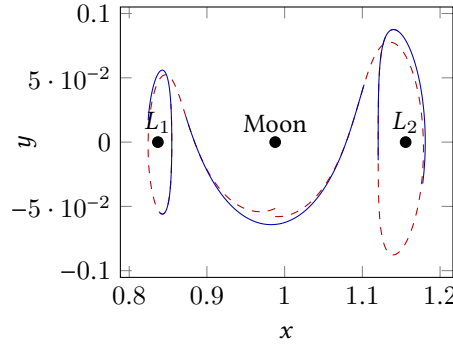


Figure 3.16 – Admissible trajectory in five parts. Dashed part are manifold trajectories, *i.e.* free parts.

Multiple Shooting for the Total Transfer

We consider here the following problem

$$\mathcal{P}_{\text{tot}}^{\text{Halo}} \left\{ \begin{array}{l} C_{\text{tot}} = \min \int_0^{t_{\text{tot}}} \|u\|^2 dt, \\ \dot{x} = F_0(x) + \frac{\epsilon}{m} \sum_{i=1}^3 u_i F_i(x), \\ \dot{m} = -\beta_s \epsilon \|u\|, \\ \|u\| \leq 1, \\ x(0) = \xi_0^* \in \text{Halo}_1, \quad m(0) = m_0^*, \\ x(t_{\text{tot}}) = \xi_5^* \in \text{Halo}_2. \end{array} \right.$$

The transfer time t_{tot} is defined as

$$t_{\text{tot}} = t_0 + t_1 + t_2 + t_3 + t_4,$$

where t_0 , t_2 and t_4 are the times previously introduced for the three short transfers. Time t_1 is the duration of trajectory A_{M_1} in the unstable manifold from Halo₁ from which we subtract the two times we used to perturb points for the local transfers around L_1 and U_2 . This gives us

$$t_1 = t_{M_1} - t_{\mathcal{A}_1}^{L_1} - t_{\mathcal{A}_1}^{U_2}.$$

And we defined t_3 in a similar way as

$$t_3 = t_{M_2} - t_{\mathcal{A}_2}^{L_2} - t_{\mathcal{A}_2}^{U_2}.$$

As in Section 3.2.4, we introduced the shooting function with four nodes (for the Lyapunov to Lyapunov mission, we had two nodes). Because we are considering a spatial mission, we get the following shooting function

$$\mathcal{S}_{\text{multi}}^{\text{Halo}}(Z) = \begin{pmatrix} \phi_{1,\dots,7}^{\text{ext}}(t_0, \xi_0^*, m_0^*, P_0) - X_1 \\ \phi_{8,\dots,14}^{\text{ext}}(t_0, \xi_0^*, m_0^*, P_0) - P_1 \\ \phi_{1,\dots,7}^{\text{ext}}(t_1, X_1, P_1) - X_2 \\ \phi_{8,\dots,14}^{\text{ext}}(t_1, X_1, P_1) - P_2 \\ \phi_{1,\dots,7}^{\text{ext}}(t_2, X_2, P_2) - X_3 \\ \phi_{8,\dots,14}^{\text{ext}}(t_2, X_2, P_2) - P_3 \\ \phi_{1,\dots,7}^{\text{ext}}(t_3, X_3, P_3) - X_4 \\ \phi_{8,\dots,14}^{\text{ext}}(t_3, X_3, P_3) - P_4 \\ \phi_{1,\dots,6}^{\text{ext}}(t_4, X_4, P_4) - \xi_5^* \\ \phi_{14}^{\text{ext}}(t_4, X_4, P_4) \end{pmatrix} \in \mathbf{R}^{4 \times 14 + 7},$$

where the vector Z is defined as

$$Z = \underbrace{(p_0, p_m^0)}_{P_0}, \underbrace{(\xi_1, m_1)}_{X_1}, \underbrace{(p_1, p_m^1)}_{P_1}, \underbrace{(\xi_2, m_2)}_{X_2}, \underbrace{(p_2, p_m^2)}_{P_2}, \underbrace{(\xi_3, m_3)}_{X_3}, \underbrace{(p_3, p_m^3)}_{P_3}, \underbrace{(\xi_4, m_4)}_{X_4}, \underbrace{(p_4, p_m^4)}_{P_4} \in \mathbf{R}^{63}.$$

We initialize the shooting method with the values that we get from the local transfers and with a zero adjoint vector for the free parts. The shooting method converges easily.

As for the two previous missions, we decrease the maximal authorized thrust by continuation. We then optimize the terminal points ξ_0^* and ξ_5^* to satisfy the transversality conditions. We manage to get the result in 4.16 min. The final trajectory is plotted in Figure 3.17 and the corresponding control in Figure 3.18. The resulting cost is summarized in table 3.4 as well as the numerical values of the parameters. Because we are not comparing this mission with other published results, we just write the physical cost C_{tot}^3 in the international system of units (see (3.9)).

Remark 3.5:

Note that we do not get the turnpike properties, indeed, in this case, there is no “steady-state” natural trajectory asymptotically connecting the two periodic orbits.

Initial Mass	Transfer time	T_{\max}
1500 kg	9.543 645 446 282 8 or 41.50 days	0.3 N

	C_{tot}^3	Mass of fuel
Halo to Halo Problem	0.004 619 126 477 355 13	7.415 872 590 999 92 kg

Table 3.4 – Numerical results for the final trajectory of the Halo to Halo Mission.

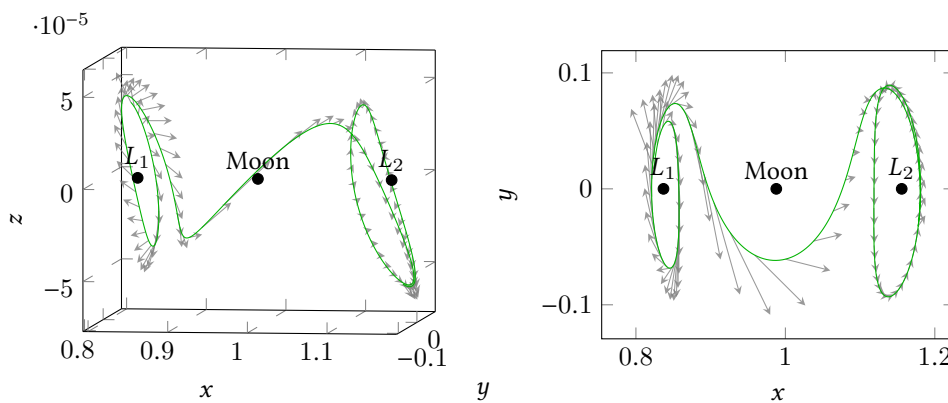


Figure 3.17 – Optimal trajectory for the Halo to Halo transfer. Left: a 3 dimensional view. Right: a view in the (x, y) -plane. The control is represented by arrows.

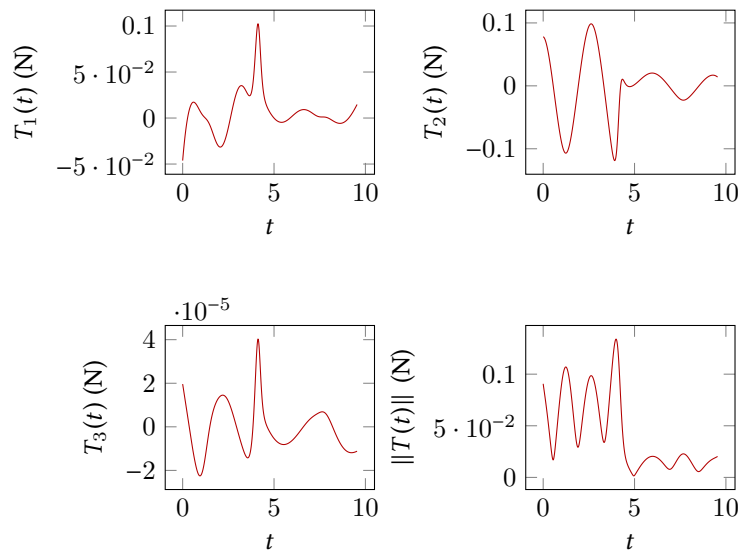


Figure 3.18 – Optimal control for the Halo to Halo Mission $T(\cdot) \in \mathbf{R}^3$ in Newton.

Missions Departing from the Geostationary Earth Orbit

Contents

4.1	Definition of the Mission	126
4.2	An Invariant Manifold as a Gravitational Current	127
4.3	Three-Part Trajectory	129
4.3.1	From GEO to the free trajectory	129
4.3.2	From the free trajectory to the LO	130
4.3.3	The Admissible Trajectory	130
4.4	Hybrid Optimization Method	132
4.4.1	The Algorithm	133
4.4.2	Numerical results	134
4.5	Other Missions	135
4.5.1	GEO to Lyapunov Missions: Two Cases	136
4.5.2	3D case, from the GEO to a Halo orbit	138
4.5.3	About the Maximal Thrust	139

In this chapter, we design admissible trajectories departing from the geostationary Earth orbit (GEO). We consider different target orbits such as Lyapunov and Halo orbits around L_1 and a Lunar orbit (LO). The principle is to reach a free trajectory of an invariant manifold with a final state continuation, and near the targeted orbit, to perform a final transfer. The obtained trajectory is designed with three parts, including an uncontrolled one that follows a gravitational current. This trajectory is computed in a few minutes, and yields a satisfactory value of the cost.

Of course because we impose an uncontrolled part, these trajectories are sub-optimal (but optimal in each part). Because we are considering a long part along invariant manifolds, the multiple shooting method is not sufficiently robust (recall that invariant manifolds can be sensitive). We introduce in Section 4.4, a hybrid optimization method where we optimize the state variables (in position and velocity) of the matching points with a gradient descent (direct method) coupled with initial and final state continuation (indirect method) on each of the three parts. Using the PMP principle, one can show that the gradient of the global cost

function at the matching points is given by the gap between the costates (see Section 4.4), so it is available as a by-product of the indirect methods on each part.

The hybrid optimization procedure allows to decrease the cost function but does not nullify the gradient. The first matching point, initialized on the free trajectory, is moved towards the GEO during the iterations of the gradient descent. Indeed, the closer the targeted point is to the GEO, the cheaper the transfer to reach it is. We add a “box constraint” (see Section 4.4.2) around each matching point (initialized with the two end-points of the free trajectory) to stop the gradient descent which does not manage to nullify the gradient in reasonable time. As could be expected, the gradient descent saturates this constraint with the closest point to the GEO. Although the L^2 -norm of the control decreases during the optimization, the solution is in practice made less interesting by the fact that the final mass also decreases. We still present the method because of the interesting mathematical aspects: the costate gives us the gradient of the value function. For all these reasons and because the hybrid optimization does not improve sufficiently the cost in reasonable time, we conclude that the main advantage of the method is to get an admissible trajectory with a free middle part following the invariant manifold.

We have deduced from our experiments that, a meaningful factor is the energy of the invariant manifolds. Indeed, the energy of the GEO embedded in the CRTBP¹ is

$$\mathcal{E}_{\text{GEO}} \simeq -4.864\,220\,3,$$

and we have seen in Section 1.3 page 37 that to allow the spacecraft to go to the realm of the Moon, we have to reach the energy of the point L_1 which is

$$\mathcal{E}_{L_1} \simeq -1.600\,200\,4.$$

The gap to fill is significantly larger than for the missions in chapter 3 in which we connected two Halo orbits of respective energies -1.5939 and -1.5805 .

We start with a GEO to LO mission, we explain in detail the method that we apply for this particular example. We finally give other examples of missions that we can design with invariant manifolds such as GEO to a Lyapunov orbit or a Halo orbit.

4.1 Definition of the Mission

We consider the geostationary Earth orbit embedded in the circular restricted three body problem.

Definition 17: *The geostationary orbit, geostationary Earth orbit or geosynchronous equatorial orbit (GEO) is a circular orbit 35 786 kilometers above Earth’s equator (radius of 42 164 km) and following the direction of Earth’s rotation.* \diamond

In Table 4.1, we summarize some values of this orbit in the normalized system of units of the CRTBP. Recall that the different CRTBP parameters are the ones given in Table 1.1.

	Radius of orbit	Velocity	Period
IS units	42 164 km	3.0746 km s ⁻¹	23.934 461 2 days
CRTBP units	0.109 687 254 48	2.891 357 831 71	0.036 494 731 216 772 6

Table 4.1 – Numerical values for the geostationary Earth orbit embedded in the CRTBP.

1. We see in this chapter that the GEO is only slightly modified by the Moon.

This periodic two-body orbit is stable even though it is not periodic when embedded in the CRTBP. In Figure 4.1, we plot it for an integration time of 3.0 which corresponds to nearly 100 rotations.

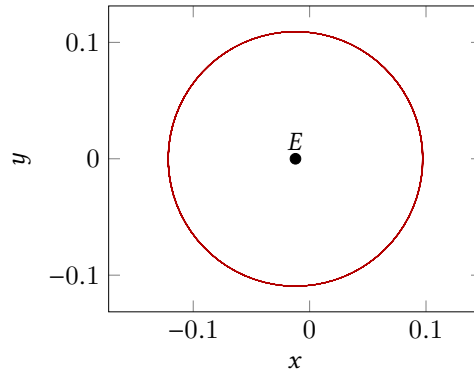


Figure 4.1 – Plot of the propagation in the CRTBP of the initial conditions of the GEO in the 2 body problem. The duration of the propagation is 3.0 and corresponds to nearly 100 revolutions. We see that the embedded trajectory is stable with respect to the perturbation of the Moon.

We then consider a periodic orbit around the Moon as defined in the SMART1 mission [72], and presented in [31]. The Lunar Orbit (LO) is described in the phase space by a radius around the Moon $r_{LO} = 13.084 \times 10^3$ m and a velocity $v = \sqrt{\frac{\mu_E}{r}} = \sqrt{\frac{1-\mu}{r}}$. We summarize these values in Table 4.2 and plot the trajectory in Figure 4.1.

	Radius of orbit	Velocity	Period
IS units	13 084 km	0.612 890 340 94 km s ⁻¹	9.246 086 041 days
CRTBP units	0.034	0.597 941 796 04	0.357 272 734 329 6

Table 4.2 – Numerical values for the LO embedded in the CRTBP.

As we can see in Figure 4.2, this periodic orbit in the 2 body problem centered on the Moon, is not very stable when it is embedded in the CRTBP, but it stays nearly periodic.

The Mission. The mission is to start on the GEO and to end on the LO minimizing the L^2 -norm of the cost. We first design an admissible trajectory in three part as we have done for the Lyapunov to Lyapunov mission (or Halo to Halo) in chapter 3.

4.2 An Invariant Manifold as a Gravitational Current

We start by computing a Lyapunov orbit at a given energy around the Lagrange point L_1 . We propagate the stable manifold in the Earth's realm and the unstable manifold in the Moon's realm. Then, using the method described in Section 2.1.1, we are able to choose a free trajectory performing the connection between the Earth's realm and the Moon's realm. Indeed, because the invariant manifolds are separatrices of the dynamics, a trajectory inside of the tube stays in it. Such a trajectory is called a transit orbit.

We then compute the section with the Poincaré cut U_2 in the Moon's realm and we choose, in this (y, \dot{y}) -plane, a point inside the set delimited by the invariant manifold. Then,

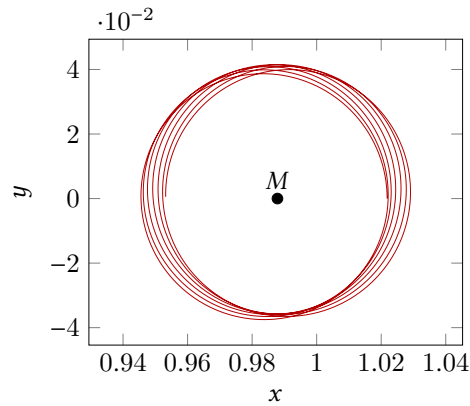
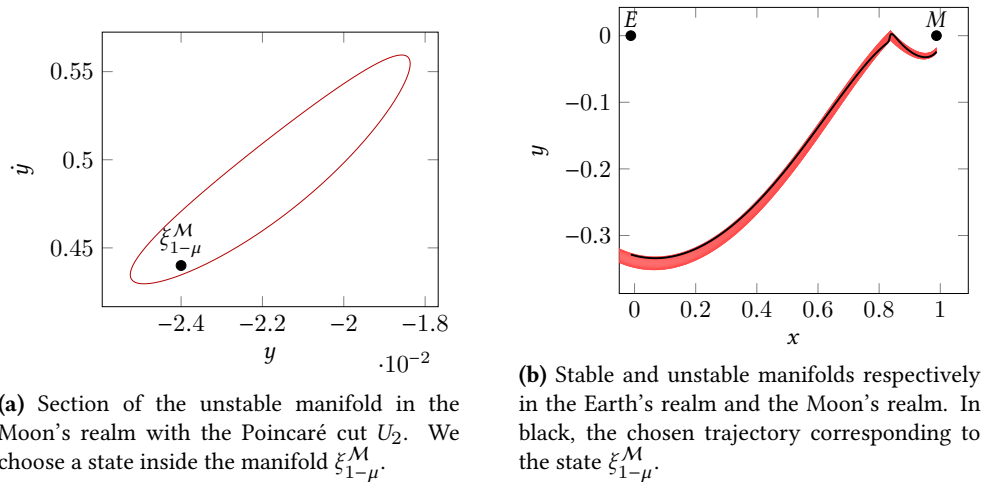


Figure 4.2 – Plot of the propagation in the CRTBP of an initial condition of a LO in the 2 body problem. The duration of the propagation is 3.0 and corresponds to nearly 10 revolutions. We see that the embedded trajectory is not periodic anymore but stays nearly periodic. The rotation of the Moon is taken into account.

we compute as usual the value of \dot{x} using the energy, and finally, we get a point of a trajectory that goes from one realm to the other (see Figure 4.3).



(a) Section of the unstable manifold in the Moon's realm with the Poincaré cut U_2 . We choose a state inside the manifold $\xi_{1-\mu}^M$.

(b) Stable and unstable manifolds respectively in the Earth's realm and the Moon's realm. In black, the chosen trajectory corresponding to the state $\xi_{1-\mu}^M$.

Figure 4.3 – Choice of a condition in the section U_2 , and the trajectory inside the invariant manifolds.

Thanks to the computation, we get a free trajectory going from the realm around the Earth to the realm around the Moon. This trajectory has the energy of the periodic orbit we have chosen. Here, we picked

$$\mathcal{E}_{\text{Lya}_1} = -1.6001.$$

We have propagated backward the initial condition in the U_2 -section until the trajectory reaches the plane defined by $x = -\mu$. We denote by \mathcal{A}_M this trajectory, and respectively by $\xi_{-\mu}^M$ and $\xi_{1-\mu}^M$ its first and last points.

We now want to use this trajectory to design a complete mission from the GEO to the LO.

4.3 Three-Part Trajectory

In this section, we design an admissible trajectory with three parts: a transfer from a point on the GEO to the first point $\xi_{-\mu}^M$ on the free trajectory that we have computed, a free part following \mathcal{A}_M , and the final transfer from the last point $\xi_{1-\mu}^M$ to a point on the LO orbit.

Recall that we use the parameters of the CRTBP given in Table 1.1, and for the modeling of the engine, as before, we chose $I_{sp} = 2000$ s and $g_0 = 9.81$ m/s².

4.3.1 From GEO to the free trajectory

To perform the transfer from a fixed point on the GEO to the point $\xi_{-\mu}^M$, we use the final state continuation. To do that, we have to choose a transfer time t_0 . There is no general method to do that, so we consider the period of the GEO orbit and we compute a transfer time with a given number of revolution and a factor greater than one. For instance for this transfer, we picked

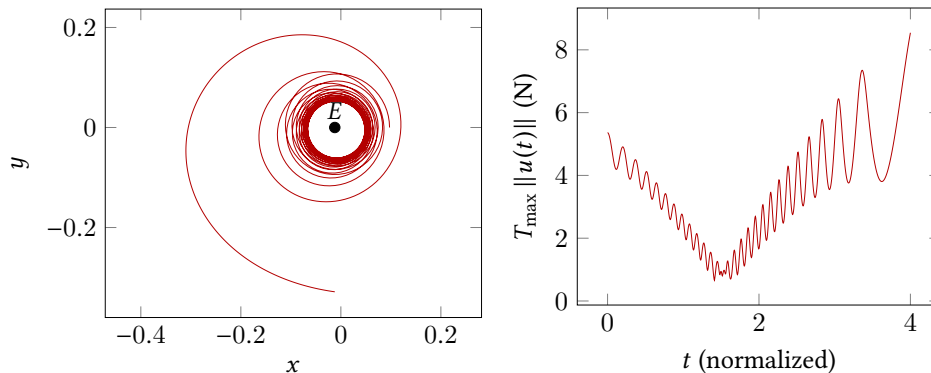
$$t_0 = 4.0,$$

in the normalized system of units. Note that a resolution for the minimization of the *minimum time transfer* should tell us which to pick.

Remark 4.1:

For all our numerical tests, the problem is not very sensitive to variation in time, and it is easy to find a suitable transfer time.

Moreover, once we have a transfer time, with a continuation on the time parameter, one can choose another time, especially to allow for a lower thrust.



(a) Optimal trajectory to reach the free trajectory from a point on the GEO. (b) The control of the optimal trajectory to reach the free trajectory from a point on the GEO.

Figure 4.4 – Transfer from a fixed point on the GEO to a fixed point on the free trajectory inside the tube connecting the Earth’s realm to the Moon’s realm. Left: the trajectory. Right: the norm of the control.

We plot the obtained trajectory (see Figure 4.4a) associated to an optimal control with a maximal thrust of 10 N (see Figure 4.4b).

We summarize the different parameters for the transfer in Table 4.3: we remark in particular that the computation time on a standard desktop computer is small.

	Transfer time			Computation time			
	4.0 or 17.397 days			cpu 173.86s			
	x	y	z	\dot{x}	\dot{y}	\dot{z}	m
Initial	9.736331E-002	0.0	0.0	0.0	2.891357	0.0	1500
Final	-1.215616E-02	-3.285562E-01	0.0	1.702750	-2.384994E-01	0.0	

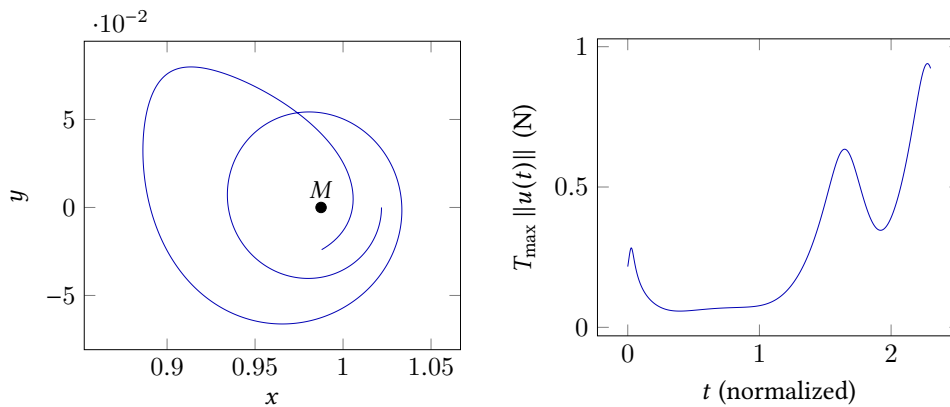
Table 4.3 – Parameters for the transfer between the GEO and the free trajectory.

4.3.2 From the free trajectory to the LO

Now, we consider the transfer from the free trajectory and more precisely from its end point $\xi_{51-\mu}^M$ to a point on the LO. As in the previous section, we choose a transfer time to perform the transfer to the LO. It is easier here because the invariant manifold in the Moon's realm is close to the LO orbit. Hence, the transfer is fast to compute. We have chosen a transfer time of

$$t_2 = 2.3.$$

We plot the obtained trajectory and the associated optimal control in, figures 4.5a and 4.5b. Moreover, we summarize the different parameters for the transfer in Table 4.4.



(a) Optimal trajectory to reach the LO from a point on the free trajectory.

(b) The control of the optimal trajectory to reach the LO orbit from a point on the free trajectory.

Figure 4.5 – Transfer between a fixed point on the free trajectory to a fixed point on LO. Left: the trajectory. Right: the norm of the control.

We summarize the different parameters for the transfer in Table 4.4, in particular the computation time on a standard desktop computer.

4.3.3 The Admissible Trajectory

Recall that we have defined three time parameters: t_0 , the transfer time from the GEO to the free trajectory, t_1 , the transfer time following the free trajectory and t_2 , the transfer time from the free trajectory to the LO. Then, we define the total transfer time as

$$t_f = t_0 + t_1 + t_2.$$

	Transfer time			Computation time			
	2.3 or 10.003 days			cpu 15.27s			
	x	y	z	\dot{x}	\dot{y}	\dot{z}	m
Initial	0.987847	-0.023997	0.0	0.763387	0.440095	0.0	1313.274585
Final	1.021843	0.0	0.0	0.0	0.597941	0.0	

Table 4.4 – Parameters for the transfer between the free trajectory and the LO.

We finally obtain a three-part admissible trajectory with, as the middle part, a free trajectory inside the invariant manifold that connects both realms. In terms of fuel consumption, we obtain a good result, the final mass is indeed $m(t_f) = 1301.228\,912$ kg. Of course, the first part is the most costly part. Indeed, recalling that $m(0) = 1500$ kg,

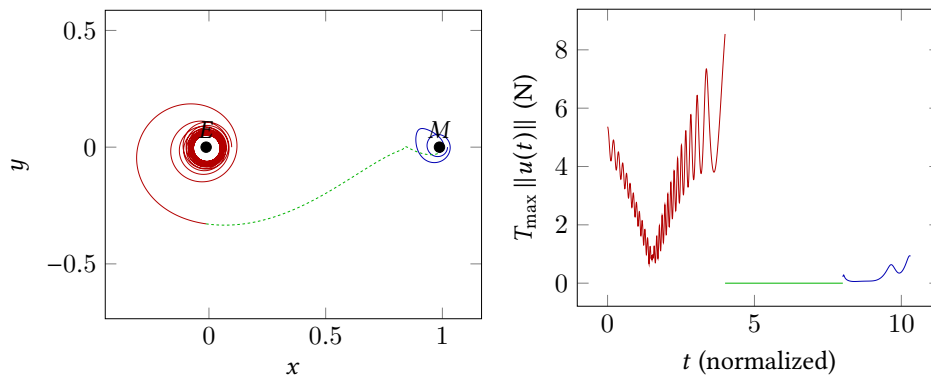
$$m(t_0) = 1313.274\,585 \text{ kg},$$

and $m(t_0 + t_1) = m(t_0)$ because we follow a free transit trajectory.

In Figure 4.6a, we plot the admissible trajectory as well as the corresponding control in Figure 4.6b. The admissible control is discontinuous, and of larger magnitude on the first part of the trajectory. Indeed, we start on the GEO trajectory of energy nearly $-4.864\,220\,3$, and we reach the energy of -1.6001 of the manifold.

We first tried to use the multiple shooting method following the method that we have previously introduced for the Lyapunov to Lyapunov mission (Section 3.2.4 page 110). Unfortunately, this multiple shooting method does not converge. Indeed, the discontinuity in the costate at the matching points $\xi_{-\mu}^M$ and $\xi_{1-\mu}^M$ is too large to be resorbed.

To overcome this difficulty, we tried to develop a hybrid method.



(a) Optimal trajectory to reach the LO from a point on the GEO. **(b)** The control in three parts. The first part is the main controlled part.

Figure 4.6 – Admissible trajectory in three parts from the GEO to the LO.

4.4 Hybrid Optimization Method

Thanks to the construction of the admissible trajectory, we develop an alternative to the multiple shooting method. Indeed, we denote as previously, the state including the mass by $X = (\xi, m)$. Then, we denote by

$$X_1 = (\xi_1, m_1) \text{ and } X_2 = (\xi_2, m_2),$$

the matching points in \mathbf{R}^7 of an admissible trajectory in three parts, initialized with $\xi_1 = \xi_{-\mu}^M$ and $\xi_2 = \xi_{1-\mu}^M$. These two matching points can be viewed as parameters of an optimization problem with the three *fixed* transfer time t_0 , t_1 and t_2

$$\min_{X_1 \in \mathbf{R}^7, X_2 \in \mathbf{R}^7} \mathcal{V}_{\text{tot}}(X_1, X_2), \quad (4.1)$$

where

$$\mathcal{V}_{\text{tot}}(X_1, X_2) = \mathcal{V}_0(t_0, X_0^*, X_1) + \mathcal{V}_1(t_1, X_1, X_2) + \mathcal{V}_2(t_2, X_2, \xi_f^*). \quad (4.2)$$

Recall that $X_0^* = (\xi_0^*, m_0^*)$ is the fixed initial condition, and ξ_f^* is the fixed final condition with a free final mass. The functions \mathcal{V}_i , $i \in \llbracket 0, 2 \rrbracket$, are value functions respectively for the three following control problems

$$\mathcal{P}_0 \left\{ \begin{array}{l} C_0 = \min \int_0^{t_0} \|u\|^2 dt, \\ \dot{x} = F_0(x) + \frac{\epsilon}{m} \sum_{i=1}^2 u_i F_i(x), \\ \dot{m} = -\beta_* \epsilon \|u\|, \\ \|u\| \leq 1, \\ x(0) = \xi_0^*, \quad m(0) = m_0^* \\ x(t_0) = \xi_1, \quad m(t_0) = m_1. \end{array} \right. \quad \mathcal{P}_1 \left\{ \begin{array}{l} C_1 = \min \int_{t_0}^{t_1} \|u\|^2 dt, \\ \dot{x} = F_0(x) + \frac{\epsilon}{m} \sum_{i=1}^2 u_i F_i(x), \\ \dot{m} = -\beta_* \epsilon \|u\|, \\ \|u\| \leq 1, \\ x(t_0) = \xi_1, \quad m(0) = m_1 \\ x(t_1) = \xi_2, \quad m(t_1) = m_2. \end{array} \right. \quad \mathcal{P}_2 \left\{ \begin{array}{l} C_2 = \min \int_{t_1}^{t_2} \|u\|^2 dt, \\ \dot{x} = F_0(x) + \frac{\epsilon}{m} \sum_{i=1}^2 u_i F_i(x), \\ \dot{m} = -\beta_* \epsilon \|u\|, \\ \|u\| \leq 1, \\ x(t_1) = \xi_2, \quad m(t_1) = m_2 \\ x(t_2) = \xi_f^*. \end{array} \right.$$

The value function is the cost obtained for an optimal solution (which corresponds to an optimal control). It is also a solution of the Hamilton-Jacobi-Bellman equations (HJB) for which there exist concepts such as viscosity solutions. We refer to [7] (and references therein) for a textbook on optimal control and viscosity solutions of the HJB equations.

We solve problem (4.2) with a gradient descent, and so, we want to compute the gradient of the cost function \mathcal{V}_{tot} , *i.e.*:

$$\nabla_{X_1, X_2} \mathcal{V}_{\text{tot}}. \quad (4.3)$$

It holds that

$$\frac{\partial \mathcal{V}_{\text{tot}}}{\partial \xi_1} = \frac{\partial \mathcal{V}_0}{\partial \xi_1} + \frac{\partial \mathcal{V}_1}{\partial \xi_1},$$

$$\frac{\partial \mathcal{V}_{\text{tot}}}{\partial \xi_2} = \frac{\partial \mathcal{V}_1}{\partial \xi_2} + \frac{\partial \mathcal{V}_2}{\partial \xi_2},$$

$$\frac{\partial \mathcal{V}_{\text{tot}}}{\partial m_1} = \frac{\partial \mathcal{V}_0}{\partial m_1} + \frac{\partial \mathcal{V}_1}{\partial m_1},$$

and

$$\frac{\partial \mathcal{V}_{\text{tot}}}{\partial m_2} = \frac{\partial \mathcal{V}_1}{\partial m_2} + \frac{\partial \mathcal{V}_2}{\partial m_2}.$$

It is well known (see [7, chap. 1, sec. 6]) that, when the value function is smooth, its *sensitivity* with respect to the state perturbation is given by the costate. This relation gives

us the following equations

$$\begin{aligned}
\frac{\partial \mathcal{V}_{\text{tot}}}{\partial \xi_1} &= \frac{\partial \mathcal{V}_0}{\partial \xi_1} + \frac{\partial \mathcal{V}_1}{\partial \xi_1} = p_\xi^0(t_0) - p_\xi^1(t_0), \\
\frac{\partial \mathcal{V}_{\text{tot}}}{\partial \xi_2} &= \frac{\partial \mathcal{V}_1}{\partial \xi_2} + \frac{\partial \mathcal{V}_2}{\partial \xi_2} = p_\xi^1(t_1) - p_\xi^2(t_1), \\
\frac{\partial \mathcal{V}_{\text{tot}}}{\partial m_1} &= \frac{\partial \mathcal{V}_0}{\partial m_1} + \frac{\partial \mathcal{V}_1}{\partial m_1} = p_m^0(t_0) - p_m^1(t_0), \\
\frac{\partial \mathcal{V}_{\text{tot}}}{\partial m_2} &= \frac{\partial \mathcal{V}_1}{\partial m_2} + \frac{\partial \mathcal{V}_2}{\partial m_2} = p_m^1(t_1) - p_m^2(t_1),
\end{aligned} \tag{4.4}$$

where we denote by $p_\xi^i(\cdot)$ the costate part of the extremal solution of problem \mathcal{P}_i relative to the variable² ξ , and by $p_m^i(\cdot)$ the costate part of the extremal solution of the problem \mathcal{P}_i relative to variable m .

Thanks to this result, we establish a two level optimization method: the first indirect step, solves the three optimal control problems connecting the two matching points X_1 and X_2 , and the second step consists in moving these two parameters (in $\mathbf{R}^7 \times \mathbf{R}^7$) following the gradient descent for the sum of the three value functions (4.2) we want to minimize.



If the necessary optimality condition for problem (4.1) is satisfied, *i.e.*, a zero of the gradient (4.3) has been found, then the gap between the costates at the matching points has also been resorbed.

Hence, the necessary conditions correspond to an extremal solution of the global problem, and we obtain the necessary conditions given by the PMP.

This method is initialized with the three-part admissible trajectory obtained in the previous section (Section 4.3.3), a first transfer to reach the free trajectory, the free part inside the invariant manifold, and the final transfer to reach the LO.

Indirect Methods as a Black Box

As previously explained, we use indirect method to solve each of the “local” optimal control problems on each of the three parts. Recall that the three transfer times are fixed. Hence, when the gradient descent “moves” the parameters X_1 and X_2 , the indirect methods are called to “adjust” the initial costate on each part. Once again, this is done with a final state continuation. Each continuation can itself be performed with a single or multiple shooting method.

In the remainder of this chapter, we denote this black box by `IndirectSolve`. As in the previous chapter, we label $P = (p_\xi, p_m)$, and the black box `IndirectSolve` updates the previous costates $P_0 = (p_\xi^0(0), p_m^0(0))$, $P_1 = (p_\xi^1(0), p_m^1(0))$ and $P_2 = (p_\xi^2(0), p_m^2(0))$ to reach respectively X_1 , X_2 and ξ_f^* .

4.4.1 The Algorithm

We have implemented a simple gradient method to solve this problem. We describe it in detail in Algorithm 4.1. For the sake of completeness and because of the difficulties we encountered, we also implemented the resolution of the minimization problem with the C++ IpOpt library (see [88] for the documentation of IpOpt).

². We added the subscript ξ , because of the superscript and the possible confusion with the usual notation p^0 for the PMP.

We denote by $\nabla\mathcal{V}_{\text{tot}}$ the gradient of the function \mathcal{V}_{tot} we want to minimize. Recall that this is given by the gap between the costates at the matching points (equation (4.4)).

Algorithm 4.1: Gradient Bi-Level Optimization

Require: Initial X_1^0 and X_2^0 associated with P_0^0, P_1^0 and P_2^0 .

- 1: Initialization of the gradient step: α (e.g. 1×10^{-2})
- 2: Initialization of the precision: ϵ (e.g. 1×10^{-8})
- 3: **while** $\|\nabla_{X_1, X_2} \mathcal{V}_T\| > \epsilon$ **do**
- 4: $(X_1^{i+1}, X_2^{i+1}) \leftarrow (X_1^i, X_2^i) - \alpha \nabla_{X_1, X_2} \mathcal{V}_{\text{tot}}(X_1^i, X_2^i)$
- 5: $(P_0^{i+1}, P_1^{i+1}, P_2^{i+1}) \leftarrow \text{IndirectSolve}$ (Adjust the corresponding costates)
- 6: **end while**

4.4.2 Numerical results

The algorithm works and allows to decrease the sum of the three value functions (all terms in the sum are positive here). But, we observe that some problems appear. First, we do not reach the necessary optimal condition in reasonable time. Second, we observe that, because we initialize the second part with an invariant manifold trajectory which is a slow trajectory (it passes close to the equilibrium point L_1), the perturbation of the matching points requires to pass further away from L_1 as can be observed in Figure 4.7. Indeed, the time is fixed on each of the three parts. A patch could be applied to allow the time to decrease for the middle part.

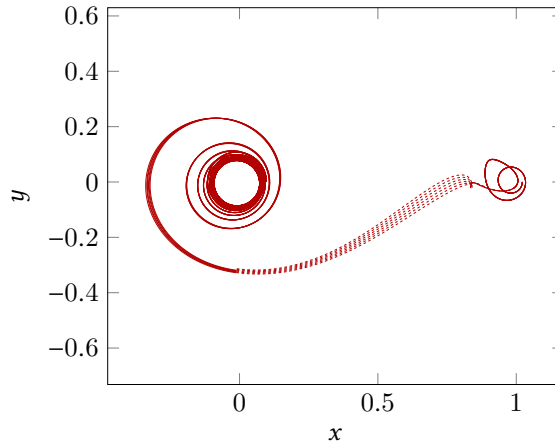


Figure 4.7 – Evolution of the three-part trajectory during the gradient descent. Note that near the equilibrium point L_1 , the spacecraft makes a detour before coming back to the matching point.

During the steps of the gradient method, we observe that the value we want to minimize decreases (equation (4.1)). Unfortunately, the corresponding final mass increases during the iterations. This evolution is plotted in Figure 4.8. Of course, it is possible to increase the final mass during the minimization of the L^2 -norm of the control, but, in practice, this is not interesting. Note that IpOpt does not give a better result and takes more time to decrease the objective function.

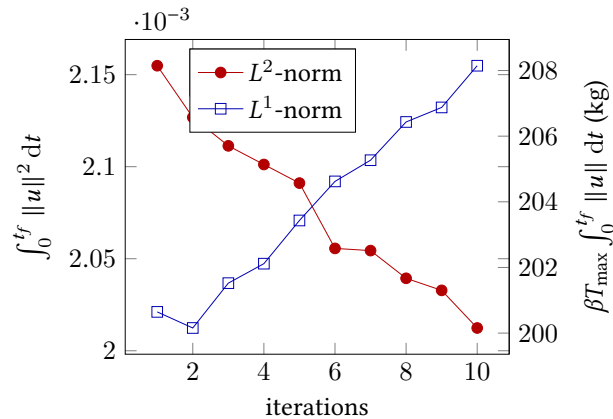


Figure 4.8 – Evolution of the two costs during the optimization. The L^2 -norm of the control decreases as expected, but unfortunately the L^1 -norm of the control increases, so the fuel consumption increases during the optimization.

Constraint box

We note in Figure 4.7 that during the gradient descent, ξ_1 , the matching point in \mathbf{R}^6 , goes closer to the starting orbit around the Earth (GEO). It seems intuitive that the closer the targeted point is to the GEO, the cheaper the transfer is, and in turn the smaller the norm of the final costate is. Recall that we initialize the transfer with a zero costate for the second part of the admissible trajectory, so it is not surprising to observe this behavior.

Hence, to stop the gradient method (and the IpOpt algorithm), we have introduced a “constraint box” around the initial states ξ_1 and ξ_2 . We add the following constraint

$$\xi_1^l \leq \xi_1 \leq \xi_1^u \text{ and } \xi_2^l \leq \xi_2 \leq \xi_2^u,$$

where the inequalities are component per component. The larger the box is, the longer the optimization takes because both algorithms saturate the constraint. We observe that even though the gradient descent allows to get better sub-optimal trajectories, we do not manage to get an optimal trajectory. Moreover, the gain on the cost (L^2 -norm) is not sufficient to justify this quite long optimization. Finally, as we have already mentioned, the L^1 -norm increases during this hybrid optimization, and so, there is no physical improvement.

4.5 Other Missions

We apply the method to other missions to check whether the numerical investigation gives us the same kind of result. Energy is not the only meaningful parameter: we observe that the insertion point onto the free trajectory is also a crucial parameter. Indeed, on a particular example we show that waiting for the second intersection with the Poincaré cut U_1 could save more than 30 kg of propellant.

As expected, the method works in the 3D case without any problem for a GEO to Halo mission. Finally, we discuss the maximal thrust problem, considering that a continuation on the transfer time would allow to decrease the maximal thrust.

4.5.1 GEO to Lyapunov Missions: Two Cases

We design admissible trajectories for missions of the type GEO to Halo orbit. We define two missions, both with an energy of $\mathcal{E}_{L_1} = -1.60$. For the first one, we reach the invariant manifold at the first intersection with the plane U_1 , and for the second mission we reach the invariant manifold at the second intersection. Note that this is possible when invariant manifolds are stable and keep their structure over a long propagation time. This property depends mostly on the energy for each type of periodic orbit, and some periodic orbits generate more stable invariant manifolds than others, for instance, the “eight-shaped” periodic orbit (see [6]).

We note first that the two first admissible trajectories with an uncontrolled part are computed in less than 2 min, this is the main advantage of our method. Moreover, the final masses, summarized in Table 4.5, are $m_1(t_f) = 1291.882\,048\,768\,7$ kg and $m_2(t_f) = 1326.062\,368\,222\,8$ kg, and the costs $\int_0^{t_f} \|u\|^2 dt$ follow the same relation of order (see Table 4.5).

	1st cut with U_1	2nd cut with U_1
final mass $m(t_f)$	1291.882 048 kg	1326.062 368 2 kg
final cost	0.003 891 10+1.804 152 5 $\times 10^{-11}$	0.0026117+1.712 344 26 $\times 10^{-11}$

Table 4.5 – Numerical results for the two GEO to Lyapunov missions using the first and second intersections with the Poincaré cut U_1 .

The times of the two controlled parts are

$$t_0 = 3.0, \text{ and } t_2 = 1.0$$

The time of the uncontrolled part depends on the insertion point. In the case of the first intersection

$$t_1^1 = 4.462\,618\,863\,7,$$

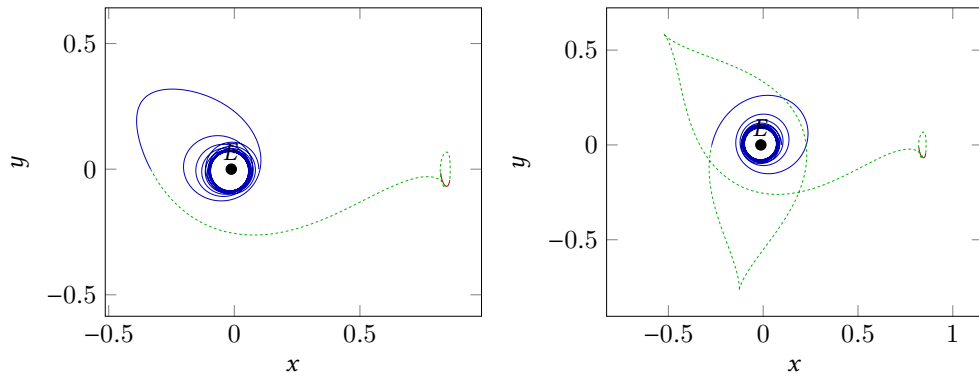
whereas for the second intersection it is

$$t_1^2 = 8.807\,734\,161\,9.$$

We plot both trajectories in Figures 4.9a and 4.9b.

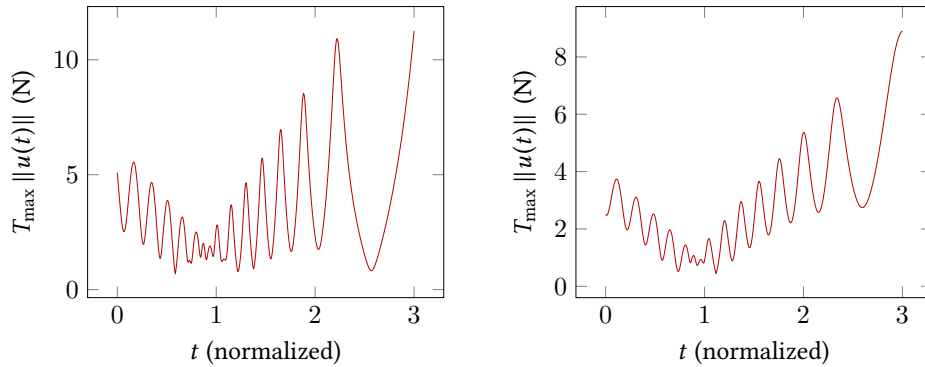
Once again, we tried to optimize the matching points with the bi-level optimization method that we have developed. Unfortunately, we obtain the same results, the L^2 -norm decreases, whereas the L^1 -norm increases during the optimization. Because we have implemented a simple gradient descent with constant step, the method is quite slow and we lose the main advantage of our method: *the short computational time*. We do not report the results of our numerical tests here because of the similarities with the previous set of tests.

We plot the norm of the control in Figure 4.10 for the part on which it is most active (GEO to the free trajectory). Note that the structure of the control is very similar in both cases, we observe oscillations corresponding to the revolutions the spacecraft performs around the Earth.



(a) The insertion point is the first point belonging to the Poincaré map U_1 . (b) The insertion point is the second point belonging to the Poincaré map U_1 .

Figure 4.9 – Two trajectories connecting the GEO to a Lyapunov orbit with different inserting points on the manifold. The energy is $\mathcal{E} = -1.60$.



(a) Control to reach the first point belonging to the Poincaré map U_1 . (b) Control to reach the second point belonging to the Poincaré map U_1 .

Figure 4.10 – Norm of the control for both trajectories connecting the GEO to the free trajectory of the stable manifold of the Lyapunov orbit. The energy is $\mathcal{E} = -1.60$.



With these two examples, we note that the insertion point onto the invariant manifold is crucial. Indeed, waiting for the second intersection with the Poincaré cut U_1 , we manage to save around 30 kg of propellant.

In fact, we should optimize the insertion point using the transversality condition of the PMP as for the Lyapunov to Lyapunov mission (see Section 3.2.6). Indeed, we want the optimal insertion point onto a natural trajectory, and the transversality condition is

$$p_{\xi}(t_f) \perp T_{x(t_{\text{tot}})}\mathcal{A},$$

where \mathcal{A} is the free trajectory belonging to the stable manifold of the Lyapunov orbit. A different point of view would be to introduce a discrete parameter (number of revolutions around the primary) and use hybrid optimization. This is more coherent with the concept of Interplanetary Transport Network (see remark 2.1) and it is, in a certain sense, more general if we see this method as an initialization with patched three body problems.

4.5.2 3D case, from the GEO to a Halo orbit

We now apply the method to build an admissible trajectory to perform a transfer in the 3D case from the GEO to a Halo orbit. This illustrates the efficiency of the method. Although we are not able to get a trajectory which satisfies the necessary condition of optimality, we manage to get an admissible trajectory (satisfying the necessary conditions on each part). Once again the computational time is low, less than 4 min, including the computation of the invariant manifold and the longer computation of the transfer from the GEO to the free trajectory of the stable manifold.

We consider a Halo orbit of energy $\mathcal{E}_{\text{Halo}} = -1.59$. The final and initial points on the GEO are defined in Table 4.6.

	Transfer time		Computation time	
	17.508 920 222 or 76.149 days		cpu 233.52s	
	x	y	z	m
Initial	9.73633112e-02	0.0	0.0	1500
Final	8.5376544e-01	-5.0569202e-02	-1.2077010e-02	
	\dot{x}	\dot{y}	\dot{z}	
Initial	0.0	2.8913578317	0.0	
Final	-2.5488886e-02	-8.2648076e-02	5.0635069e-02	

Table 4.6 – Parameters for the transfer between the GEO and the Halo orbit.

The admissible trajectory is plotted in Figure 4.11 with the three parts. We observe that the end of the controlled trajectory looks like a manifold trajectory. As usual, we have to pick the transfer time for each part. For the middle part, it is given by the duration of the free trajectory, whereas for the two others it must be chosen carefully. Once again, the study of the minimum time problem could give us a hint as to what time to choose. The problem is however not very sensitive with respect to this parameter, and it is in fact easy to find suitable times. The first transfer is performed with a transfer time

$$t_0 = 12.0.$$

The time of propagation of the uncontrolled part is

$$t_1 = 4.508520222.$$

And finally, the last controlled transfer time is

$$t_2 = 1.0.$$

The total transfer time is then

$$t_f = 17.508920222 = 76.149 \text{ days.}$$

The obtained controls for the two controlled parts are plotted in Figure 4.12. As can be expected from the plot of the first part trajectory which looks like a manifold, the norm of the control decreases during the transfer. Finally, starting with an initial mass of 1500 kg, we obtain a final mass of

$$m(t_f) = 1366.969 975 7 \text{ kg,}$$

which is an efficient transfer that uses a small amount of propellant. Note that this efficient trajectory was obtained in only a few minutes.

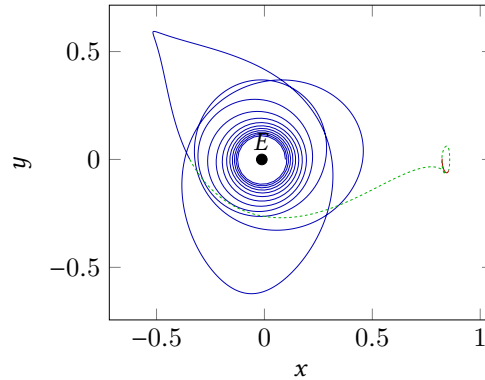
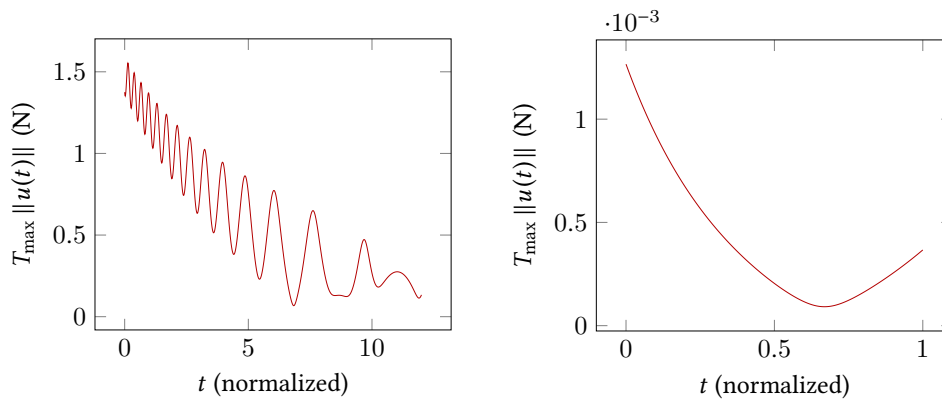


Figure 4.11 – Admissible trajectory for the transfer from the GEO to the Halo orbit.



(a) Control of the first controlled part to reach the point belonging to the invariant manifold in the Poincaré map U_1 . **(b)** Control of the last controlled part to reach the point belonging to the Halo orbit.

Figure 4.12 – Norm of the control for the two controlled parts of the admissible trajectory connecting the GEO to the Halo orbit. The energy is $\mathcal{E} = -1.59$.

4.5.3 About the Maximal Thrust

We do not investigate the maximal thrust constraint here for several reasons. The first reason is that the main purpose of this method is to provide us with admissible trajectories which are an initial guess for another level of optimization. Hence, the maximal thrust is chosen in such a way that the control does not saturate the constraint. Of course we can decrease the maximal thrust by a continuation, and this works as long as the final point is in the admissible set. If not, one can perform a continuation on the final time.

The second reason is that the way to allow a fast decrease of the control is to perform a continuation on time without waiting for the control to saturate the constraint. Indeed, for the GEO to Halo mission, we plot in Figure 4.13 two different norms of the control for a transfer from the GEO to the stable manifold orbit, one with a transfer time of 3.0 (normalized time) and the other with a transfer time of 12.0. In Figure 4.14, we plot the

corresponding admissible trajectories. We observe that the maximal, not saturating, control is approximately 11 N for the short transfer whereas the maximal thrust is approximately 1.6 N for the longer one. The main advantage is that we perform this continuation in less than two minutes on a standard desktop computer.

Relaxing the constraint that the second part must be uncontrolled allows to further reduce the cost of the control for the first transfer, and consequently, to save energy (or propellant consumption) for the first part. This can be viewed as a diffusion of the control from the first to the second part of the trajectory.

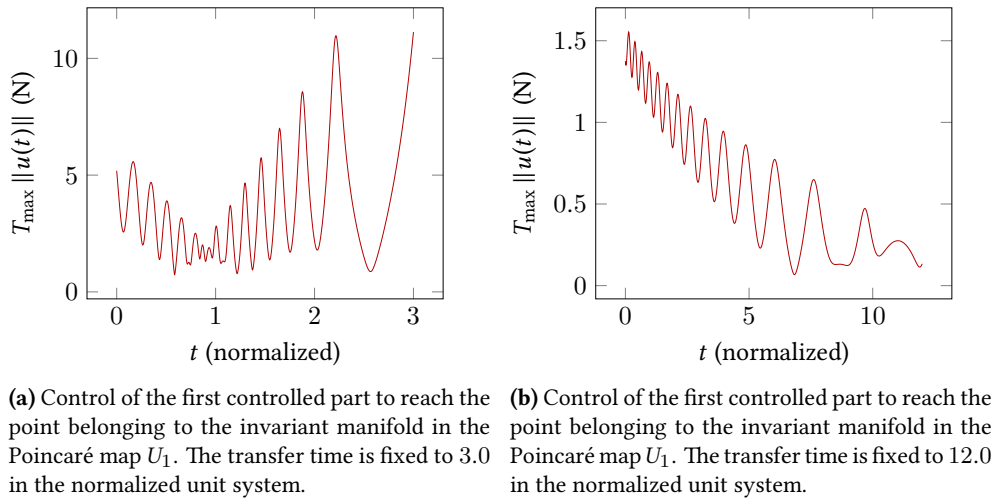


Figure 4.13 – Norm of the control for the two controlled times to reach the invariant manifold trajectory. The energy is $\mathcal{E} = -1.59$.

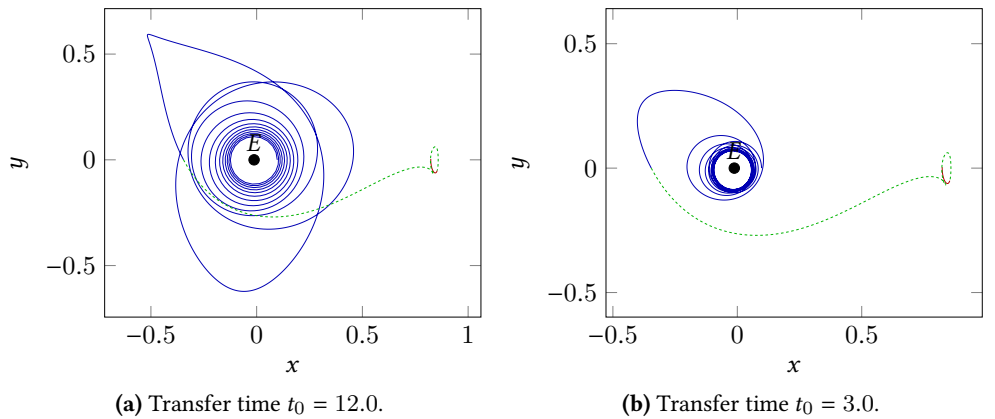


Figure 4.14 – The two admissible trajectories for different times of transfer for the first controlled part of the admissible trajectory. The energy is $\mathcal{E} = -1.59$.

Conclusion

Contribution

The first objective of this work was to understand the dynamical properties of the circular restricted three body problem in order to use them to design low consumption missions for spacecrafts with a low thrust engine. This work can be viewed as a continuation of the work in [6]. Our work was originally driven by Philippe Augros from Airbus Defence and Space (DS) and was funded by Airbus DS. A code in FORTRAN90 was developed for Airbus DS to compute efficiently the different properties of the CRTBP such as periodic orbits around equilibrium points (Halo, Lyapunov and “Eight-Shaped” orbits), as well as associated invariant manifolds. We introduced a new continuation method to compute the family of periodic orbits using energy as the continuation parameter.

Following the Interplanetary Transport Network (ITN) concept, invariant manifolds are very useful to design spacecraft missions because they are *gravitational currents* in the CRTBP. For this purpose, a large part of this work was devoted to designing a numerical method that performs an optimal transfer between invariant manifolds. The method is to use the impulsive transfer method in order to build an Optimal Control Problem. After having obtained the optimal control problem formulation, we developed a robust method based on various continuations: final state continuation, thrust continuation and cost continuation. This last continuation performs an homotopy between the minimization of the L^2 -norm of the control and the minimization of the L^1 -norm of the control. This is a well known method which works quite well and it is used because the L^2 -minimization is numerically easier to perform than the L^1 -minimization. For the different numerical experiments of transfers between invariant manifolds, the developed method shows good results, managing to compute the L^1 -minimization and shows robustness with respect to the different parameters. A study of the crucial transfer time parameter was also conducted and we concluded that the method is robust with respect to transfer time. Moreover, at the limit where the transfer time goes to 0, the control appears to converge to the corresponding impulse ΔV .

The most important achievement of this work is Chapter 3. With the algorithm developed to achieve transfers between invariant manifolds, we design missions between periodic orbits around the Lagrange points L_1 and L_2 . The basic idea is to initialize a multiple shooting method with an admissible trajectory that contains an uncontrolled part following the natural dynamics. To illustrate the method, we perform different missions. First, three-part admissible trajectories that contain a heteroclinic trajectory are built (the two periodic orbits share the same energy). For different values of the energy, the considered heteroclinic orbits perform either one or two revolutions around the primary. In each case the method succeeded. A last example consists of a 3D mission, where no heteroclinic orbit exists. In that case, the admissible trajectory is built with 5 parts including two free parts that follow the two invariant manifolds. In all these examples, the method is both robust and efficient. The results in terms of cost and consumption are very good, and the computation time is

very small. The most time consuming step in our method is the end-point position optimization but, this optimization, although improving just a little the cost of the transfer, allows to obtain the intuitive *turnpike property* when heteroclinic orbit exists. Because of the too small effective maximal thrust, the continuation on the cost to obtain the maximization of the final mass fails, hence, only the L^2 -minimization is solved in this chapter.

The last contribution of this thesis is to apply the methods we developed to missions starting from the geostationary Earth orbit (GEO). We reach a lunar orbit, as well as Lyapunov and Halo orbits. We are able to compute admissible trajectories composed of three parts: one to reach a transit free trajectory, then one following the natural dynamics (invariant manifolds), and the last one to reach the targeted orbit from the free trajectory. These admissible trajectories are computed within a very short time (a few minutes). Unfortunately, because of the energy gap between the GEO and invariant manifolds (greater than the energy of L_1), the multiple shooting fails in this particular case. We developed a hybrid optimization method consisting of both direct and indirect methods. The efficiency of this method is based on the fact that solving the three transfers with indirect methods enables to perform a gradient descent method. Indeed, at each matching point, the (required) gradient of the global value function (the sum of the three local ones) is given by the difference between the final and initial costate at these points. We show that if we obtain the necessary condition for the gradient method, then we have a one-part trajectory performing the transfer and satisfying the PMP necessary condition. This hybrid method does not converge in reasonable computation time, and hence, we restrict the optimization of the two matching points position with a “constraint box”. We observe that the constraint is saturated in the direction of the GEO. Moreover, although the L^2 -cost decreases during this optimization, the physically interesting L^1 -cost increases. Hence, the main advantage of the method is to obtain an admissible trajectory with low consumption in a very short computation time. We present different examples of transfers departing from the GEO, and we observe that the choice of the insertion point onto the transit trajectory is crucial. The duration of the more expensive part (the first one) is also an important parameter, and allows to significantly decrease the maximum thrust.

Perspectives

In each of our transfers, the first order necessary conditions for optimality of the PMP give us the optimal control, but we do not check that the sufficient second order conditions are satisfied (nor the necessary second order conditions). This could be done using the conjugate locus theory which is well developed for applications in mission design. However, the good results in terms of cost do point toward the optimality of our trajectories.

Design of spacecraft missions is a very rich and vast subject of research. Understanding the numerical problems is a big issue. The study of the instability of the Hamiltonian system could explain the difficulties we encountered for the convergence of the multiple shooting method, especially along the natural trajectory part following the invariant manifolds. Moreover, studying the instability of invariant manifolds in depth, following the Lyapunov exponent approach, and linking that with the success of the multiple shooting method could provide us with important information. Also, the more systematic numerical study of the turnpike property, proved for static equilibrium points, could help the theoretical study of the turnpike property with natural drift.

Our methods and algorithm could be further improved in many ways. First, to help the L^2 to L^1 -minimization continuation, one could add tools to determine the structure of the bang-bang targeted control. For instance, when oscillations are detected, we could consider a corresponding bang-bang structure and add switching times as parameters. The hybrid

method developed for the missions departing from the GEO should be improved, in particular by allowing the time adaptation in the middle part initialized with a natural uncontrolled trajectory. Indeed, we observe that the fixed time on this part implies that, during the gradient descent, the trajectories make a detour around the equilibrium point L_1 . An adaptive duration of the middle part should improve the method.

Finally, the most important perspective is to couple CRTBP to design interplanetary spacecraft missions. The complete study of the patched three body approximation with a low thrust engine should be done. In this subject, many unexplored subjects pop up: one can introduce a discrete parameter counting the revolutions of invariant manifolds around primaries (we saw that the insertion point on invariant manifolds is crucial). Moreover, the stability of the embedding of the three body problem trajectories into the four body problem, and the embedded control may be an issue depending on the considered three-body problems.

Richardson's Constants

Here, we recall Richardson's constants obtained in his work [74]. See section 1.4.3 for explanations of what are all these constants and parameters.

$$\begin{aligned}
 a_{21} &= \frac{3c_3(\kappa^2 - 2)}{4(1 + 2c_2)}, \\
 a_{22} &= \frac{3c_3}{4(1 + 2c_2)}, \\
 a_{23} &= -\frac{3c_3\lambda}{4\kappa d_1} [3\kappa^3\lambda - 6\kappa(\kappa - \lambda) + 4], \\
 a_{24} &= -\frac{3c_3\lambda}{4\kappa d_1} (2 + 3\kappa\lambda) \\
 a_{31} &= -\frac{9\lambda}{4d_2} (4c_3(\kappa a_{23} - b_{21}) + \kappa c_4(4 + \kappa^2)) + \left(\frac{9\lambda^2 + 1 - c_2}{2d_2} \right) (3c_3(2a_{23} - \kappa b_{21}) + c_4(2 + 3\kappa^2)), \\
 a_{32} &= -\frac{1}{d^2} \left(\frac{9\lambda}{4} (4c_3(\kappa a_{24} - b_{22}) + \kappa c_4) + \frac{3}{2} (9\lambda^2 + 1 - c_2) (c_3(\kappa b_{22} + d_{21} - 2a_{24}) - c_4) \right), \\
 b_{21} &= -\frac{3c_3\lambda}{2d_1} (3\kappa\lambda - 4), \\
 b_{22} &= \frac{3c_3\lambda}{d_1}, \\
 b_{31} &= \frac{3}{8d_2} \left(8\lambda (3c_3(\kappa b_{21} - 2a_{23}) - c_4(2 + 3\kappa^2)) + (9\lambda^2 + 1 + 2c_2) (4c_3(\kappa a_{23} - b_{21}) + \kappa c_4(4 + \kappa^2)) \right), \\
 b_{32} &= \frac{1}{d_2} \left(9\lambda (3c_3(\kappa b_{22} + d_{21} - 2a_{24}) - c_4) + \frac{3}{8} (9\lambda^2 + 1 + 2c_2) (4c_3(\kappa a_{24} - b_{22}) + \kappa c_4) \right) \\
 d_{21} &= -\frac{c_3}{2\lambda^2}, \\
 d_{31} &= \frac{3}{64\lambda^2} (4c_3 a_{24} + c_4), \\
 d_{32} &= \frac{3}{64\lambda^2} (4c_3 a_{23} - d_{21} + c_4(4 + \kappa^2)),
 \end{aligned}$$

where

$$d_1 = \frac{3\lambda^2}{\kappa} (\kappa(6\lambda^2 - 1) - 2\lambda)$$

and

$$d_2 = \frac{8\lambda^2}{\kappa} (\kappa(11\lambda^2 - 1) - 2\lambda)$$

s_1 and s_2 are defined by

$$s_1 = \frac{\frac{3}{2}c_3(2a_{21}(\kappa^2 - 2) - a_{23}(\kappa^2 + 2) - 2\kappa b_{21}) - \frac{3}{8}(3\kappa^4 - 8\kappa^2 + 8)}{2\lambda(\lambda(1 + \kappa^2) - 2\kappa)},$$

$$s_2 = \frac{\frac{3}{2}c_3(2a_{22}(\kappa^2 - 2) - a_{24}(\kappa^2 + 2) + 2\kappa b_{22} + 5d_{21}) + \frac{3}{8}c_4(12 - \kappa^2)}{2\lambda(\lambda(1 + \kappa^2) - 2\kappa)},$$

where $\kappa = \frac{1}{2\lambda}(\lambda^2 + 1 + 2c_2)$, and λ is solution of

$$\lambda^4 + (c_2 - 2)\lambda^2 - (c_2 - 1)(1 + 2c_2) = 0.$$

Constants l_1 and l_2 are defined by

$$l_1 = a_1 + 2l^2s_1 \quad \text{et} \quad l_2 = a_2 + 2l^2s_2,$$

where $a_1 = -\frac{3}{2}c_3(2a_{21} + a_{23} + 5d_{21}) - \frac{3}{8}c_4(12 - k^2)$ and $a_2 = \frac{3}{2}(a_{24} - 2a_{22}) + \frac{9}{8}c_4$.

User guide for the Uacamol program – v1.4

This document is a documentation of a code developed for Airbus Defence of Space, at les Mureaux.

B.1 Introduction

This document is a user documentation for the program **Uacamol**. The code is not described here, and we invite the reader to see the doxygen documentation for a description of the source code of the program and its structure.

B.2 A Short Review of the Three Body Problem

We consider the motion of the spacecraft P of negligible mass moving under the gravitational influence of the two masses M_1 and M_2 , referred to as the primary masses, or simply the *primaries* (here Earth and Moon). We denote these primaries by P_1 and P_2 . Moreover, we assume that the primaries have circular orbits around their common center of mass. The particle P is free to move all around the primaries but cannot affect their motion.

The system is made nondimensional by the following choice of units: the unit of mass is taken to be $M_1 + M_2$; the unit of length is chosen to be the constant separation between P_1 and P_2 ; the unit of time is chosen such that the orbital period of P_1 and P_2 around their center of mass is 2π . The universal constant of gravitation then becomes $G = 1$. The conversion from units of distance, velocity and time in the unprimed, normalized system to the primed, dimensionalized system is

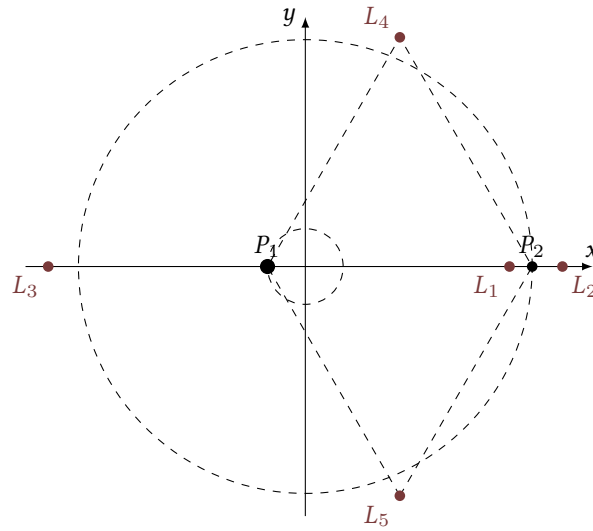
$$\begin{aligned}
 \text{distance} & \quad d' = l_* d, \\
 \text{velocity} & \quad s' = v_* s, \\
 \text{time} & \quad t' = \frac{t_*}{2\pi} t,
 \end{aligned}
 \tag{B.1}$$

where we call l_* the distance between P_1 and P_2 , v_* the orbital velocity of P_1 and t_* the orbital period of P_1 and P_2 .

We define the only parameter of this system as

$$\mu = \frac{M_2}{M_1 + M_2}, \quad (\text{B.2})$$

and call it the *mass parameter*, assuming that $M_1 > M_2$.



B.2.1 Equations of Motion

We in fact consider two coordinate systems, the first described in the previous section called the Cross coordinate system (centered on the center of mass of the two primaries and with the distance between the two primaries normalized to one), and a second, the Richardson system centered on the considered Lagrange L_i point and with the distance between L_i and P_2 normalized to one.

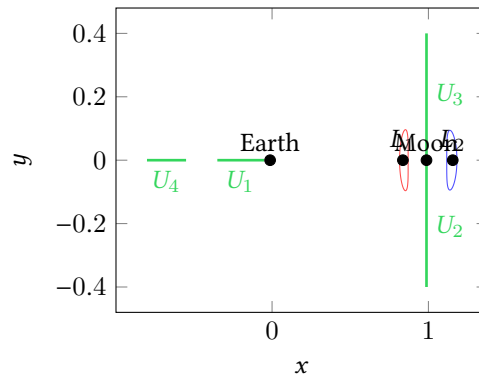
Almost all computations and results are given in Richardson coordinates.

We give here the equations of motion in Cross coordinates (see the thesis of Gregory Archaubeau for the details on how to change coordinates).

$$\begin{cases} \dot{x}_1 = x_4 \\ \dot{x}_2 = x_5 \\ \dot{x}_3 = x_6 \\ \dot{x}_4 = x_1 + 2x_5 - (1 - \mu) \frac{x_1 - x_1^0}{r_1^3} - \mu \frac{x_1 - x_2^0}{r_2^3} \\ \dot{x}_5 = x_2 - 2x_4 - (1 - \mu) \frac{x_2}{r_1^3} - \mu \frac{x_2}{r_2^3} \\ \dot{x}_6 = -(1 - \mu) \frac{x_3}{r_1^3} - \mu \frac{x_3}{r_2^3} \end{cases}$$

B.2.2 The Poincaré Cuts

We plot here in the Earth-Moon example the four cuts U_1 , U_2 , U_3 and U_4 used to compute sections of invariant manifolds.



B.3 Compile Uacamol

We give a Makefile to create the executable program **Uacamol** with the binary `uacamolF`. In the Exec directory, you just have to make:

```
user@machine:Exec/ > make
```

The Makefile file must be adjusted to chose the compiler (gfortran or ifort). The `blas` and `lapack` file in the `Sources/lib/lapack-3.5.0/` directory must be compiled. Once again, there are two possible compilers, gfortran or ifort and two files are provided: `make.inc.gfortran` and `make.inc.ifort`, the file `make.inc` must be replaced by the right file. See the Makefile file.

B.4 Files to Feed Uacamol

B.4.1 Addresses File

Uacamol has a necessary argument when we execute it. It is the file of the different addresses given to the main program.

```
user@machine:Input/ > uacamolF inputFile.txt
```

This file must have the exact following structure:

```

1 ===== INPUT FILES =====
2 # Parameter File
3 './inL1.dat'
4 # Initialisation Guess File ('' if not)
5 ''
6
7 ===== OUTPUT FILES =====
8 # Output dir
9 '../Output'
10 # Generic name for manifolds trajectories : NAME_S/I_R/L_i etc.
11 'Traj'
```

- In line 3, the address and name of the parameter input file are given. They will be described in the section B.4.2.

- In line 5, we give, if the user chooses this option, the address of a file containing an initial guess point for a periodic orbit is given (to replace the analytical approximations given by the program). If not, an empty string '' should be given. If an input is given, this file must have the following structure (dummy example):

```

1 # period    x(1)  x(2)  x(3)  x(4)  x(5)  x(6)
2 2.34d0     1.d0  2.d0  3.d0  4.d0  5.d0  6.d0

```

- In line 9, the directory of all different outputs is given.
- In line 11, the directory and the *generic* name of all the trajectories produced when the program computes the four manifolds is given. There are four types (for this particular example):

1. ../Output/Traj_S_R_i.dat for the *stable right manifold*, *i* is a formatted integer, e.g. 0001.
2. ../Output/Traj_S_L_i.dat for the *stable left manifold*.
3. ../Output/Traj_I_R_i.dat for the *unstable right manifold*.
4. ../Output/Traj_I_L_i.dat for the *unstable left manifold*.

Indeed, for each periodic orbit around a Lagrange point there are four associated manifolds: two stable, and two unstable. Spatially, there is one stable manifold to the left of the periodic orbit and one to the right. It is the same for the unstable manifolds. The counter *i* is formatted with four numbers, starting at 1 (e.g. 0001).

Remark B.1:

Note that for the stable manifolds, trajectories are integrated and printed *backward*.

B.4.2 Parameters Input File

We give all parameters in one file that we describe in this section. First, we give an example of such a file.

```

1 # M1 M2 Distance Periode Li
2 5.972d24 7.349d22 384402d3 2.361d6 1
3 # intOrbite
4 100
5 # boolprop Tprop dtMani epsMani
6 1 6.d0 1d-02 1d-04
7 # readInit
8 0
9 # boolOrbType Az boolEnergy energy stepCont familyPrint
10 1 630d5 1 -1.56 0.001d0
11 # relerr abserr epstol factor
12 1d-14 1d-14 1d-12 1d02
13 # sectionU2 sectionU3 sectionU14 tourNbr printTraj
14 0 1 0 0 1
15 # verbose RichCross
16 1 0

```

The structure of this the file must be respected. Odd numbered lines are for comments, and even numbered lines are used to provide the values of the parameters separated by spaces.

Next, we describe all the parameters line by line.

Masses, distance, period and Lagrange point

In line 2, we give:

M1: Mass of the first primary (*real (kg)*).

M2: Mass of the second primary (*real (kg)*).

Distance: Distance between primaries (*real (km)*).

Period: Period of revolution of the two primaries around their center of mass (*real (s)*).

Li: The considered Lagrange point, here L_1 or L_2 (*integer =1 or 2*).

Discretization of periodic orbit

In line 4, we give:

intOrbit: Number of points for the discretization of the periodic orbit. This also defines how many trajectories will be used to approximate an invariant manifold (which is an infinite set of orbits) (*integer >1*).

Propagation of invariant manifolds

In line 6, we give:

boolprop: To choose if we want to propagate and save the trajectories of the invariant manifolds using the generic prefix given in the addresses file (*0 (no) or 1 (yes)*).

Tprop: Time of propagation in normalized system (*real*).

dtMani: Time interval between two consecutive points on the trajectory of the invariant manifold that are saved to the file (*real*).

epsMani: Small parameter, perturbation of periodic orbit along eigenvectors of the monodromy matrix to get manifolds (*real (small)*).

Periodic orbit

In line 8, we give:

readInit: To choose if we want to initialize the first shooting method by a given point and a period in an input file (see previous section), or if we use the analytical approximation given by the program explained in the next description. If `readInit==1`, then the 2 parameters `boolOrbType` and `Az` are useless and their values will be ignored ¹ (*=1 if we give a file, else =0*).

In line 10, we give:

1. We will not provide an example with this parameter active because it is not really relevant but a file to test it is given in the snapshot of the program (Input directory).

boolOrbType: To choose the type of periodic orbit we want to compute. We chose between Halo/Lissajous (diffeomorphic to a circle) or Eight-shaped orbit (we call it Archambeau orbit) (`=0 (Halo) or 1 (Eight)`). If `Az==0.d0`, only Halo choice is possible and we get a Lissajous orbit.

Az: Initial excursion along the z-axis for the analytical approximation that serves as an initial guess in the shooting method to get a periodic orbit (`real (km)`).

boolEnergy: To choose if we want to compute by a continuation an orbit of a given energy greater than the energy of the Lagrange point. A test is done to verify this last properties. (`=0 (no) or 1 (yes)`).

energy: The energy to reach if the previous parameter is set to one (`real (in Cross coordinates)`).

stepCont: Initial step for the continuation predictor-corrector (`real (small)`).

familyPrint: To choose if we want to print all the intermediate periodic orbits computed during the continuation on energy. The output files are named `FOutput/FamPeri` where *i* is a formatted counter. (`=0 (no) or 1 (yes)`).

Parameters for HYBDR and DOP853

In line 12, we give:

relerr: Relative error for dop853 (`real (~1d-12)`).

abserr: Absolute error for dop853 (`real (~1d-12)`).

epstol: Tolerance for HYBRD (`real (~1d-14)`).

factor: Factor for HYBRD (`real`).

Section of manifolds

In line 14, we give:

sectionU2: To choose if we want to compute the intersection of the correct manifolds (depending on the considered Lagrange point) with the plane (defined in Cross coordinates)

$$U_2 = \{(x, y), x = 1 - \mu, y < 0\}.$$

The manifold is the right unstable (resp. left stable) manifold if `Li==1` (resp. `Li==2`) (`=0 (no) or 1 (yes)`).

sectionU3: To choose if we want to compute the intersection of the correct manifolds (depending on the considered Lagrange point) with the plane (defined in Cross coordinates)

$$U_3 = \{(x, y), x = 1 - \mu, y > 0\}.$$

The manifold is the right stable (resp. left unstable) manifold if `Li==1` (resp. `Li==2`) (`=0 (no) or 1 (yes)`).

sectionU14: To choose if we want to compute the intersection of the correct manifolds (depending on the considered Lagrange point) with the plane (defined in Cross coordinates)

$$U_1 = \{(x, y), x > -\mu, y = 0\},$$

or

$$U_4 = \{(x, y), x < -\mu, y = 0\}.$$

If $Li==1$, then we compute the intersection with the “left” invariant manifolds, one forward (unstable) the other backward (stable). If $Li==2$, then we compute the intersection with the “right” invariant manifolds, one forward (unstable) the other backward (stable). (=0 (no) or 1 (yes)).

tourNbr: Number of rotations around the second primary before we compute the section. If we want the first intersection, we give 0 rotation, the second, 1 rotation, etc. (integer).

printTraj: Integer that allow to save trajectories of the manifolds that intersect the U_2 or U_3 cuts depending on the previous options. The files of trajectories respects the `dtMani` parameter previously described (=1 if save traj. else 0).

Verbose and Coordinate Output

In the last line, we give:

verbose: If we want the program to tell us what it is doing and get the information in the standard output, *i.e.* the terminal (=0 (no messages) or 1 (messages)).

RichCross: We choose here the coordinate system of the output trajectories. All computations are done in Richardson coordinates in the program, but we can choose to get the output trajectory files in Richardson or Cross coordinates (=0 for Richardson, 1 for Cross).

B.5 Outputs

Depending on what options the user chose we get the following files in the user defined directory. We denote by `FOutput`, the directory of outputs. All trajectories saved in files have the following structure:

```

1  time  y(1)  y(2)  y(3)  y(4)  y(5)  y(6)
2  .      .      .      .      .      .      .
3  .      .      .      .      .      .      .
4  .      .      .      .      .      .      .

```

`FOutput/Parameters.txt`: All the input parameters plus the computed ones in a summary file.

`FOutput/RichardsonConst.txt`: Constants computed and used to obtain either the Richardson analytical approximation or the Archambeau analytical approximation.

`FOutput/Richardson.txt`: The initial guess obtained by the Richardson analytical approximation (Halo/Lissajous) propagated during the approximate period (does not look like a periodic orbit).

`FOutput/Archambeau.txt`: The initial guess obtained by the Archambeau analytical approximation (eight-shaped) propagated during the approximate period (does not look like a periodic orbit).

`FOutput/PeriodicExc.txt`: The periodic orbit obtained after the shoot with fixed excursion using the analytical approximation as an initial guess.

FOutput/PeriodicEn.txt: The periodic orbit obtained after the continuation to reach the given energy.

Family of periodic orbits: Already described.

Trajectories of the four manifolds: Already described.

Trajectories stopping at the Poincaré cuts: Files are named using the prefix given in the address file (see section B.4) with the suffixes `_U2_sec_i`, `_U3_sec_i`, `_U14back_sec_i` or `_U14_sec_i` where $i \in \{1, \dots, \text{intOrbite}\}$.

B.6 Examples of Application

The four examples presented in this section are available in the sources of the code in the directory `Input`.

We note that a complete computation of one of these examples does not take more than a few seconds on a standard desktop computer.

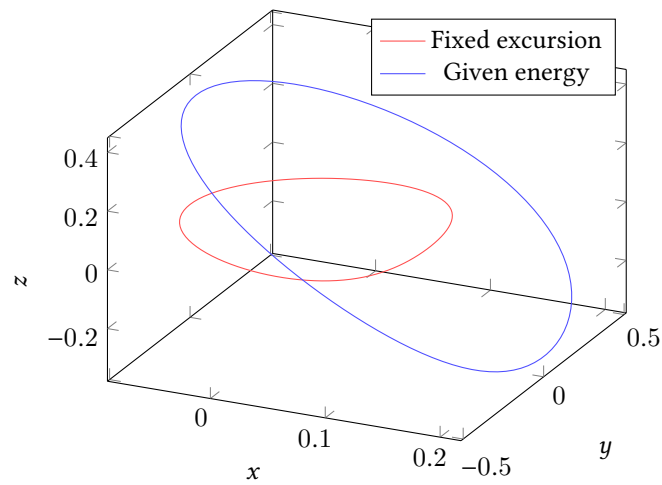
B.6.1 Halo Orbit around L_1 – System Earth-Moon

```

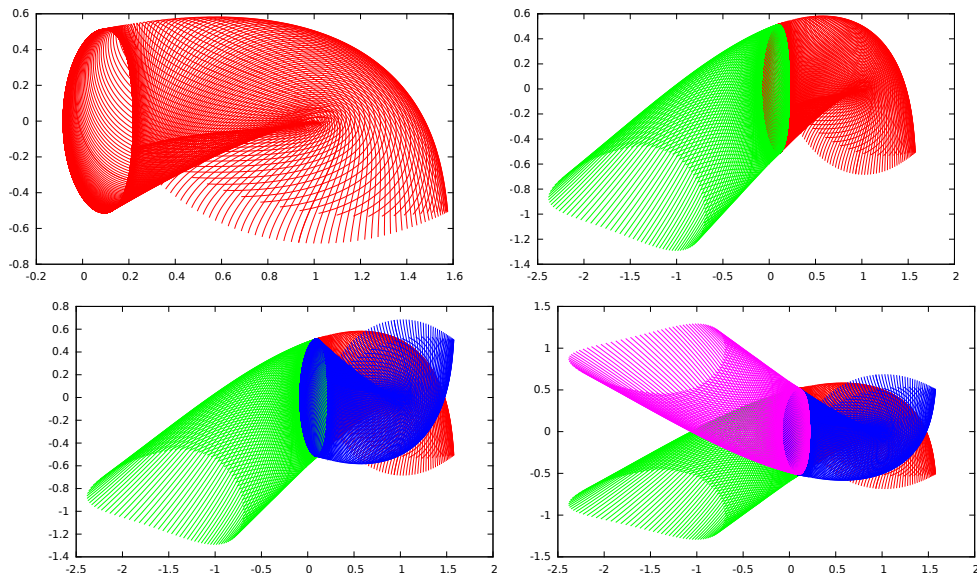
1  # M1 M2 Distance Periode Li
2  5.972d24 7.349d22 384402d3 2.361d6 1
3  # intOrbite
4  100
5  # boolprop Tprop dtMani epsMani
6  1 6.d0 1d-02 1d-04
7  # readInit
8  0
9  # boolOrbType Az boolEnergy energy stepCont printFamily
10 0 300.d3 1 -1.58 0.001d0 0
11 # relerr abserr epstol factor
12 1d-14 1d-14 1d-12 1d02
13 # sectionU2 sectionU3 sectionU14 tourNbr printTraj
14 0 0 0 0 0
15 # verbose RichCross
16 1 0

```

Periodic Orbits.



Four Manifolds.



B.6.2 Lissajous Orbit around L_2 – System Earth-Moon

```

1 # M1 M2 Distance Periode Li
2 5.972d24 7.349d22 384402d3 2.361d6 2
3 # intOrbite
4 100
5 # boolprop Tprop dtMani epsMani
6 1 5.d0 1d-02 1d-04
7 # readInit
8 0
9 # boolOrbType Az boolEnergy energy stepCont printFamily
10 0 0.d0 1 -1.5900004d0 0.01d0
11 # relerr abserr epstol factor
12 1d-14 1d-14 1d-12 1d02

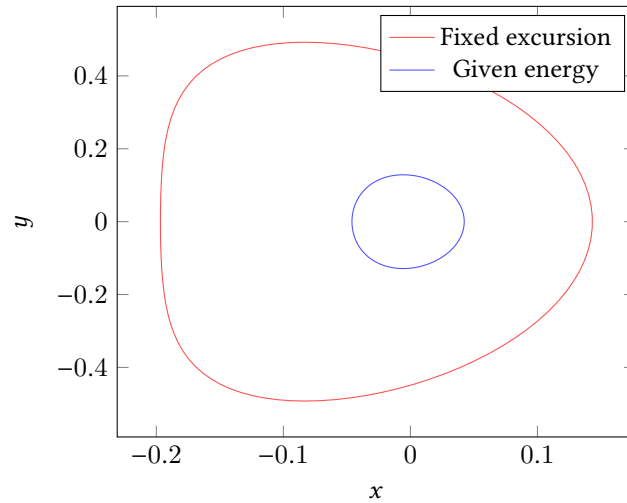
```

```

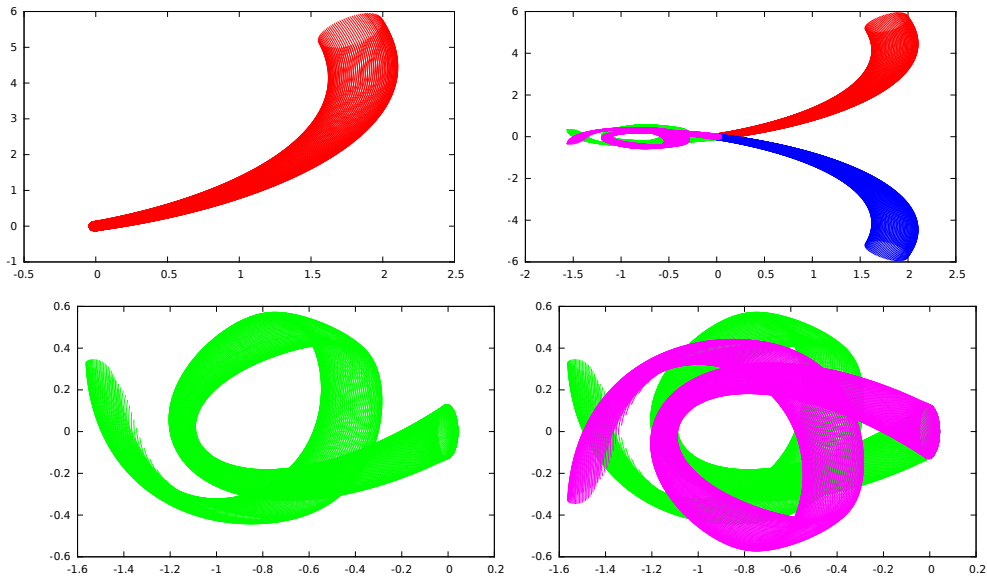
13 # sectionU2 sectionU3 sectionU14 tourNbr printTraj
14 1 1 0 2 0
15 # verbose RichCross
16 1 0

```

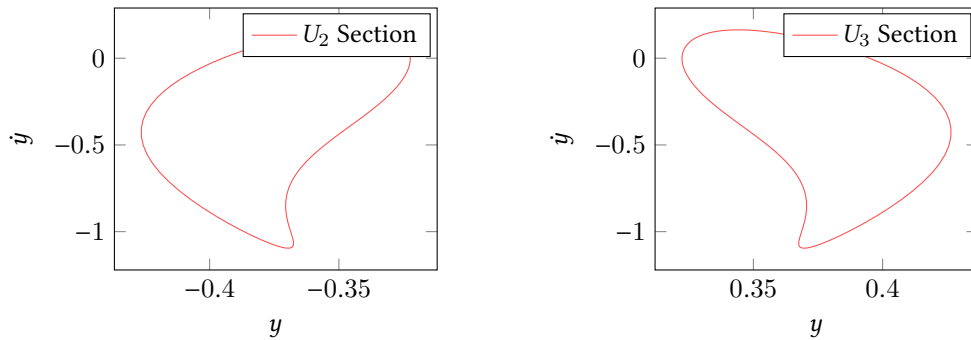
Periodic Orbits.



Four Manifolds.



Section with U_2 and U_3 after one rotation. Here we plot the section in the plane $((y, \dot{y}))$ with the cuts U_2 and U_3 . Because we have a fixed energy (Hamiltonian system), the \dot{x} value is deduced.



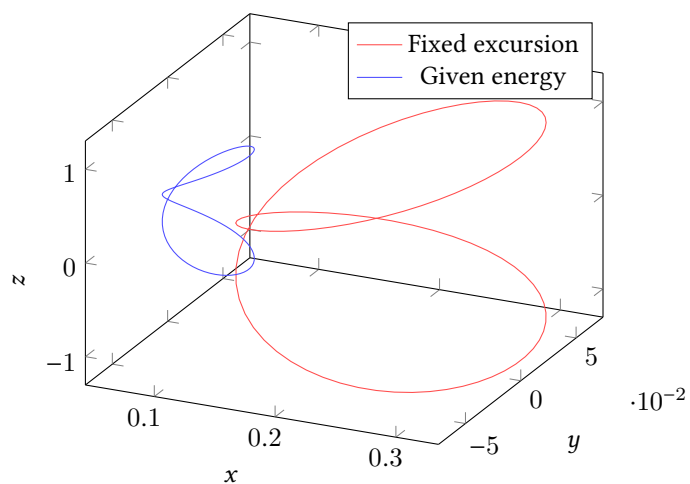
B.6.3 Eight-shaped Orbit around L_1 – System Earth-Moon

```

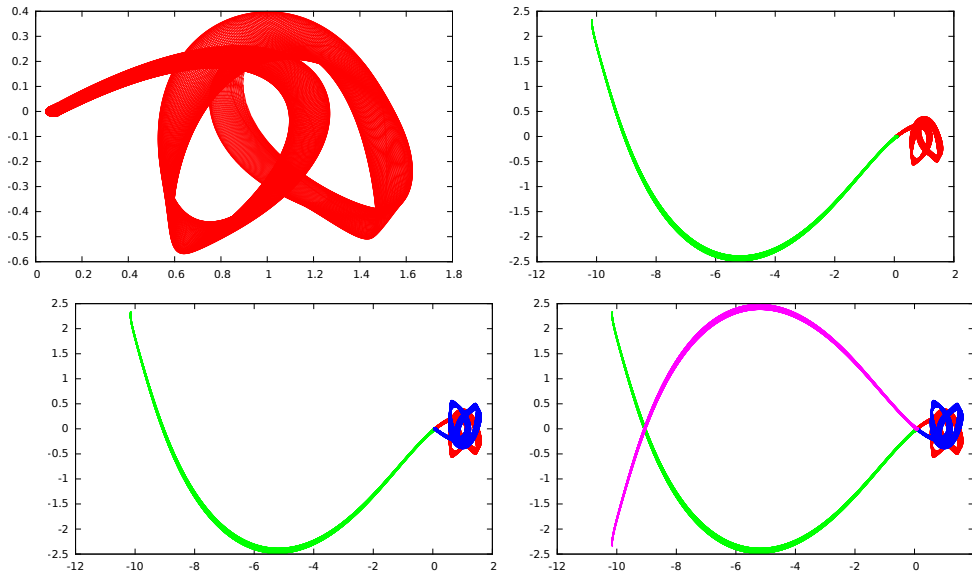
1 # M1 M2 Distance Periode Li
2 5.972d24 7.349d22 384402d3 2.361d6 1
3 # intOrbite
4 100
5 # boolprop Tprop dtMani epsMani
6 1 6.d0 1d-02 1d-04
7 # readInit
8 0
9 # boolOrbType Az boolEnergy energy stepCont printFamily
10 1 630d5 1 -1.58 0.001d0
11 # relerr abserr epstol factor
12 1d-14 1d-14 1d-12 1d02
13 # sectionU2 sectionU3 sectionU14 tourNbr printTraj
14 1 1 0 2 1
15 # verbose RichCross
16 1 0

```

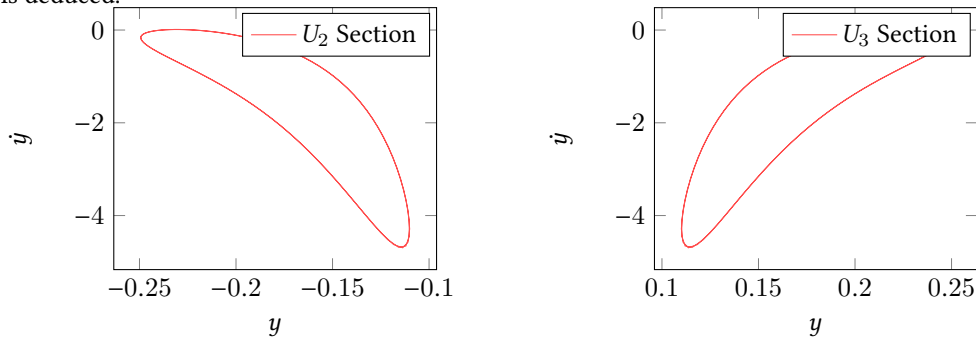
Periodic Orbits.



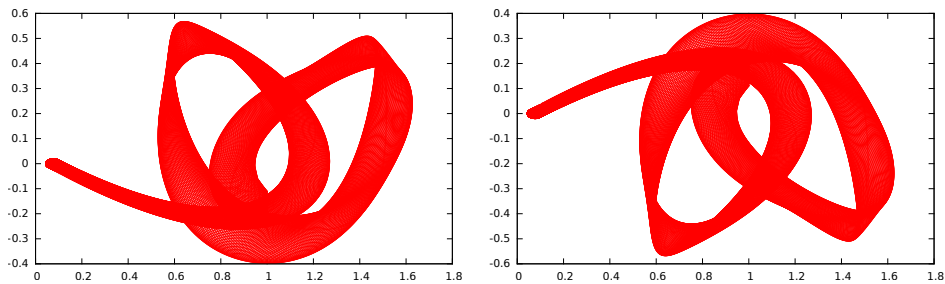
Four Manifolds.



Section with U_2 and U_3 after two rotations. Here we plot the section in the plane $((y, \dot{y}))$ with the cuts U_2 and U_3 . Because we have a fixed energy (Hamiltonian system), the \dot{x} value is deduced.



Plot of the two manifolds stopping at the U_2 and U_3 cuts.



Manifold stopping at the second intersection with U_2 .

Manifold stopping at the second intersection with U_3 .

B.6.4 Halo Orbit around L_1 – System Sun-Earth

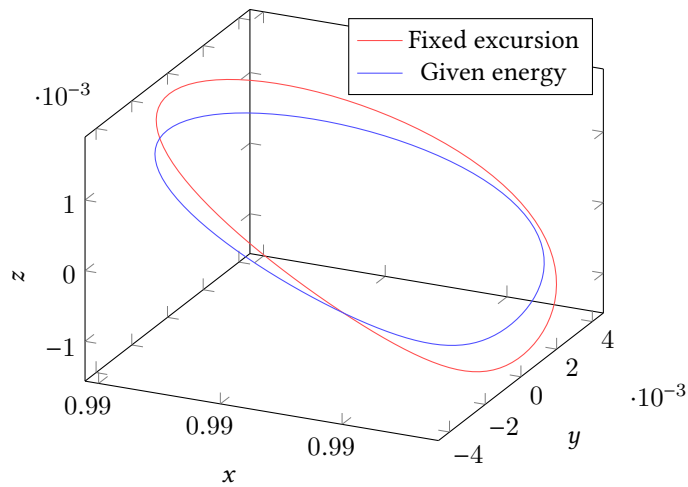
Parameter Input File. We note that we use the Cross coordinates.

```

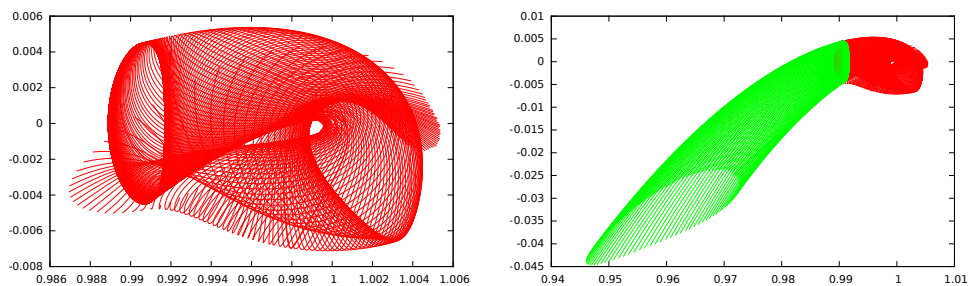
1 # M1 M2 Distance Periode Li
2 1.989E6 5.972 149597870E3 2.361d6 1
3 # intOrbite
4 100
5 # boolprop Tprop dtMani epsMani
6 1 5.d0 1d-02 1d-04
7 # readInit
8 0
9 # boolorbType Az boolEnergy energy stepCont printFamily
10 0 240.d6 1 -1.50041 0.001d0
11 # relerr abserr epstol factor
12 1d-14 1d-14 1d-12 1d02
13 # sectionU2 sectionU3 sectionU14 tourNbr printTraj
14 0 1 0 0 1
15 # verbose RichCross
16 1 1

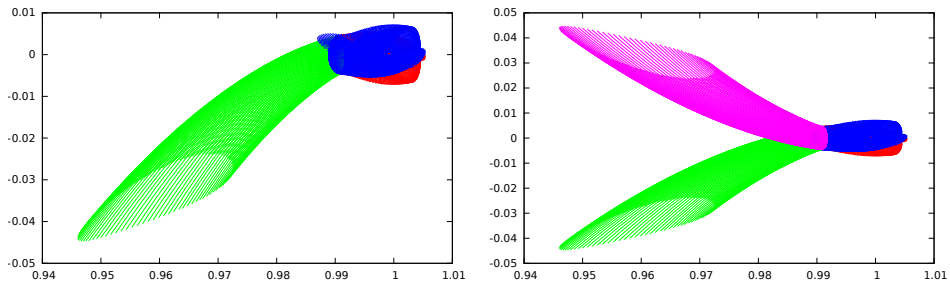
```

Periodic Orbits.

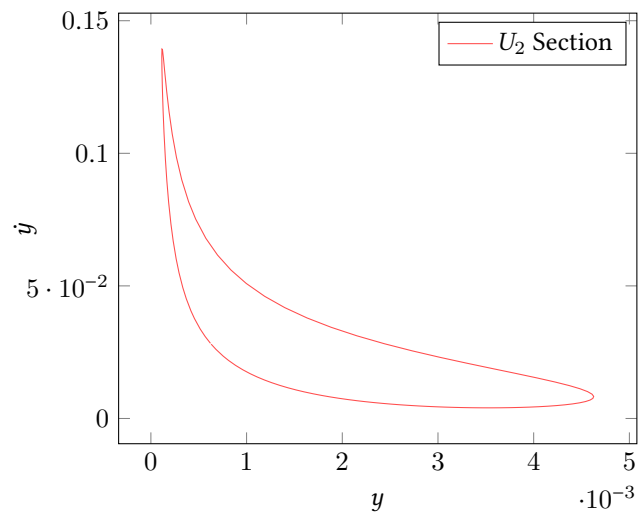


Four Manifolds.

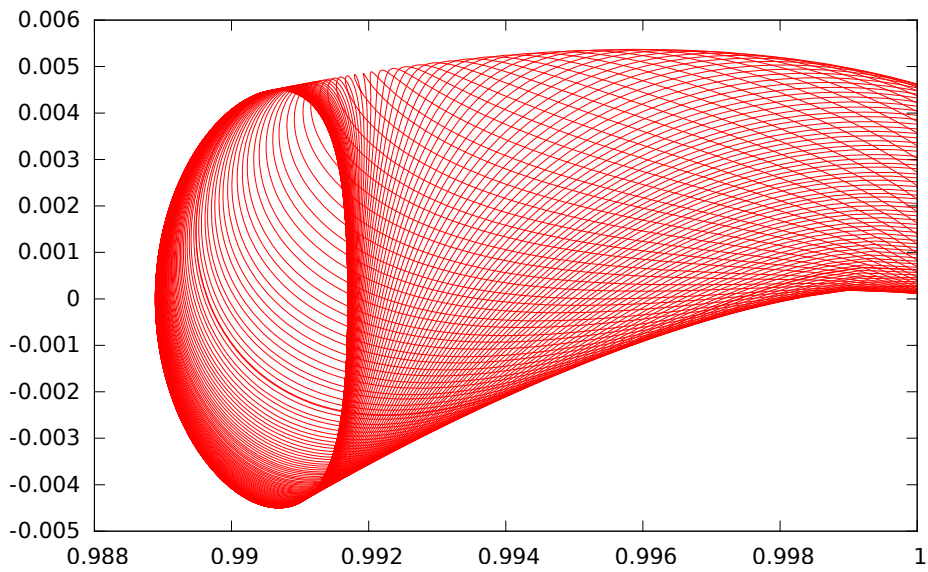




Section with U_3 after zero rotations. Here we plot the section in the plane $((y, \dot{y}))$ with the cut U_3 . Because we have a fixed energy (Hamiltonian system), the \dot{x} value is deduced.



Plot of the two manifolds stopping at the U_2 cut.



Manifold stopping at the second intersection with U_2 .

Input File for the Code Performing Transfers between Invariant Manifolds

We describe here the input file of the program performing the transfer between two invariant manifolds.

C.1 Principle

The main idea is to give two states in \mathbf{R}^6 denoted by ξ_0^U and ξ_1^U (as in Section 2.6) belonging to two different invariant manifolds. Then we follow the method explained in section 2.6. See figure 2.10 for the description of how the program works.

Here, we restrict ourselves to describing the input file of the program that we have developed. The program is more general and can be used for other purposes such as computing a transfer between natural trajectories in the CRTBP.

C.2 Input File

The input file is of the form

```
1 # M1      M2      Distance(m)  period
2 5.972E24 ; 7.349E22 ; 384402e3 ; 2.361e6
3 # TMAXinit(N) TMAXobj(N)
4 30. ; 30.
5 # ContinuationStep (initial)
6 0.01
7 # deltaT1 deltaT2 TransferTime ObjTransferTime
8 1.0 ; 2.0 ; 0.0 ; 0.0
9 # L2minToL1min printHom initCostate 2Bto3B HomTemps
10 0 ; 1 ; 0 ; 0 ; 1.0
11 # ConditionsFile
```

```

12 conditions.txt
13 # ISP(s)   g0(m.s^2)
14 2000 ; 9.81
15 # IncreaseTTir   placeofL2toL1(1,2,3)
16 0 ; 3
17 # HybrdEps   HybrdFact
18 1E-12 ; 1E-03
19 # integrator   pertubCostate
20 1 ; 0
21 # optEndpoints   ADJOINT0
22 0 ; 1E00

```

The structure of this the file must be respected. Odd numbered lines are for comments, and even numbered lines are used to provide the values of the parameters separated by semicolons.

Next, we describe all the parameters line by line.

Masses, distance, period

M1: Mass of the first primary (real (kg)).

M2: Mass of the second primary (real (kg)).

Distance: Distance between primaries (real (km)).

Period: Period of revolution of the two primaries around their center of mass (real (s)).

Maximal Thrust

TMAXinit: Initial value of the allowed maximal thrust (real (Newton)).

TMAXObj: Objective maximal thrust. If it is different from **TMAXinit**, then a continuation on the maximal thrust is performed. (real (Newton)).

Initial Continuation Step

ContinuationStep: Initial continuation step for all the different continuations. (real between 1e09 and 0.1).

Transfer Times

deltaT1: Backward propagation time of the first initial condition, see below (real (normalized time)).

deltaT2: Forward propagation time of the second initial condition, see below (real (normalized time)).

TransferTime: If **deltaT1** or **deltaT2** are zero, then, **TransferTime** determines the transfer time to perform the transfer between initial conditions (real (normalized time)).

ObjTransferTime: If **deltaT1** or **deltaT2** are different from **TransferTime**, then a continuation on the transfer time is performed (real (normalized time)).

Several Parameters

L2minToL1min: Integer parameter that enables the continuation on the cost, from the default L^2 -minimization (0) to the L^1 -minimization (1) (integer: 0 or 1)

printHom: Integer parameter to enable the creation of directories for the different continuations. In each directory, some files are created such as a file param and each successful trajectory TrajX.dat (where X is a number) .

initCostate: Integer to enable reading an initialization for the initial costate (the default initialization choice is zero) (integer 0 for no, 1 for yes).

2Bto3B: Integer to enable a continuation from the two body problem to the CRTBP (integer 0 for no, 1 for yes).

HomTemps: Parameter α_T defined in Section 2.6 to start the transfer with the closer states. This parameter allows to start the resolution with two points denoted by $\xi_0^{\alpha_T}$ and $\xi_1^{\alpha_T}$ and defined as

$$\xi_0^{\alpha_T} = \phi(-\alpha_T t_{\mathcal{A}_0}, \xi_0^U), \quad \text{and} \quad \xi_1^{\alpha_T} = \phi(\alpha_T t_{\mathcal{A}_1}, \xi_1^U).$$

These two points are closer than the two end-points defined as

$$\xi_0^* = \phi(-t_{\mathcal{A}_0}, \xi_0^U), \quad \text{and} \quad \xi_1^* = \phi(t_{\mathcal{A}_1}, \xi_1^U)$$

We then reach the two objective states ξ_0^* and ξ_1^* by continuation on the initial and final states as described in section 2.7.1. When **HomTemps**= 1.0 no continuation is performed. (real >0 and <=1.0).

Initial and Final condition

ConditionFile: Name of the file containing the initial (in \mathbf{R}^7) and final states (in \mathbf{R}^6), The file must contain two lines with on each the two states where the components are separated by semicolons (string).

Engine Specifications

ISP: Specific Impulse of the engine. (real (s)).

g0: Acceleration at Earth's surface (real (m/s²)).

Time Increasing and Place of the Cost Continuation

IncreaseTTir: Integer parameter that enables the increase of the transfer time if we reach a saturation ration of 0.85. (integer 0 for no, 1 for yes).

placeofL2toL1: Integer parameter to choose the place of the continuation on the cost if **L2minToL1min** is set to 1. See figure 2.10 for the different places (integer 1,2 or 3).

HYBRD Parameters

Two parameters of the HYBRD Fortran subroutine are available with our interface. The first one is also used for the integrator precision.

HybrdEps: Input variable used to determine a suitable step length for the forward-difference approximation. this approximation assumes that the relative errors in the functions are of the order of **HybrdEps**. If **HybrdEps** is less than machine precision, it is assumed that the relative errors in the functions are of the order of machine precision.
(real). (string).

HybrdFact: Positive input variable used to determine the initial step bound. In most cases **HybrdFact** should lie in the interval (.1,100.). 100. is a generally recommended value. For more detail see the HBRD documentation (real).

Integrator and Costate Perturbation

integrator: Choice between two integrators: DOP853. f if 0 or ode. f if 1 (integer 0 or 1).

pertubCostate: Integer parameter that allows to randomly perturb the initial zero costate.
(integer 0 for no, 1 for yes).

Last parameters

optEndpoints: Integer parameter that allows the optimization of the end-point positions on the natural dynamics (to obtain the transversality conditions of PMP)
(integer 0 for no, 1 for yes).

ADJOINT0: Choice of the value of p^0 in the PMP for the normalization of the costate
(real >0).

Index

- N*-body choreography, 15
- N*-body problem, 62
- adjoint vector, 72
- admissible trajectory, 130
- analytical approximation, 43
- ballistic capture, 17
- bang-bang control, 86
- boundary value problem, 75
- Cassini-Huygens mission, 16
- characteristic multiplier, 52
- circular three-body problem, 27
- continuation, 76
- continuation method, 47
- control vector field, 69
- costate, 72
- Cross coordinates, 31
- direct method, 73
- discrete continuation, 47, 77
- drift vector field, 69
- Duffing equation, 42
- dynamics, 31
- eight-shape periodic orbit, 45
- energy surface, 37
- equilibrium points, 32
- excursion, 42, 44
- extremal, 73
 - abnormal, 73
 - normal, 73
- family of orbits, 48
- final state continuation, 88
- Floquet multiplier, 52
- fly-by, 16
- forbidden realm, 37
- Galileo, 16
- geostationary Earth orbit, 15, 125
- gravitational assist, 63
- gravitational current, 49, 59, 62
- gravity assist maneuver, 16
- Greek asteroid, 36
- Halo orbit, 41
- Hamiltonian, 36
- heteroclinic orbit, 65
- Hill's region, 37
- HJB, 132
- homoclinic orbit, 65
- homotopy, 76
- homotopy method, 47
- indirect method, 73, 74
- integral of motion, 36
- invariant manifold, 49
- ion thruster, 17
- Jacobi integral, 37
- Lagrange points, 32
- Legendre polynomials, 40
- libration points, 32
- Lindstedt-Poincaré Method, 42
- linearization, 35
- linearized Hamiltonian, 56
- Lissajous orbit, 41
- LO, 127
- low Earth Orbit, 82
- low Earth orbit, 15
- lunar orbit, 125, 127
- Lyapunov orbit, 41
- Lyapunov-Poincaré, 40
- Lyapunov-Poincaré center theorem, 40
- minimization: L^2 -norm control, 86
- monodromy matrix, 51
- Moser theorem, 44

- multiple shooting function, 75
- multiple shooting method, 75
- multiplier, 41
- neck, 38
- nontrivial multiplier, 41
- parking orbit, 82
- patched conic approximation, 16
- PCRTBP, 65
- periodic orbits, 39
- piecewise linear continuation, 78
- planar circular restricted three body problem, 63
- planar restricted circular three body problem, 65
- Poincaré map, 53
- Poincaré cut, 65
- Poincaré surfaces, 63
- potential, 31
- primaries, 27
- primary, 28
- Richardson coordinates, 34
- Rosetta, 16, 17
- secondary, 28
- secular term, 45
- separatrix, 57
- shooting function, 42
- shooting method, 73
- single shooting method, 74
- stability, 35
- swing-by, 16
- thrust continuation, 89
- transition map, 31
- Trojan asteroid, 36
- tube, 54
- turnpike property, 113
- turnpike structure, 117
- value function, 132
- Voyager, 16
- zero path, 76
- zero velocity curve, 37

Bibliography

- [1] A. Agrachev and Y. Sachkov. *Control Theory from the Geometric Viewpoint*. Control theory and optimization. Springer, 2004.
- [2] E. L. Allgower and K. Georg. “Continuation and path following”. In: *Acta numerica, 1993*. Acta Numer. Cambridge Univ. Press, Cambridge, 1993, pp. 1–64.
- [3] E. L. Allgower and K. Georg. *Introduction to Numerical Continuation Methods*. Ed. by Springer-Verlag. Springer series in computational mathematics. 1990.
- [4] E. L. Allgower and K. Georg. “Piecewise linear methods for nonlinear equations and optimization”. In: *Journal of Computational and Applied Mathematics* 124.1–2 (2000). Numerical Analysis 2000. Vol. IV: Optimization and Nonlinear Equations, pp. 245–261.
- [5] E. Allgower and K. Georg. “Simplicial and continuation methods for approximating fixed points and solutions to systems of equations”. In: *SIAM Rev.* 22.1 (1980), pp. 28–85.
- [6] G. Archambeau, P. Augros, and E. Trélat. “Eight-shaped Lissajous orbits in the Earth-Moon system”. In: *Mathematics in Action* 4.1 (2011). Accepted for publication in Mathematics in Action, pp. 1–23.
- [7] M. Bardi and I. Capuzzo-Dolcetta. *Optimal control and viscosity solutions of Hamilton-Jacobi-Bellman equations*. With appendices by Maurizio Falcone and Pierpaolo Soravia. Birkhäuser Boston Inc., 1997, pp. xviii+570.
- [8] R. Bate, D. Mueller, and J. White. *Fundamentals of Astrodynamics*. Dover Books on Aeronautical Engineering Series. Dover Publications, 1971.
- [9] R. Battin. *An Introduction to the Mathematics and Methods of Astrodynamics*. AIAA education series. American Institute of Aeronautics & Astronautics, 1999.
- [10] E. A. Belbruno and J. K. Miller. “Sun-perturbed Earth-to-moon transfers with ballistic capture”. In: *Journal of Guidance Control Dynamics* 16 (Aug. 1993), pp. 770–775.
- [11] L. Berkovitz and N. Medhin. *Nonlinear Optimal Control Theory*. Chapman & Hall/CRC Applied Mathematics & Nonlinear Science. Taylor & Francis, 2012.
- [12] R. Bertrand and R. Epenoy. “New smoothing techniques for solving bang–bang optimal control problems—numerical results and statistical interpretation”. In: *Optimal Control Applications and Methods* 23.4 (2002), pp. 171–197.
- [13] J. T. Betts. *Practical Methods for Optimal Control Using Nonlinear Programming*. SIAM, 2001.
- [14] F. Bonnans, P. Martinon, D. Giorgi, V. Grélard, S. Maindrault, and O. Tissot. *BOCOP 2.0.4 - User Guide*. Nov. 2015.
- [15] J. Bonnans, J. Gilbert, C. Lemaréchal, and C. Sagastizábal. *Numerical Optimization – Theoretical and Practical Aspects*. Universitext. Springer Verlag, Berlin, 2006.

- [16] B. Bonnard and M. Chyba. *Singular Trajectories and Their Role in Control Theory*. Mathématiques et Applications. Springer, 2003.
- [17] B. Bonnard, J.-B. Caillau, and E. Trélat. “Second order optimality conditions in the smooth case and applications in optimal control”. In: *ESAIM: Control, Optimisation and Calculus of Variations* 13.2 (2007), pp. 207–236.
- [18] B. Bonnard, L. Faubourg, and E. Trélat. *Mécanique céleste et contrôle des véhicules spatiaux*. Ed. by Springer. 2009.
- [19] A. Bressan and B. Piccoli. *Introduction to the mathematical theory of control*. Vol. 2. AIMS Series on Applied Mathematics. American Institute of Mathematical Sciences (AIMS), Springfield, MO, 2007, pp. xiv+312.
- [20] R. Broucke. “Stability of periodic orbits in the elliptic, restricted three-body problem.” In: *AIAA Journal* 7 (1969), pp. 1003–1009.
- [21] W. I. Z. C. B. Garcia. “An Approach to Homotopy and Degree Theory”. In: *Mathematics of Operations Research* 4.4 (1979), pp. 390–405.
- [22] J.-B. Caillau, O. Cots, and J. Gergaud. “Differential continuation for regular optimal control problems”. In: *Optim. Methods Softw.* 27.2 (2012), pp. 177–196.
- [23] J.-B. Caillau and B. Daoud. “Minimum Time Control of the Restricted Three-Body Problem”. In: *SIAM Journal on Control and Optimization* 50.6 (2012), pp. 3178–3202.
- [24] J.-B. Caillau. “Contribution à l’étude du contrôle en temps minimal des transferts orbitaux”. Thèse de doctorat. Toulouse, France: Institut National Polytechnique de Toulouse, Nov. 2000.
- [25] J.-B. Caillau and J. Noailles. “Coplanar control of a satellite around the Earth”. In: *ESAIM Control, Optimisation and Calculus of Variations* 6 (février 2001), pp. 239–258.
- [26] Z. Chen, J.-B. Caillau, and Y. Chitour. *L_1 -minimization for mechanical systems*. Version 1. Mar. 2015. arXiv: 1506.00569 [math.OC]¹.
- [27] A. Chenciner and R. Montgomery. “A remarkable periodic solution of the three-body problem in the case of equal masses”. In: *Annals of Mathematics-Second Series* 152.3 (2000), pp. 881–902.
- [28] M. Chupin, T. Haberkorn, and E. Trélat. “Low-Thrust Lyapunov to Lyapunov and Halo to Halo Missions with L^2 -Minimization”. In: *ESAIM: Mathematical Modelling and Numerical Analysis* (June 2016). accepted.
- [29] C. C. Conley. “Low Energy Transit Orbits in the Restricted Three-Body Problems”. In: *SIAM Journal on Applied Mathematics* 16.4 (1968), pp. 732–746. eprint: <http://dx.doi.org/10.1137/0116060>.
- [30] O. Cots, J.-B. Caillau, and J. Gergaud. “Differential pathfollowing for regular optimal control problems”. anglais. In: *Optim. Methods Software* 27.2 (2012), pp. 177–196.
- [31] B. Daoud. “Contribution au contrôle optimal du problème circulaire restreint des trois corps”. français. Thèse de doctorat. Université de Bourgogne, Nov. 2011.
- [32] R. Epenoy. “Optimal long-duration low-thrust transfers between libration point orbits”. In: *IAC-2012* (2012).
- [33] R. Epenoy. “Recent Advances in Celestial and Space Mechanics”. In: ed. by B. Bonnard and M. Chyba. Cham: Springer International Publishing, 2016. Chap. Low-Thrust Transfers Between Libration Point Orbits Without Explicit Use of Manifolds, pp. 143–178.

1. <http://arxiv.org/abs/1506.00569>

- [34] L. Euler. “De motu rectilineo trium corpörum se mutuo attrahentium”. In: *Novi commentarii academiae scientiarum Petropolitanae Oeuvres*, Seria Secunda tome XXv Commentationes Astronomicae (1767), pp. 144–151.
- [35] R. W. Farquhar and A. A. Kamel. “Quasi-periodic orbits about the translunar libration point”. English. In: *Celestial mechanics* 7.4 (1973), pp. 458–473.
- [36] R. W. Farquhar, D. P. Muhonen, C. R. Newman, and H. S. Heuberger. “Trajectories and Orbital Maneuvers for the First Libration-Point Satellite”. In: *Journal of Guidance, Control, and Dynamics* 3.6 (1980), pp. 549–554.
- [37] R. Fourer, D. M. Gay, B. W. Kernighan, R. F. D. M. Gay, and B. W. Kernighan. *AMPL: A mathematical programming language*. 1989.
- [38] E. Gawlik, J. Marsden, P. Du Toit, and S. Campagnola. “Lagrangian coherent structures in the planar elliptic restricted three-body problem”. English. In: *Celestial Mechanics and Dynamical Astronomy* 103.3 (2009), pp. 227–249.
- [39] J. Gergaud and T. Haberkorn. “Homotopy Method for minimum consumption orbit transfer problem”. anglais. In: *ESAIM: Control, Optimisation and Calculus of Variations* 12.2 (avril 2006), pp. 294–310.
- [40] G. Gomez and J. Masdemont. “Some Zero Cost Transfers between Libration Point Orbits”. In: *POINT ORBITS, AAS PAPER 00-177, AAS/AIAA ASTRODYNAMICS SPECIALIST CONFERENCE*. 2000.
- [41] G. Gómez, J. Masdemont, and C. Simó. “Lissajous Orbits Around Halo Orbits”. In: *AAS* (1997), pp. 97–106.
- [42] G. Gómez, J. Masdemont, C. Simó, and A. Jorba. “Study Refinement of Semi-analytical Halo Orbit Theory: Executive Summary”. In: *ESOC Contract No.: 8625/89/D/MD (SC)* (1991).
- [43] T. Haberkorn and E. Trélat. “Convergence Results for Smooth Regularizations of Hybrid Nonlinear Optimal Control Problems”. In: *SIAM Journal on Control and Optimization* 49.4 (2011), pp. 1498–1522. eprint: <http://dx.doi.org/10.1137/100809209>.
- [44] T. Haberkorn. “Transfert orbital a pousse faible avec minimisation de la consommation: resolution par homotopie differentielle”. Thèse de doctorat. Toulouse, France: Institut National Polytechnique de Toulouse, Oct. 2004.
- [45] E. Hairer, S. Nørsett, and G. Wanner. *Solving Ordinary Differential Equations I: Nonstiff Problems*. Springer Series in Computational Mathematics. Springer Berlin Heidelberg, 2008.
- [46] P. Hartman. *Ordinary Differential Equations*. Second. Society for Industrial and Applied Mathematics, 2002. eprint: <http://epubs.siam.org/doi/pdf/10.1137/1.9780898719222>.
- [47] L. Hascoët and V. Pascual. “The Tapenade Automatic Differentiation tool: Principles, Model, and Specification”. In: *ACM Transactions On Mathematical Software* 39.3 (2013).
- [48] F. Jean. *Stabilité et commande des systèmes dynamiques*. Ed. by L. P. de l’ENSTA. Sept. 2011.
- [49] F. Jiang, H. Baoyin, and J. Li. “Practical Techniques for Low-Thrust Trajectory Optimization with Homotopic Approach”. In: *Journal of Guidance, Control, and Dynamics* 35.1 (2012). doi: 10.2514/1.52476, pp. 245–258.
- [50] À. Jorba and J. Masdemont. “Dynamics in the center manifold of the collinear points of the Restricted Three Body Problem”. In: *Physica D* (1997).

- [51] V. Jurdjevic. *Geometric Control Theory*. Cambridge Studies in Advanced Mathematics. Cambridge University Press, 1997.
- [52] W. S. Koon, M. W. Lo, J. E. Marsden, and J. E. Ross. *Dynamical Systems, the Three-Body Problem, And Space Mission Design*. Springer-Verlag New York Inc, 2006, p. 336.
- [53] W. S. Koon, M. W. Lo, J. E. Marsden, and S. D. Ross. “Heteroclinic connections between periodic orbits and resonance transitions in celestial mechanics”. In: *Chaos: An Interdisciplinary Journal of Nonlinear Science* 10.2 (2000), pp. 427–469.
- [54] J.-L. Lagrange. “Essai sur le problème des trois corps”. In: *Prix de l’académie royale des Sciences de paris, tome IX Oeuvres de Lagrange* 6, Gauthier-Villars (1772), pp. 272–282.
- [55] L. Landau and E. Lifshitz. *Mechanics*. Butterworth Heinemann. Butterworth-Heinemann, 1976.
- [56] E. B. Lee and L. Markus. *Foundations of optimal control theory*. Second. Robert E. Krieger Publishing Co., Inc., Melbourne, FL, 1986, pp. xii+576.
- [57] A. Lindstedt. “Sur la détermination des distances mutuelles dans le problème des trois corps”. In: *Ann. Sci. École Norm. Sup. (3)* 1 (1884), pp. 85–102.
- [58] J. Llibre and C. Piñol. “On the elliptic restricted three-body problem”. In: *Celestial Mechanics and Dynamical Astronomy* 48.4 (), pp. 319–345.
- [59] A. M. Lyapunov. *The general problem of the stability of motion*. Taylor & Francis, Ltd., London, 1992, pp. x+270.
- [60] J. E. Marsden and T. S. Ratiu. *Introduction to Mechanics and Symmetry*. 1998.
- [61] C. Martin and B. A. Conway. “Optimal Low-Thrust Trajectories Using Stable Manifolds”. In: *Spacecraft Trajectory Optimization*. Ed. by B. A. Conway. Cambridge Books Online. Cambridge University Press, 2010, pp. 238–262.
- [62] K. Meyer, G. Hall, and D. Offin. *Introduction to Hamiltonian Dynamical Systems and the N-Body Problem*. Applied Mathematical Sciences. Springer New York, 2010.
- [63] G. Mingotti, F. Topputo, and F. Bernelli-Zazzera. “Combined Optimal Low-Thrust and Stable-Manifold Trajectories to the Earth-Moon Halo Orbits”. In: *AIP Conference Proceedings* 886.1 (2007), pp. 100–112.
- [64] G. Mingotti, F. Topputo, and F. Bernelli-Zazzera. “Low-energy, low-thrust transfers to the Moon”. English. In: *Celestial Mechanics and Dynamical Astronomy* 105.1-3 (2009), pp. 61–74.
- [65] G. Mingotti, F. Topputo, and F. Bernelli-Zazzera. “Optimal Low-Thrust Invariant Manifold Trajectories via Attainable Sets”. In: *Journal of guidance, control, and dynamics*. 4th ser. 34 (2011), pp. 1644–1655.
- [66] J. Moser. “On the generalization of a theorem of A. Liapounoff”. In: *Communications on Pure and Applied Mathematics* 11.2 (1958), pp. 257–271.
- [67] J. Olympio. “Optimisation and optimal control methods for planet sequence design of low-thrust Interplanetary transfer problems with gravity-assists”. Theses. École Nationale Supérieure des Mines de Paris, Oct. 2008.
- [68] M. T. Ozimek and K. C. Howell. “Low-Thrust Transfers in the Earth-Moon System, Including Applications to Libration Point Orbits”. In: *Journal of Guidance, Control, and Dynamics* 33.2 (2010). doi: 10.2514/1.43179, pp. 533–549.
- [69] H. Poincaré. *Les méthodes nouvelles de la mécanique céleste: Invariants intégraux. Solutions périodiques du deuxième genre. Solutions doublement asymptotiques*. 1899. Les méthodes nouvelles de la mécanique céleste. Gauthier-Villars et fils, 1899.

- [70] H. Poincaré. *Les méthodes nouvelles de la mécanique céleste. Tome II. Les Grands Classiques Gauthier-Villars*. [Gauthier-Villars Great Classics]. Librairie Scientifique et Technique Albert Blanchard, Paris, 1987, pp. viii+487.
- [71] L. Pontryagin, V. Boltianski, R. Gamkrélidzé, and E. Michtchenko. *Théorie mathématique des processus optimaux*. Ed. by É. Mir. 1974.
- [72] G. D. Racca, B. H. Foing, and M. Coradini. “Smart-1: The First Time Of Europe To The Moon; Wandering in the Earth–Moon Space”. In: *Earth, Moon, and Planets* 85 (), pp. 379–390.
- [73] W. C. Rheinboldt. “Numerical continuation methods: a perspective”. In: *J. Comput. Appl. Math.* 124.1-2 (2000). Numerical analysis 2000, Vol. IV, Optimization and non-linear equations, pp. 229–244.
- [74] D. L. Richardson. “Analytic Construction of periodic orbits about the collinear points”. In: *Celestial mechanics* 22.3 (Oct. 1980).
- [75] C. Roberts. “The SOHO Mission L1 Halo Orbit Recovery From the Attitude Control Anomalies of 1998”. In: *Libration Point Orbits and Applications*. 2011. Chap. 9, pp. 171–217.
- [76] S. Ross. “The Interplanetary Transport Network”. In: *Amer. Scientist* 94.3 (2006), p. 230.
- [77] J.-M. Sarlat. *Les chorégraphies*. <http://melusine.eu.org/syracuse/swf/1-nbody/>. 2011.
- [78] J. Senent, C. Ocampo, and A. Capella. “Low-Thrust Variable-Specific-Impulse Transfers and Guidance to Unstable Periodic Orbits”. In: *Journal of Guidance, Control, and Dynamics* 28.2 (2005). doi: 10.2514/1.6398, pp. 280–290.
- [79] C. Simó. “European Congress of Mathematics: Barcelona, July 10–14, 2000, Volume I”. In: ed. by C. Casacuberta, R. M. Miró-Roig, J. Verdera, and S. Xambó-Descamps. Basel: Birkhäuser Basel, 2001. Chap. New Families of Solutions in N-Body Problems, pp. 101–115.
- [80] T. Starchville and R. Melton. “Optimal Low-Thrust Trajectories to Earth-Moon L2 Halo Orbits (Circular Problem)”. In: *Proceedings of the AAS/AIAA Astrodynamics Specialists Conference*. Ed. by P. of the AAS/AIAA Astrodynamics Specialists Conference. American Astro- nomical Soc., 1997, pp. 97–714.
- [81] J. Stoer and R. Bulirsch. *Introduction to Numerical Analysis*. Ed. by Springer. 2002.
- [82] E. Stuhlinger. *Ion propulsion for space flight*. McGraw-Hill series in missile and space technology. McGraw-Hill, 1964.
- [83] V. G. Szebehely. *Theory of Orbits - The Restricted Problem of Three Bodies*. Academic Press, 1967.
- [84] E. Trélat. *Contrôle Optimal*. Ed. by Vuibert. 2008.
- [85] E. Trélat. “Optimal Control and Applications to Aerospace: Some Results and Challenges”. In: *J. Optimization Theory and Applications* 154 (2012).
- [86] E. Trélat and E. Zuazua. “The turnpike property in finite-dimensional nonlinear optimal control”. In: *Journal of Differential Equations* 258 (2015), pp. 81–114.
- [87] K. Vogtman, A. Weinstein, and V. Arnold. *Mathematical Methods of Classical Mechanics*. Graduate Texts in Mathematics. Springer New York, 1997.
- [88] A. Wächter and T. L. Biegler. “On the implementation of an interior-point filter line-search algorithm for large-scale nonlinear programming”. In: *Mathematical Programming* 106.1 (2005), pp. 25–57.

-
- [89] L. Watson. *HOMPACK90: FORTRAN 90 Codes for Globally Convergent Homotopy Algorithms*. Department of Computer Science, Virginia Polytechnic Institute and State University, 1996.
- [90] F. B. Zazzera, F. Topputo, and M. Massari. *Assessment of mission design including utilisation of libration points and weak stability boundaries*. Tech. rep. 03-4103b. Available on line at www.esa.int/act. European Space Agency, the Advanced Concepts Team, 2004.
- [91] C. Zhang, F. Topputo, F. Bernelli-Zazzera, and Y.-S. Zhao. “Low-Thrust Minimum-Fuel Optimization in the Circular Restricted Three-Body Problem”. In: *Journal of Guidance, Control, and Dynamics* 38.8 (2015). doi: 10.2514/1.G001080, pp. 1501–1510.

INTERPLANETARY TRANSFERS WITH LOW CONSUMPTION USING THE PROPERTIES OF THE RESTRICTED THREE BODY PROBLEM

Abstract

The first objective of this work is to understand the dynamical properties of the circular restricted three body problem in order to use them to design low consumption missions for spacecrafts with a low thrust engine. A fundamental property is the existence of invariant manifolds associated with periodic orbits around Lagrange points. Following the Interplanetary Transport Network concept, invariant manifolds are very useful to design spacecraft missions because they are gravitational currents. A large part of this work is devoted to designing a numerical method that performs an optimal transfer between invariant manifolds. The cost we want to minimize is the L^1 -norm of the control which is equivalent to minimizing the consumption of the engines. We also consider the L^2 -norm of the control which is easier to minimize numerically. The numerical methods are indirect ones coupled with different continuations on the thrust, on the cost, and on the final state, to provide robustness. These methods are based on the application of the Pontryagin Maximum Principle. The algorithms developed in this work allow for the design of real life missions such as missions between the realms of libration points. The basic idea is to initialize a multiple shooting method with an admissible trajectory that contains controlled parts (local transfers) and uncontrolled parts following the natural dynamics (invariant manifolds). The methods developed here are efficient and fast (less than a few minutes to obtain the whole optimal trajectory). Finally, we develop a hybrid method, with both direct and indirect methods, to adjust the position of the matching points on the invariant manifolds for missions with large energy gaps. The gradient of the value function is given by the values of the costates at the matching points and does not require any additional computation. Hence, the implementation of the gradient descent is easy.

Keywords: optimal control, circular restricted three body problem, continuation method, shooting method, indirect methods, spacecraft mission, invariant manifolds

TRANSFERTS INTERPLANÉTAIRES À FAIBLE CONSOMMATION UTILISANT LES PROPRIÉTÉS DU PROBLÈME RESTREINT DES TROIS CORPS

Résumé

Le premier objectif de cette thèse est de bien comprendre les propriétés de la dynamique du problème circulaire restreint des trois corps et de les utiliser pour calculer des missions pour satellites pourvus de moteurs à faible poussée. Une propriété fondamentale est l'existence de variétés invariantes associées à des orbites périodiques autour des points de LAGRANGE. En suivant l'idée de l'*Interplanetary Transport Network*, la connaissance et le calcul des variétés invariantes, comme courants gravitationnels, sont cruciaux pour le *design* de missions spatiales. Une grande partie de ce travail de thèse est consacrée au développement de méthodes numériques pour calculer le transfert entre variétés invariantes de façon optimale. Le coût que l'on cherche alors à minimiser est la norme L^1 du contrôle car elle est équivalente à minimiser la consommation des moteurs. On considère aussi la norme L^2 du contrôle car elle est, numériquement, plus facile à minimiser. Les méthodes numériques que nous utilisons sont des méthodes indirectes rendues plus robustes par des méthodes de continuation sur le coût, sur la poussée, et sur l'état final. La mise en œuvre de ces méthodes repose sur l'application du Principe du Maximum de Pontryagin. Les algorithmes développés dans ce travail permettent de calculer des missions réelles telles que des missions entre des voisinages des points de LAGRANGE. L'idée principale est d'initialiser un tir multiple avec une trajectoire admissible composée de parties contrôlées (des transferts locaux) et de parties non-contrôlées suivant la dynamique libre (les variétés invariantes). Les méthodes mises au point ici, sont efficaces et rapides puisqu'il suffit de quelques minutes pour obtenir la trajectoire optimale complète. Enfin, on développe une méthode hybride, avec à la fois des méthodes directes et indirectes, qui permettent d'ajuster la positions des points de raccord sur les variétés invariantes pour les missions à grandes variations d'énergie. Le gradient de la fonction valeur est donné par les valeurs des états adjoints aux points de raccord et donc ne nécessite pas de calculs supplémentaires. Ainsi, l'implémentation de l'algorithme du gradient est aisée.

Mots clés : contrôle optimal, problème circulaire restreint des trois corps, méthode de continuation, méthode de tir, mission spatiale, méthodes indirectes, variétés invariantes

